論文 / 著書情報
Article / Book Information

題目(和文)	乾式再処理プロセスに向けての溶融ハロゲン化物の物理化学的研究
Title(English)	Physicochemical study on the molten halides for the pyroprocess of the pyrochemical reprocessing
著者(和文)	松宮正彦
Author(English)	
出典(和文)	学位:博士(工学), 学位授与機関:東京工業大学, 報告番号:甲第4359号, 授与年月日:2000年3月26日, 学位の種別:課程博士, 審査員:富安 博
Citation(English)	Degree:Doctor (Engineering), Conferring organization: Tokyo Institute of Technology, Report number:甲第4359号, Conferred date:2000/3/26, Degree Type:Course doctor, Examiner:
学位種別(和文)	博士論文
Type(English)	Doctoral Thesis

Physicochemical study on the molten halides for the pyroprocess of the pyrochemical reprocessing

Department of Nuclear Engineering,
Tokyo Institute of Technology

by Masahiko Matsumiya

Supervisor: Professor Dr. Hiroshi Tomiyasu
Professor Dr. Ryuzo Takagi

Contents

Chapter I

Introduction

Chapter I Introduction

There are some advantages for molten salts as follows.

(1) The temperature range is wide and vapor pressure is low.

(2) The thermal capacity, solubility and chemical stability is high.

(3) The electrochemical window is wider than the aqueous solution.

Good electric conduction is one of the characteristics of many, though not all, molten salts. The good electric conduction has been or is to be utilized industrially in electrolytic production of metals, electrorefining, batteries, fuel cells, etc. Owing to these characteristics, molten salts are used as the solvents for electrowinning of Al and Na. Nowadays, many metals including alkali, alkaline-earth, rare earth, as well as U are deposited by an electrorefining method. In addition, molten salts technology has also been applied to nuclear technology by its high stability against radiation. At the heart of the Integral Fast Reactor (IFR) fuel processing program at Argonne National Laboratory (ANL) is the recovery of U and Pu from spent IFR fuel via the pyrochemical process unknown as electrorefining. The development of this program at ANL has benefited greatly from the wealth of work done here in pyrochemistry during the 1960s and 1970s. To contribute further to this program the literature on electrorefining of U and Pu has been comprehensively and critically reviewed. The last literature review of this subject was published in 1973 by Martinot and Caligara[1]. Since that time, however, progress has continued in this area in the US and abroad, including the recent efforts in electrorefining spent IFR fuel.

On the other hand, from a fundamental viewpoint, molten salts are regarded as strong coulombic liquid systems and therefore the electric conduction in electrolytes such as molten salts based on statistical mechanics, i.e., the linear response theory[2, 3]. In recently, the development of computer science calculating speed and storage volume becomes much faster and larger, respectively. The technique of molecular dynamics simulation (MD) can yield some experimentally information. Professor Okada et al. have proposed that the strong correlation between the internal mobility and the self-exchange velocity (SEV) in molten alkali nitrates and chlorides.

§ I - i Electrodeposition of U and Pu by liquid metallic cathodes

The first use of a liquid metal cathode in the electrodeposition of U or Pu was reported by Brodsky and Carleson in 1962[4]. They added U^{3+} as $CsUCl_6$ to a LiCl-KCl melt at 973K and electrodeposited U metal at a liquid Pb cathode contained in a MgO crucible. Analysis of the deposit, however, revealed that a large portion of it was UO_2, not metallic U as had been expected. They believed that the oxide had formed by a reaction between the U-Pb alloy and the MgO crucible. An extensive search of the literature has revealed that, other than Brodsky and Carleson and the work related to the IFR program at ANL, only one other laboratory has investigated electrodeposition of actinides from molten salt solutions at liquid metal electrodes. However, this one laboratory, at the S. M. Kirov Urals Polytechnic Institute in Sverdlovsk, USSR, has been very active in this area for the last twenty years. Their publications in this area generally fall into two groups. The first group of publications describe the investigation of the thermodynamics of molten salt electrodeposition at liquid metal electrodes and are authored by V. A. Lebedev and coworkers. The second group of publications, authored by S. L. Gol'dshtein and coworkers, focused on optimizing the electrodeposition process by various means, most notably pulsed current electrodeposition. The more basic thermodynamic studies of Lebedev and coworkers will be discussed first. In 1974 Lebedev et al. began to examine the initial stage of solid phase formation in the deposition of rare elements from molten salts on molten metal cathodes. Using an approach developed by Gutsov[5], they measured the nucleation overpotential, the time required to reach that overpotential, the work required to form the nucleus and the number of atoms in a nucleus, all as a function of temperature and current density. The system they studied were La-Zn[6], U-Zn[7], U-Al[8], U-In[9], U-Bi[10], U-Ga[11], and U-Sb[12]. The full texts of these papers are Russian and have been obtained from VINITI, a Soviet document depository. Fortunately, brief English summaries of these papers are also available. Before Gol'dshtein and coworkers became interested in liquid metal electrodes, they did some initial studies of electrodeposition at solid cathodes. In this work, they developed a model for determining initial currents for potentiostatic electrolysis of a molten salt system at a

solid cathode[13]. The model predicts the initial electrolysis current, taking into consideration the response performance of the potentiostat in addition to the diffusion coefficients of the species in the molten salt phase. Shortly thereafter, the focus shifted to electrodeposition at liquid cathodes with an examination of Zr electrodeposition on liquid Zn from a NaCl-KCl melt containing 25wt% K_2ZrF_6[14]. In comparing the results from constant current and pulsed current electrodeposition, Gol'dshtein et al. found that the pulsed current approach improved the current efficiency from 63 to 89%. Furthermore, they found that pulsing the current resulted in a product that was more homogeneous and had a higher Zr is not explicitly stated in the paper, the paper implies that it was indeed metallic Zr being deposited. Several other papers were published on the electrodeposition of Zr[15-20] and U[21,22] at liquid Zn cathodes. Similar studies have been made of La[23-25], U[8,26-27], and Ce[28] electrodeposition at liquid Al cathodes as well as electrodeposition of U[29] and Zr[19] at liquid Bi cathodes. These reports demonstrate that in the case of liquid metal electrodes, pulsed current electrodeposition is clearly superior to constant current electrodeposition with respect to efficiency and maximum yield. In most of these papers, Gol'dshtein et al. attribute the observed increase in efficiency and homogeneity to two observed increase in efficiency and homogeneity to two distinct effects arising from the pulsating current. The primary effect is a decrease in the thickness of the diffusion layer. After each pulse, the diffusion layers in the liquid metal and in the electrolyte are given the opportunity to relax and approach bulk conditions. Because near-bulk concentrations are present at the interface when the next pulse is applied, higher deposition current densities can be used without a loss of efficiency. In the early Zn cathode studies, Gol'dshtein et al.[14] observed that the pulsed current caused a regular and periodic movement of the surface of the liquid metal. They regarded this effect as beneficial because it facilitates the removal of the oxide film from the Zn/melt boundary of separation, prevents the formation of a solid crust of intermetallic compound, and favors its uniform distribution in the volume of the melt.

§ I - ii Pyrometallurgical Process Development

§ I - ii - i Pyrochemical reprocessing process proposed by JAERI

The combination of nitride fuels and pyrochemical reprocessing is being studied in Japan Atomic Energy Research Institute (JAERI) as a viable option for the minor-actinide recycling for a dedicated actinide burner system. One of the advantages of applying pyrochemical process to nitride is the ease of ^{15}N recovery. The current status of JAERI thermochemical data file for prediction of pyrochemical processes is also presented. In JAERI, the concepts of dedicated systems for burning minor actinides (MA: Np, Am and Cm) are being studied. A combination of the nitride fuels and pyrochemical reprocessing has being chosen for the fuel cycle of the dedicated MA burner systems for the following reasons:

(1) Excellent thermal properties: actinide nitrides are characterized by refractoriness and high thermal conductivities.

(2) Mutual solubility: the isotope vector of the actinides strongly depends on the commercial spent-fuel history as well as the recycle mode in a burner system. The fuel should accommodate a wide range of the combination and composition of actinides. The mutual solubility among the actinide mononitrides is expected to be high, which is in contrast with that among the respective metal elements.

(3) MA handling: MA is characterized by a significantly large α-decay heat and fast-neutron emission. A compact fuel cycle facility should be realized to economically cope with this problem. Pyrochemical reprocessing based on molten-salts technology may be adaptable to this purpose. Process concepts have been proposed[30-32] as shown in **Fig. 1-1-1**.

(4) ^{15}N recycling: a highly ^{15}N-enriched nitrogen would have to be used for nitride fuels in order to prevent the formation of ^{14}C, which itself is a long-term radiological concern. By applying pyrochemical process, ^{15}N could be readily recovered.

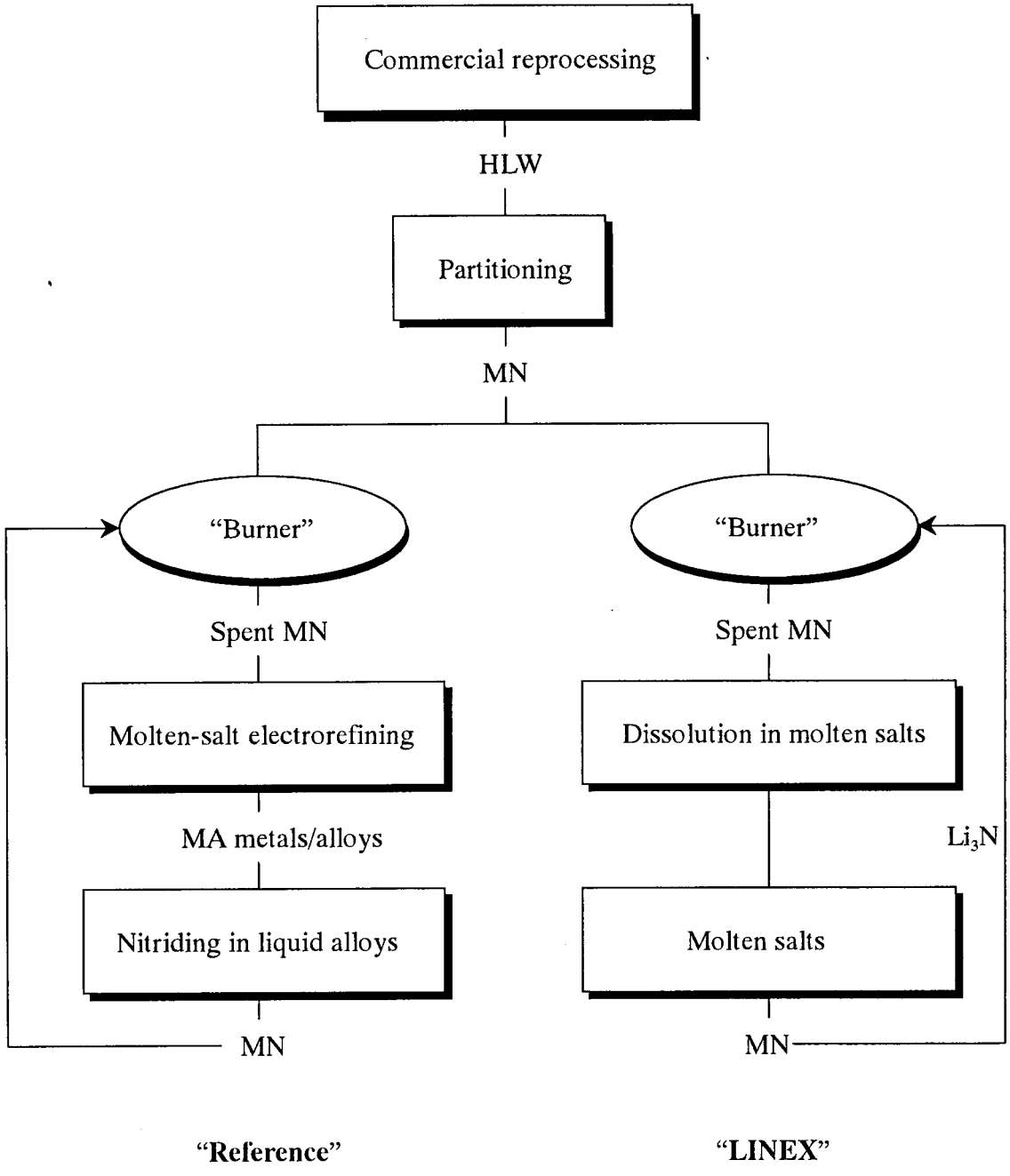

Fig. 1-1-1 Concepts of nitride/pyroprocess for MA burning.

§ I - ii - ii Pyrometallurgical partitioning technology proposed by CRIEPI

Central Research Institute of Electric Power Industry (CRIEPI) has been developing the pyro-reprocessing technology as the way to realize the advanced fuel cycle concept. The pyrometallurgical processing was originally developed by Argonne National Laboratory for recycling the metal fuel with keeping compactness, economy and diversion resistance[33-35]. CRIEPI has started studying pyrometallurgical processing since 1986[36-38]. The study was first dedicated on the assessment of physico-chemical properties such as standard potentials, equilibrium distribution data, diffusion coefficients etc. for evaluating the feasibility of pyrometallurgical processing, resulting in experimental measurements of the lacking data.

The pyrometallurgical partitioning technology to recover actinides from HLW (high level radioactive wastes) generated in PUREX reprocessing facility is being developed at CRIEPI[38-40]. The process consists of four main steps as shown in **Fig. 1-1-2**:

(1) denitration of HLW to oxides by heating,

(2) chlorination to convert oxides to chlorides,

(3) reductive extraction to reduce actinides in a molten salt by lithium metal and to extract them into liquid cadmium,

(4) electrorefining in LiCl-KCl eutectic salt to separate actinides from liquid cadmium anode.

Elements contained in HLW are classified into three groups based on Gibbs free energies of formation of chlorides as shown in **Table 1-1-1**:

(1) active metals such as alkali metal, alkaline earth, samarium and europium

(2) actinides and most of REs (rare earth elements)

(3) noble metals such as ruthenium, technetium and molybdenum

Active metals remain in the salt during the reductive extraction step and noble metals remain in the cadmium anode during the electrorefining.

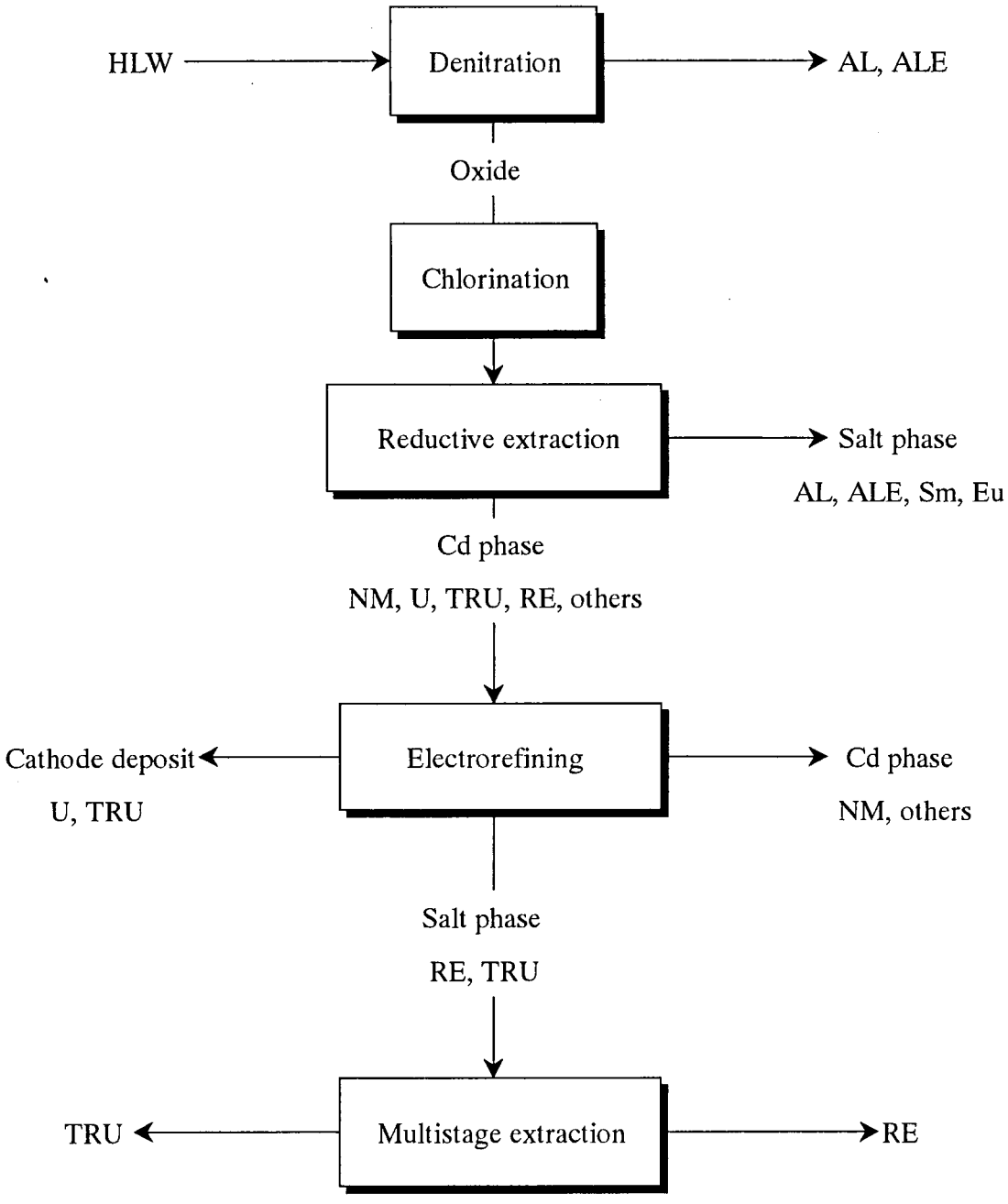

Fig. 1-1-2 Flow diagram of pyrometallurgical partitioning process.

Table 1-1-1 Standard free energy of formation of chlorides at 773K.

Chlorides	ΔG_f^0 (kJ/mol-Cl)	Comment
$BaCl_2$	-367.56	
CsCl	-366.65	
KCl	-363.76	*Molten Salt*
RbCl	-361.76	-Alkali Metals
$SrCl_2$	-353.75	-Alkaline Earths
$SmCl_2$	-345.91	-Rare Earths
LiCl	-345.27	
$YbCl_2$	-343.71	
NaCl	-339.58	
$CaCl_2$	-337.82	
$LaCl_3$	-293.62	
$PrCl_3$	-288.89	
$CeCl_3$	-287.37	
$NdCl_3$	-281.45	
$SmCl_3$	-278.10	
$GdCl_3$	-273.02	
YCl_3	-272.50	
$HoCl_3$	-269.09	
$ErCl_3$	-269.02	
$AmCl_3$	-266.38	
$DyCl_3$	-265.92	
$CmCl_3$	-264.99	
$TmCl_3$	-263.15	
$PuCl_3$	-261.41	*Cathode*
$MgCl_2$	-258.33	-Actinides
$YbCl_3$	-257.77	
$ScCl_3$	-247.65	

$EuCl_3$	-245.39	
$NpCl_3$	-242.91	
UCl_3	-232.35	
UCl_4	-198.75	
$ZrCl_4$	-195.28	
$ZrCl_2$	-194.18	
$BeCl_2$	-190.18	
$NpCl_4$	-189.76	
$MnCl_2$	-189.36	
VCl_2	-168.08	
UCl_5	-159.21	
$ZnCl_2$	-150.93	
$CrCl_2$	-148.58	
$CdCl_2$	-136.30	
VCl_3	-135.37	
$FeCl_2$	-124.36	
HCl(g)	-99.26	
$NiCl_2$	-94.25	
AgCl(l)	-86.43	
WCl_2	-81.89	*Anode*
$MoCl_3$	-67.96	-Transition Metals
$ZrCl_3$	-67.22	-Noble Metals
$TcCl_2$	-46.02	

§ I - ii - iii Aqua-Pyro partitioning process proposed by Toshiba Corporation

A new TRU recovery process named "Aqua-Pyro partitioning process" is shown in **Fig. 1-1-3**[41-44]. In the first step, TRUs and REs are precipitated from HLLW (High-Level Liquid Waste) is an aqueous solution. Simple separation of TRUs from REs in the aqueous solution is difficult to be achieved. A pyrochemical process is more effective for separating TRUs from REs than an aqueous one. TRUs are separated from REs by electrorefining in molten salt in the final step.

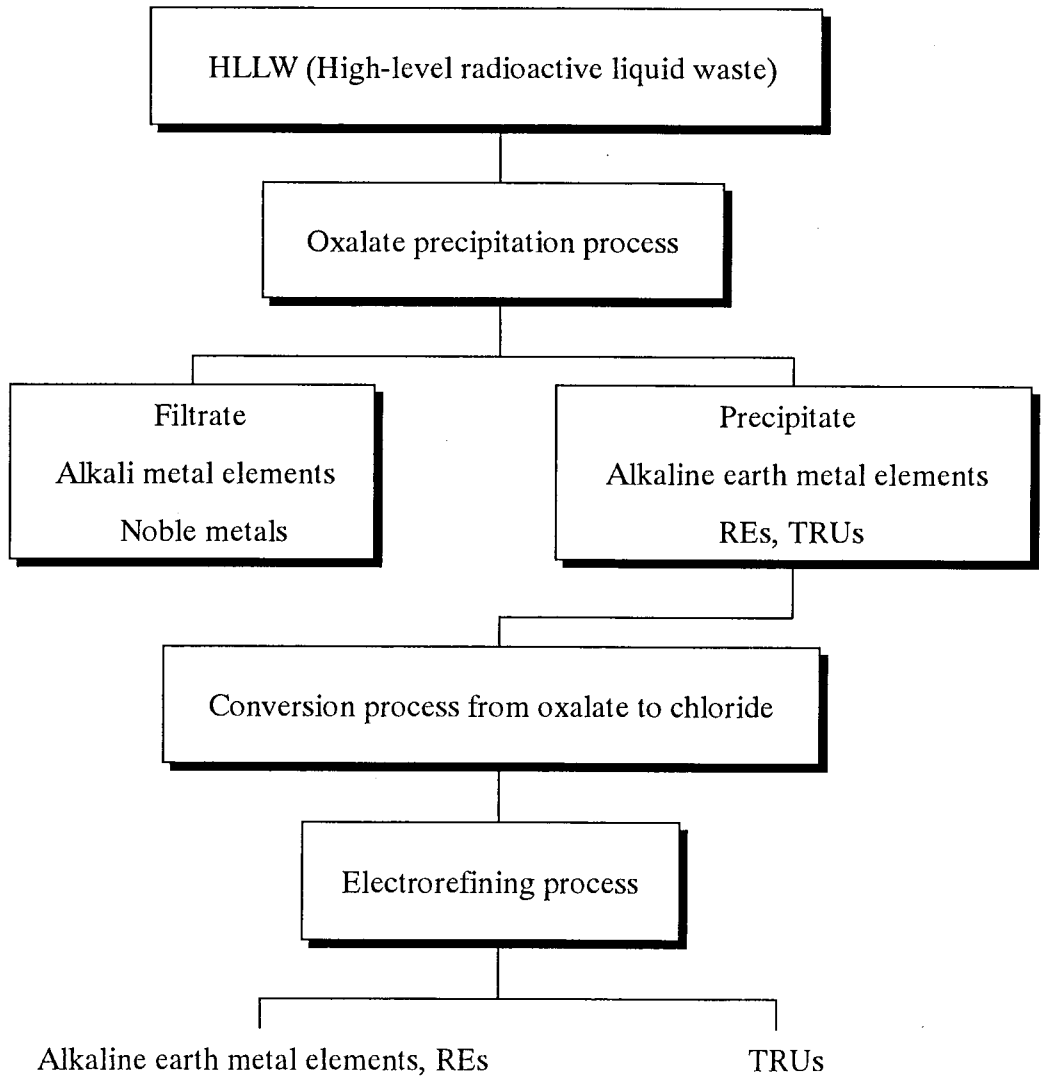

Fig. 1-1-3 Process flow of the "Aqua-Pyro" partitioning process.

§ I - iii Self-Consistent Nuclear Energy System

§ I - iii - i Background

The PUREX method was originally planned for separation of U and Pu. Many investigators have proposed several nuclear fuel cycle concepts by modifying the PUREX method, in most of which radioactive materials are to be vitrified to inorganic matrix and stored in the underground. The Integral Fast Reactor (IFR) concept proposed by Argonne National Laboratory[45] contains a sophisticated idea of pyrochemical treatment in the nuclear fuel cycle. After electrowinning U as well as transuranium elements (TRU), a small amount of the fuel elements and a large amount of fission products are left in the melt bath. In the IFR concept, after removal of the fuel materials, the salt bath containing fission products will be occluded into the zeolites and stocked as the deposits. However, from a standpoint of the harmonization of nuclear systems with global environment,

(a) we should remove the residue of U and TRU completely for minimization of nuclear waste and utilization of rare fuel elements,

(b) we should also make an effort to separate the fission products each other for incineration or utilization of medical tracers, rare materials and so on.

Thus, Shimizu and Fujii-e have proposed Self-Consistent Nuclear Energy System (SCNES)[46], which aims at zero release of radioactive materials out of the fuel cycle[47], as shown in **Fig. 1-2-1**. In the SCNES we need to separate fuel elements and fission products into the following groups;

(1) U and TRU should be recycled as fuel elements

(2) A series of fission products whose half-lives are more than 1 year should be returned back to the reactor core for their incineration, and the other should be cooled down and released from the fuel cycle.

§ I - iii - ii The purpose of this study

As one of the most feasible candidates for the SCNES is a metallic fuel fast breeder reactor (FBR), we have adopted pyrochemical treatment of metallic fuel as a chemical separation process. One of concepts using molten chlorides as solvent is shown in **Fig. 1-2-2**. After the electrorefining and drawdown process, all alkali halides, alkaline-earth halides and some amounts of rare earth halides from fission products still remain in the salt bath. Thus, in order to use the salt bath repeatedly, we have applied a countercurrent electromigration method and an electowinning method.

The electromigration method has an advantage for the pyrochemical treatment due to its simple construction for being able to use the same container with the conductive melt bath. Iwasaki and Takagi have already demonstrated enrichment of La in the NaCl-KCl equimolar mixture bath[48]. Moreover, Matsuura et al. have also demonstrated enrichment of Cs, Sr and Gd as examples of fission products in the LiCl-KCl eutectic system[49]. In this present work, we have carried out the experiments for the following purposes;

(a) Scientific aspects; evaluation of mobilities for molten alkali chlorides by comparison with MD simulation

(b) Technological aspects; possibility of application of the continuous countercurrent electromigration method for nuclear waste treatment process

Additionally, it is difficult to recover some fission products like alkali and alkaline-earth elements from the salt phase, because of their more negative reduction potentials[50] than the solvent components as shown in **Table 1-1-2**. However, if we can find adequate liquid metal which forms stable alloy with the electrochemically negative elements (Cs^+, Eu^{2+}, Sr^{2+} and Ba^{2+}) making less interaction with the solvent, because it is found that the liquid Cd metal forms stable alloy with Pu.

(a) Scientific aspects; electrochemical behavior of the electrochemically negative elements on several solid and liquid metallic electrodes in the fluoride and chloride baths.

(b) Technological aspects; possibility of recovery of the electrochemically negative elements on several liquid metallic cathodes in the fluoride and chloride baths.

Table 1-1-2 Standard electromotive forces for molten chlorides and fluorides[50].

Metal Ion	Chlorides (at 1073K) [V]	Fluorides (at 1073K) [V]
Eu^{2+}	------	5.602
Sm^{2+}	3.661	5.385
Ba^{2+}	3.568	5.310
Sr^{2+}	3.469	5.364
Li^{+}	3.457	5.256
K^{+}	3.441	4.674
Cs^{+}	3.362	4.367
Ca^{2+}	3.323	5.350
Na^{+}	3.240	4.818
La^{3+}	2.997	5.174
Ce^{3+}	2.945	5.097
Pr^{3+}	2.911	5.109
Sm^{3+}	2.861	4.992
Nd^{3+}	2.856	5.004
Eu^{3+}	2.828	4.790
Be^{2+}	------	4.247
Zr^{3+}	------	4.255
U^{3+}	2.280	------
Zr^{4+}	------	4.045
U^{4+}	1.974	4.015
Zn^{2+}	1.476	3.068
Fe^{2+}	1.118	2.905
Cd^{2+}	1.193	2.826
Ni^{2+}	0.875	2.697

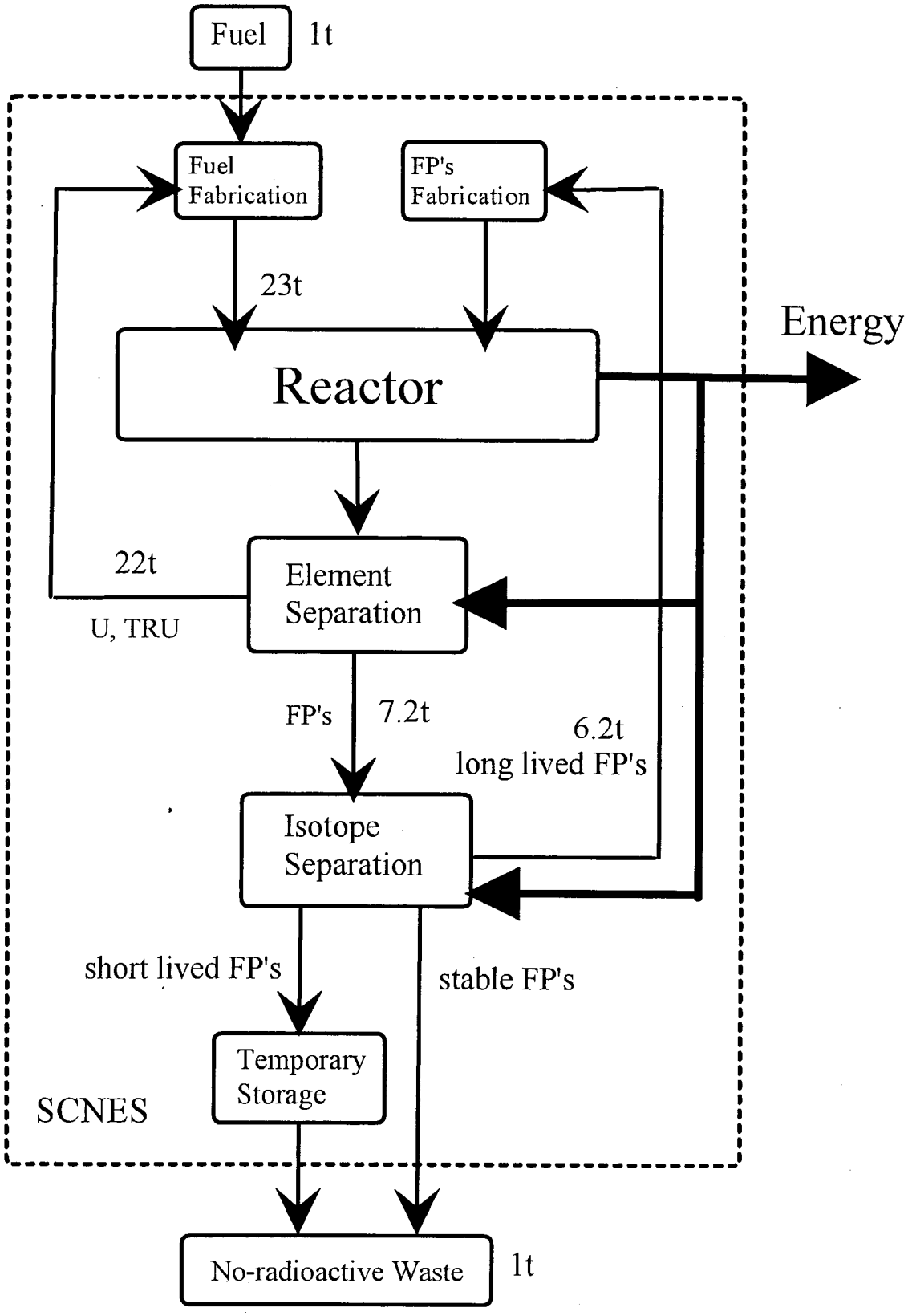

Fig. 1-2-1 Self-consistent nuclear energy system

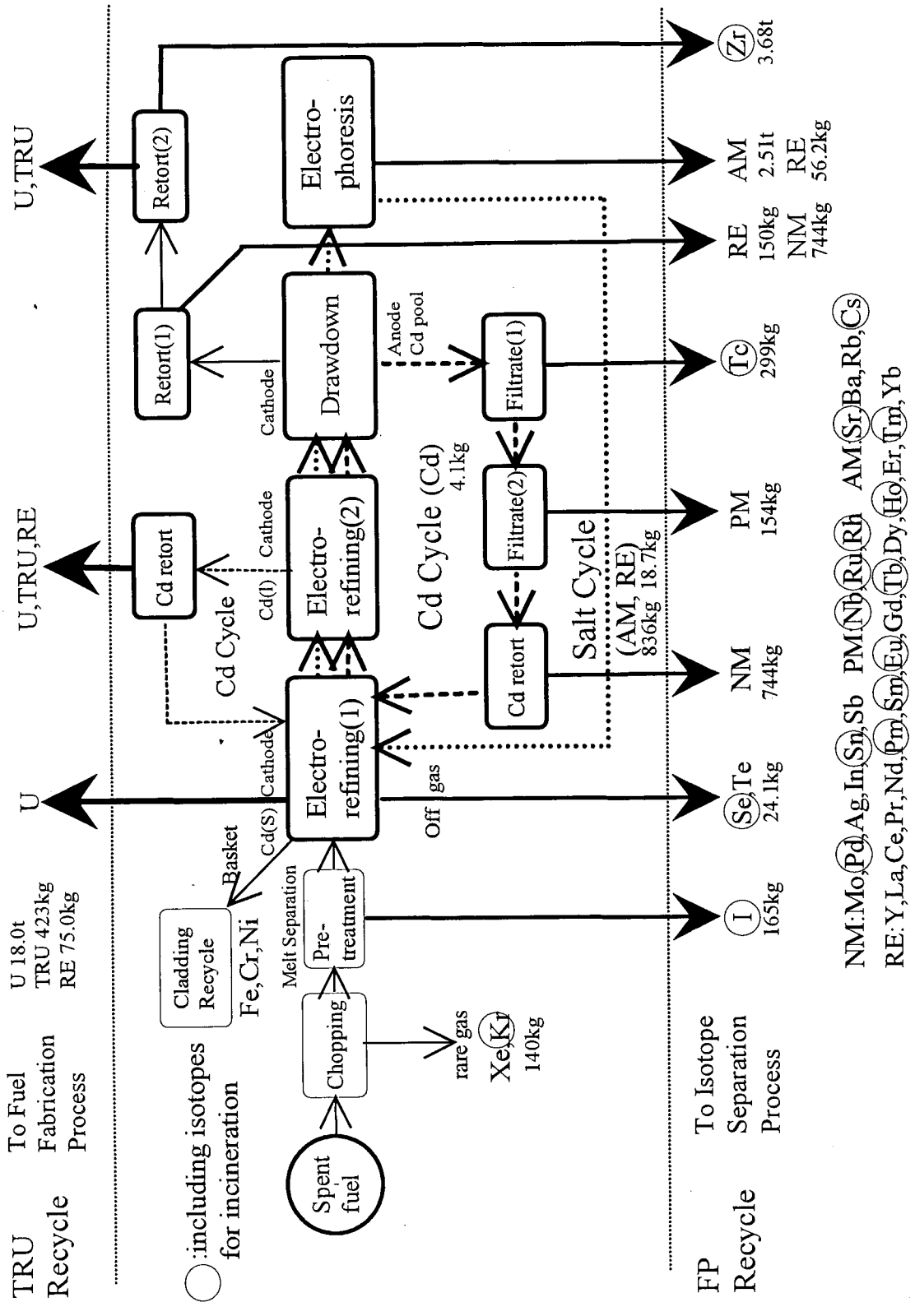

Fig. 1-2-2 One of the concepts for pyrochemical process using molten chlorides

§ I - iv References

(1) L. Martinot and F. Caligara, *At. Energy Rev.*, **11**, 3 (1973).

(2) R. Kubo, *J. Phys. Soc. Jpn.*, **12**, 570 (1957).

(3) B. F. Markov, *D. A. N. SSSR*, **110**, 441 (1956).

(4) M. B. Brodsky and B G. F. Carleson, *J. Inorg. Nucl. Chem.*, **24**, 1675 (1962).

(5) Iv. Gutsov, Izv. Inst. Fizikokhim., Bulgar. Akad. Nauk 4, 69-88 (1964).

(6) V. A. Lebedev, V. I. Pyatkov and V. G. Prokop'ev, *Russ. J. Phys. Chem.*, **49**, 478 (1975).

(7) V. A. Lebedev, V. I. Pyatkov and V. V. Prokop'ev, *Russ. J. Phys. Chem.*, **49**, 804 (1975).

(8) V. A. Lebedev, V. I. Sal'nikov and V. A. Cherkezov, *Russ. J. Phys. Chem.*, **49**, 945 (1975).

(9) V. A. Lebedev and V. A. Cherkezov, *Russ. J. Phys. Chem.*, **49**, 1092 (1975).

(10) V. A. Lebedev, V. I. Pyatkov and V. G. Prokop'ev, *Russ. J. Phys. Chem.*, **49**, 1097 (1975).

(11) V. A. Lebedev and V. A. Cherkezov, *Russ. J. Phys. Chem.*, **49**, 1266 (1975).

(12) V. A. Lebedev, V. I. Pyatkov and V. G. Prokop'ev, *Russ. J. Phys. Chem.*, **49**, 1268 (1975).

(13) S. L. Gol'dshtein, V. A. Lebedev, I. F. Nichkov and S. P. Raspopin, *Sov. Electrochem.*, **7**, 258-261 (1971).

(14) S. L. Gol'dshtein, D. F. Rakipov and S. P. Raspopin, *Sov. Electrochem.*, **10**, 1277-1279 (1973).

(15) S. L. Gol'dshtein, D. F. Rakipov and S. P. Raspopin, *Sov. Electrochem.*, 12, 128-130 (1974).

(16) (a) S. L. Gol'dshtein, D. F. Rakipov and S. P. Raspopin, *Electrolytic Preparation of Zn-Zr Compositions*, USSR Patent 449, 994 (1974).

(b) S. L. Gol'dshtein, D. F. Rakipov and S. P. Raspopin, *Electrolytic Production of Zn-Zr Alloys*, USSR Patent 589, 289 (1976).

(17) S. L. Gol'dshtein, D. F. Rakipov and S. P. Raspopin, *Non-Ferrous Metal*, **6**, 48 (1974); *Tsvetn. Met.*, **9**, 46 (1975).

(18) S. L. Gol'dshtein, D. F. Rakipov and S. P. Raspopin, *Non-Ferrous Metal*, **9**, 51 (1975); *Tsvetn. Met.*, **9**, 50 (1975).

(19) S. L. Gol'dshtein, D. F. Rakipov, S. P. Raspopin and Y. P. Shepelev, *Izv. Vyssh. Uxhebn. Zaved., Tsvetn. Metall.*, **2**, 114 (1976).

(20) S. L. Gol'dshtein, D. F. Rakipov and S. P. Raspopin, *Sov. Non-Ferrous Metal. Res.*, **2**, 80 (1977); *Izv. Vyssh. Uchebn. Zaved., Tsvetn. Metall.*, **2**, 151 (1977).

(21) S. L. Gol'dshtein, S. M. Zakhar'yash, D. F. Rakipov and S. P. Raspopin, *Sov. At. Energy*, **42**, 136 (1977); *At. Energy*, **42**, 125 (1977).

(22) S. L. Gol'dshtein, S. P. Raspopin, G. B. Smirnov and A. A. Khusnutdinov, *Sov. At. Energy*, **43**, 826 (1977); *At. Energ.*, **43**, 199 (1977).

(23) S. L. Gol'dshtein, S. P. Raspopin and V. A. Fedorov, *Sov. Non-Ferrous Metal. Res.*, **4**, 355 (1981); *Izv. Vyssh. Uchebn. Zaved., Tsvetn. Metall.*, 83 (1981).

(24) S. L. Gol'dshtein, S. P. Raspopin, V. L. Sergeev and V. A. Fedrov, *Sov. Non-Ferrous Metal. Res.*, **1**, 18 (1978); *Izv. Vyssh. Uchebn. Zaved., Tsvetn. Metall.*, **1**, 59 (1978).

(25) S. L. Gol'dshtein, S. P. Raspopin and V. A. Fedrov, *Sov. Electrochem.*, **17**, 1110 (1981); *Elektrokhimiya*, **17**, 1350 (1981).

(26) S. L. Gol'dshtein, S. V. Gudkov, S. P. Raspopin and V. L. Sergeev, *Sov. Electrochem.*, **17**, 1043 (1981); *Elektrokhimiya*, **17**, 1267 (1981).

(27) S. L. Gol'dshtein, S. P. Raspopin, V. L. Sergeev and V. A. Fedrov, *Al-La Master Alloy*, USSR Patent, **657**, 92 (1979).

(28) S. L. Gol'dshtein, S. P. Raspopin, A. V. Tunin and V. A. Fedrov, *Izv. Vyssh. Uchebn. Zaved., Tsvetn. Khim. Tekhnol.*, **20**, 1096 (1977).

(29) S. L. Gol'dshtein, S. M. Zokhar'gash, D. F. Rahipoz, S. P. Raspopin and D. A. Kukiev, *Izv. Vyssh. Uchebn. Zaved., Tsvetn. Metall.*, **3**, 119 (1978).

(30) T. Ogawa et al., "Dense fuel cycles for actinide burning and thermodynamic database", *Proc. of Int. Conf. Evaluation of Emerging Nuclear Fuel Cycle Systems-Global 1995, Sept. 11-14, 1995, Versailles, France.*

(31) T. Ogawa et al., "Nuclear fuel cycles on pyrochemistry", *Proc. of Int. Conf. Future Nuclear Systems-Global'97, Oct. 5-10, 1997, Yokohama, Japan*, **2**, 812 (1997).

(32) F. Kobayashi et al., *J. Am. Ceram. Soc.*, **78**, 2279 (1995).

(33) Y. I. Chang, "The Integral Fast Reactor", *J. Nucl. Technol.*, **88**, 129 (1989).

(34) J. J. Leidler et al., *Proceedings of GLOBAL'93*, 1061 (1993).

(35) J. E. Battles et al., *Proceedings of RECOD'91*, Ⅵ, 342 (1991).

(36) M. Tokiwai et al., *Proceedings of FR91*, Ⅷ**12**, 7-1 (1991).

(37) T. Inoue et al., *Nuclear Technology*, **69**, 206 (1991).

(38) T. Koyama et al., *J. Nucl. Sci. Technol.*, **34(4)**, 384 (1997).

(39) Sakata, M. et al., *Proc. Int. Conf. On Fast Reactors and Related Fuel Cycles*, Vol. Ⅱ, 19-7 (1991).

(40) Inoue, T. et al., *IAEA-TECDOC-783*, p.137 (1995).

(41) Y. Akai, and R. Fujita, *J. Nucl. Sci. Technol.*, **32**, 1064 (1995).

(42) Y. Akai, and R. Fujita, *J. Nucl. Sci. Technol.*, **33**, 807 (1996).

(43) Y. Akai and R. Fujita, *Proc. of Int. Conf. Future Nuclear Systems, Global'97, Yokohama, Japan, Oct. 5-10*, **2**, 1418 (1997).

(44) R. Fujita, and Y. Akai, *J. Alloys and Compounds.*, **271-273**, 563 (1998).

(45) Y. I. Chang et al., *ANL-IFR-125* (1990).

(46) A, Shimizu and Y. Fujii-e, *Prog. Nucl. Energy*, **29**, (*Suppl.*) 25 (1995).

(47) R. Takagi et al., *Prog. Nucl. Energy*, **29**, (*Suppl.*) 471 (1995).

(48) M. Iwasaki and R. Takagi, *J. Nucl. Sci. Technol.*, **31**, 751 (1994).

(49) H. Matsuura, R. Takagi, I. Okada, R. Fujita, *J. Nucl. Sci. Technol.*, **35**, 304 (1997).

(50) W. J. Hamer, M. S. Malmberg, B. Rubin, *J. Electrochem. Soc.*, **112**, 750 (1965).

Chapter II

Principle

Chapter II Principle

§ II- i - i Principle of countercurrent electromigration

For explaining the principle, a schematic diagram for the electromigration is shown in **Fig. 2-1-1**. When the electrical field is applied between anode and cathode, cations migrate toward the cathode. The migration mobilities of each cation, u_1 and u_2 depend on cationic radii, valences, polarizabilities, molar volumes, and so on. During migration, there occurs a back flow for cations, which is caused by osmotic force keeping the liquid level constant. This flow is called a *countercurrent flow*, u_c, which is equal to all kinds of species. Due to this countercurrent flow, a cation with lower mobility is enriched toward the anode.

§ II- i - ii Derivation of mass balance equation

Let us assume a mixture consisting of cations 1, 2 and a common anion 3. In a separation tube the flow J_i per cross sectional area in the direction from the anode to cathode is expressed by,

$$J_1 = (v_1 - v_c)c_1 - D_1 \nabla c_1 \tag{2.1.1}$$

$$J_2 = (v_2 - v_c)c_2 - D_2 \nabla c_2 \tag{2.1.2}$$

$$J_3 = (-v_3 - v_c)c_3 - D_3 \nabla c_3 \tag{2.1.3}$$

where J_i is the net flow of each component i, v_i: the scalar component of the external velocity, v_c: the velocity of countercurrent flow with reference to the wall, D_i: the effective diffusion coefficient, c_i: equivalent concentration.

In the right-hand of Eq. (2.1.1), $v_1 c_1$, $v_c c_1$ and $D_1 \nabla c_1$ represent the migration, the countercurrent and the diffusion flow, respectively. The convection flow can be neglected in the migration tube.

In a plane B where the concentration does not change during electromigration, the diffusion flow is neglected.

$$J_1 = (v_1 - v_c)c_1 \tag{2.1.4}$$

$$J_2 = (v_2 - v_c)c_2 \tag{2.1.5}$$

$$J_3 = (-v_3 - v_c)c_3 \tag{2.1.6}$$

From the electrical neutrality

$$c_1 + c_2 - c_3 = 0 \tag{2.1.7}$$

The electrical current density I_d at the plane B is

$$I_d = I/S = F\left(J_1 + J_2 - J_3\right) \tag{2.1.8}$$

where S is the cross sectional area at the plane B, F Faraday constant and the constant current I is assumed for simplicity.

ε is defined as

$$\varepsilon = \frac{\left(v_1 - v_2\right)\left(c_1 + c_2\right)}{\left\{\left(v_1 + v_3\right)c_1 + \left(v_2 + v_3\right)c_2\right\}} \tag{2.1.9}$$

From Eqs. (2.1.4), (2.1.5), (2.1.6), (2.1.7) and (2.1.8)

$$I_d/F = J_1 + J_2 - J_3 = v_1c_1 + v_2c_2 + v_3c_3 = \left(v_1 + v_3\right)c_1 + \left(v_2 + v_3\right)c_2 \tag{2.1.10}$$

From Eqs. (2.1.9) and (2.1.10)

$$v_1 + v_3 = \left(\frac{I_d}{c_3F}\right)\left\{1 + \left(\frac{c_2}{c_3}\right)\varepsilon\right\} \tag{2.1.11}$$

$$v_2 + v_3 = \left(\frac{I_d}{c_3F}\right)\left\{1 - \left(\frac{c_1}{c_3}\right)\varepsilon\right\} \tag{2.1.12}$$

Dividing both sides of Eqs. (2.1.11) and (2.1.12) by voltage per unit length E at the plane B gives u_1 and u_2, internal mobilities of 1 and 2, respectively;

$$u_1 = \left(\frac{I_d}{c_3EF}\right)\left\{1 + x_2\varepsilon\right\} \tag{2.1.13}$$

$$u_2 = \left(\frac{I_d}{c_3EF}\right)\left\{1 - x_1\varepsilon\right\} \tag{2.1.14}$$

where x_1 and x_2 are equivalent fractions of 1 and 2, respectively, at the plane B, that is before electromigration; $x_1+x_2=1$.

Since electrical conductivity of the mixture at the plane B, $\kappa = I_d/E$ and equivalent volume of the mixture at the plane B, $V_m = 1/c_3$

$$u_1 = \left(\frac{\kappa V_m}{F}\right)\left\{1 + x_2\varepsilon\right\} \tag{2.1.15}$$

$$u_2 = \left(\frac{\kappa V_m}{F}\right)\left\{1 - x_1\varepsilon\right\} \tag{2.1.16}$$

In countercurrent electromigration of molten salts, there is generally no volume flow

along the separation tube, in other words, such a condition can be fulfilled and therefore across the plane B

$$J_1V_{13} + J_2V_{23} = 0 \tag{2.1.17}$$

where V_{13} and V_{23} are equivalent volumes of pure melts 13 and 23, respectively. The additivity of the molar volume is assumed, which is found to be generally the case.

$$v_c(t) = \left(v_1c_1V_{13} + v_2c_2V_{23}\right)/\left(c_1V_{13} + c_2V_{23}\right) \tag{2.1.18}$$

$v_c(t)$ could be a function of t, but actually independent of t, as far as $v_1(t)$ and $v_2(t)$ are independent of t.

If the volume between A and B is V, the equivalent quantity of 13 there, $N_1(t)$ is

$$N_1(t) = c_1V - \int_0^t J_1(t)Sdt = c_1V - \left(v_1 - v_2\right)c_1c_2V_{23}St/\left(c_1V_{13} + c_2V_{23}\right) \tag{2.1.19}$$

Similarly, the equivalent quantity of 23, $N_2(t)$ is

$$N_2(t) = c_2V - \int_0^t J_2(t)Sdt = c_2V - \left(v_2 - v_1\right)c_1c_2V_{13}St/\left(c_1V_{13} + c_2V_{23}\right) \tag{2.1.20}$$

From Eqs. (2.1.19) and (2.1.20),

$$v_1 - v_2 = -\left(\frac{1}{St}\right)\left\{\frac{N_1(t)}{c_1} - \frac{N_2(t)}{c_2}\right\} \tag{2.1.21}$$

It follows from Eqs. (2.1.10) and (2.1.21) that

$$\frac{\left(v_1 - v_2\right)}{\left\{\left(v_1 + v_3\right)x_1 + \left(v_2 + v_3\right)x_2\right\}} = -\left(\frac{F}{It}\right)\left\{\frac{N_1(t)}{x_1} - \frac{N_2(t)}{x_2}\right\} \tag{2.1.22}$$

Therefore,

$$\varepsilon = \frac{\left(u_1 - u_2\right)}{\left(x_1u_1 + x_2u_2\right)} = -\left(\frac{F}{Q}\right)\left\{\frac{N_1(t)}{x_1} - \frac{N_2(t)}{x_2}\right\} \tag{2.1.23}$$

Equation (2.1.23) was derived by Klemm[1] and Ljubimov and Lunden[2].

Even if $J_1V_{13} + J_2V_{23} = \alpha \neq 0$ in Eq. (2.1.17), Eq. (2.1.23) is same, because the term corresponding to α vanishes when the equation corresponding to Eq. (2.1.19) is subtracted by that of Eq. (2.1.20).

The standard deviation of ε is represented as follows,

$$\sigma_\varepsilon = \sqrt{\left(\frac{\partial \varepsilon}{\partial x_1}\right)^2 \sigma_{x_1}^2 + \left(\frac{\partial \varepsilon}{\partial x_2}\right)^2 \sigma_{x_2}^2 + \sum_{i=1}\left(\frac{\partial \varepsilon}{\partial N_{1i}}\right)^2 \sigma_{N_{1i}}^2 + \sum_{i=1}\left(\frac{\partial \varepsilon}{\partial N_{2i}}\right)^2 \sigma_{N_{2i}}^2}$$

$$= \sqrt{\left(\frac{F}{Q}\right)^2 \left(\frac{\sum_{i=1} N_{1i}}{x_1^2}\right)^2 \sigma_{x_1}^2 + \left(\frac{F}{Q}\right)^2 \left(\frac{\sum_{i=1} N_{2i}}{x_2^2}\right)^2 \sigma_{x_2}^2 + \sum_{i=1}\left(\frac{F}{Q}\right)^2 \left(\frac{1}{x_1}\right)^2 \sigma_{N_{1i}}^2 + \sum_{i=1}\left(\frac{F}{Q}\right)^2 \left(\frac{1}{x_2}\right)^2 \sigma_{N_{2i}}^2}$$

$$= \left(\frac{F}{Q}\right) \sqrt{\left(\frac{\sum_{i=1} N_{1i}}{x_1^2}\right) \sigma_{x_1}^2 + \left(\frac{F}{Q}\right)^2 \left(\frac{\sum_{i=1} N_{2i}}{x_2^2}\right)^2 \sigma_{x_2}^2 + \left(\frac{1}{x_1}\right)^2 \sum_{i=1} \sigma_{N_{1i}}^2 + \left(\frac{1}{x_2}\right)^2 \sum_{i=1} \sigma_{N_{2i}}^2}$$

Therefore, standard deviations of internal mobilities σ_{u_1} and σ_{u_2}, respectively.

$$\sigma_{u_1} = \sqrt{\left(\frac{\partial u_1}{\partial x_2}\right)^2 \sigma_{x_2}^2 + \left(\frac{\partial u_1}{\partial \varepsilon}\right)^2 \sigma_\varepsilon^2}$$

$$= \sqrt{\left(\frac{\kappa V_m}{F}\right)^2 \varepsilon^2 \sigma_{x_2}^2 + \left(\frac{\kappa V_m}{F}\right)^2 x_2^2 \sigma_\varepsilon^2}$$

$$= \left(\frac{\kappa V_m}{F}\right) \sqrt{\varepsilon^2 \sigma_{x_2}^2 + x_2^2 \sigma_\varepsilon^2}$$

$$\sigma_{u_2} = \sqrt{\left(\frac{\partial u_2}{\partial x_1}\right)^2 \sigma_{x_1}^2 + \left(\frac{\partial u_2}{\partial \varepsilon}\right)^2 \sigma_\varepsilon^2}$$

$$= \sqrt{\left(\frac{\kappa V_m}{F}\right)^2 \varepsilon^2 \sigma_{x_1}^2 + \left(\frac{\kappa V_m}{F}\right)^2 x_1^2 \sigma_\varepsilon^2}$$

$$= \left(\frac{\kappa V_m}{F}\right) \sqrt{\varepsilon^2 \sigma_{x_1}^2 + x_1^2 \sigma_\varepsilon^2}$$

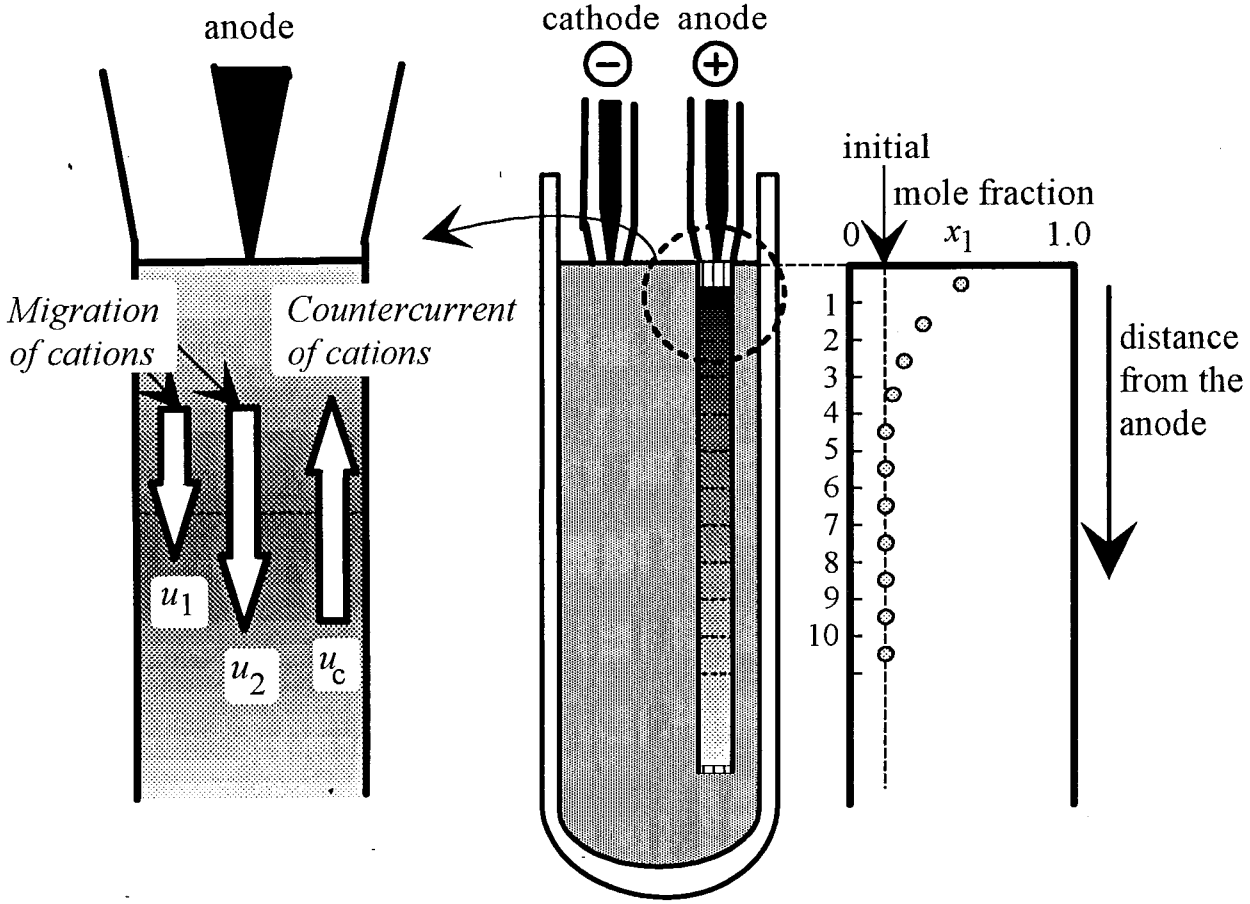

Fig. 2-1-1 Schematic diagram for countercurrent electromigration

§ II- ii Derivation of General Mass Transfer Equation

In this section we discuss the general partial differential equations that govern mass transfer; these will be used frequently in subsequent chapters for the deviation of equations appropriate to the different electrochemical techniques. Mass transfer in solution occurs because of a gradient in electrochemical potential $\overline{\mu}$ (i.e., by diffusion and migration) and by convection. Consider a section of solution where, for a certain species j at two points in the solution, r and s (an infinitesimal distance from one another). This difference of $\overline{\mu_j}$ over a distance (or gradient of electrochemical potential) can arise because of differences of concentration (or activity) of species j at r and s (a concentration gradient) or because of differences of ϕ at r and s (an electric field or potential gradient). In general, a flux of species j will occur to alleviate this difference of $\overline{\mu_j}$. The flux, $\mathbf{J}_j$ (mol sec^{-1} cm^{-2}), is proportional to the gradient , **grad** or ∇, of $\overline{\mu_j}$:

$$\mathbf{J}_j \propto \mathbf{grad}\,\overline{\mu_j} \qquad \text{or} \qquad \nabla\overline{\mu_j} \tag{2.2.1}$$

where grad or ∇ is a vector operator. For linear (one-dimensional) mass transfer $\nabla = \mathbf{i}(\partial/\partial x)$ (where $\mathbf{i}$ is the unit vector along the axis and x is distance), and for rectangular mass transfer

$$\nabla = \mathbf{i}\frac{\partial}{\partial x} + \mathbf{j}\frac{\partial}{\partial y} + \mathbf{k}\frac{\partial}{\partial z} \tag{2.2.2}$$

When the constant of proportionality is added to (2.2.1), we obtain

$$\mathbf{J}_j = -\left(\frac{C_j D_j}{RT}\right)\nabla\overline{\mu}_j \tag{2.2.3}$$

or for linear mass transfer,

$$J_j(x) = -\left(\frac{C_j D_j}{RT}\right)\frac{\partial\overline{\mu}_j}{\partial x} \tag{2.2.4}$$

The minus sign in (2.2.3) arises because the direction of the flux opposes the direction of increasing $\overline{\mu}_j$. If, in addition to this $\overline{\mu}$ gradient, the solution is moving so that an element of solution [with j at a concentration $C_j(s)$] moves from s with a velocity, $\mathbf{v}$, an additional term is added to the flux equation, yielding

$$\mathbf{J}_j = -\left(\frac{C_j D_j}{RT}\right)\nabla\bar{\mu}_j + C_j\mathbf{v} \tag{2.2.5}$$

or for linear mass transfer

$$J_j(x) = -\left(\frac{C_j D_j}{RT}\right)\left(\frac{\partial\bar{\mu}_j}{\partial x}\right) + C_j v(x) \tag{2.2.6}$$

For $a_j \cong C_j$, we obtain the *Nernst-Planck* equations, which can be written as

$$J_j(x) = -\left(\frac{C_j D_j}{RT}\right)\left[\frac{\partial}{\partial x}\left(RT\ln C_j + \frac{\partial}{\partial x}\left(z_j F\phi\right)\right)\right] + C_j v(x) \tag{2.2.7}$$

$$J_j(x) = -D_j\frac{\partial C_j(x)}{\partial x} - \frac{z_j F}{RT}D_j C_j\frac{\partial\phi(x)}{\partial x} + C_j v(x) \tag{2.2.8}$$

or in general

$$\mathbf{J}_j = -D_j\nabla C_j - \frac{z_j F}{RT}D_j C_j\nabla\phi + C_j\mathbf{v} \tag{2.2.9}$$

In this chapter we are considered with systems in which convection is absent. Under these conditions, that is, in an unstirred or stagnant solution with no density gradients, the solution velocity **v** is zero, and the general flux equation for species *j*, (2.2.9), becomes

$$\mathbf{J}_j = -D_j\nabla C_j - \frac{z_j F}{RT}D_j C_j\nabla\phi \tag{2.2.10}$$

For linear mass transfer (2.2.10) is given by

$$J_j(x) = -D_j\left(\frac{\partial C_j(x)}{\partial x}\right) - \frac{z_j F}{RT}D_j C_j\left(\frac{\partial\phi(x)}{\partial x}\right) \tag{2.2.11}$$

where the terms on the right-hand side of (2.2.11) represent the contributions of diffusion and migration, respectively, to the total mass transfer. If species *j* is charged, then the flux J_j is equivalent to a current density. Let us consider a linear mass-flow system with a cross-sectional area *A* normal to the axis of mass flow. Then J_j (mol sec^{-1} cm^{-2}) is equal to $-i_j/z_j FA$, where i_j is current component at any value of *x* arising from a flow of species *j*. Equation (2.2.11) can then be written:

$$-J_j = \frac{i_j}{z_j FA} = \frac{i_{d,j}}{z_j FA} + \frac{i_{m,j}}{z_j FA} \tag{2.2.12}$$

with

$$\frac{i_{d,j}}{z_j FA} = D_j \frac{\partial C_j}{\partial x} \tag{2.2.13}$$

$$\frac{i_{m,j}}{z_j FA} = \frac{z_j F D_j}{RT} C_j \frac{\partial \phi}{\partial x} \tag{2.2.14}$$

where $i_{d,j}$ and $i_{m,j}$ are *diffusion* and *migration currents* of species j, respectively. The factor $|z_j| FD_j / RT$ is the mobility u_j, so that

$$\frac{i_{m,j}}{|z_j| FA} = u_j C_j \frac{\partial \phi}{\partial x} \tag{2.2.15}$$

At any location in solution during electrolysis, the total current i is made up of contributions from all species; that is,

$$i = \sum_j i_j \tag{2.2.16}$$

and the current for each species is made up of a diffusional component arising from a concentration gradient and a migrational component arising from a potential gradient.

§ II-iii Controlled Potential Techniques-Potential Sweep Methods

§ II-iii-i Solution of the Boundary Value Problem for Nernstian (Reversible) Systems

We consider the reaction O + ne^- ⇔ R, assuming semi-infinite linear diffusion and a solution initially containing only species O, with the electrode held initially at a potential E_i, where no electrode reaction occurs. The potential is swept linearly at v V/sec so that the potential at any time is

$$E(t)=E_i-vt \tag{2.3.1}$$

With the assumption that the rate of electron transfer is so rapid at the electrode surface that species O and R immediately adjust to the ratio dictated by the Nernst equation, which can be written more clearly as

$$\frac{C_O(0,t)}{C_R(0,t)} = f(t) = \exp\left[\frac{nF}{RT}(E_i - vt - E^{0'})\right] \tag{2.3.2}$$

to show that this ratio is now a function of time. The difference is significant, since the Laplace transformation of (2.3.2) cannot be obtained. This inability to use the Laplace transform procedure greatly complicates the mathematics in this case. The problem was first considered by Randles[3] and Sevcik[4]; the treatment and notation here follow the latter work of Nicholson and Shain[5]. The boundary condition (2.3.2) can be written

$$\frac{C_O(0,t)}{C_R(0,t)} = \theta e^{-\sigma t} = \theta S(t) \tag{2.3.3}$$

where $S(t) = e^{-\sigma t}$, $\theta = \exp\left[\left(\frac{nF}{RT}\right)(E_i - E^{0'})\right]$, and $\sigma = \left(\frac{nF}{RT}\right)v$. Application of the Laplace transform to the diffusion equations and the boundary conditions leads to

$$\bar{C}_O(x,s) = \frac{C_O^*}{s} + A(s)\exp\left[-\left(\frac{s}{D_O}\right)^{1/2} x\right] \tag{2.3.4}$$

We note that the transform of the current is given by

$$\bar{i}(s) = nFAD_O\left[\frac{\partial \bar{C}_O(x,s)}{\partial x}\right]_{x=0} \tag{2.3.5}$$

Combining this with (2.3.4) and investigating, by making use of the convolution theorem, we obtain

$$C_O(0,t) = C_O^* - \left[nFA(\pi D_O)^{1/2}\right]^{-1} \int_0^t i(\tau)(t-\tau)^{-1/2} d\tau \tag{2.3.6}$$

By letting

$$f(\tau) = \frac{i(\tau)}{nFA} \tag{2.3.7}$$

(2.3.6) can be written

$$C_O(0,t) = C_O^* - (\pi D_O)^{-1/2} \int_0^t f(\tau)(t-\tau)^{-1/2} d\tau \tag{2.3.8}$$

An expression for $C_R(0, t)$ can be obtained (assuming R is initially absent):

$$C_R(0,t) = (\pi D_R)^{-1/2} \int_0^t f(\tau)(t-\tau)^{-1/2} d\tau \tag{2.3.9}$$

The derivation of (2.3.8) and (2.3.9) employed only the linear diffusion equations, initial conditions, semi-infinite conditions, and the flux balance. No assumption related to electrode kinetics or technique has been made, so that (2.3.8) and (2.3.9) are completely general. From these equations and the boundary condition for LSV, (2.3.3), we obtain

$$\int_0^t f(\tau)(t-\tau)^{-1/2} d\tau = \frac{C_O^*}{\left[\theta S(t)(\pi D_R)^{-1/2} + (\pi D_O)^{-1/2}\right]} \tag{2.3.10}$$

$$\int_0^t i(\tau)(t-\tau)^{-1/2} d\tau = \frac{nFA\pi^{1/2} D_O^{1/2} C_O^*}{\left[\theta S(t)\xi + 1\right]} \tag{2.3.11}$$

where, as before, $\xi = \left(\frac{D_O}{D_R}\right)^{1/2}$. The solution of this integral equation would be of the form $i(t)$=(constant)$g(t)$ [where $g(t)$ is some function of time], and would thus yield the desired current-time curve or, since potential is linearly related to time, the current-potential equation. A closed-form solution of (2.3.11) cannot be obtained, and a numerical method must be employed. Before solving (2.3.11) numerically, it is convenient (a) to change from $i(t)$ to $i(E)$, since that is the way in which the data are usually considered, and (b) to put the equation in a dimensionless form so that a single

numerical solution will give results that will be useful under any experimental conditions. This is accompanied by using the following substitution:

$$\sigma t = \frac{nF}{RT} vt = \left(\frac{nF}{RT}\right)(E_i - E) \tag{2.3.12}$$

Let $f(\tau) = g(\sigma\tau)$. With $z = \sigma t$, so that $\tau = z/\sigma$, $d\tau = dz/\sigma$, z=0 at τ=0, and $z = \sigma t$ at $\tau = t$, we obtain

$$\int_0^t f(\tau)(t-\tau)^{-1/2} d\tau = \int_0^{\sigma t} g(z)\left(t - \frac{z}{\sigma}\right)^{-1/2} \frac{dz}{\sigma} \tag{2.3.13}$$

so that (2.3.11) can be written

$$\int_0^{\sigma t} g(z)(\sigma t - z)^{-1/2} \sigma^{-1/2} dz = \frac{C_O^*(\pi D_O)^{1/2}}{1 + \xi\theta S(\sigma t)} \tag{2.3.14}$$

or finally, dividing by $C_o^*(\pi D_o)^{1/2}$, we obtain

$$\int_0^{\sigma t} \frac{\chi(z)dz}{(\sigma t - z)^{1/2}} = \frac{1}{1 + \xi\theta S(\sigma t)} \tag{2.3.15}$$

where

$$\chi(z) = \frac{g(z)}{C_O^*(\pi D_O \sigma)^{1/2}} = \frac{i(\sigma t)}{nFAC_O^*(\pi D_O \sigma)^{1/2}} \tag{2.3.16}$$

Note that (2.3.15) is the desired equation in terms of the dimensionless variables $\chi(z)$, ξ, θ, $S(\sigma t)$ and σt. The current can be obtained from (2.3.16)

$$i = nFAC_O^*(\pi D_O \sigma)^{1/2} \chi(\sigma t) \tag{2.3.17}$$

Thus at any value of $S(\sigma t)$, which is a function of E, $\chi(\sigma t)$ can be obtained by solution of (2.3.15) and, from it, by (2.3.17), the current is available. Note that $\chi(\sigma t)$ at any given point is a pure number, so that (2.3.17) gives the functional relationship between the current at any point on the LSV curve and the variables. Specially, i is proportional to C_o^* and $v^{1/2}$. The solution of (2.3.15) has been carried out numerically by computer [Nicholson and Shain[5]], by a series solution [Sevcik[4], Reinmuth[6]] and analytically, in terms of an integral that must be evaluated numerically [Matsuda and Ayabe[7], Gokhshtein[8]]. The general result of solving (2.3.15) is a table of values of $\chi(\sigma t)$ as a function of σt or $n(E - E_{1/2})$ (see **Table 2-3-1** and **Figure 2-**

3-1).

§ II-iii-ii Peak Current and Potential

The function $\pi^{1/2}\chi(\sigma t)$, and hence the current, reaches a maximum at 0.4463. From (2.3.17) the *peak current* i_p is

$$i_p = 0.4463nFAC_O^*\left(\frac{nF}{RT}\right)^{1/2} v^{1/2}D_O^{1/2} \tag{2.3.18}$$

or, for A in cm^2, D_O in cm^2/sec, C_o^* in mol/cm^3, and v in V/sec, i_p in amperes is

$$i_p = (2.69\times10^5)n^{3/2}AD_O^{1/2}v^{1/2}C_O^* \tag{2.3.19}$$

$$E_p - E_{1/2} = E_p - E^{0'} + \left(\frac{RT}{nF}\right)\ln\xi = -1.109\left(\frac{RT}{nF}\right) \tag{2.3.20}$$

Because the peak is somewhat broad, so that the peak potential may be difficult to determine, it is sometimes more convenient to report the potential at $1/2i_p$, called the *half-peak potential*, $E_{p/2}$, which is

$$E_{p/2} = E_{1/2} + 1.09\frac{RT}{nF} \tag{2.3.21}$$

Note that the polarographic $E_{1/2}$ value is located just about midway between E_p and $E_{p/2}$, and that a convenient diagnostic for a nernstian wave is

$$\left|E_p - E_{p/2}\right| = 2.2\frac{RT}{nF} \tag{2.3.22}$$

Thus for a reversible wave, E_p is independent of scan rate, and i_p (as well as the current at any point on the wave) is proportional to $v^{1/2}$. [The latter property indicates diffusion control and is analogous to the variation of i_d with $h^{1/2}$ in polarography. A convenient constant in LSV is (sometimes called *the current function*), which depends on $n^{3/2}$ and $D_o^{1/2}$. This constant can be used to estimate n for an electrode reaction, if a value of D_O can be estimated, for example, from the LSV of a compound of similar size or structure, which undergoes an electrode reaction with known n value.

§ II-iii-iii The boundary value problem for totally irreversible systems

For a totally irreversible reaction (O + ne^- → R) the nernstian boundary condition,

(2.3.2), is replaced by

$$\frac{i}{nFA} = D_O\left[\frac{\partial C_O(x,t)}{\partial x}\right]_{x=0} = k_f(t)C_O(0,t) \qquad (2.3.23)$$

where

$$k_f(t) = k^0 \exp\left\{-\alpha n_a f\left[E(t) - E^{0'}\right]\right\} \qquad (2.3.24)$$

Introducing $E(t)$ from (2.3.1) into (2.3.24) yields

$$k_f(t)C_O(0,t) = k_{fi}C_O(0,t)e^{bt} \qquad (2.3.25)$$

where

$$k_{fi} = k^0 \exp\left[-\alpha n_a f(E_i - E^{0'})\right] \qquad (2.3.26)$$

$$b = \alpha n_a f v \qquad f = \frac{F}{RT} \qquad (2.3.27)$$

The solution follows in an analogous manner to that described in Section II - iii - i [5],[7] and again requires a numerical solution of an integral equation. The current is given by

$$i = nFAC_O^*(\pi D_O b)^{1/2}\chi(bt) \qquad (2.3.28)$$

$$i = nFAC_O^* D_O^{1/2} v^{1/2}\left(\frac{\alpha n_a F}{RT}\right)^{1/2}\pi^{1/2}\chi(bt) \qquad (2.3.29)$$

where $\chi(bt)$ is a tabulated function [different from $\chi(\sigma t)$, **Table 2-3-2**] Again i at any point on the wave varies with $v^{1/2}$ and C_o^*.

§ II - iii - iv **Peak current and potential**

The function $\chi(bt)$ goes through a maximum at $\pi^{1/2}\chi(bt) = 0.4958$. Introduction of this value into (2.3.29) yields the following for the peak current (in amperes):

$$i_p = (2.99\times10^5)n(\alpha n_a)^{1/2} AC_O^* D_O^{1/2} v^{1/2} \qquad (2.3.30)$$

where the units are the same as for (2.3.19). This value occurs when

$$\alpha n_a(E_p - E^{0'}) + \left(\frac{RT}{F}\right)\ln\left[\frac{(\pi D_O b)^{1/2}}{k^0}\right] = -5.34\text{mV} \qquad (2.3.31)$$

or (in millivolts)

$$E_p = E^{0'} - \frac{RT}{\alpha n_a F}\left[0.780 + \ln\left(\frac{D_O^{1/2}}{k^0}\right) + \ln\left(\frac{\alpha n_a F v}{RT}\right)^{1/2}\right] \qquad (2.3.32)$$

$$\left|E_p - E_{p/2}\right| = \frac{1.857RT}{\alpha n_a F} \qquad (2.3.33)$$

Thus, for a totally irreversible wave, i_p is also proportional to C_o^* and $v^{1/2}$, but E_p is a function of scan rate, shifting (for a reduction) in a negative direction by an amount $1.15RT/\alpha n_a F$ for each tenfold increase in v. Note that in this case E_p occurs beyond $E^{0'}$ by an activation overpotential related to k^0. An alternate expression for i_p in terms of E_p can be obtained by combining (2.3.32) with (2.3.29), so that the result contains the value of $\chi(bt)$ at the peak. After rearrangement and evaluation of the constants, the following equation is obtained[5],[8]:

$$i_p = 0.227nFAC_O^* k^0 \exp\left[-\left(\frac{\alpha n_a F}{RT}\right)\left(E_p - E^{0'}\right)\right] \qquad (2.3.34)$$

A plot of $\ln(i_p)$ *vs.* E_p-$E^{0'}$ (assuming $E^{0'}$ could be obtained) determined at different scan rates should have a slope of $-\alpha n_a f$ and an intercept proportional to k^0.

For spherical electrodes, a procedure analogous to that employed at planar electrodes has been proposed. The spherical correction factor, $\phi(bt)$, when can be employed in the equation

$$i = i(\text{plane}) + \frac{nFAD_O C_O^* \phi(bt)}{r_0} \qquad (2.3.35)$$

is tabulated in Table 2-3-2.

§ II - iii - v Quasi-reversible systems

The treatment of these systems was first described by Matsuda and Ayabe[7], who coined the term *quasi-reversible* for reactions that show electron transfer kinetic limitations where the reverse reaction has to be considered. The boundary condition for this case is

$$D_O\left(\frac{\partial C_O(x,t)}{\partial x}\right)_{x=0} = k^0 \exp(-\alpha nf\left[E(t) - E^{0'}\right])\left\{C_O(0,t) - C_R(0,t)\exp(nf\left[E(t) - E^{0'}\right])\right\} \qquad (2.3.36)$$

The shape of the peak and the various peak parameters were shown to be functions of α and the parameter Λ, defined as

$$\Lambda = \frac{k^0}{\left[D_O^{1-\alpha} D_R^{\alpha} \left(\frac{nF}{RT}\right) v\right]^{1/2}} \tag{2.3.37}$$

or, for $D_O = D_R = D$,

$$\Lambda = \frac{k^0}{D^{1/2} \left(\frac{nF}{RT}\right)^{1/2} v^{1/2}} \tag{2.3.38}$$

The current is given by

$$i = nFAC_O^* D_O^{1/2} \left(\frac{nF}{RT}\right)^{1/2} \Psi(E) v^{1/2} \tag{2.3.39}$$

Note that when $\Lambda \geq 10$, the behavior approaches that of a reversible system. The i_p, E_p and $E_{1/2}$ values depend on Λ and α. The appropriate expression for the peak current is

$$i_p = i_p(\text{rev}) K(\Lambda, \alpha) \tag{2.3.40}$$

where i_p(rev) is the value for the reversible i_p value (equation 2.3.18). Note that for a quasi-reversible reaction, i_p is not proportional to $v^{1/2}$. The peak potential is

$$E_p - E_{1/2} = -\Xi(\Lambda, \alpha) \left(\frac{RT}{nF}\right) \tag{2.3.41}$$

For the half-peak potential, we have

$$E_{p/2} - E_p = \Delta(\Lambda, \alpha) \left(\frac{RT}{nF}\right) \tag{2.3.42}$$

These parameters attain limiting values characteristic of reversible or totally irreversible processes as Λ varies. For example, consider Δ (Λ , α). For $\Lambda \geq 10$, $\Delta(n, \alpha) \approx 2.2$, yielding the $E_p - E_{p/2}$ value characteristic of a reversible wave (2.3.22). For $\Lambda \leq 10^{-2}$ and $\alpha = 0.5$, $\Delta(\Lambda, \alpha) \approx 3.7$, yielding the totally irreversible characteristic (2.3.33). Thus a system may show nernstian, quasi-reversible, or totally irreversible behavior, depending on Λ, or experimentally, on the scan rate employed. The appearance of kinetic effects depends on the time window of the experiment, which is

essentially the time needed to traverse the LSV wave. At small v (or long times), systems may yield reversible waves, while at large v (or short times), irreversible behavior is observed. Matsuda and Ayabe suggest the following zone boundaries:

Reversible (nernstian) $\Lambda \geq 15; k^0 \geq 0.3v^{1/2}\text{cm/sec}$

Quasi-reversible $15 \geq \Lambda \geq 10^{-2(1+\alpha)}; 0.3v^{1/2} \geq k^0 \geq 2\times10^{-5}v^{1/2}\text{cm/sec}$

Totally irreversible $\Lambda \leq 10^{-2(1+\alpha)}; k^0 \leq 2\times10^{-5}v^{1/2}\text{cm/sec}$

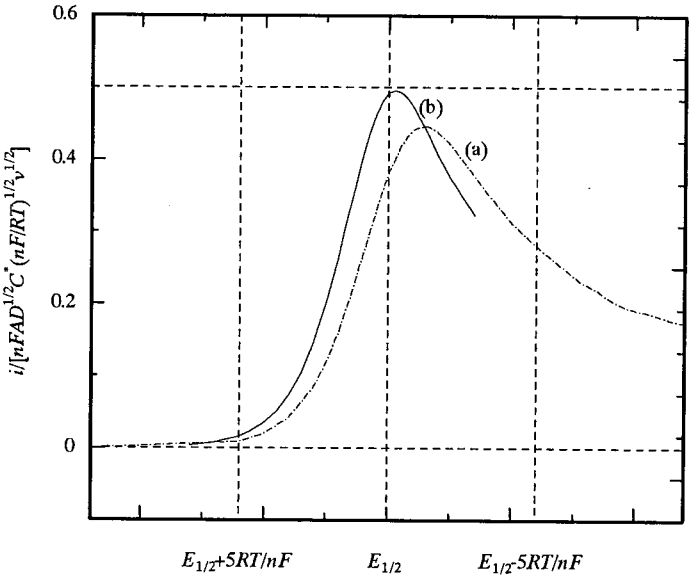

Fig. 2-3-1 Linear potential sweep voltammogram in terms of dimensionless current function. (a) reversible (b) irreversible

Table 2-3-1 Current functions $\sqrt{\pi}\chi(\sigma t)$ for reversible charge transfer

$(E-E_{1/2})n$/mV*	$\sqrt{\pi}\chi(\sigma t)$	$\phi(\sigma t)$	$(E-E_{1/2})n$/mV*	$\sqrt{\pi}\chi(\sigma t)$	$\phi(\sigma t)$
120	0.009	0.008	-5	0.400	0.548
100	0.020	0.019	-10	0.418	0.596
80	0.042	0.041	-15	0.432	0.641
60	0.084	0.087	-20	0.441	0.685
50	0.117	0.124	-25	0.445	0.725
45	0.138	0.146	-28.50	0.4463	0.7516
40	0.160	0.173	-30	0.446	0.763
35	0.185	0.208	-35	0.443	0.796
30	0.211	0.236	-40	0.438	0.826
25	0.240	0.273	-50	0.421	0.875
20	0.269	0.314	-60	0.399	0.912
15	0.298	0.357	-80	0.353	0.957
10	0.328	0.403	-100	0.312	0.980
5	0.355	0.451	-120	0.280	0.991
0	0.380	0.499	-150	0.245	0.997

* $E_{1/2} = E^{0'} + (RT/nF)\ln(D_R/D_O)^{1/2}$

Table 2-3-2 Current functions $\sqrt{\pi}\chi(\sigma t)$ for irreversible charge transfer

Potential/mV	$\sqrt{\pi}\chi(\sigma t)$	$\phi(\sigma t)$	Potential/mV	$\sqrt{\pi}\chi(\sigma t)$	$\phi(\sigma t)$
160	0.003	------	15	0.437	0.323
140	0.008	------	10	0.462	0.396
120	0.016	------	5	0.480	0.482
110	0.024	------	0	0.492	0.600
100	0.035	------	-5	0.496	0.685
90	0.050	------	-5.34	0.4958	0.694
80	0.073	0.004	-10	0.493	0.755
70	0.104	0.010	-15	0.485	0.823
60	0.145	0.021	-20	0.472	0.895
50	0.199	0.042	-25	0.457	0.952
40	0.264	0.083	-30	0.441	0.992
35	0.300	0.115	-35	0.423	1.00
30	0.337	0.154	-40	0.406	------
25	0.372	0.199	-50	0.374	------
20	0.406	0.253	-70	0.323	------

§ II-iv Convolutive or semi-integral techniques

§ II-iv-i Principles and Definitions

By proper treatment of the linear potential sweep data, the voltammetric *i-E* (or *i-t*) curves can be transformed into forms, closely resembling the steady-state voltammetric curves, which are frequently more convenient for further data processing. This transformation makes use of the convolution principle and has been facilitated by the availability of digital computers for the processing and acquisition of data. The solution of the diffusion equation for semi-infinite linear diffusion conditions, and for species O initially present at a concentration C_o^*, yields for any electrochemical technique, the expression (see equations (2.3.4) to (2.3.6))

$$C_O(0,t) = C_O^* - \frac{1}{nFAD_O^{1/2}}\left[\frac{1}{\pi^{1/2}}\int_0^t \frac{i(u)}{(t-u)^{1/2}}du\right] \tag{2.4.1}$$

If the term in brackets, which represents a particular (convolutive) transformation of the experimental $i(t)$ data, is defined as $I(t)$, then equation (2.4.1) becomes[9]

$$C_O(0,t) = C_O^* - \frac{I(t)}{nFAD_O^{1/2}} \tag{2.4.2}$$

where

$$I(t) = \frac{1}{\pi^{1/2}}\int_0^t \frac{i(u)}{(t-u)^{1/2}}du \tag{2.4.3}$$

Following the generalized definition of Riemann-Liouville operators, this integral can be considered as *semi-integral* of $i(t)$, generated by the operator $d^{-1/2}/dt^{-1/2}$, so that[10],[11]

$$\frac{d^{-1/2}}{dt^{-1/2}}i(t) = m(t) = I(t) \tag{2.4.4}$$

Both $m(t)$ and $I(t)$, which represent the integral in equation (2.4.3), have been used in discussing this transformation technique; closely the convolutive[9] and semi-integral [10],[11] approaches are equivalent. Thus the transformed current data can be used directly, by (2.4.2), to obtain $C_o(0,t)$. Under conditions where $C_O(0, t)=0$ (i.e., under purely diffusion-controlled conditions), $I(t)$ reaches its limiting or maximum value, I_l [or, in semi-integral notation, $m(t)_{max}$] where

$$I_l = nFAD_O^{1/2}C_O^* \tag{2.4.5}$$

or

$$C_O(0,t) = \frac{[I_l - I(t)]}{nFAD_O^{1/2}} \tag{2.4.6}$$

Note the similarity between this expression for the transformed current and that for the steady-state concentration in terms of the actual current. Similarly for species R, assumed absent initially, the expression that results is (see equation (2.3.9))

$$C_R(0,t) = \frac{I(t)}{nFAD_R^{1/2}} \tag{2.4.7}$$

Let us stress that these equations hold for any form of signal excitation in any electrochemical technique applied under the above conditions (semi-infinite diffusion, absence of migration, convection etc.), and no assumptions have been made concerning the reversibility of the charge transfer reaction or even the form of the dependence of $C_O(0, t)$ and $C_R(0, t)$ on E. Thus, with the application of any excitation signal that eventually drives $C_O(0, t)$ to zero, the transformed current $I(t)$ will attain a limiting value, I_l, that can be used to determine C_o^* by equation (2.4.5)[11]. If the electron transfer reaction is nernstian, the application of equations (2.4.6) and (2.4.7) immediately yields

$$E = E_{1/2} + \frac{RT}{nF}\ln\frac{I_l - I(t)}{I(t)} \tag{2.4.8}$$

where $E_{1/2} = E^{0'} + \frac{RT}{2nF}\ln\frac{D_R}{D_O}$. Note that this expression is identical in form to those for the steady-state or sampled-current *i-E* curves. Transformation of a linear potential sweep *i-E* response thus converts the peaked *i-E* curve to an S-shaped one resembling a polarogram (**Figure 2-4-1**).

§ II-iv-ii Transformation of the Current-Evaluation of $I(t)$

Although analog circuits that approximate $I(t)$ have been proposed[12], the function is usually evaluated by a numerical integration technique on a computer. Several different algorithms have been proposed for the evaluation[13],[15]. The *i-t* data are usually divided into N equally spaced time intervals between t=0 and $t=t_f$, indexed by j;

then $I(t)$ becomes $I(k\Delta t)$ (where k varies between 0 and N, representing t=0 and t=t_f; Δt=t_f/N) (**Figure 2-4-2**). One convenient algorithm, which follows directly from the definition of $I(t)$, is shown in reference[13]

$$I(t) = I(k\Delta t) = \frac{1}{\pi^{1/2}} \sum_{j=1}^{j=k} \frac{i(j\Delta t - \frac{1}{2}\Delta t)\Delta t}{\sqrt{k\Delta t - j\Delta t + \frac{1}{2}\Delta t}} \tag{2.4.9}$$

which is obtained by using $t=k\Delta t$ and $u=j\Delta t$, and measuring i at the midpoint of each interval. This can be simplified to

$$I(k\Delta t) = \frac{1}{\pi^{1/2}} \sum_{j=1}^{j=k} \frac{i(j\Delta t - \frac{1}{2}\Delta t)\Delta t^{1/2}}{\sqrt{k - j + \frac{1}{2}}} \tag{2.4.10}$$

Another algorithm, which is especially convenient for digital computer processing, is

$$I(k\Delta t) = \frac{1}{\pi^{1/2}} \sum_{j=1}^{j=k} \frac{\Gamma(k - j + \frac{1}{2})}{(k-j)!} \Delta t^{1/2} i(j\Delta t) \tag{2.4.11}$$

where $\Gamma(x)$ is the Gamma function of x, where $\Gamma(1/2)=\pi^{1/2}$, $\Gamma(3/2)=1/2\pi^{1/2}$, $\Gamma(5/2)=3/2 \cdot 1/2\pi^{1/2}$, etc. Other algorithms based on standard methods of numerical evaluation of definite integrals also have been used [9-11),(14),(15)].

§ II-iv-iii Irreversible and Quasi-Reversible Reactions

The convolutive form for a totally irreversible reaction follows directly from the i-E expression, with no back reaction:

$$i = nFAk^0 C_O(0,t)\exp[-\alpha nf(E - E^{0'})] \tag{2.4.12}$$

and the expression for $C_O(0, t)$, equation (2.4.6). Thus [9]

$$i(t) = k^0 D_O^{-1/2}[I_l - I(t)]\exp[-\alpha nf(E - E^{0'})] \tag{2.4.13}$$

or

$$E = E^{0'} - \frac{RT}{\alpha nF}\ln\frac{D_O^{1/2}}{k^0} - \frac{RT}{\alpha nF}\ln\frac{i(t)}{I_l - I(t)} \tag{2.4.14}$$

For a quasi-reversible reaction, along with equations (2.4.6) and (2.4.7), to yield

$$i(t) = k^0\{D_O^{-1/2}[I_l - I(t)]\exp[-\alpha nF(E - E^{0'})] - D_R^{-1/2} I(t)\exp[(1-\alpha)nf(E - E^{0'})]\}$$

(2.4.15)

$$i(t) = k^0 D_O^{-1/2} \exp[-\alpha nF(E - E^{0'})]\{I_l - I(t)[1 + \xi \exp[nf(E - E^{0'})]]\}$$

(2.4.16)

$$E = E^{0'} + \frac{RT}{\alpha nF} \ln \frac{k^0}{D_O^{1/2}} + \frac{RT}{\alpha nF} \ln \frac{\{I_l - I(t)[1 + \xi \exp[(nF/RT)(E - E^{0'})]]\}}{i(t)}$$

(2.4.17)

where $\xi = \left(D_O / D_R\right)^{1/2}$.

In deriving (2.4.14) and (2.4.17), we assumed that the Butler-Volmer expression for the rate constant for electron transfer applied. Indeed this assumption (or the adoption of some other model) is necessary a priori before equations can be derived for a particular electrochemical method. However, with the convolutive approach, this assumption is not needed and the rate law can be written in the general form [16]:

$$i(t) = nFAk_f(E)\{C_O(0,t) - C_R(0,t)\exp[(nF/RT)(E - E^{0'})]\} \qquad (2.4.18)$$

where $k_f(E)$ is the potential-dependent rate constant of the forward reaction. Thus, with (2.4.6) and (2.4.7),

$$\ln k_f(E) = \ln D_R^{1/2} - \ln\left\{\frac{I_l - I(t)[1 + \xi \exp[(nF/RT)(E - E^{0'})]}{i(t)}\right\} \qquad (2.4.19)$$

Analysis of experimental linear potential sweep experiments according to (2.4.19) or the equivalent expression for a totally irreversible reduction

$$\left\{\xi \exp\left[\left(nF/RT\right) \times \left(E - E^{0'}\right)\right] << 1\right\}, \quad \ln k_f(E) = \ln D_O^{1/2} - \ln \frac{[I_l - I(t)]}{i(t)} \qquad (2.4.20)$$

yields $\ln k_f(E)$ as a function of E at different v. If pure Butler-Volmer kinetic apply, then a plot of $\ln k_f(E)$ vs. E should be linear with a slope $\alpha nF/RT$. In an analysis of experimental data for the electroreduction of tertnitrobutane in aprotic solvents, Saveant and Tessier[16] noted significant deviations from linearity (after necessary corrections for double-layer effects were carried out), demonstrating that the α value was potential dependent, as is indeed predicted by other theories of electron transfer reactions.

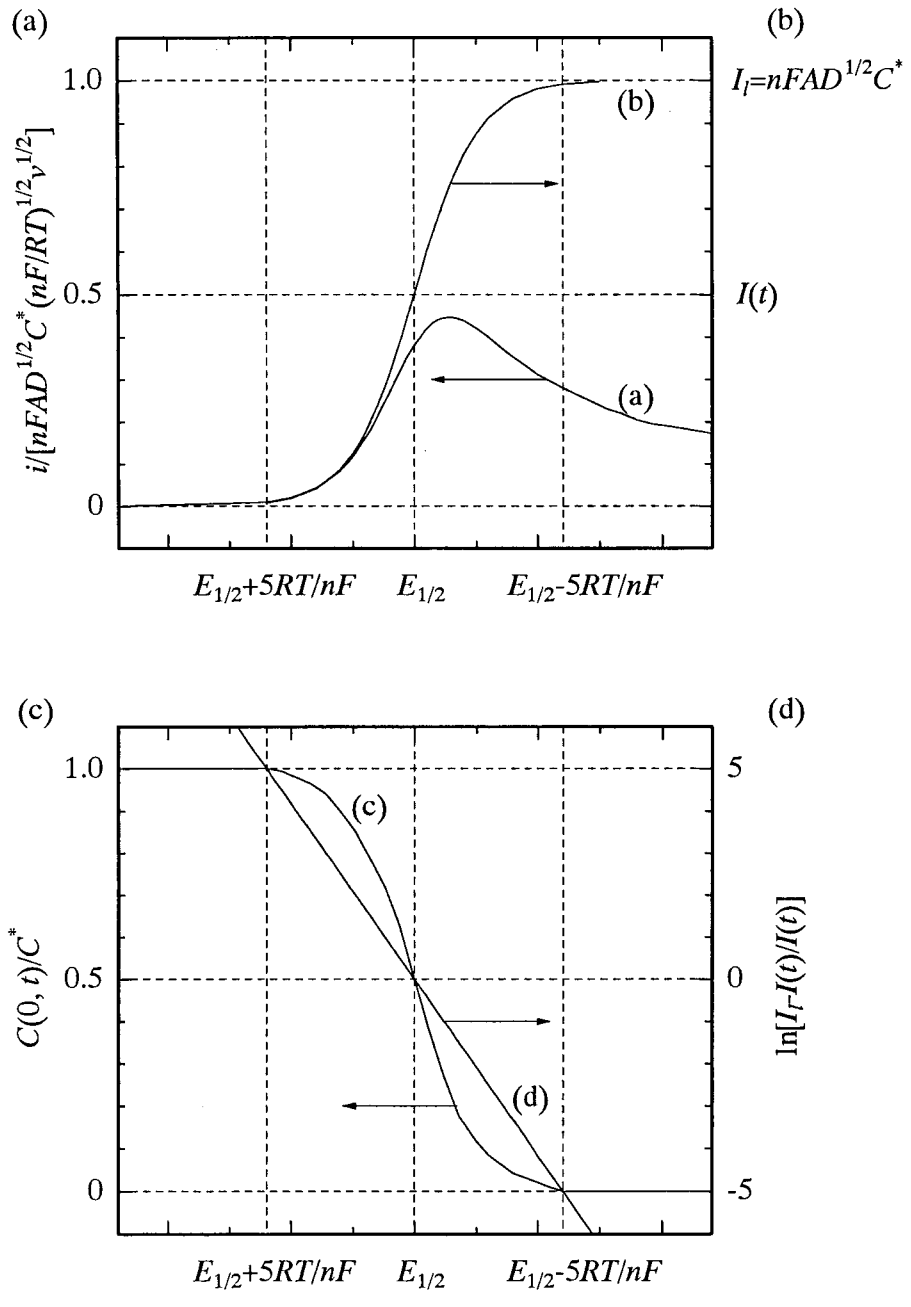

Fig. 2-4-1 Variation of i, I, $C_O(0,t)/C_O^*$, and $\ln\left[\left(I_l - I\right)/I\right]$ with E.

[Adapted from J. C. Imbeaux and J. M. Saveant, *J. Electroanal. Chem.*, **44**, 169 (1973)]

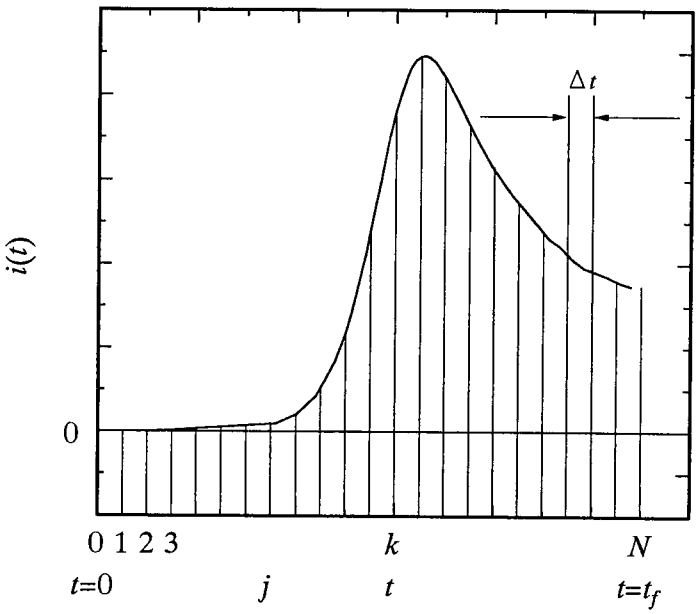

Fig. 2-4-2 Division of experimental $i(t)$ *vs.* t [or *vs.* $E(t)$] curve for digital evaluation of $I(t)$.

§ II- v Semi-differential techniques

§ II- v - i Theory[17]

The preliminary findings on a new voltammetric technique, semi-differential electroanalysis, were recently announced[18]. In the present article, the theory is extended to encompass irreversible electrode reactions. The complicating effects of electrode sphericity are also analyzed.

We adopted the symbolism of Goto and Ishii[18]. In particular, we use the symbol e to denote the semi-derivative[19] of the current with respect to time

$$e = \frac{d^{1/2}i}{dt^{1/2}} = \frac{dm}{dt} = \frac{1}{\sqrt{\pi}}\frac{d}{dt}\int_0^t \frac{i(\tau)d\tau}{\sqrt{t-\tau}} \tag{2.5.1}$$

Note, however, that there is some ambiguity in reference[18] in that the symbol e is also used to denote the semi-derivative of current with respect to potential. Consider the application of the potential ramp

$$E = E_0 - vt \tag{2.5.2}$$

to a working electrode immersed in a solution containing, in addition to excess supporting electrolyte, a concentration c of the electroreducible species Ox. This species undergoes the n-electron reduction

$$\mathrm{Ox} + ne^- \rightarrow \mathrm{Red} \tag{2.5.3}$$

to the initially-absent species Red. The initial potential E_0 is sufficiently positive that reaction (2.5.3) does not occur at time t=0. Subsequently, however, a faradaic current i does flow as the electrode potential becomes progressively more negative. A plot of i versus $-E$ (or versus t) arising in this way is termed, among other names, a "stationary electrode polarogram"[5]; a plot of the semi-integral m versus $-E$ is known as a "neopolarogram"[20]; and an appropriate name for a plot of the semi-derivative e versus $-E$ is a "derivative neopolarogram".

It will be assumed throughout this article that the transport of Ox to, and (in the reversible case) of Red from, the electrode is solely by semi-infinite diffusion. First, we shall derive the shape of the e versus E curve for an electrode to which diffusion occurs linearly. In this case the equations

$$(C_{bulk} - C_O)\sqrt{D_O} = \frac{m}{n}AF = C_R\sqrt{D_R} \qquad (2.5.4)$$

have been shown to relate the current semi-integral m uniquely to the surface concentrations of Ox and Red[10]. Later, we shall turn to the more complex, but more practically useful, case in which semi-differential electroanalysis is carried out with a spherical diffusion field.

§ II-v-ii Reversible reaction; linear diffusion

If reaction (2.5.3) is reversible, the Nernst equation

$$E = E_S + \frac{RT}{nF}\ln\frac{f_O C_O}{f_R C_R} = E_{1/2} + \frac{RT}{nF}\ln\left(\frac{C_O\sqrt{D_O}}{C_R\sqrt{D_R}}\right) \qquad (2.5.5)$$

relates the potential to the surface concentrations. Using this relationships, with Eqns. (2.5.4) and (2.5.2), and the definition (2.5.1) of e, one may derive

$$e = \frac{n^2F^2A\nu C_{bulk}\sqrt{D_O}}{4RT}\operatorname{sech}^2\left[\frac{nF}{2RT}\left[E - E_{1/2}\right]\right] \qquad (2.5.6)$$

as was demonstrated by Goto and Ishii[18].

Equation (2.5.6) represents a symmetric peak. The peak height is

$$e_p = -\frac{n^2F^2A\nu C_{bulk}\sqrt{D_O}}{4RT} \qquad (2.5.7)$$

and the potential corresponding to the peak is simply

$$E_p = E_{1/2} \qquad (2.5.8)$$

the polarographic half-wave potential. Moreover, since $\operatorname{arcsech} 2^{-1/2} = \pm 0.882$, it follows that

$$e = \frac{1}{2}e_p\left\{\begin{array}{l}\text{when} E = E_b = E_{1/2} + \dfrac{1.764RT}{nF} \\ \text{and. when} E = E_a = E_{1/2} - \dfrac{1.764RT}{nF}\end{array}\right\} \qquad (2.5.9)$$

Here E_b and E_a are the two potentials (one before the peak, the other after) at which e acquires a value equal to one-half of the peak semiderivative e_p. The peak width (the width of the peak at an ordinate value equal to one-half of the peak height) is therefore

$$W_p = E_b - E_a = \frac{3.53RT}{nF} \tag{2.5.10}$$

Notice that the peak shape is very dependent upon n, the number of transferred electrons: as n increases, the peak becomes narrower and much higher.

§ II - v - iii **Irreversible reaction: linear diffusion**

If reaction (2.5.3) is totally irreversible and is taken to obey the Volmer equation

$$\frac{i}{nAF} = k_S C_O \exp\left[\frac{\alpha nF}{RT}(E - E_S)\right] \tag{2.5.11}$$

then a solution to Eqns. (2.5.1), (2.5.2) and (2.5.4) was shown by Goto and Oldham[21] to be

$$m = -nFAC\sqrt{D}\sum_{j=1}^{\infty}(-)^j \exp\frac{jz}{(j!)^{1/2}} \tag{2.5.12}$$

where z is defined by

$$z = \frac{\alpha nF}{RT}(E_S - E) + \frac{1}{2}\ln\left(\frac{RTk_S^2}{\alpha nFvD}\right) = \frac{\alpha nF}{RT}(E_* - E) \tag{2.5.13}$$

Here E_* is a characteristic potential; expression (2.5.13) contains its definition, and its relation to features in some electroanalytical techniques is summarized in **Table 2-5-1**. In compiling this Table the relationship[22]

$$E_{1/2} = E_S + \frac{RT}{\alpha nF}\ln\left(\frac{1.35k_S\tau^{1/2}}{D^{1/2}}\right) \tag{2.5.14}$$

for the half-wave potential in classical (dropping electrode) polarography was used, as well as data relating to linear potential sweep techniques[5,21]. Differentiation of eqn. (2.5.12) is aided by the chain rule in the form $e = \frac{dm}{dt} = \left(\frac{dm}{dz}\right)\left(\frac{dz}{dE}\right)\left(\frac{dE}{dt}\right)$ and yields

$$e = -\left(\frac{\alpha n^2 ACF^2 vD^{1/2}}{RT}\right)\sum_{j=1}^{\infty}(-)^j j \exp\frac{jz}{(j!)^{1/2}} \tag{2.5.15}$$

as the expression for the shape of a totally irreversible derivative neopolarogram. Values of the summation term in eqn. (2.5.15) are listed in **Table 2-5-2** for an assortment of z values. The asymmetry, however, is mild enough to escape casual

notice. From Table 2-5-2 the maximum value of the summation term is 0.2970, whence it follows that

$$e_p = -\frac{\alpha n^2 F^2 A \nu C_{\text{bulk}} \sqrt{D_O}}{3.367RT} \tag{2.5.16}$$

From the fact that the maximum value of the summation occurs when z equals –0.055, it follows that

$$E_p = E_* + \frac{0.055RT}{\alpha nF} \begin{cases} E_b = E_* + \dfrac{1.642RT}{\alpha nF} \\ E_a = E_* - \dfrac{1.299RT}{\alpha nF} \end{cases} \tag{2.5.17}$$

Likewise the tabular data permit the peak width to be predicted; whence

$$W_p = E_b - E_a = \frac{2.94RT}{\alpha nF} \tag{2.5.18}$$

§ II-v-iv **Digital Techniques**[23]

Several algorithms for numerical semi-differentiation have been described[10]. The simplest, so called G1 algorithm, uses N equally spaced current data to complete e by the concentration scheme

$$\frac{t^{1/2}}{N^{1/2}} e = \left[\left[\left[\cdots\left[i_1\left(\frac{2N-5}{2N-2}\right)+i_2\right]\left(\frac{2N-7}{2N-4}\right)+i_3\right]\cdots\right]\left(\frac{1}{4}\right)+i_{N-1}\left[\left(-\frac{1}{2}\right)+i_N\right]\right]$$

Which is very easily implemented by a multiplication-addition-multiplication-$\cdots$ multiplication-addition procedure. In this algorithm, i_1, i_2, i_3, $\cdots$ i_{N-1} and i_N denote the instantaneous currents at times t/N, $2t/N$, $3t/N$, $\cdots$ $(N\text{-}1)t/N$, and t. As with all algorithms, there is a discretization error implicit in this G1 formula; its magnitude diminishes as N increases.

Table 2-5-1 The relationship to the characteristic potential E_* of features in some electroanalytical techniques applied to totally irreversible electroreductions.

Technique	Feature	Relation
Semi-integral electroanalysis	Half-wave potential of neopolarogram	$E_{1/2} = E_* + 0206(RT/\alpha nF)$
Stationary electrode polarography	Peak of linear scan voltammogram	$E_p = E_* - 0.780(RT/\alpha nF)$
Semi-differential electroanalysis	Peak of derivative neopolarogram	$E_p = E_* + 0055(RT/\alpha nF)$
Classical DME polarography	Half-wave potential of neopolarogram	$E_{1/2} = E_* + 0300(RT/\alpha nF)$ $+ (RT/2\alpha nF)\ln(\alpha nF\nu\tau/RT)$

Table 2-5-2 Values of the function that describes the shape of a totally irreversible derivative neopolarogram.

z	$-\sum_{j=1}^{\infty}(-)^j\, j \exp(jz)/(j!)^{1/2}$	$0.2970 - 0.105(z+0.055)^2$
-2.000	0.1122	
-1.750	0.1368	
-1.642	0.1485(b)	
-1.500	0.1645	
-1.250	0.1945	
-1.000	0.2251	
-0.750	0.2539	0.2463
-0.500	0.2778	0.2762
-0.250	0.2930	0.2930
-0.055	0.2970(p)	0.2970
0.000	0.2966	0.2970
0.250	0.2868	0.2872
0.500	0.2641	0.2647
0.750	0.2316	0.2290
1.000	0.1938	
1.250	0.1557	
1.299	0.1485(a)	
1.500	0.1209	

§ II-vi General Theory of Controlled Current Methods

§ II-vi-i Mathematics of Semi-Infinite Linear Diffusion

We again consider the simple electron transfer reaction, O + ne^- → R. A planar working electrode and an unstirred solution are assumed, with only species O initially present at a concentration C_o^*. The diffusion equations and general boundary conditions apply:

$$\frac{\partial C_O(x,t)}{\partial t} = D_O\left[\frac{\partial^2 C_O(x,t)}{\partial x^2}\right] \tag{2.6.1}$$

$$\frac{\partial C_R(x,t)}{\partial t} = D_R\left[\frac{\partial^2 C_R(x,t)}{\partial x^2}\right] \tag{2.6.2}$$

$$\left\{\begin{matrix} t = 0 \quad (for\ all\ x) \\ x \to \infty\ (for\ all\ t) \end{matrix}\right\} \quad C_O(x,t) = C_O^* \quad C_R(x,t) = 0 \tag{2.6.3}$$

$$D_O\left[\frac{\partial C_O(x,t)}{\partial x}\right]_{x=0} + D_R\left[\frac{\partial C_R(x,t)}{\partial x}\right]_{x=0} = 0 \tag{2.6.4}$$

Since the applied current $i(t)$ is presumed unknown, the flux at the electrode surface is also known at any time, by the equation:

$$D_O\left[\frac{\partial C_O(x,t)}{\partial x}\right]_{x=0} = \frac{i(t)}{nFA} \tag{2.6.5}$$

Note that this boundary condition involving the concentration gradient allows the diffusion problem to be solved without reference to the rate of the electron transfer reaction, in contrast with the concentration-potential boundary conditions required for controlled potential methods. Although in many controlled current experiments the applied current is constant, the more general case for any arbitrary applied current $i(t)$, can be solved readily and includes the constant current case, as well as reversal experiments and several others of interest.

As before, application of the Laplace transform method to (2.6.1) and (2.6.3) yields

$$\overline{C}_O(x,s) = \frac{C_O^*}{s} + B(s)\exp\left[-\left(\frac{s}{D_O}\right)^{1/2} x\right] \tag{2.6.6}$$

The transform of (2.6.5) is

$$D_O\left[\frac{\partial \bar{C}_O(x,s)}{\partial x}\right]_{x=0} = \frac{\bar{i}(s)}{nFA} \tag{2.6.7}$$

The combination of (2.6.6) and (2.6.7) with elimination of the integration constant $B(s)$ finally yields

$$\bar{C}_O(x,s) = \frac{C_O^*}{s} - \left[\frac{\bar{i}(s)}{nFAD_O^{1/2}s^{1/2}}\right]\exp\left[-\left(\frac{s}{D_O}\right)^{1/2}x\right] \tag{2.6.8}$$

By substitution of the known function, $i(s)$, and employing the inverse transform, $C_O(x, t)$ can be obtained. Similarly, the following expression for $C_R(x, s)$ can be derived:

$$\bar{C}_R(x,s) = \left[\frac{\bar{i}(s)}{nFAD_R^{1/2}s^{1/2}}\right]\exp\left[-\left(\frac{s}{D_R}\right)^{1/2}x\right] \tag{2.6.9}$$

Note that direct inversion of (2.6.8) and (2.6.9) using the convolution property leads to (2.3.6) and (2.3.9). These integral forms are also convenient for solving controlled current problems.

§ II-vi-ii Constant Current Electrolysis-The Sand Equation

If $i(t)=i$ (constant), then $i(s)=i/s$ and (2.6.8) becomes

$$\bar{C}_O(x,s) = \frac{C_O^*}{s} - \left[\frac{i}{nFAD_O^{1/2}s^{3/2}}\right]\exp\left[-\left(\frac{s}{D_O}\right)^{1/2}x\right] \tag{2.6.10}$$

The inverse transform of this equation yields the expression for $C_O(x, t)$:

$$C_O(x,t) = C_O^* - \frac{i}{nFAD_O}\left\{2\left(\frac{D_Ot}{\pi}\right)^{1/2}\exp\left(-\frac{x^2}{4D_Ot}\right) - x\,\mathrm{erfc}\left[\frac{x}{2(D_Ot)^{1/2}}\right]\right\} \tag{2.6.11}$$

Note that $\left[\partial C_o(x,t)/\partial x\right]_{x=0}$ is constant at all times after the onset of electrolysis and $C_O(0, t)$ decreases continually. An expression for $C_O(0, t)$ can be obtained by setting $x=0$ in (2.6.11), or directly by inverse transform of (2.6.8) with $x=0$:

$$\bar{C}_O(0,s) = \frac{C_O^*}{s} - \frac{i}{nFAD_O^{1/2}s^{3/2}} \tag{2.6.12}$$

to yield

$$C_O(0,t) = C_O^* - \frac{2it^{1/2}}{nFAD_O^{1/2}\pi^{1/2}} \tag{2.6.13}$$

At a certain characteristic time τ, called the *transition time*, $C_O(0, t)$ drops to zero. At this point (2.6.13) becomes

$$\frac{i\tau^{1/2}}{C_O^*} = \frac{nFAD_O^{1/2}\pi^{1/2}}{2} = 85.5nD_O^{1/2}A\frac{\text{mAsec}^{1/2}}{\text{cm}^2\text{mM}} \tag{2.6.14}$$

This equation, known as the *Sand equation*, was first derived by H. J. S. Sand[25]. The flux of O to the electrode surface beyond the transition time is not large enough to satisfy the applied current, and the potential jumps to a value where another electrode process can occur (**Figure 2-6-1**). The actual shape of the *E-t* curve is discussed in the next sections. The measured value of τ at known i (or better, the values of $i\tau^{1/2}$ obtained at various currents) can be used to determine C_o^* or D_O. A lack of constancy of the *transition time constant*, $i\tau^{1/2}/C_o^*$, with i or C_o^* indicates complications to the electrode reaction from coupled homogeneous chemical reactions, adsorption, or measurement artifacts. Note that (2.6.11) can be written in a convenient form with dimensionless groupings $C_o(x,t)/C_o^*, t/\tau, and\ \lambda_o = x/2(D_o t)^{1/2}\ for (0 \le t \le \tau)$:

$$\frac{C_O(x,t)}{C_O^*} = 1 - \left(\frac{t}{\tau}\right)^{1/2}\left[\exp\left(-\lambda_O^2\right) - \pi^{1/2}\lambda_O \text{erfc}(\lambda_O)\right] \tag{2.6.15}$$

$$\frac{C_O(0,t)}{C_O^*} = 1 - \left(\frac{t}{\tau}\right)^{1/2} \tag{2.6.16}$$

In a similar way, the following equations hold for $C_R(x, t)$ when $(0 \le t \le \tau)$:

$$\frac{C_R(x,t)}{C_O^*} = \xi\left(\frac{t}{\tau}\right)^{1/2}\left[\exp\left(-\lambda_R^2\right) - \pi^{1/2}\lambda_R \text{erfc}(\lambda_R)\right] \tag{2.6.17}$$

where

$$\lambda_R = \frac{x}{2(D_R t)^{1/2}} \text{ and } \xi = \left(\frac{D_O}{D_R}\right)^{1/2}$$

$$C_R(0,t) = \frac{2it^{1/2}}{nFA\pi^{1/2}D_R^{1/2}} = \xi\left(\frac{t}{\tau}\right)^{1/2} C_O^* \tag{2.6.18}$$

§ II-vi-iii Programmed Current Chronopotentiometry

It is possible to use currents that are programmed to vary with time in a special way, rather than remaining constant[26]. For example, a constant that increases linearly with time could be used:

$$i(t) = \beta t \tag{2.6.19}$$

The treatment follows that for a constant current electrolysis. In this case the transform is

$$\bar{i}(s) = \frac{\beta}{s^2} \tag{2.6.20}$$

so that (2.6.9) becomes, at x=0,

$$\bar{C}_O(0,s) = \frac{C_O^*}{s} - \frac{\beta}{nFAD_O^{1/2}s^{5/2}} \tag{2.6.21}$$

$$C_O(0,t) = C_O^* - \frac{2\beta t^{3/2}}{nFAD_O^{1/2}\Gamma(5/2)} \tag{2.6.22}$$

where $\Gamma(5/2)$ is the Gamma function ,equal with this argument to 1.33. This same treatment can be employed with any power function of time.

A particular interesting applied current is one varying with the square root of time:

$$i(t) = \beta t^{1/2} \tag{2.6.23}$$

$$\bar{i}(s) = \frac{\beta\pi^{1/2}}{2s^{3/2}} \tag{2.6.24}$$

$$\bar{C}_O(0,s) = \frac{C_O^*}{s} - \frac{\beta\pi^{1/2}}{2nFAD_O^{1/2}s^2} \tag{2.6.25}$$

$$C_O(0,t) = C_O^* - \frac{\beta\pi^{1/2}t}{2nFAD_O^{1/2}} \tag{2.6.26}$$

Again, defining the transition time τ as that time when $C_O(0, t)$=0, an expression equivalent to the constant current Sand equation, but with τ (rather than $\tau^{1/2}$) proportional to C_o^* and β, results:

$$\frac{\beta\tau}{C_O^*} = 2nFA\pi^{-1/2}D_O^{1/2} \tag{2.6.27}$$

Because this current excitation function is fairly difficult to generate, the technique has

not been used very much. Nevertheless, it would be especially advantageous for stepwise electron transfer reactions and multi-component systems.

§ II-vi-iv Reversible (Nernstian) Waves

For rapid electron transfer, the Nernst equation applies. Substitution of the expressions for $C_O(0, t)$ and $C_R(0, t)$ (equations 2.6.16 and 2.6.18) into it yields[27]

$$E = E_{\tau/4} + \frac{RT}{nF}\ln\frac{\tau^{1/2} - t^{/2}}{t^{1/2}} \tag{2.6.28}$$

where E, the *quarter-wave potential*, is

$$E_{\tau/4} = E^{0'} - \frac{RT}{2nF}\ln\frac{D_O}{D_R} \tag{2.6.29}$$

so that E is chronopotentiometric equivalent of the voltammetric $E_{1/2}$ value (Figure 2-6-1). The test for reversibility of an E-t curve is linearity of an E vs. $\log\left[\left(\tau^{1/2} - t^{1/2}\right)/t^{1/2}\right]$ plot with a slope of 0.059/n V, or a value of $\left|E_{\tau/4} - E_{3\tau/4}\right| = 47.9/n$ mV (at 298K).

§ II-vi-v Totally Irreversible Waves

For a totally irreversible cathodic reaction, i is related to E by either of the following equations[28]:

$$\frac{i}{nFA} = k_f^0 C_O(0,t)\exp\left[\frac{-\alpha n_a FE}{RT}\right] \tag{2.6.30}$$

$$\frac{i}{nFA} = k^0 C_O(0,t)\exp\left[\frac{-\alpha n_a F(E - E^{0'})}{RT}\right] \tag{2.6.31}$$

When the expression for $C_O(0,t)$, (2.6.16), is substituted into these equations, the following expressions result:

$$E = \frac{RT}{\alpha n_a F}\ln\left(\frac{nFAC_O^* k_f^0}{i}\right) + \frac{RT}{\alpha n_a F}\ln\left[1 - \left(\frac{t}{\tau}\right)^{1/2}\right] \tag{2.6.32a}$$

$$E = E^{0'} + \frac{RT}{\alpha n_a F}\ln\left(\frac{nFAC_O^* k_f^0}{i}\right) + \frac{RT}{\alpha n_a F}\ln\left[1 - \left(\frac{t}{\tau}\right)^{1/2}\right] \tag{2.6.32b}$$

Equivalent expressions can be obtained by using the Sand equation and substituting for $\tau^{1/2}$:

$$E = \left(\frac{RT}{\alpha n_a F}\right)\ln\left[\frac{2k_f^0}{(\pi D_O)^{1/2}}\right] + \left(\frac{RT}{\alpha n_a F}\right)\ln\left(\tau^{1/2} - t^{1/2}\right) \qquad (2.6.33a)$$

$$E = E^{0'} + \left(\frac{RT}{\alpha n_a F}\right)\ln\left[\frac{2k_f^0}{(\pi D_O)^{1/2}}\right] + \left(\frac{RT}{\alpha n_a F}\right)\ln\left(\tau^{1/2} - t^{1/2}\right) \qquad (2.6.33b)$$

Thus, for a totally irreversible reduction wave, the whole *E-t* wave shifts toward more negative potentials with increasing current, with a tenfold increase in current causing a shift of $2.3RT/\alpha n_a F$. Note that uncompensated resistance between the reference and working electrode will also cause the *E-t* curve to shift with increasing *i*. For a totally irreversible wave, $\left|E_{\tau/4} - E_{3\tau/4}\right| = 33.8/\alpha n_a$ mV at 298K.

§ II-vi-vi Quasi-Reversible Waves

The general equation for the *E-t* curve results from combining the general current-potential-concentration characteristic, with the equations for $C_O(0, t)$, (2.6.13), and $C_R(0, t)$, (2.6.18), (including, so that a starting equilibrium potential can be defined, an initial concentration of R of C_R) [29],[30]. The result, in terms of η, is

$$\frac{i}{i_0} = \left[1 - \frac{2i}{nFAC_O^*}\left(\frac{t}{\pi D_O}\right)^{1/2}\right]e^{-\alpha nf\eta} - \left[1 + \frac{2i}{nFAC_R^*}\left(\frac{t}{\pi D_R}\right)^{1/2}\right]e^{(1-\alpha)nf\eta} \qquad (2.6.34)$$

Alternate forms can be written, for example,

$$j = k_f\left[nFC_O^* - 2j\left(\frac{t}{\pi D_O}\right)^{1/2}\right] - k_b\left[nFC_R^* + 2j\left(\frac{t}{\pi D_R}\right)^{1/2}\right] \qquad (2.6.35a)$$

or, when C_R=0,

$$j = nFk_f C_O^* - \frac{2jt^{1/2}}{\pi^{1/2}}\left(\frac{k_f}{D_O^{1/2}} + \frac{k_b}{D_R^{1/2}}\right) \qquad (2.6.35b)$$

where k_f and k_b are defined as follows, and j is the current density.

$$k_f = k^0 \exp\left[-\alpha n f\left(E - E^{0'}\right)\right] \tag{2.6.35c}$$

$$k_b = k^0 \exp\left[(1-\alpha) n f\left(E - E^{0'}\right)\right] \tag{2.6.35d}$$

where $f = F/RT$, and k^0 and α are adjustable parameters called *the standard rate constant* and *transfer coefficient*, respectively.

Usually the study of the kinetics of quasi-reversible electrode reactions by constant current techniques (generally called the galvanostatic or current step method) involves the use of such small current perturbations that the potential change is small. When both O and R are initially present, the linearized current-potential-concentration characteristic, can then be employed; and combination of that with (2.6.13) and (2.6.18) yields

$$-\eta = \frac{RT}{nF} i \left[\frac{2t^{1/2}}{nFA\pi^{1/2}} \left(\frac{1}{C_O^* D_O^{1/2}} + \frac{1}{C_R^* D_R^{1/2}} \right) + \frac{1}{i_0} \right] \tag{2.6.36}$$

thus a plot of η *vs.* $t^{1/2}$, for small values of η, will be linear, and i_0 can be obtained from the intercept. This method is the constant current analog of the potentiostatic or potential step method.

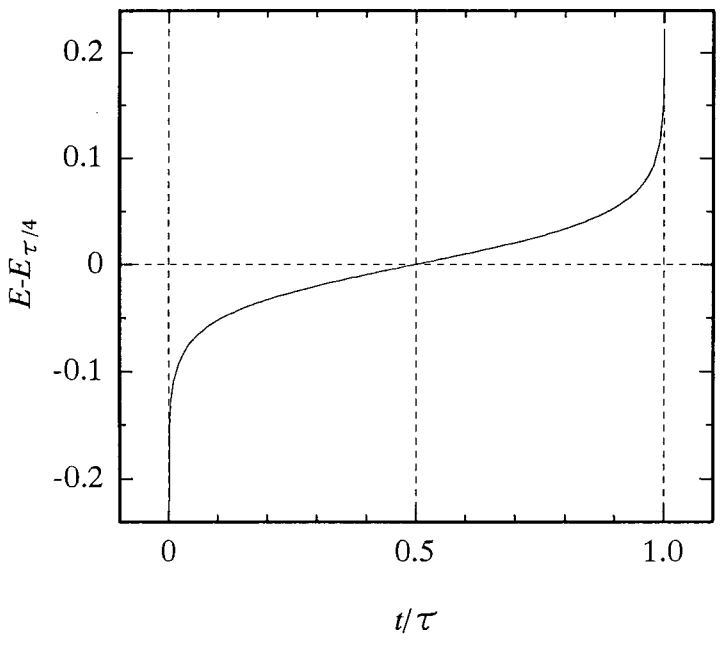

Fig. 2-6-1 Theoretical chronopotentiogram for a nernstian electrode process

§ II-vii Molecular Dynamics Simulation

One of the main features of the liquid state is the mobility of the constituent particles. The study of their motions may be done by the molecular dynamics technique[31]. Such treatments have already been used to describe the properties of liquid rare gases[32-34], of simple molecular liquids[35] and of the classical one-component plasma[36].

Consider a set of N particles ($N/2$ anions and $N/2$ cations) in an elementary cubic box of side L. According to the periodic boundary conditions the infinite system is set up by replicas of this parent cube translated by a positive or negative multiple of L along its edges.

The equations of classical mechanics describing the motion of the ions are numerically integrated to yield a time record of their position and velocity coordinates[32-34].

The interaction potential $\Phi_{ij}(r)$ between two particles i and j is assumed to be independent of the position of neighboring particles. For sufficiently small time intervals Δt the successive positions $\mathbf{r}_i$ are computed according to Verlet's algorithm [32, 33] :

$$\mathbf{r}_i(t+\Delta t) = -\mathbf{r}_i(t-\Delta t) + 2\mathbf{r}_i(t) + (\Delta t)^2\left(d\sum_{j\neq i}^{N}\Phi_{ij}(r)/d\mathbf{r}_i\right)m_i^{-1} \qquad (2.7.1)$$

m_i represents the mass of the particles i; at the time t velocities and temperatures are given by

$$\mathbf{v}_i(t) = \left(\mathbf{r}_i(t+\Delta t) - \mathbf{r}_i(t-\Delta t)\right)/2\Delta t \qquad (2.7.2)$$

$$T_s(t) = \left(3N_s k\right)^{-1}\sum_{i=1}^{N_s} m_i v_i^2(t) \qquad (2.7.3)$$

The temperatures are evaluated for the two species s: anion and cation (for a sufficiently long time interval the average values of the anion and cation temperatures should be equal).

This calculation was performed with a pair potential of the Born-Mayer-Huggins form[37] :

$$\Phi_{ij} = \xi_i \xi_j r^{-1} + b \exp\left(B\left(\sigma_{ij} - r\right)\right) + C_{ij} r^{-6} + D_{ij} r^{-8} \qquad (2.7.4)$$

The values of the parameters b, B, C_{ij}, D_{ij} are calculated from the solid-state properties of alkali halides[37] The initial positions for the integration process are those of a face-centered cubic lattice, and the initial velocities are chosen at random according to a Maxwell-Boltzmann distribution ; then the system evolves until equilibrium is reached. This is the case when two conditions are fulfilled :

(1) the temperature does not systematically drift;

(2) the configuration corresponds to a liquid phase, i.e., the melting factor $\rho_m = \sum_{i=1}^{N} \cos\left(\mathbf{k} \cdot \mathbf{r}_i\right)$ fluctuates around zero[34].

With the exception of the r^{-1} term, all quantities of the pair potential (equation (2.7.4)) converge rapidly as soon as the distance r_{ij} is greater than a few atomic radii. As for the coulombic term, the studies of Brush et al.[38], and, more recently, of Woodcock and Sangster[39] and of Hansen[40] have shown that Ewald's expansion[41] leads to rapidly convergent sums. In this treatment two mutually canceling normalized gaussian charge distributions are added to the ion point charge distribution (half-width)[42]. In this case the expression of the Coulomb energy takes the form[39].

$$\Phi^e = \Phi_I^e + \Phi_{II}^e \qquad (2.7.5)$$

$$\Phi_I^e = \frac{1}{2}\left\{\sum_i \xi_i \left[\sum_j \xi_j \sum_{\mathbf{n}} \frac{1 - \operatorname{erf}\left(\alpha r_{ij\mathbf{n}}\right)}{r_{ij\mathbf{n}}} - \frac{\xi_i \alpha}{\sqrt{\pi}}\right]\right\} \qquad (2.7.6)$$

$$\Phi_{II}^e = \frac{1}{2\pi L} \sum_i \sum_j \xi_i \xi_j \sum_{\mathbf{n}} \frac{\exp\left(-\pi^2 |\mathbf{n}|^2 / \alpha^2 L^2\right)}{|\mathbf{n}|^2} \cos\left(2\pi \mathbf{n} \cdot \mathbf{r}_{ij} / L\right) \qquad (2.7.7)$$

Where $\mathbf{n}$ is a vector with integer components n_x, n_y, n_z and $\mathbf{r}_{ij\mathbf{n}}=\mathbf{r}_i-\mathbf{r}_j+L\mathbf{n}$. In Φ_I^e, $i=j$ is omitted when $\mathbf{n}=(0,0,0)$ and in Φ_{II}^e, n=(0,0,0) is omitted.

To avoid time-consuming calculations it is important to know the relative contribution of the terms in Φ_I^e and Φ_{II}^e. For this reason we have calculated the values of the first terms of these series by evaluating the Φ_I^e terms up to $r_{ij\mathbf{n}}=3L/2$ and the Fourier series Φ_{II}^e up to $|\mathbf{n}|^2 = 12$.

Since they are based on Newton's equation, molecular dynamics calculations directly depend on the forces $\mathbf{F}_{ij} = d\Phi_{ij}/d\mathbf{r}_{ij}$ and the cut-off values have to be carefully selected. No particular problem arises in the differentiation of the short-range forces. These forces are negligible for r_{ij} greater than $L/2$, i.e., three ionic diameters for N=1000.

The Coulomb force $\mathbf{F}_i^e$ acting on a particle i is calculated by differentiation of Ewald's potential, and thus may be divided into two parts : $\mathbf{F}_i^e = \mathbf{F}_{Ii}^e + \mathbf{F}_{IIi}^e$. The components of these two forces are

$$F_{xIi}^e = \frac{1}{2}\xi_i \sum_j \xi_j \sum_{\mathbf{n}} \left[-\frac{2\alpha}{\sqrt{\pi}} \frac{1}{r_{ijn}} \exp\left(-\alpha^2 r_{ijn}^2\right) - \frac{\operatorname{erfc}\left(\alpha r_{ijn}\right)}{r_{ijn}^2} \right] \frac{x_{ijn}}{r_{ijn}} \tag{2.7.8}$$

$$F_{xIIi}^e = -\frac{1}{L}\xi_i \sum_j \xi_j \sum_{\mathbf{n}} \frac{\exp\left(-\pi^2|\mathbf{n}|^2/\alpha^2 L^2\right)}{|\mathbf{n}|^2} n_x \sin\left(2\pi \mathbf{n}\mathbf{r}_{ij}/L\right) \tag{2.7.9}$$

The components on the other two axes O_y and O_z are obtained by substituting x_{ijn} and n_x respectively by y_{ijn}, n_y and z_{ijn}, n_z (x_{ijn}, y_{ijn}, z_{ijn} are the components of r_{ijn}). The total force on i, $\mathbf{F}_i = \sum_j^N \mathbf{F}_{ij}$, is the resultant of two main contributions : the Coulomb forces $\mathbf{F}_i^e = \mathbf{F}_{Ii}^e + \mathbf{F}_{IIi}^e$ and the repulsion $\mathbf{F}^{rep}$. A precision of a few parts in 10^3 is required to obtain a good conservation of the internal energy of the system. This condition may be fulfilled by expanding the F series up to the term , which corresponds to 80 vectors. In this case the computing time required per integration step is about 4s. The average value of the resultant of the first neglected vectors represents 0.15 per cent of the average total force. However, the increasing disorder introduces a significant decrease in the relative value of the neglected vectors. Let us remark that the particular values chosen ($r_{ijn} \le L$ and $|\mathbf{n}|^2 \le 6$) are dictated by practical computation considerations; the required precision might be obtained using $r_{ijn} \le L/2$, $|\mathbf{n}|^2 \le 27$ and $\alpha_{min} = 5.6/L$.

§ II-viii References

(1) A. Klemm, *Z. Naturforsch.*, **1**, 252 (1946) [in German].

(2) V. Ljubimov and A. Lunden, *Z. Naturforsch.*, **21a**, 1592 (1966).

(3) J. E. B. Randles, *Trans. Faraday Soc.*, **44**, 327 (1948).

(4) A. Sevcik, *Collect. Czech. Chem. Commun.*, **13**, 349 (1948).

(5) R. S. Nicholson and I. Shain, *Anal. Chem.*, **36**, 706 (1964).

(6) W. H. Reinmuth, *J. Am. Chem. Soc.*, **79**, 6358 (1957).

(7) H. Matsuda and Y. Ayabe, *Z. Elecktrochem.*, **59**, 494 (1955).

(8) Y. P. Gokhshtein, *Dokl. Akad. Nauk SSSR*, **126**, 598 (1959).

(9) J. C. Imbeaux and J. M. Saveant , *J. Electroanal. Chem.*, **44**, 1969 (1973).

(10) K. B. Oldham and J. Spanier, *ibid.*, **26**, 331 (1970).

(11) K. B. Oldham, *Anal. Chem.*, **44**, 196 (1972).

(12) K. B. Oldham, *ibid.*, **45**, 39 (1973).

(13) R. J. Lawson and J. T. Maloy, *ibid.*, **46**, 559 (1974).

(14) J. H. Carney and H. C. Miller, *ibid.*, **45**, 2175 (1973).

(15) P. E. Whitson, H. W. Vanden Born, and D. H. Evans, *ibid.*, **45**, 1298 (1975).

(16) J. M. Saveant and D. Tessier, *J. Electroanal. Chem.*, **65**, 57 (1975).

(17) P. Dalrymple-Alford, M Goto, and K. B. Oldham, *J. Electroanal. Chem.*, **85**, 1 (1977).

(18) M. Goto and D. Ishii, *J. Electroanal. Chem.*, **61**, 361 (1975).

(19) K. B. Oldham and J. Spanier, *The Fractional Calculus*, Academic Press, New York, 1974.

(20) M. Goto and K. B. Oldham, *Anal. Chem.*, **45**, 2043 (1973).

(21) M. Goto and K. B. Oldham, *Anal. Chem.*, **48**, 1671 (1976).

(22) J. Koutecky, *Collect. Czech. Chem. Commun.*, **18**, 597 (1953).

(23) P. Dalrymple-Alford, M Goto, and K. B. Oldham, *Anal. Chem.*, **49**, 1390 (1977).

(24) K. B. Oldham and J. Spanier, "*The Fractional Calculus*", Academic Press, New York, 1974.

(25) H. J. S. Sand, *Phil. Mag.*, **1**, 45 (1901).

(26) R. W. Murray and C. N. Reilley, *J. Electroanal. Chem.*, **3**, 64, 182 (1962).

(27) Z. Karaoglanoff, *Z. Elektrochem.*, **12**, 5 (1906).

(28) P. Delahay and T. Berzins, *J. Am. Chem. Soc.*, **75**, 2486 (1953).

(29) L. B. Anderson and D. J. Macero, *Anal. Chem.*, **37**, 322 (1965).

(30) Y. Okinaka, S. Toshima, and H. Okaniwa, *Talanta*, **11**, 203 (1964).

(31) B. J. Alder, and T. E. Wainwright, *J. Chem. Phys.*, **31**, 459 (1959); Ibid., **33**, 1439 (1960).

(32) A. Rahman, *Phys. Rev. A*, **136**, 405 (1964).

(33) L. Verlet, *Phys. Rev.*, **159**, 98 (1967).

(34) L. Verlet, *Phys. Rev.*, **165**, 21 (1968).

(35) J. Barojas, D. Levesque, and B. Quentrec, *Phys. Rev. A*, **7**, 1092 (1973).

(36) J. P. Hansen, E. L. Pollock, and I. R. McDonald, *Phys. Rev. Lett.*, **32**, 277 (1974).

(37) M. P. Tosi, and F. G. Fumi, *J. Phys. Chem. Solids*, **25**, 31 (1964).

(38) S. G. Brush, H. L. Sahlin, and E. Teller, *J. Chem. Phys.*, **45**, 2102 (1966).

(39) L. V. Woodcock, and K. Singer, *Trans. Faraday Soc.*, **67**, 12 (1971).

(40) J. P. Hansen, *Phys. Rev. A*, **8**, 3096 (1973).

(41) P. P. Ewald, *Ann. Phys.*, **21**, 1087 (1921).

(42) C. Kittel, Introduction to Solid State Physics, 2nd edition, (John Wiley), p571 (1961).

Chapter III

Molten Ternary System (Na, K, Cs)Cl

ChapterIII Molten Ternary System (Na, K, Cs)Cl

§ III- i Background

The ionic mobilities in mixtures of molten salts have been interpreted in terms of anion polarization[1] and complex formation[2]. The Chemla effect[3] refers to the phenomenon that in a charge symmetrical mixture with a common anion the mobility isotherms of the two cations cross at some concentration. In the molten alkali chloride mixtures (Li, Na)Cl[4], (Li, K)Cl[1,2,5,6], (Li, Rb)Cl[7], (Li, Cs)Cl[2, 8], (Na, K)Cl[2], (Na, Cs)Cl[2] and (Li, Na, K)Cl[9,10] the internal cation mobilities have been measured. As far as we know, the electric conductivity and the internal mobility have not been measured in molten (Na, K, Cs)Cl system. For (Na, K)Cl, the internal mobilities were measured by the EMF method[2], which involves large errors in some cases[11,12]. Therefore, in the present study the internal mobilities of the ternary alkali chloride systems have been measured by the Klemm method, which yields the most accurate and precise data among the available methods.

On the other hand, we have proposed to apply the electromigration method to enrich the solute, because the electromigration method has an advantage for the pyrochemical treatment due to its simple construction for being able to use the same container with the conductive melt bath. In addition, it was recently pointed out a possibility of high enrichment of Cs, Sr and Gd[13] in the LiCl-KCl eutectic mixture. In the case of the enrichment of Cs by countercurrent electromigration method, it is necessary to know that the limitation of enrichment degree for Cs, i.e., the Chemla crossing point. In recently, it was also investigated the relative differences in the internal mobilities for Cs, Sr and Ba[14] in the NaCl-KCl equimolar mixtures. Therefore, it is also important for the technological fields to investigate the internal mobilities in molten alkali chlorides. Furthermore, from MD simulation, we calculated the electric conductivity used by Kubo formula and self-exchange velocity for molten alkali ternary system, because it has reported that the strong correlation between internal mobilities and SEV's for some alkali binary chlorides and nitrates.

§ III- ii Experimental

§ III- ii - i Electromigration and Electrical Conductivity

The chemicals NaCl, KCl and CsCl were of reagent grade. The finely crushed NaCl and KCl were mixed in the desired portion (NaCl:50mol%, KCl:50mol%) and were introduced in a quartz tube. The mixture was kept at 973K under vacuum for about 7h and melted above 1073K. The solute CsCl was introduced in a quartz cell and kept at about 673K under vacuum for about 24h. The electromigration cell was similar to that shown in reference[6]. The anode was made of a super fine graphite rod (5mmϕ, Tokai Carbon Co., Ltd.). The cathode consists of the glassy carbon (3.0mm ϕ, Nilaco Co.) was connected to the graphite rod with the ceramic binder for protection from corrosion because the glassy carbon does not make the intermetallic compounds with alkali metals. Chlorine gas which was dried by passing through conc. sulfuric acid was bubbled into the melt around the cathode in order to convert electrodeposited metal into the chloride. The migration tubes were made of the quartz glass. The upper part of the migration tube had an outlet for Cl_2 gas. The lower part of the migration tube was packed with alumina powder (100μmϕ, Nishio Chemical Ind.) in order to prevent convection of the melt in the migration tube. The temperature was kept at 1023K with a temperature controller and measured by a Chromel-Alumel thermocouple during electromigration. A constant DC current supplier (Kikusui Electronics. Corp. PAD 500-0.6A) fed electric currents less than 0.2A. The transported charge was measured by a Cu coulometer or the Desital Coulometer (HIOKI 3187, AC/DC Power HITESTER). After several thousand Coulombs of charge was transported, the migration tube was taken out from the bath and the salt was quenched quickly. The tube was cleaned outside and cut into several pieces of about 10mm length. The salt in each fraction was dissolved to distilled water. The amount of Cs in each fraction was determined by absorption spectrometry (Hitachi Corp. Z-6100). The amount of Na and K was analyzed by ICP emission spectrometry (Seiko Denshi Kogyo SPS-7000).

The electric conductivity of the mixture was measured by the direct current method by Duke and Bissel[15] as shown in **Fig. 3-1**. The cell was made of quartz and four

platinum wires were used as electrodes. The standard resistance used in the circuit was 10 Ω. The cell constant was measured at 295K to be 22.03cm^{-1}, using KCl standard aqueous solutions prepared according to the specifications by Jones and Bradshaw[16]. The accuracy of this cell was checked by measuring the electric conductivity of molten $NaNO_3$ and KNO_3.

§ III- ii - ii Molecular Dynamics Simulation

For MD simulation of the ternary alkali chloride system (Na, K, Cs)Cl, 1000 or 800 particles were disposed in a periodic cube whose edge length L was determined from the molar volume calculated from those of the pure melts on the assumption of additivity. This assumption is justified since the excess molar volumes on mixing two alkali chlorides are very small[17].

The pair potentials of the Born-Mayer-Huggins type were used:

$$\Phi_{ij} = \frac{z_i z_j e^2}{4\pi\varepsilon_0 r} + A_{ij} b \exp\left[\left(\sigma_i + \sigma_j - r\right)/\rho\right] - \frac{c_{ij}}{r^6} - \frac{d_{ij}}{r^8} \tag{3-1}$$

$$A_{ij} = \left(1 + \frac{z_i}{n_i} + \frac{z_j}{n_j}\right) \tag{3-2}$$

where z is the positive or negative charge number, e the elementary charge, ε_0 the permittivity of vacuum and A the Pauling factor. For pure alkali halide crystals of the NaCl-type, values of b, σ and ρ have been given by Tosi and Fumi[18], and values of c and d by Mayer[19], while the third and fourth terms represent the dipole-dipole and dipole-quadrupole dispersion energies with parameters. The corresponding parameters for the mixture were determined by the combination rule presented by Larsen et al.[20]. The parameters shown in **Tables 3-1-1** and **3-1-2** are employed for alkali ternary chloride system (Na, K, Cs)Cl and binary systems (Li, Cs)Cl, (Rb, Cs)Cl, respectively. The Ewald method[21] was used for the calculation of the Coulomb forces; the cutoff distance in real space was $L/2$, and the reciprocal lattice vectors $|\mathbf{n}^2|$ were counted up to 27. The convergence parameter α was $5.6/L$ and time step 2fs. At the beginning, MD runs were performed with the constant temperature method proposed by

Woodcock[22]. After constant temperature runs of several thousand steps, these were switched to constant energy runs. From the runs during more than 5000 time steps using Verlet's algorithm after attainment of equilibrium, the structure and the other properties were obtained.

§ III-iii Results and Discussion

§ III-iii-i Electric Conductivity and Internal Cation Mobilities

. Data on the electric conductivity are shown in **Fig. 3-2**. From a least square method, the conductivity κ (Scm^{-1}) are expressed in the range $933K \leqq T \leqq 1023K$ by

$$\kappa_1 = 0.354 + 1.059 \times 10^{-3} T + 5.758 \times 10^{-7} T^2 \quad (x_{Cs} = 0.202 \pm 0.006) \tag{3-3a}$$

$$\kappa_2 = -0.833 + 3.048 \times 10^{-3} T - 4.735 \times 10^{-7} T^2 \quad (x_{Cs} = 0.397 \pm 0.002) \tag{3-3b}$$

$$\kappa_3 = -0.446 + 2.001 \times 10^{-3} T - 0.076 \times 10^{-7} T^2 \quad (x_{Cs} = 0.592 \pm 0.003) \tag{3-3c}$$

$$\kappa_4 = -1.370 + 3.707 \times 10^{-3} T - 9.318 \times 10^{-7} T^2 \quad (x_{Cs} = 0.782 \pm 0.013) \tag{3-3d}$$

where T is an absolute temperature and x_{Cs} is the mole fraction of Cs. It is shown that the relationship between the mole fraction of caesium and the conductivity at 1023K in **Fig. 3-3**. This relationship is also expressed by

$$\kappa = 2.481 - 2.447 x_{Cs} + 1.888 x_{Cs}^2 - 0.513 x_{Cs}^3 \tag{3-4}$$

The relative differences of the mobilities for the 3 cation pairs are defined as

$$\varepsilon_{12} = (b_1 - b_2)/\bar{b} \tag{3-5a}$$

$$\varepsilon_{13} = (b_1 - b_3)/\bar{b} \tag{3-5b}$$

$$\varepsilon_{23} = (b_2 - b_3)/\bar{b} \tag{3-5c}$$

where the subscripts 1, 2 and 3 denote Na, K and Cs, respectively, and

$$\bar{b} = x_{Na} b_{Na} + x_K b_K + x_{Cs} b_{Cs} = \kappa V / F \tag{3-6}$$

where V is molar volume and F is Faraday's constant.

The ε_{12} can be determined from chemical analysis and the transported charge quite similarly to the case of binary mixtures:

$$\varepsilon_{12} = -\frac{F}{Q}\left(\frac{N_1}{x_1} - \frac{N_2}{x_2}\right) \tag{3-7}$$

where N_1 and N_2 are the total amounts of species 1 and 2 in the pieces of the separation tube, respectively, after passage of the charge Q, in which the mole fractions are

different from the original ones x_1 and x_2, respectively. The ε values can be obtained from an equation based on the material balance and the charge balance[23]. The ε_{12}, ε_{13} and ε_{23} values thus obtained and the main experimental conditions are tabulated in **Table 3-2**. The internal mobilities of the each cations are calculated from the following equations using ε and κ values thus obtained.

$$b_{Na} = (\kappa V/F)(1 + x_K \varepsilon_{NaK} + x_{Cs} \varepsilon_{NaCs}) \quad (3\text{-}8a)$$

$$b_K = (\kappa V/F)(1 - x_{Na} \varepsilon_{NaK} + x_{Cs} \varepsilon_{KCs}) \quad (3\text{-}8b)$$

$$b_{Cs} = (\kappa V/F)(1 - x_{Na} \varepsilon_{NaCs} - x_K \varepsilon_{KCs}) \quad (3\text{-}8c)$$

The molar volumes V were calculated from those of pure melts on the assumption of additivity. Internal mobiliteis calculated from (8a-8c) and isotherms of b_{Na}, b_K and b_{Cs} in this system at 1023K are shown in Table 3-2 and **Fig. 3-4**, respectively. The orders of the internal mobilities are expressed by

$$b_{Cs} < b_{Na} < b_K \ (x_{Cs}=0.099 \pm 0.001) \quad (3\text{-}9a)$$

$$b_{Na} < b_{Cs} < b_K \ (x_{Cs}=0.137 \pm 0.007) \quad (3\text{-}9b)$$

$$b_{Na} < b_K < b_{Cs} \ (x_{Cs}>0.607 \pm 0.011) \quad (3\text{-}9c)$$

These behaviors mean that the Chemla effect occurs in this system.

§ III-iii-ii Self-Exchange Velocity(SEV) Calculated by MD

The separating motion of neighboring cation and anion can be expressed in terms of the self-exchange velocity (SEV)[7, 24] which can be calculated by molecular dynamics simulation. The SEV is defined by

$$v_{+-} = \frac{(R_2 - \langle R(0) \rangle)}{\tau} \quad (3\text{-}10)$$

where R_2 is the distance where the cation-anion correlation function crosses unity for the second time and $\langle R(0) \rangle$ is the average distance between cation and anion within R_2 at a given time origin. The SEV's calculated in the present study are shown in **Fig. 3-5** and **Table 3-3**. The orders of the v's are as follows.

$$v_{Cs} < v_{Na} < v_K \ (x_{Cs}=0.10) \quad (3\text{-}11a)$$

$$v_{Na} < v_{Cs} < v_K \ (x_{Cs}=0.14) \quad (3\text{-}11b)$$

$$v_{Na} < v_K < v_{Cs} \ (x_{Cs}>0.60) \quad (3\text{-}11c)$$

These orders are relatively in good agreement with those for the internal mobilities obtained experimentally. It is reported that the strong correlation between internal mobilities and SEV's for some alkali chlorides[7]. It is shown that the relationship between internal mobilities and SEV's in this experiment in **Fig. 3-6**. It seems that there is an approximately linear relation between two entities. Thus, the assumption seems to be verified and the Chemla effect of this system is reproduced by the SEV's obtained from the simulation.

§ III-iii-iii Transport Number Estimated by Original Equation

On the other hand, we can estimate the order of mobility from calculating the transport number using the software (Mathematica Ver2.2). The definition of the mobilities for the ternary system can not be defined accurately because the total transported charge is used for separation of two cations in the ternary system. Therefore, we revised the equation as follows.

$$\frac{t_1}{x_1}-\frac{t_2}{x_2}=\frac{-F}{(t_1+t_2)Q}\left(\frac{N_1}{x_1}-\frac{N_2}{x_2}\right) \tag{3-12a}$$

$$\frac{t_1}{x_1}-\frac{t_3}{x_3}=\frac{-F}{(t_1+t_3)Q}\left(\frac{N_1}{x_1}-\frac{N_3}{x_3}\right) \tag{3-12b}$$

$$\frac{t_2}{x_2}-\frac{t_3}{x_3}=\frac{-F}{(t_2+t_3)Q}\left(\frac{N_2}{x_2}-\frac{N_3}{x_3}\right) \tag{3-12c}$$

$$t_1+t_2+t_3=1 \tag{3-12d}$$

where t_1, t_2 and t_3 are transport numbers for each cation. $(t_1+t_2)Q$ means the transported charge for separation between cation 1 and 2. The transported numbers, which are calculated by (12a)-(12d) equations, divided by the mole fraction of Cs are shown in **Fig. 3-7**. It is speculated the order of the mobilities for each cation as follows.

$$b_{Cs}<b_{Na}<b_K \ (x_{Cs}<0.2) \tag{3-13a}$$

$$b_{Na}<b_K<b_{Cs} \ (x_{Cs}>0.6) \tag{3-13b}$$

It is reported the mobilities in the CsCl-NaCl system from estimating the EMF methods[2] and this tendency is consistent with our results.

The pair correlation function $g_{ij}(r)$ of j about i is defined as follows.

$$g_{ij}(r) = \left\langle \frac{1}{N_i} \sum_{i=1}^{N_i} \frac{n_{ij}(r, r+\Delta r)}{4\pi\rho_j r^2 \Delta r} \right\rangle \tag{3-14}$$

The running coordination number $n_{ij}(r)$ of j about i is defined by

$$n_{ij}(r) = 4\pi \frac{N_j}{V} \int_0^r r'^2 g_{ij}(r') dr' \tag{3-15}$$

where N_j is the number of atoms j in V which is the volume of the simulation cell. Here, the first coordination shell of ion j about ion i can be defined by the distance at which $g_{ij}(r)$ becomes unity for the second time, or by the distance r where $g_{ij}(r)$ reached its first minimum. The pair correlation function and running coordination numbers of the pure CsCl salt and of the binary and ternary mixtures for various compositions are shown in **Fig. 3-8** and **Table 3-4**. The position of the first peaks of the pair correlation functions $g_{\text{Na-Cl}}$, $g_{\text{K-Cl}}$ and $g_{\text{Cs-Cl}}$ are much the same in the binary mixture and the pure salts. As for the peak heights, $g_{\text{Na-Cl}}$ and $g_{\text{K-Cl}}$ are more sharply peaked in the ternary mixture than in the binary mixtures. $g_{\text{Cs-Cl}}$ is less sharply peaked in the ternary mixtures than in the pure CsCl salt. The increasing rate of the peak heights for Na and K is larger than for Cs. The position of the second peak of g_{+-} is more distant for NaCl, KCl and less distant for CsCl in the ternary mixture than in the respective binary and pure salts, with increasing the ratio of Cs, as shown in Fig. 3-8. The position of the second peaks is strongly affected by the number density, as pointed out for pure salts in reference[25]. To explain this point, Dixon and Sangster[25, 26] have presumed that with decreasing density the second-neighbor ions move out, having more space available to them, and consequently unlike ions can cluster round a reference ion with less interference from the second neighbors. Another characteristic of g_{+-} of the mixture as compared to that of the pure salts is the more rapid disappearance of the pair correlation in the long distance. This is due to the presence of cations with quite different sizes in the mixture.

The self-diffusion coefficients were calculated from the mean square displacements, which is shown in **Fig. 3-9-1**, according to the Einstein formula

$$D = \frac{1}{6}\frac{d}{d\tau}\left\langle \left\{ r_i(t+\tau) - r_i(t) \right\}^2 \right\rangle \tag{3-16}$$

where τ is the period during which the mean square displacement lies on a straight line and brackets denote an ensemble average of time origins. The results obtained with the simulation as shown in **Fig. 3-9-2** predict that in this ternary mixture the order of the self-diffusion coefficient for each cation would be the following order.

$$D_{Cs} < D_{Na} < D_K \ (x_{Cs}=0.1) \tag{3-17a}$$

$$D_{Na} < D_{Cs} < D_K \ (x_{Cs}=0.6) \tag{3-17b}$$

This is consistent with observations on our experimental results, where the Chemla effect is observed for pair of Na-Cs.

It can be understood by the potential for the cations located between two Cl^- ions as shown in **Figs. 3-10-1** and **3-10-2**. These potentials are obtained by combining the pair potentials for Li^+-Cl^-, Na^+-Cl^-, K^+-Cl^- and Cs^+-Cl^-. We can consider the one-dimensional motion of the cations leaving the reference Cl^- ion. As the concentration of Cs^+ increases, the molar volume and the average Cl^--Cl^- distance increase d_1 to d_2. Figure 3-10-1 shows that the barrier h_1 to h_2 becomes higher with increasing the molar volume and its rate of increase is very rapid for the Na^+ ion. When d is small, the Cs^+ ion can move away from the reference Cl^- ion, as the two Cl^- ions separate. At large d, the Na^+ ion has to wait for a longer time than the Cs^+ ion and h becomes so low that the cation can move away from the reference Cl^- ion. In other words, Na^+-Cs^- pair is more associated, Thus, the SEV will decrease with increasing d, but the decreasing rate is larger for Na than for Cs. Thus, the SEV's of Na and Cs will have a crossing point and isotherms of two internal mobilities have a Chemla crossing point.

§ III-iii-iv Electric Conductivity Calculated by MD

In general, in the case of the calculation of electric conductivity for molten salt system, Nernst-Einstein equation cannot be applied. Therefore the electric conductivity is calculated from the integral of the current auto-correlation function according to the following relation.

$$\sigma = \frac{1}{kT}\int_0^\infty \langle \mathbf{j}(0)\cdot\mathbf{j}(t)\rangle, \quad \mathbf{j}(t) = \sum_i z_i e \mathbf{v}_i(t) \tag{3-18}$$

One of the current auto-correlation function, **j**(t) and the electric conductivity profiles in molten ternary system at x_{Cs}=0.1 as shown in **Figs. 3-11-1** and **3-11-2**, respectively. Time step is 5fs and MD step is up to 5×10^6 steps. **Fig. 3-12** shows that the electric conductivity calculated from MD compared with the experimental results. The values calculated from MD simulation are smaller than the experimental results. This might be due to not supplementing by taking into account the polarization effects of CsCl. Recently, Wilson and Madden proposed a polarizable ion model (PIM)[27]. According to this model, ions are not simply charged hard spheres; their properties change profoundly with their environment and they may undergo polarization and dispersion interactions. The details are described elsewhere[28)-(30)]. However, both tendencies are reproduced by MD simulation, i.e., the electric conductivity is decreasing with increasing the Cs concentration.

On the other hand, the electric conductivity for (Li, Cs)Cl calculated by MD is compared with (Rb, Cs)Cl, which is selected as the candidate has extremely difference in ionic radii. One of the auto-correlation function and the electric conductivity profiles for molten binary system (Li, Cs)Cl and (Rb, Cs)Cl show in **Figs. 3-13-1** and **3-13-2**, respectively. The calculation results are similar tendency for experimental results as shown in **Fig. 3-13-3**. The difference of the electric conductivities between (Li, Cs)Cl and (Rb, Cs)Cl is caused by the difference of the self-diffusion coefficients for them as shown in **Fig. 3-14**. It was demonstrated that this mechanism is arose from the Chemla effect proposed by Markov[31, 32], which means that the mobilities for each cation changes by the compositions.

Table 3-1-1 Parameters for the pair potentials used in the MD simulations as for the molten ternary system (Na, K, Cs)Cl at 1023K.

System NaCl-KCl-CsCl	Number of ions Na^+ K^+ Cs^+ Cl^-	Density kg/m^3	Ion pair	A_{ij}	c_{ij} $10^{-79}Jm^6$	d_{ij} $10^{-99}Jm^8$
(45:45:10)	225 225 50 500	1.706	Na-Na	1.25	1.68	0.80
			Na-K	1.25	6.27	4.59
			Na-Cs	1.25	15.06	17.36
			Na-Cl	1.00	11.22	14.07
			K-K	1.25	24.3	24.0
			K-Cs	1.25	60.11	84.65
			K-Cl	1.00	47.61	71.88
			Cs-Cs	1.25	152.0	278.0
			Cs-Cl	1.00	126.74	244.66
			Cl-Cl	0.75	121.07	246.01

b=0.338 × 10^{-19}J, r_{Na}=117.0pm, r_K=146.3pm, r_{Cs}=172.0pm, r_{Cl}=158.5pm, ρ =32.43pm, AL=3.3418129nm

System NaCl-KCl-CsCl	Number of ions Na^+ K^+ Cs^+ Cl^-	Density kg/m^3	Ion pair	A_{ij}	c_{ij} $10^{-79}Jm^6$	d_{ij} $10^{-99}Jm^8$
(43:43:14)	172 172 56 400	1.766	Na-Na	1.25	1.68	0.80
			Na-K	1.25	6.27	4.59
			Na-Cs	1.25	15.06	17.36
			Na-Cl	1.00	11.25	14.11
			K-K	1.25	24.3	24.0
			K-Cs	1.25	60.11	84.65
			K-Cl	1.00	47.70	72.02
			Cs-Cs	1.25	152.0	278.0
			Cs-Cl	1.00	126.96	245.13
			Cl-Cl	0.75	121.42	246.79

b=0.338 × 10^{-19}J, r_{Na}=117.0pm, r_K=146.3pm, r_{Cs}=172.0pm, r_{Cl}=158.5pm, ρ =32.32pm, AL=3.1201063nm

System NaCl-KCl-CsCl	Number of ions Na^+ K^+ Cs^+ Cl^-	Density kg/m^3	Ion pair	A_{ij}	c_{ij} $10^{-79}Jm^6$	d_{ij} $10^{-99}Jm^8$
(35:35:30)	175 175 150 500	1.984	Na-Na	1.25	1.68	0.80
			Na-K	1.25	6.27	4.59
			Na-Cs	1.25	15.06	17.36
			Na-Cl	1.00	11.33	14.23
			K-K	1.25	24.3	24.0
			K-Cs	1.25	60.11	84.65
			K-Cl	1.00	47.04	72.61
			Cs-Cs	1.25	152.0	278.0
			Cs-Cl	1.00	127.83	246.97
			Cl-Cl	0.75	122.81	249.94

b=0.338 × 10^{-19}J, r_{Na}=117.0pm, r_K=146.3pm, r_{Cs}=172.0pm, r_{Cl}=158.5pm, ρ =31.89pm, AL=3.43732nm

System NaCl-KCl-CsCl	Number of ions Na^+ K^+ Cs^+ Cl^-	Density kg/m^3	Ion pair	A_{ij}	c_{ij} $10^{-79}Jm^6$	d_{ij} $10^{-99}Jm^8$
(30:30:40)	150 150 200 500	2.107	Na-Na	1.25	1.68	0.80
			Na-K	1.25	6.27	4.59
			Na-Cs	1.25	15.06	17.36
			Na-Cl	1.00	11.39	14.31
			K-K	1.25	24.3	24.0
			K-Cs	1.25	60.11	84.65
			K-Cl	1.00	48.26	72.97
			Cs-Cs	1.25	152.0	278.0
			Cs-Cl	1.00	128.37	248.13
			Cl-Cl	0.75	123.69	251.92

b=0.338 × 10^{-19}J, r_{Na}=117.0pm, r_K=146.3pm, r_{Cs}=172.0pm, r_{Cl}=158.5pm, ρ =31.62pm, AL=3.48320nm

System NaCl-KCl-CsCl	Number of ions Na^+ K^+ Cs^+ Cl^-	Density kg/m^3	Ion pair	A_{ij}	c_{ij} 10^{-79}Jm^6	d_{ij} 10^{-99}Jm^8
(25:25:50)	125 125 250 500	2.221	Na-Na	1.25	1.68	0.80
			Na-K	1.25	6.27	4.59
			Na-Cs	1.25	15.06	17.36
			Na-Cl	1.00	11.44	14.38
			K-K	1.25	24.3	24.0
			K-Cs	1.25	60.11	84.65
			K-Cl	1.00	48.47	73.34
			Cs-Cs	1.25	152.0	278.0
			Cs-Cl	1.00	128.92	249.29
			Cl-Cl	0.75	124.56	253.92

b=0.338 × 10^{-19}J, r_{Na}=117.0pm, r_K=146.3pm, r_{Cs}=172.0pm, r_{Cl}=158.5pm, ρ =31.35pm, AL=3.52789nm

System NaCl-KCl-CsCl	Number of ions Na^+ K^+ Cs^+ Cl^-	Density kg/m^3	Ion pair	A_{ij}	c_{ij} 10^{-79}Jm^6	d_{ij} 10^{-99}Jm^8
(20:20:60)	100 100 300 500	2.326	Na-Na	1.25	1.68	0.80
			Na-K	1.25	6.27	4.59
			Na-Cs	1.25	15.06	17.36
			Na-Cl	1.00	11.49	14.46
			K-K	1.25	24.3	24.0
			K-Cs	1.25	60.11	84.65
			K-Cl	1.00	48.69	73.71
			Cs-Cs	1.25	152.0	278.0
			Cs-Cl	1.00	129.46	250.45
			Cl-Cl	0.75	125.45	255.93

b=0.338 × 10^{-19}J, r_{Na}=117.0pm, r_K=146.3pm, r_{Cs}=172.0pm, r_{Cl}=158.5pm, ρ =31.35pm, AL=3.5713944nm

System NaCl-KCl-CsCl	Number of ions Na^+ K^+ Cs^+ Cl^-	Density kg/m^3	Ion pair	A_{ij}	c_{ij} $10^{-79}Jm^6$	d_{ij} $10^{-99}Jm^8$
(15:15:70)	75 75 350 500	2.424	Na-Na	1.25	1.68	0.80
			Na-K	1.25	6.27	4.59
			Na-Cs	1.25	15.06	17.36
			Na-Cl	1.00	11.55	14.54
			K-K	1.25	24.3	24.0
			K-Cs	1.25	60.11	84.65
			K-Cl	1.00	48.90	74.08
			Cs-Cs	1.25	152.0	278.0
			Cs-Cl	1.00	130.00	251.61
			Cl-Cl	0.75	126.33	257.95

b=0.338 × 10^{-19}J, r_{Na}=117.0pm, r_K=146.3pm, r_{Cs}=172.0pm, r_{Cl}=158.5pm, ρ =30.81pm, AL=3.6139375nm

System NaCl-KCl-CsCl	Number of ions Na^+ K^+ Cs^+ Cl^-	Density kg/m^3	Ion pair	A_{ij}	c_{ij} $10^{-79}Jm^6$	d_{ij} $10^{-99}Jm^8$
(10:10:80)	50 50 400 500	2.515	Na-Na	1.25	1.68	0.80
			Na-K	1.25	6.27	4.59
			Na-Cs	1.25	15.06	17.36
			Na-Cl	1.00	11.602	14.616
			K-K	1.25	24.3	24.0
			K-Cs	1.25	60.11	84.65
			K-Cl	1.00	49.121	74.446
			Cs-Cs	1.25	152.0	278.0
			Cs-Cl	1.00	130.548	252.773
			Cl-Cl	0.75	127.220	259.980

b=0.338 × 10^{-19}J, r_{Na}=117.0pm, r_K=146.3pm, r_{Cs}=172.0pm, r_{Cl}=158.5pm, ρ =30.54pm, AL=3.65569nm

System NaCl-KCl-CsCl	Number of ions Na^+ K^+ Cs^+ Cl^-	Density kg/m^3	Ion pair	A_{ij}	c_{ij} 10^{-79}Jm^6	d_{ij} 10^{-99}Jm^8
(5:5:90)	25 25 450 500	2.601	Na-Na	1.25	1.68	0.80
			Na-K	1.25	6.27	4.59
			Na-Cs	1.25	15.06	17.36
			Na-Cl	1.00	11.656	14.694
			K-K	1.25	24.3	24.0
			K-Cs	1.25	60.11	84.65
			K-Cl	1.00	49.338	74.817
			Cs-Cs	1.25	152.0	278.0
			Cs-Cl	1.00	131.093	253.938
			Cl-Cl	0.75	128.112	262.017

b=0.338 × 10^{-19}J, r_{Na}=117.0pm, r_K=146.3pm, r_{Cs}=172.0pm, r_{Cl}=158.5pm, ρ =30.27pm, AL=3.696245nm

System NaCl-KCl	Number of ions Na^+ K^+ Cl^-	Density kg/m^3	Ion pair	A_{ij}	c_{ij} 10^{-79}Jm^6	d_{ij} 10^{-99}Jm^8
(50:50)	250 250 500	1.550	Na-Na	1.25	1.68	0.8
			Na-K	1.25	6.27	4.59
			Na-Cl	1.00	11.28	14.15
			K-K	1.25	24.3	24.0
			K-Cl	1.00	47.82	72.24
			Cl-Cl	0.75	121.94	247.953

b=0.338×10^{-19}J, r_{Na}=117.0pm, r_K=146.3pm, r_{Cl}=158.5pm, ρ=32.7pm, AL=3.29004nm

System CsCl	Number of ions Cs^+ Cl^-	Density kg/m^3	Ion pair	A_{ij}	c_{ij} 10^{-79}Jm^6	d_{ij} 10^{-99}Jm^8
(100)	500 500	2.680	Cs-Cs	1.25	152.0	278.0
			Cs-Cl	1.00	129.0	250.0
			Cl-Cl	0.75	129.0	260.0

b=0.338×10^{-19}J, r_{Cs}=172.0pm, r_{Cl}=158.5pm, ρ=30.0pm, AL=3.73647nm

Table 3-1-2 Parameters for the pair potentials used in the MD simulations as for (Li, Cs)Cl and (Rb, Cs)Cl.

System LiCl-CsCl	Number of ions Li^+ Cs^+ Cl^-	Density kg/m^3	Ion pair	A_{ij}	c_{ij} $10^{-79}Jm^6$	d_{ij} $10^{-99}Jm^8$
(20:80)	100 400 500	2.591	Li-Li	2.000	0.073	0.030
			Li-Cs	1.625	2.837	3.177
			Li-Cl	1.375	2.058	2.496
			Cs-Cs	1.250	152.0	278.0
			Cs-Cl	1.000	129.861	249.525
			Cl-Cl	0.750	125.339	252.450

b=0.338×10^{-19}J, r_{Li}=81.6pm, r_{Cs}=172.0pm, r_{Cl}=158.5pm, ρ=33.56pm, AL=3.57986nm

System LiCl-CsCl	Number of ions Li^+ Cs^+ Cl^-	Density kg/m^3	Ion pair	A_{ij}	c_{ij} $10^{-79}Jm^6$	d_{ij} $10^{-99}Jm^8$
(40:60)	200 300 500	2.401	Li-Li	2.000	0.073	0.030
			Li-Cs	1.625	2.837	3.177
			Li-Cl	1.375	2.032	2.462
			Cs-Cs	1.250	152.0	278.0
			Cs-Cl	1.000	128.074	246.010
			Cl-Cl	0.750	121.707	244.982

b=0.338×10^{-19}J, r_{Li}=81.6pm, r_{Cs}=172.0pm, r_{Cl}=158.5pm, ρ=33.72pm, AL=3.44248nm

System LiCl-CsCl	Number of ions Li^+ Cs^+ Cl^-	Density kg/m^3	Ion pair	A_{ij}	c_{ij} $10^{-79}Jm^6$	d_{ij} $10^{-99}Jm^8$
(60:40)	300 200 500	2.149	Li-Li	2.000	0.073	0.030
			Li-Cs	1.625	2.837	3.177
			Li-Cl	1.375	2.005	2.429
			Cs-Cs	1.250	152.0	278.0
			Cs-Cl	1.000	126.271	242.466
			Cl-Cl	0.750	118.106	237.585

b=0.338×10^{-19}J, r_{Li}=81.6pm, r_{Cs}=172.0pm, r_{Cl}=158.5pm, ρ=33.88pm, AL=3.29722nm

System LiCl-CsCl	Number of ions Li^+ Cs^+ Cl^-	Density kg/m^3	Ion pair	A_{ij}	c_{ij} $10^{-79}Jm^6$	d_{ij} $10^{-99}Jm^8$
(80:20)	400 100 500	1.834	Li-Li	2.000	0.073	0.030
			Li-Cs	1.625	2.837	3.177
			Li-Cl	1.375	1.978	2.395
			Cs-Cs	1.250	152.0	278.0
			Cs-Cl	1.000	124.451	238.894
			Cl-Cl	0.750	114.538	230.262

$b=0.338\times10^{-19}$J, r_{Li}=81.6pm, r_{Cs}=172.0pm, r_{Cl}=158.5pm, ρ=34.04pm, AL=3.12773nm

System RbCl-CsCl	Number of ions Rb^+ Cs^+ Cl^-	Density kg/m^3	Ion pair	A_{ij}	c_{ij} $10^{-79}Jm^6$	d_{ij} $10^{-99}Jm^8$
(20:80)	100 400 500	2.623	Rb-Rb	1.25	59.4	82
			Rb-Cs	1.25	94.749	152.044
			Rb-Cl	1.00	79.948	135.629
			Cs-Cs	1.25	152.0	278.0
			Cs-Cl	1.00	131.589	252.725
			Cl-Cl	0.75	129.223	260.041

$b=0.338\times10^{-19}$J, r_{Rb}=158.7pm, r_{Cs}=172.0pm, r_{Cl}=158.5pm, ρ=33.08pm, AL=3.66339nm

System RbCl-CsCl	Number of ions Rb^+ Cs^+ Cl^-	Density kg/m^3	Ion pair	A_{ij}	c_{ij} $10^{-79}Jm^6$	d_{ij} $10^{-99}Jm^8$
(40:60)	200 300 500	2.529	Rb-Rb	1.25	59.4	82
			Rb-Cs	1.25	94.749	152.044
			Rb-Cl	1.00	79.898	135.423
			Cs-Cs	1.25	152.0	278.0
			Cs-Cl	1.00	131.537	252.424
			Cl-Cl	0.75	129.435	260.070

$b=0.338\times10^{-19}$J, r_{Rb}=158.7pm, r_{Cs}=172.0pm, r_{Cl}=158.5pm, ρ=32.76pm, AL=3.66038nm

System RbCl-CsCl	Number of ions Rb^+ Cs^+ Cl^-	Density kg/m^3	Ion pair	A_{ij}	c_{ij} 10^{-79}Jm^6	d_{ij} 10^{-99}Jm^8
(60:40)	300 200 500	2.433	Rb-Rb	1.25	59.4	82
			Rb-Cs	1.25	94.749	152.044
			Rb-Cl	1.00	79.844	135.208
			Cs-Cs	1.25	152.0	278.0
			Cs-Cl	1.00	131.477	252.108
			Cl-Cl	0.75	129.635	260.076

b=0.338×10^{-19}J, r_{Rb}=158.7pm, r_{Cs}=172.0pm, r_{Cl}=158.5pm, ρ=32.44pm, AL=3.62768nm

System RbCl-CsCl	Number of ions Rb^+ Cs^+ Cl^-	Density kg/m^3	Ion pair	A_{ij}	c_{ij} 10^{-79}Jm^6	d_{ij} 10^{-99}Jm^8
(80:20)	400 100 500	2.335	Rb-Rb	1.25	59.4	82
			Rb-Cs	1.25	94.749	152.044
			Rb-Cl	1.00	79.784	134.985
			Cs-Cs	1.25	152.0	278.0
			Cs-Cl	1.00	131.408	251.776
			Cl-Cl	0.75	129.824	260.059

b=0.338×10^{-19}J, r_{Rb}=158.7pm, r_{Cs}=172.0pm, r_{Cl}=158.5pm, ρ=32.12pm, AL=3.59265nm

Table 3-2 Main experimental conditions and the internal mobilities in the molten system (Na, K, Cs)Cl at 1023K.

Run No.	x_{Cs}	Q	ε_{NaCs}	ε_{KCs}	ε_{NaK}	κ	V_m	b_{Na}	b_K	b_{Cs}
		(C)				(Sm^{-1})	(10^{-6} m^3mol^{-1})	(10^{-8} $m^2V^{-1}s^{-1}$)		
1	0.011±0.003	2088	0.0005±0.002	0.026±0.002	-0.025±0.004	245.4	43.18	10.85±0.03	11.12±0.03	10.84±0.02
2	0.013±0.005	6221	0.014±0.003	0.050±0.003	-0.036±0.006	245.0	43.22	10.78±0.02	11.18±0.02	10.63±0.03
3	0.013±0.005	7920	0.022±0.003	0.054±0.003	-0.033±0.007	245.0	43.22	10.80±0.02	11.16±0.02	10.57±0.04
4	0.019±0.008	9373	0.016±0.002	0.056±0.002	-0.040±0.006	243.5	43.34	10.73±0.03	11.16±0.02	10.55±0.03
5	0.040±0.002	4320	0.026±0.004	0.049±0.004	-0.024±0.003	239.1	43.71	10.74±0.03	11.00±0.03	10.46±0.02
6	0.099±0.001	5120	0.008±0.001	0.061±0.001	-0.054±0.003	225.9	44.91	10.27±0.06	10.83±0.07	10.19±0.07
7	0.137±0.007	4518	-0.007±0.000	0.024±0.000	-0.031±0.001	218.6	45.62	10.19±0.06	10.51±0.04	10.26±0.05
8	0.157±0.002	6523	-0.008±0.001	0.038±0.001	-0.046±0.003	214.9	46.00	10.04±0.04	10.51±0.06	10.12±0.07
9	0.574±0.018	5040	-0.057±0.003	0.002±0.003	-0.058±0.001	160.4	54.29	8.62±0.02	9.15±0.02	9.14±0.01
10	0.607±0.011	4320	-0.062±0.001	-0.014±0.001	-0.048±0.006	157.7	54.99	8.57±0.04	9.00±0.03	9.12±0.03
11	0.674±0.011	6000	-0.051±0.001	-0.016±0.001	-0.051±0.008	153.5	56.24	8.56±0.06	9.02±0.05	9.02±0.05
12	0.703±0.018	4500	-0.074±0.002	-0.019±0.002	-0.054±0.011	151.3	57.01	8.41±0.03	8.89±0.04	9.07±0.07
13	0.713±0.015	5040	-0.099±0.001	-0.008±0.001	-0.091±0.009	151.1	57.09	8.20±0.07	9.01±0.06	9.08±0.06
14	0.753±0.014	6300	-0.096±0.002	-0.012±0.002	-0.084±0.019	149.2	57.81	8.21±0.06	8.96±0.08	9.06±0.12

The sign ± for x_{Cs}, ε and b indicates the errors due to the chemical analysis.

Table 3-3 Self-exchange velocities and internal mobilities.

System	v (ms^{-1})			b ($10^{-8}m^2V^{-1}s^{-1}$)		
(Na:K:Cs)	Na-Cl	K-Cl	Cs-Cl	Na-Cl	K-Cl	Cs-Cl
45:45:10	72.37	80.06	72.15	10.27	10.83	10.19
43:43:14	70.50	78.08	72.96	10.19	10.51	10.26
20:20:60	50.89	54.37	55.05	8.57	9.00	9.12
15:15:70	44.80	47.62	60.29	8.41	8.89	9.07

Table 3-4 Characteristic values of the $g_{ij}(r)$'s for cation-anion and anion-anion pairs. R_1 and R_2 are the distances where $g_{ij}(r)$ crosses unity for the first and second time, respectively. R_M and R_m are the distances at the first maximum and minimum, respectively. $n_{eq}(R_2\text{-}R_m)$ is the partial equivalent coordination number within $R_2\text{-}R_m$ of a cation, which is equal to the coordination number of Cl^- around the cation.

System (Na:K:Cs)	Ion Pair	R_1/nm	R_M/nm	$g(R_M)$	R_2/nm	R_m/nm	$n_{eq}(R_2\text{-}R_m)$
(45:45:10)	Na-Cl	0.229	0.260	4.72	0.326	0.408	3.63-4.58
	K-Cl	0.266	0.300	3.59	0.370	0.439	4.13-5.40
	Cs-Cl	0.298	0.330	3.10	0.405	0.489	4.73-6.57
(43:43:14)	Na-Cl	0.228	0.256	4.88	0.326	0.400	3.60-4.44
	K-Cl	0.268	0.299	3.73	0.371	0.456	4.21-5.68
	Cs-Cl	0.298	0.332	3.13	0.404	0.483	4.73-6.46
(20:20:60)	Na-Cl	0.231	0.259	5.86	0.329	0.425	3.52-4.36
	K-Cl	0.268	0.299	4.44	0.371	0.465	4.00-5.29
	Cs-Cl	0.298	0.332	3.77	0.407	0.503	4.58-6.17
(15:15:70)	Na-Cl	0.229	0.261	6.17	0.327	0.422	3.48-4.31
	K-Cl	0.266	0.299	4.63	0.374	0.468	4.02-5.27
	Cs-Cl	0.298	0.330	3.88	0.404	0.512	3.60-6.19
(50:50:0)	Na-Cl	0.228	0.260	4.47	0.328	0.405	3.66-4.67
	K-Cl	0.266	0.300	3.41	0.371	0.440	4.25-5.59
(0:0:100)	Cs-Cl	0.298	0.332	4.33	0.404	0.513	4.30-5.81

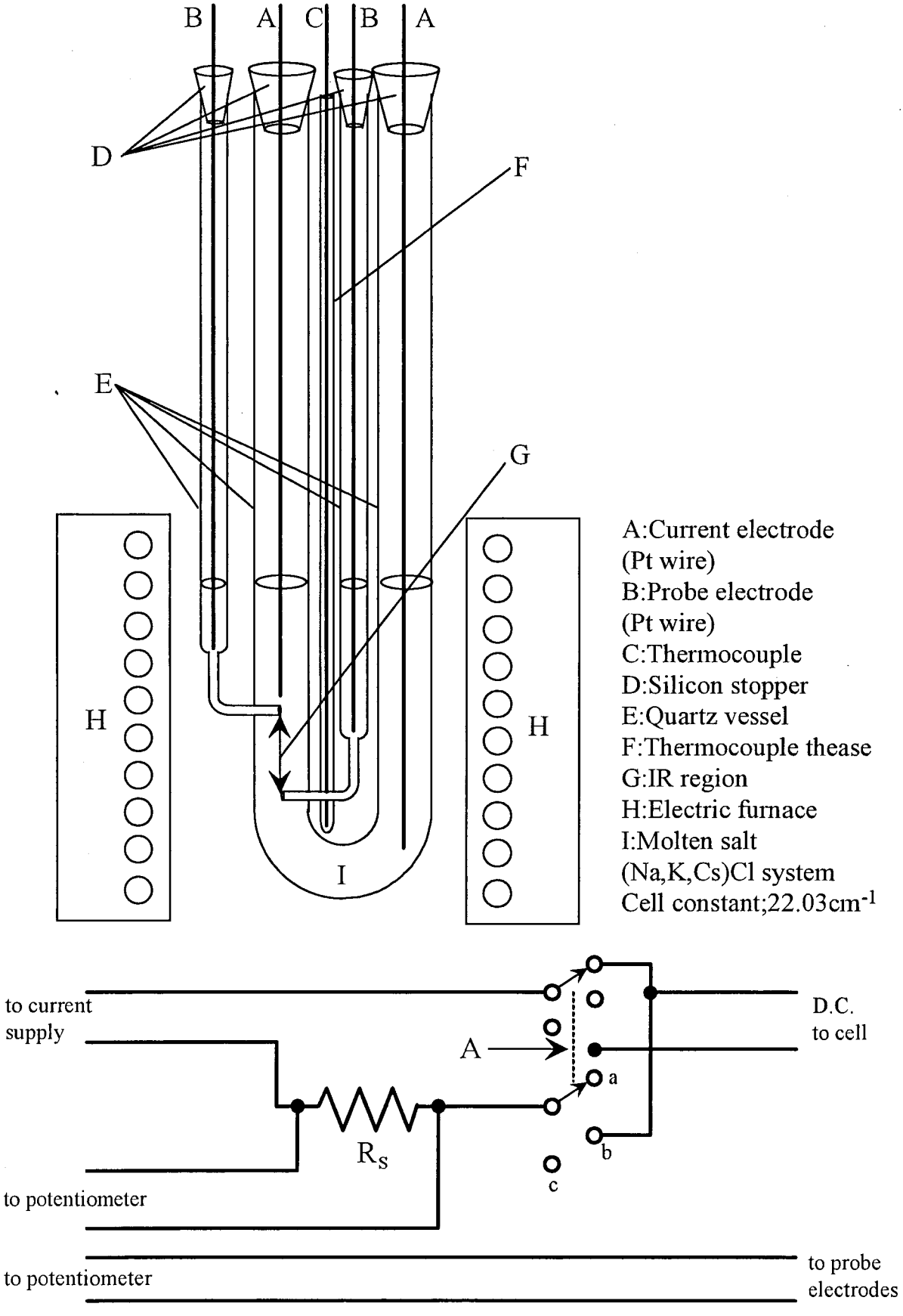

Fig. 3-1 Schematic diagram for the electric conductivity measurement

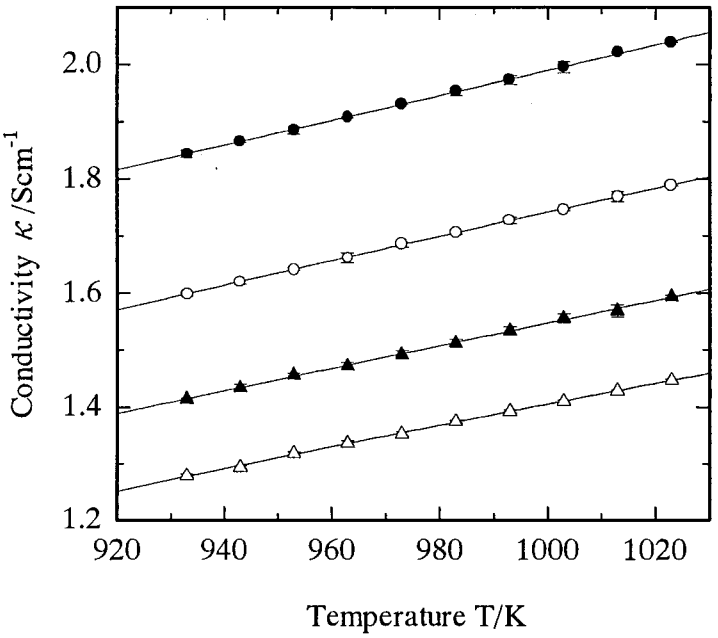

Fig. 3-2 Relationship between the temperature and the conductivities for each compositions of caesium, —●—; $\kappa_1(x_{Cs}=0.202\pm0.006)$, —○—; $\kappa_2(x_{Cs}=0.397\pm0.002)$, —▲—; $\kappa_3(x_{Cs}=0.592\pm0.003)$, —△—; $\kappa_4(x_{Cs}=0.782\pm0.013)$.

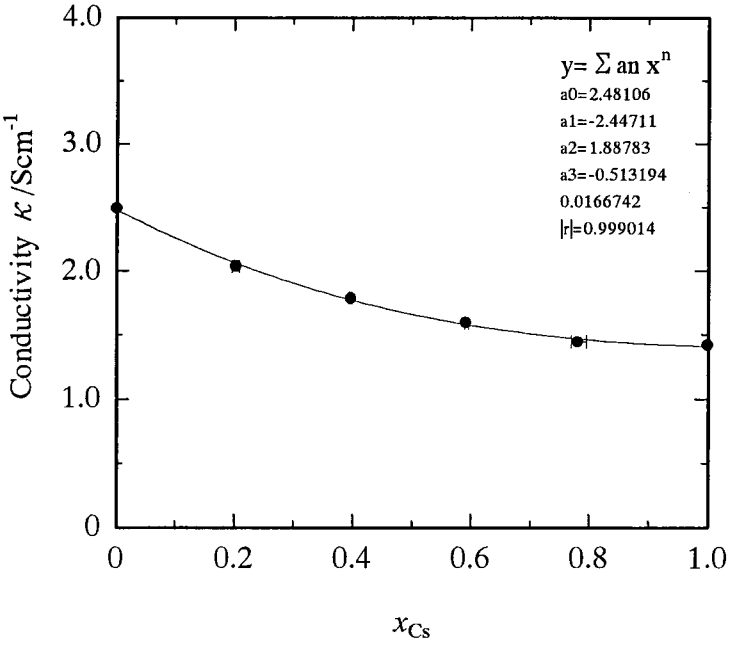

Fig. 3-3 Relationship between the mole fraction of caesium and the conductivity at 1023K.

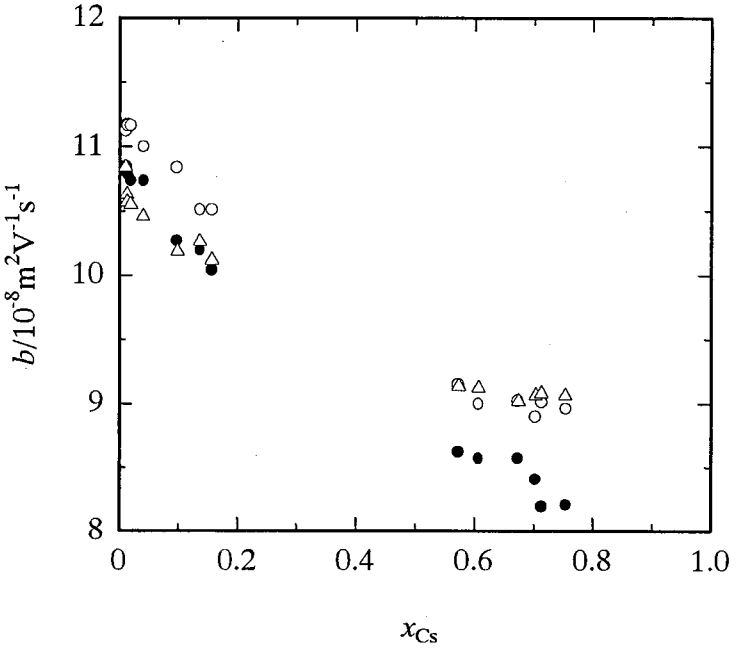

Fig. 3-4 Isotherms of b_{Na}, b_K and b_{Cs} in the molten system (Na, K, Cs)Cl at 1023K, ●: b_{Na}, ○: b_K, △: b_{Cs}

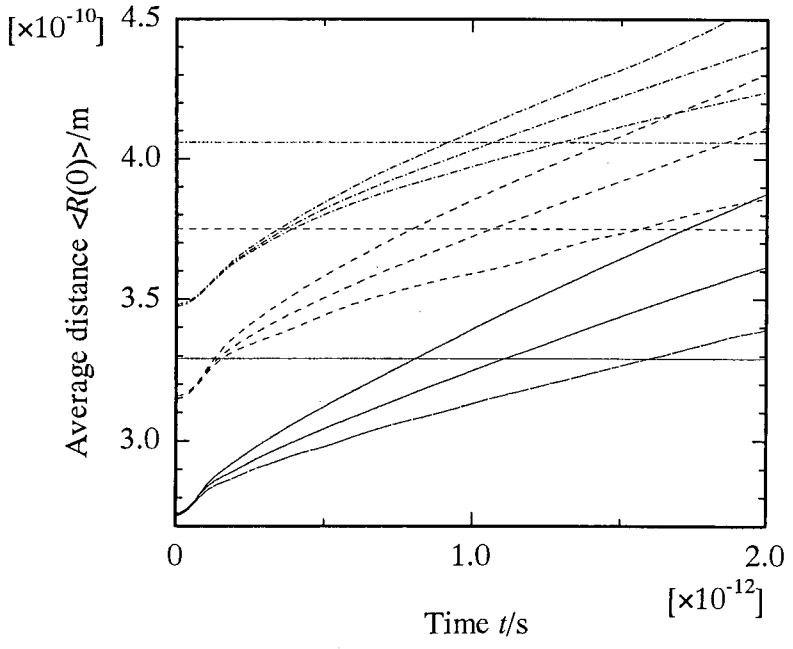

Fig. 3-5 Evolution of the average distances of marked cations from a Cl^- ion, ———; Na^+, - - - ; K^+, — - —; Cs^+

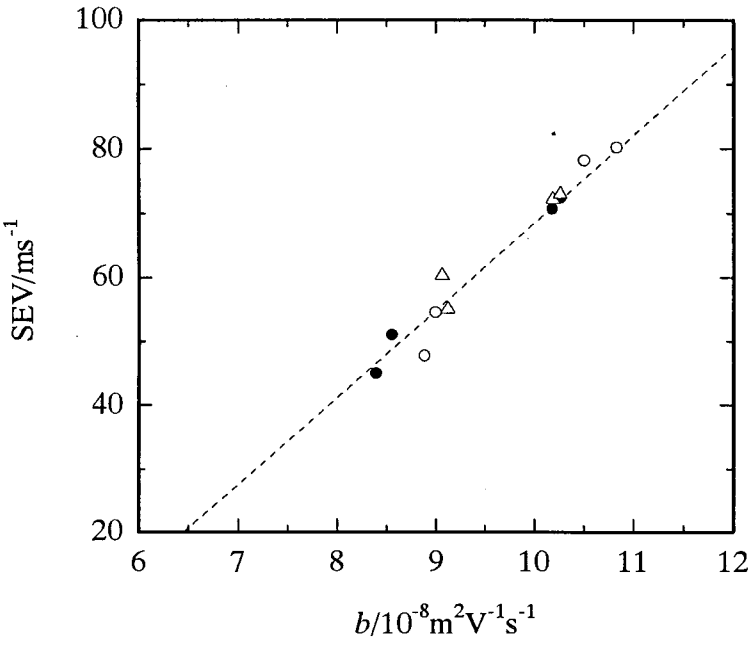

Fig. 3-6 Relationship between the internal mobilities and SEV's at 1023K,

●: b_{Na}, ○: b_K, △: b_{Cs}

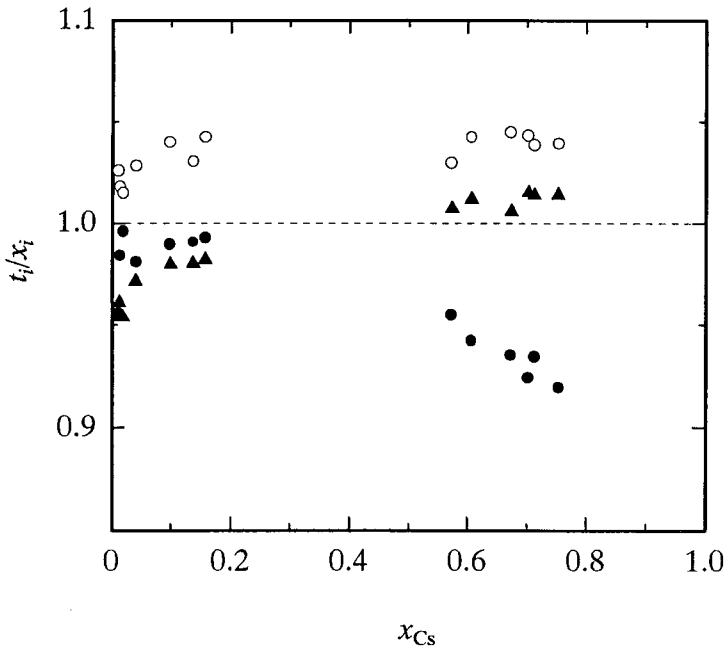

Fig. 3-7 Relationship between t_i/x_i and the mole fraction of Cs,

●: t_{Na}/x_{Na}, ○: t_K/x_K, △: t_{Cs}/x_{Cs}

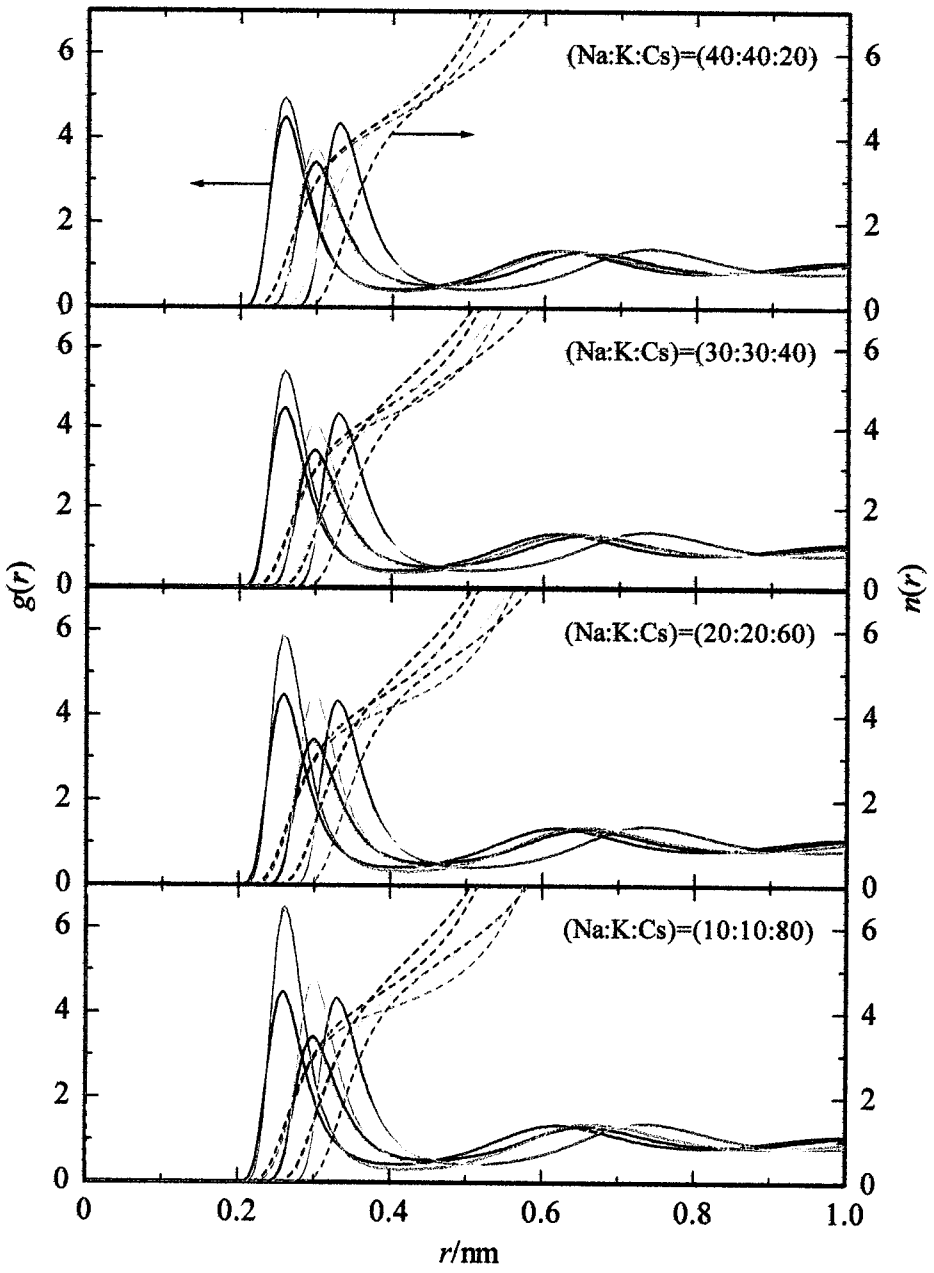

———; $g_{Cs\text{-}Cl}$ in pure CsCl system, ····· ; coordination number

———; $g_{Na\text{-}Cl}$ in binary system (Na, K)Cl, ····· ; coordination number

———; $g_{K\text{-}Cl}$ in binary system (Na, K)Cl, ····· ; coordination number

; $g_{Na\text{-}Cl}$ in ternary system (Na, K, Cs)Cl, ····· ; coordination number

; $g_{K\text{-}Cl}$ in ternary system (Na, K, Cs)Cl, ; coordination number

; $g_{Cs\text{-}Cl}$ in ternary system (Na, K, Cs)Cl, ; coordination number

Fig. 3-8 Pair correlation functions $g_{+-}(r)$ and running coordination numbers $n(r)$.

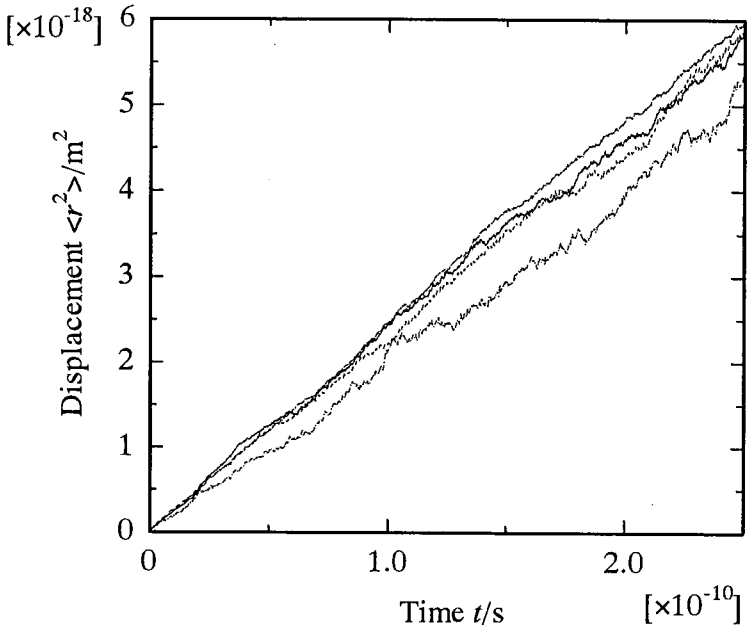

Fig. 3-9-1 Mean-square displacement of Na^+, K^+, Cs^+ and Cl^- in molten ternary system (Na, K, Cs)Cl at 1023K, x_{Cs}=0.1, ———; Na^+, - - - -; K^+, — - —; Cs^+, —·· —; Cl^-

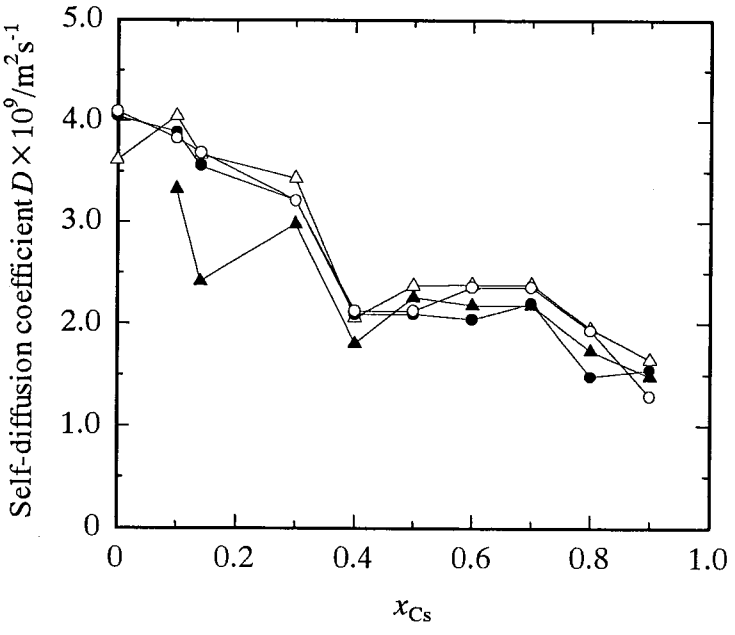

Fig. 3-9-2 Relationship between the self-diffusion coefficients and the mole fraction of Cs in molten ternary system (Na, K, Cs)Cl at 1023K, —●—; Na^+, —○—; K^+, —▲—; Cs^+, —△—; Cl^-

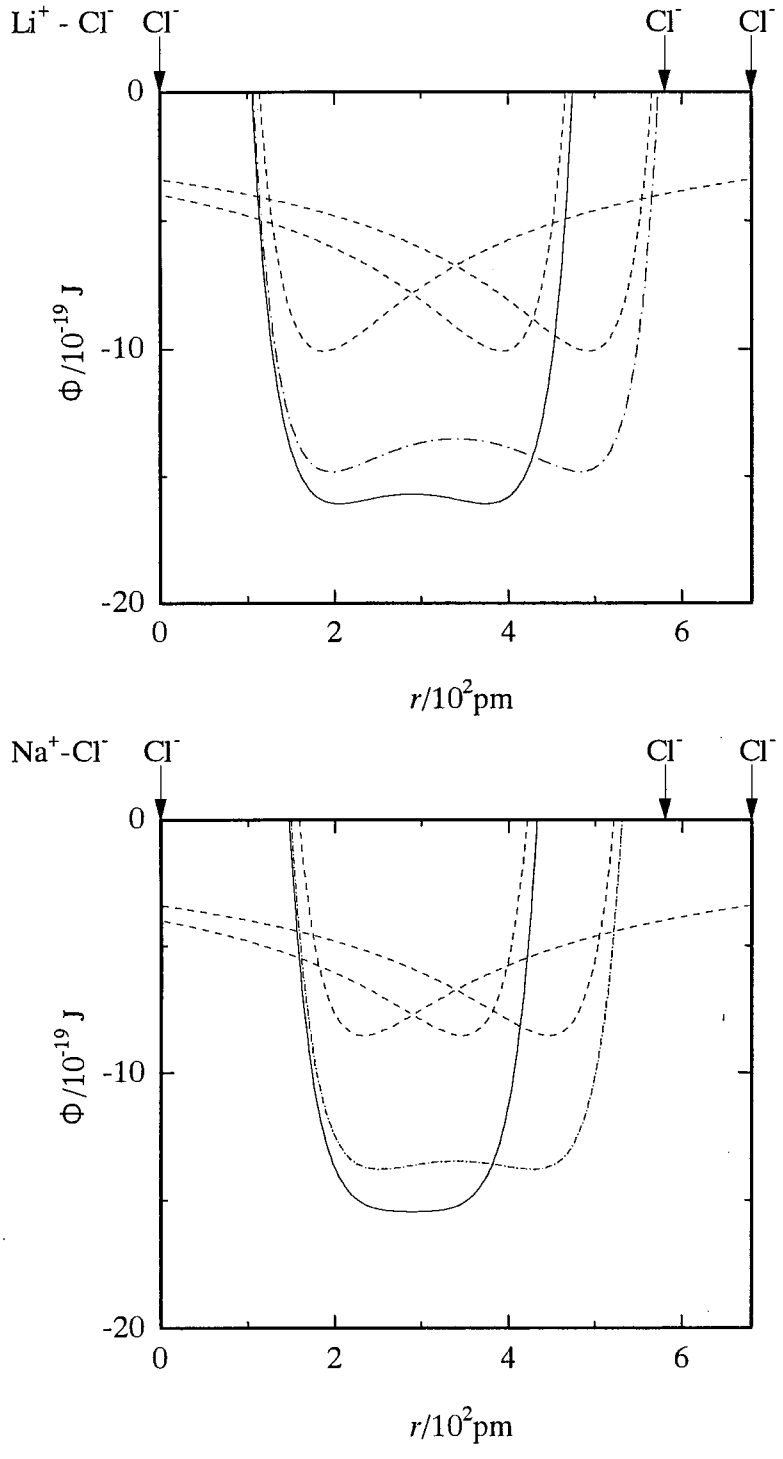

Fig. 3-10-1 The schematic diagram for the potential profiles felt by Li^+ and Na^+ ions located between two Cl^- ions separated by the distance (a) l=580pm and (b) l=680pm,

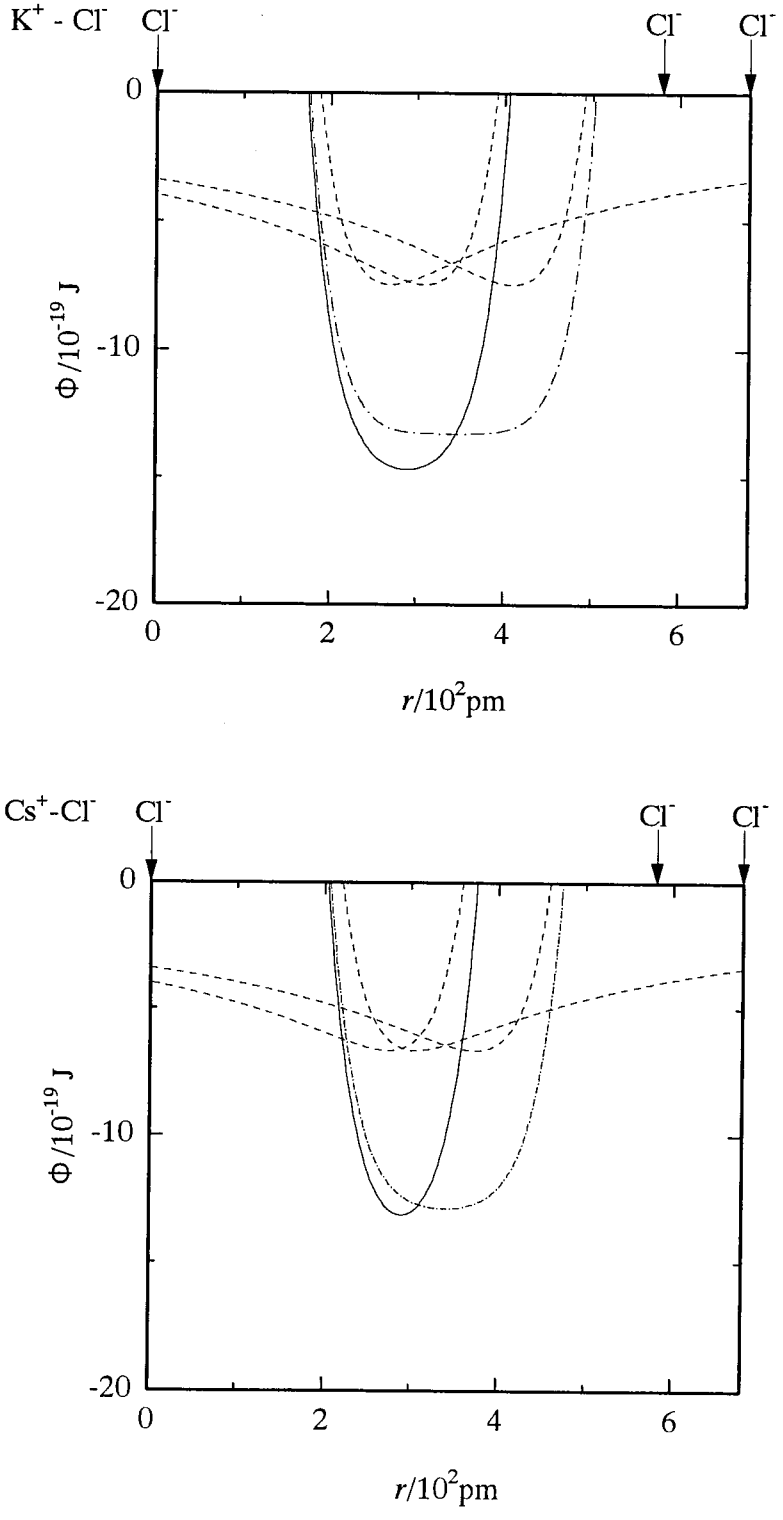

Fig. 3-10-2 The schematic diagram for the potential profiles felt by K^+ and Cs^+ ions located between two Cl^- ions separated by the distance (a) l=580pm and (b) l=680pm,

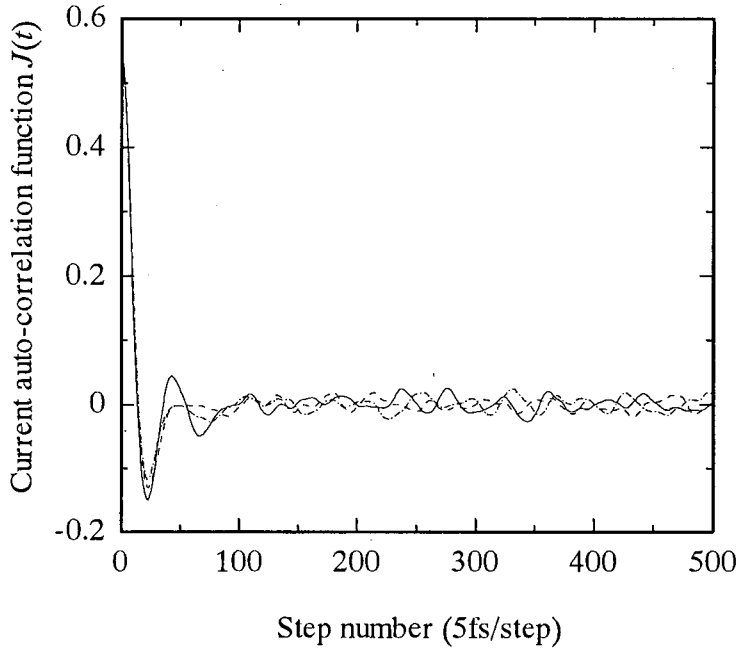

Fig. 3-11-1 One of the auto-correlation function profiles in molten ternary system (Na, K, Cs)Cl at 1023K, x_{Cs}=0.1, ———; 3×10^5 steps, - - -; 4×10^5 steps, — - —; 5×10^5 steps

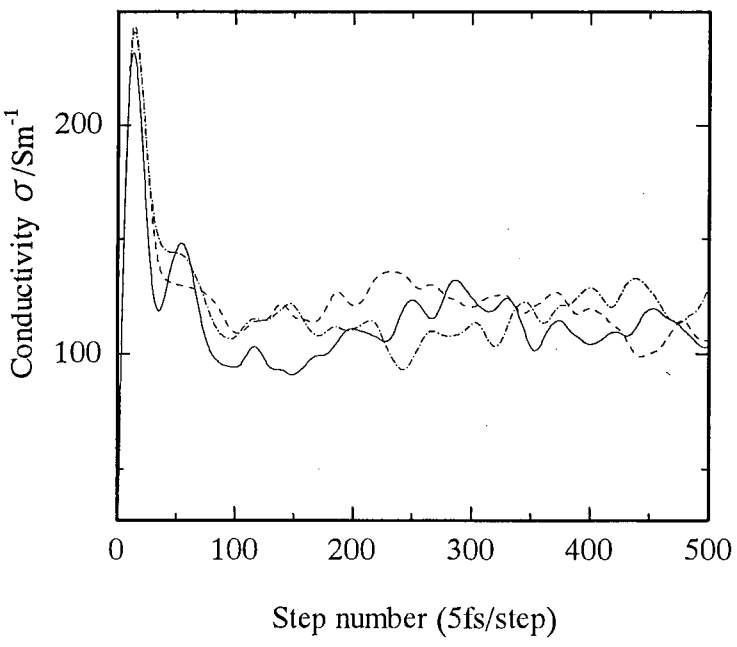

Fig. 3-11-2 One of the electric conductivity profiles in molten ternary system (Na, K, Cs)Cl at 1023K, x_{Cs}=0.1, ———; 3×10^5 steps, - - -; 4×10^5 steps, — - —; 5×10^5 steps

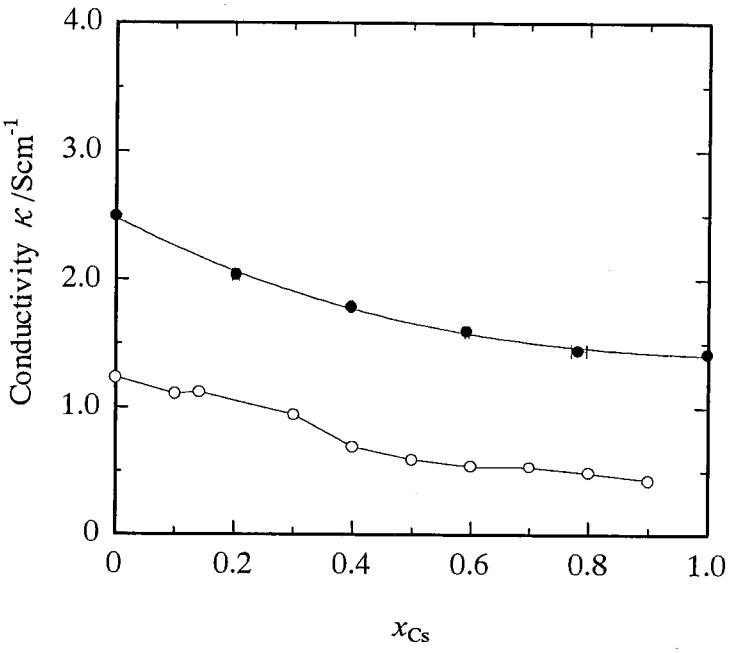

Fig. 3-12 Relationship between the electric conductivity and the mole fraction of Cs in molten ternary system (Na, K, Cs)Cl at 1023K compared with MD simulation, —●—; Experimental results, —○—; MD simulation

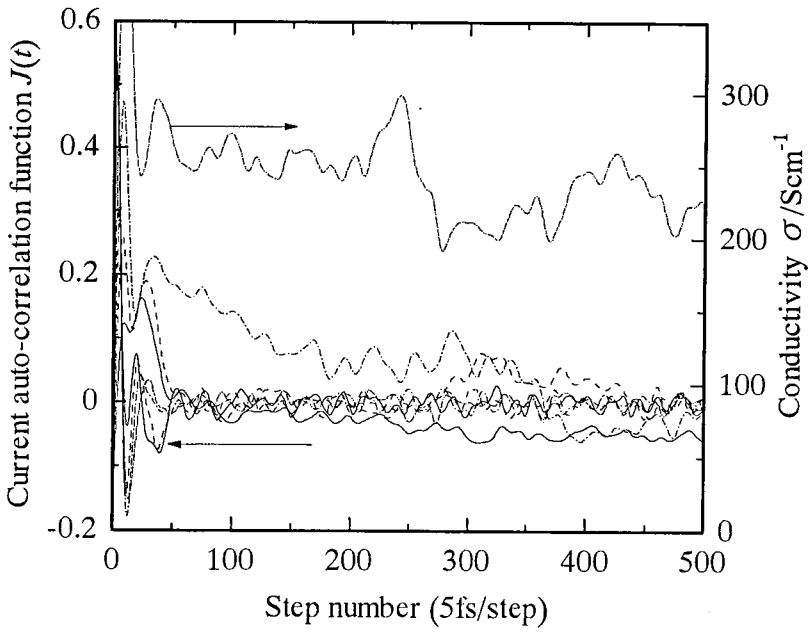

Fig. 3-13-1 One of the auto-correlation function and the electric conductivity profiles in molten binary system (Li, Cs)Cl at 1000K, 5×10^5 steps, ———; x_{Li}=0.2, - - -; x_{Li}=0.4, — - —; x_{Li}=0.6, —·—x_{Li}=0.8

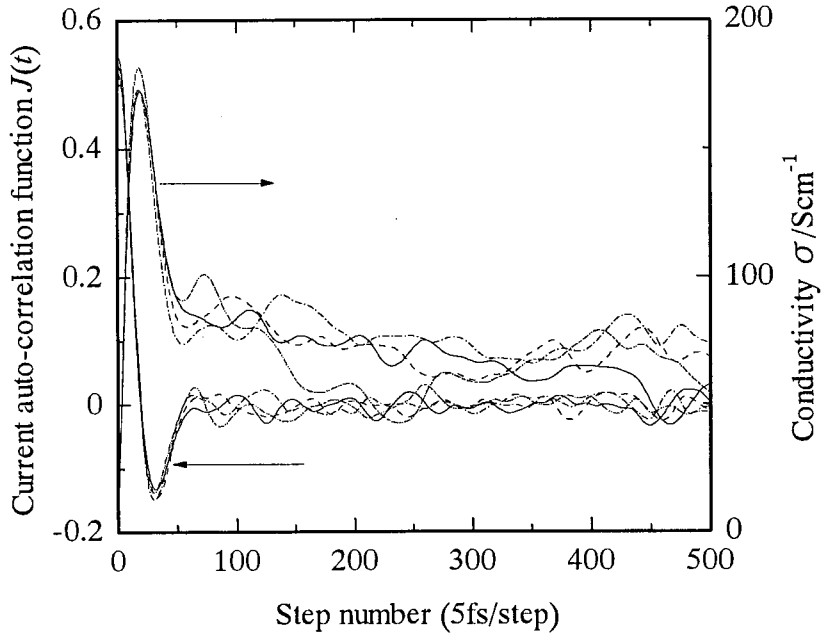

Fig. 3-13-2 One of the auto-correlation function and the electric conductivity profiles in molten binary system (Rb, Cs)Cl at 1000K, 5×10^5 steps, ———; x_{Rb}=0.2, - - - -; x_{Rb}=0.4, — - —; x_{Rb}=0.6, —·—x_{Rb}=0.8

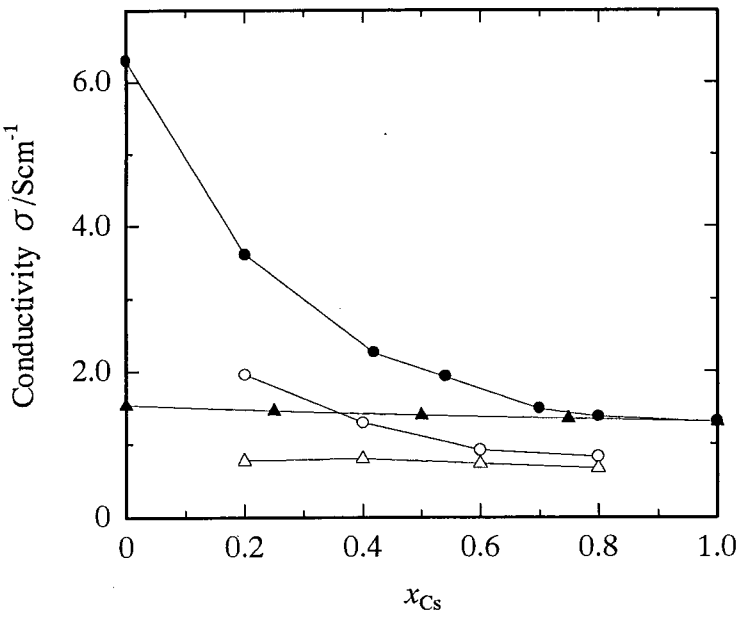

Fig. 3-13-3 Relationship between the electric conductivities and the mole fraction of Cs in molten binary system (Li, Cs)Cl and (Rb, Cs)Cl at 1000K,

—●—; Experimental results for (Li, Cs)Cl, —○—; MD simulation for (Li, Cs)Cl,

—▲—; Experimental results for (Rb, Cs)Cl, —△—; MD simulation for (Rb, Cs)Cl

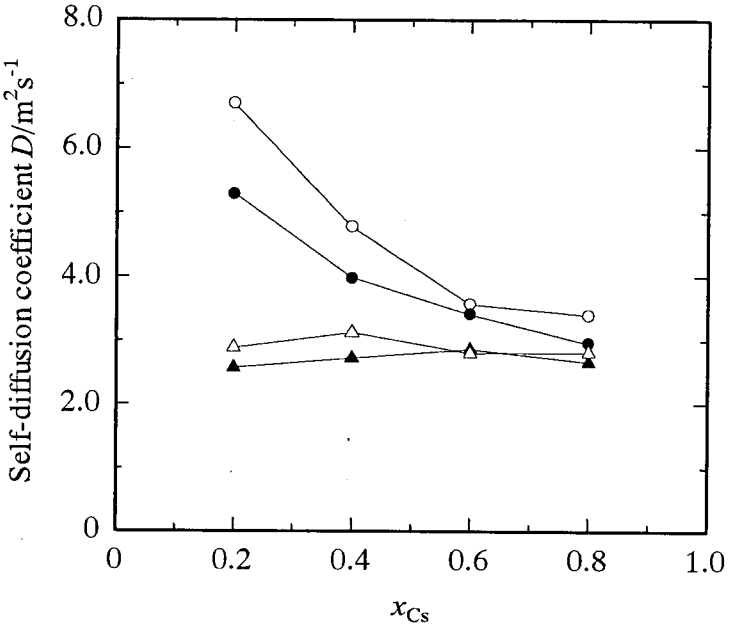

Fig. 3-14 Relationship between the self-diffusion coefficients and the mole fraction of Cs in molten binary system (Li, Cs)Cl and (Rb, Cs)Cl at 1000K, —●—; Li^+ for (Li, Cs)Cl, —○—; Cs^+ for (Li, Cs)Cl, —▲—; Rb^+ for (Rb, Cs)Cl, —△—; Cs^+ for (Rb, Cs)Cl

§ III-iv References

(1) C. T. Moynihan and R. W. Laity, *J. Phys. Chem.*, **68**, 3312 (1964).

(2) M. V. Smirnov, K. A. Aleksandsv, and V. A. Khokhlov, *Electrochim. Acta*, **22**, 543 (1977).

(3) I. Okada, R. Takagi, and K. Kawamura, *Z. Naturforsch.*, **34a**, 498 (1979).

(4) C.-C. Yang, and B.-J. Lee, *Z. Naturforsch.*, **48a**, 1223 (1993).

(5) R. Takagi, H. Shimotake, and K. J. Jensen, *J. Electrochem. Soc.*, **131**, 1280 (1984).

(6) A. Lunden and I. Okada, *Z. Naturforsch.*, **41a**, 1034 (1986).

(7) I. Okada, R. Takagi, and K. Kawamura, *Z. Naturforsch.*, **35a**, 493 (1980).

(8) I. Okada, S. Okazaki, H. Horinouchi, and Y. Miyamoto, *Materials Sci. Forum 73*, 175 (1991).

(9) A. Endoh, and I. Okada, *Z. Naturforsch.*, **43a**, 638 (1988).

(10) A. Endoh, and I. Okada, *Z. Naturforsch.*, **44a**, 1131 (1989).

(11) I. Okada, and A. Klemm, *Z. Naturforsch.*, **44a**, 747 (1989).

(12) I. Okada, and A. Ichioka, *Z. Naturforsch.*, **47a**, 781 (1992).

(13) H. Matsuura, R. Takagi, I. Okada, and R. Fujita, *J. Nucl. Sci. Technol.*, **34**, 304 (1997).

(14) M. Matsumiya, H. Matsuura, R. Takagi, and R. Fujita, *J. Alloys Comp.*, to be submitted.

(15) F. R. Duke and L. Bissell, *J. Electrochem. Soc.*, **111**, 717 (1964).

(16) G. Jones and B. C. Bradshaw, *J. Amer. Chem. Soc.*, **55**, 1780 (1933).

(17) P. Fellner, I. Votava, and M. Chrenkova-Paucirova, *Chem. Zvesti*, **34**, 330 (1980).

(18) M. P. Tosi and F. G. Fumi, *J. Phys. Chem. Solids*, **25**, 45 (1964).

(19) J. E. Mayer, *J. Chem. Phys.*, **1**, 270 (1933).

(20) B. Larsen, T. Forland, and K. Singer, *Mol. Phys.*, **26**, 1521 (1973).

(21) P. P. Ewald, *Ann. Phys.*, **64**, 253 (1921).

(22) L. V. Woodcock, *Chem. Phys. Lett.*, **10**, 257 (1971).

(23) J. Habasaki and I. Okada, *Z. Naturforsch.*, **40a**, 906 (1985).

(24) I. Okada, *Z. Naturforsch.*, **42a**, 21 (1987).

(25) M. Dixon and M. J. L. Sangster, *Phys. Chem. Liquids*, **5**, 221 (1976).

(26) M. Dixon and M. J. L. Sangster, *J. Phys. C: Solid State Phys.*, **9**, 3381 (1976).

(27) M. Wilson and P. A. Madden, *J. Phys.: Condens. Matter*, **5**, 6833 (1993); **6**, 159 (1994).

(28) R. Takagi, F. Hutchinson, P. A. Madden, A. K. Adya and M. Gaune-Escard, *J. Chem. Phys.*, to be submitted.

(29) M. Sakurai, R. Takagi, A. K. Adya and M. Gaune-Escard, *Z. Naturforsch.*, **53a** (1998).

(30) A. K. Adya, R. Takagi, M. Sakurai and M. Gaune-Escard, *Proc. 11th Int. Symp. Molten Salts*, ed. P. C. Trulove, H. De Long and S. Deki, Electrochem. Soc. Inc., Pennington, **98**, (1998).

(31) Iu. K. Delimarskii and B. F. Marcov, *"Electrochemistry of Fused Salts"*, Sigma Press (1961).

(32) B. F. Markov, *D. A. N. SSSR*, **110**, 441 (1956).

Chapter IV

Continuous Countercurrent Electromigration

ChapterⅣ Continuous Countercurrent Electromigration

§Ⅳ-ⅰ Background

The Self-Consistent Nuclear Energy System (SCNES)[1] requires zero release of radioactive materials out of the fuel cycle[2]. From a standpoint of the harmonization of nuclear systems with global environment, we should make efforts to separate the fission products from one another for incineration and utilization of medical tracers, precious materials and so on. As one of the most feasible candidates for SCNES is a metallic fuel fast breeder reactor, we have assumed the pyrochemical treatment of metallic fuel proposed by ANL as a chemical separation process. After the electrorefining and drawdown process, all alkali halides, alkaline-earth halides and some amounts of rare earth halides still remain in the salt bath. Thus, in order to re-use the salt bath, we have proposed a countercurrent electromigration method which originated from isotope separation, e.g., enrichment of ^{6}Li[3]-[6]. According to experimental cation mobilities of La^{3+}[7], Dy^{3+}[8], Ca^{2+}[9] and Cs^{+}[10] in their molten alkali mixtures, the ions can be enriched easily. Moreover, a possibility of high enrichment of Nd, U[11], Cs, Sr and Gd[12] in the LiCl-KCl eutectic mixture was pointed out recently. However, the application of the electromigration process to the practical plant has so far not developed. If we use the binary system of NaCl-KCl for our purpose, we can also use the binary system of LiCl-KCl because the decomposition potential of Na^{+} is more positive than Li^{+}. Therefore, in the present work, we have employed the molten CsCl, $SrCl_2$ and $BaCl_2$ in the NaCl-KCl equimolar mixture system as examples of fission products and arranged the column cell so as to recover the concentrated fission products continuously, i.e., we investigated the applicability of the electromigration process to the practical plant for nuclear waste reprocessing.

§ Ⅳ- ii Experimental

§ Ⅳ- ii - i Melt preparation for electromigration method

Chloride reagents used as a solvent were NaCl (Wako Chem. Ind. Ltd.:>99.5%), KCl (Kanto Chem. Ind. Ltd.:>99.5%), and those used as a solute were CsCl (Wako Chem. Ind. Ltd.:>99.0%), $SrCl_2$ (Wako Chem. Ind. Ltd.:>99.5%) and $BaCl_2$ (Wako Chem. Ind. Ltd.:>99.5%). The finely crushed NaCl and KCl were mixed at the desired composition (NaCl:50mol%, KCl:50mol%) and were introduced in a quartz tube. The mixture was kept at 973K under vacuum for about 7h and melted above 1073K. The solute CsCl was introduced in a quartz cell and kept at about 673K under vacuum for about 24h. The $SrCl_2$ and $BaCl_2$ were dried in the same way because of the hygroscopic materials. We have performed a series of electromigration experiments of CsCl in the NaCl-KCl system and employed all the reagents (CsCl; $SrCl_2$; $BaCl_2$) in the NaCl-KCl system.

Ⅳ- ii - ii Electromigration method for the practical plant

The electromigration cell for the batch experiment is similar to that in the reference[13]. The most improved cell for countercurrent electromigration system has mainly two distinctive features as shown in **Fig. 4-1**.

(1) The electromigration tube is arranged to take out enriched salt in the column from the melt bath, which is shown as the sub-unit in Fig. 4-1.

(2) The Cl_2 gas which was generated from the anode during electromigration was circulated from anode to cathode and acted as an oxidizing agent for the Na deposited on the cathode as shown in the following reaction in order to prevent the corrosion caused by Na and the NaCl melt was recycled.

$$2Na + Cl_2 \rightarrow 2NaCl \qquad (4\text{-}1)$$

It is reported that about three times the amount of chlorine gas theoretically needed for the conversion was introduced to the cathode compartment[14]. Therefore we introduced the Cl_2 gas into the cell before electromigration preliminary. The flow speed of 22.3ml/min during electromigration was estimated from the reference[14]. Additionally, we selected the glassy carbon as the candidate of the cathode as discussed

in detail in the results and discussions. The salt bath containing a NaCl-KCl equimolar mixture and additional salts CsCl, $SrCl_2$ and $BaCl_2$ was kept in a large container. The anode was made of a super fine graphite rod (5mmϕ in diameter, Tokai Carbon Co., Ltd.). The glassy carbon (3.0mmϕ in diameter, Nilaco Co.) was connected to the graphite rod with the ceramic binder for protection from corrosion and it was used as the cathode. The migration tubes (two types: 4mmϕ in diameter and 6mmϕ in diameter, 100mm in length) were made of the quartz glass. The upper part of the migration tube had an outlet for Cl_2 gas. The lower part of the migration tube was packed with alumina powder (100μmϕ, Nishio Chemical Ind.) in order to prevent convection of the melt in the migration tube. The quartz wool was packed at the bottom and at the end of the anode in contact with the melt. The temperature was kept at 1023K with a temperature controller and measured by a Chromel-Alumel thermocouple during electromigration. A constant DC current supplier (Kikusui Electronics. Corp., PAD 500-0.6A) fed electric currents less than 0.2A. The transported charge was measured by a Cu coulometer or a Desital Coulometer (HIOKI 3187, AC/DC Power HITESTER). After electromigration we closed the cock b and absorbed the enriched salt by using the roller pump in order to remove the enriched salt from the anode to the sub-unit. We could regulate the enriched salt amounts for sub-units by adjusting the rotating ratio and time of the roller pump, which is confirmed by using the distilled water preliminary. For next electromigration, the melt has already penetrated in the migration tube. The amount of Cs was determined by absorption spectrometry (Hitachi Corp. Z-6100). The amount of Sr, Ba, Na and K was estimated by ICP emission spectrometry (Seiko Denshi Kogyo, SPS-1500-VR).

§Ⅳ-ⅲ Results and Discussion

§Ⅳ-ⅲ-ⅰ The behaviors of Cs, Sr and Ba in molten NaCl-KCl system for scientific aspects

(a) System of CsCl and mixture in molten NaCl-KCl

The ε values can be determined from chemical analysis and calculated by Eq. (4-2) based on the material balance,

$$\varepsilon_{12} = -(F/Q)(N_1/x_1 - N_2/x_2) \tag{4-2}$$

where Q is the transported charge, N_M the total quantities in mole of $(1/Z)M^{Z+}$ in the separation tube from the anode to the position where the chemical composition remained unchanged during electromigration and x_M the mole fractions before electromigration. Equation (4-2) was derived by Klemm[15] and by Ljubimov and Lunden[16]. The values of ε are given in **Table 4-1** together with the main experimental conditions. The $\varepsilon<0$ means that Cs migrates slower than Na and K. According to a series of several runs, one of the results of the salt distribution along the tubes in each cell fraction in the system of CsCl in the NaCl-KCl equimolar mixture are shown in **Fig. 4-2.** In Fig. 4-2, the upper abscissa indicates the distance from the anode, showing that the electromigration method can concentrate Cs near the anode under the condition of the initial concentration $x_{Cs}<0.2$. The values of $-\varepsilon_{Cs}$ in this system are plotted against x_{Cs} in **Fig. 4-3**. Although the data of $-\varepsilon_{Cs}$ are scattered at low Cs concentration, Cs migrates more slowly than Na and K. Additionally, compared with the previous results[12], $-\varepsilon_{Cs}$ in the LiCl-KCl eutectic system at $x_{Cs}<0.2$ is larger than that in our results, which is also interpreted by the potential profiles[10,17].

The electric conductivity κ was calculated from the following equation, which is to be discussed in more detail in elsewhere[17].

$$\kappa = 2.481 - 2.447x_{Cs} + 1.888x_{Cs}^2 - 0.513x_{Cs}^3 \ (\mathrm{Scm^{-1}}) \tag{4-3}$$

For a conventional calculation, NaCl-KCl mixture was considered to be quasi-unitary, because the internal mobilities of Na and K are very similar to each other at the equimolar composition. The internal mobilities of Cs and solvent components ,i.e., Na and K are calculated from the following equations[10] using ε and κ values thus obtained.

$$b_1 = (\kappa V/F)(1 + \varepsilon_{12} x_2) \quad (4\text{-}4a)$$

$$b_2 = (\kappa V/F)(1 - \varepsilon_{12} x_1) \quad (4\text{-}4b)$$

The molar volumes V were calculated from those of pure melts on the assumption of additivity. The calculated κ and V values were listed in Table 4-1. Internal mobilities calculated from Eqs. (4a and 4b) and isotherms of b_{Cs} and $b_{solvent}$ in this system at 1023K are given in Table 1 and **Fig. 4-4**, respectively. The Chemla crossing point is defined to be the point where the isotherms of two cation mobilities as a function of the mole fraction cross with each other. For example, in the LiCl-CsCl[10] Li^+ is more mobile at a higher concentration of LiCl and Cs^+ is more mobile at a lower concentration, and therefore, from the anode side the concentration gradually shifts to that of the Chemla crossing point. As illustrated in Fig. 4-4, the orders of the internal mobilities in this work are expressed by

$$b_{Cs} < b_{Na} \approx b_K \quad (x_{Cs} < 0.2) \quad (4\text{-}5a)$$

$$b_{Na} \approx b_K < b_{Cs} \quad (x_{Cs} > 0.6) \quad (4\text{-}5b)$$

These behaviors mean that the Chemla effect occurs also in this system and it is possible to enrich Cs at most x_{Cs}=0.2 in the NaCl-KCl melts at 1023K.

(b) System of CsCl, $SrCl_2$ and $BaCl_2$ in molten NaCl-KCl

In the mixture of CsCl, $SrCl_2$ and $BaCl_2$(1mol%) in the NaCl-KCl system, Cs, Sr and Ba can be enriched near the anode as depicted in **Fig. 4-5**. The relative differences of the mobilities away each cation are indicated in **Table 4-2**, which means that $-\varepsilon_{Sr}$ and $-\varepsilon_{Ba}$ are clearly larger than $-\varepsilon_{Cs}$. It has been reported that Dy and Ca were well enriched from their low concentrations in the molten KCl-$DyCl_3$[8] and KCl-$CaCl_2$[9], respectively. Thus, this electromigration method is found to be effective for separation of multivalent cations from monovalent cations. On the other hand, **Figure 4-6** represents one of the concentration profiles in the mixture of CsCl (1mol%), $SrCl_2$ and $BaCl_2$(0.1mol%) in the NaCl-KCl system. It is possible to enrich Cs significantly under this condition. Figure 4-6 shows these are more enriched in the second fraction than in the first. The tranquilization effect[18] of Sr^{2+} and Ba^{2+} on the internal mobility of Cs^+ may account to this phenomena. The tranquilization effect occurs according to

the strong coulombic interaction between cations with the common anion Cl^-. This tendency is conspicuous in the molten KCl-$DyCl_3$[8] and KCl-$CaCl_2$[9] mixtures. **Figure 4-7** expresses the relationship between current density at anode and concentration profile in migration tube. The result allowed us to conclude that it is efficient to enrich the divalent ions, such as Sr^{2+} and Ba^{2+}, under the condition at the high current density during electromigation. It has been reported that the separation factor at the high current density in the isotope separation of $^7Li/^6Li$ is smaller than that at the low current density, which means that it is remarkable to separate ^6Li from ^7Li at the high current density[6]. This result is also consistent with our results.

§ Ⅳ - ⅲ - ⅱ A series of continuous countercurrent electromigration for technological aspects

The present study of the electromigration process was focused on the multistage removing process in order to apply the separation of Cs, Sr and Ba to the actual system. For this purpose, it was attempted to design a new original countercurrent electromigration cell which is arranged to take out concentrated solute in the column from the melt in order to apply the electromigration method to the practical plant on the basis of the above experimental results. Tables 4-3 to 4-8 designate the results of the continuous countercurrent electromigration together the experimental conditions. The recovered weight means the amounts of the removed melts after electromigration. The ratio of the electrochemically base elements (Cs, Sr and Ba) for the solvent components (Na and K) by the electromigration is defined as follows.

$$\frac{N_M}{N_{total}} = \frac{N_M}{N_{Na} + N_K} \times 100(\%) \qquad (4\text{-}6)$$

where N_M is the molar concentration of the main elements (M=Cs, Sr and Ba) in the migration tube and N_{total} is the total mole concentration of the solvent components in the migration tube. Although the Cs/(Na+K) ratio in the CsCl-NaCl-KCl system is not so high, it is confirmed that the ratio is about two or three times larger than the ratio of the initial composition as shown in **Table 4-3**. This result enables us to remove the Cs enriched salt from the melt bath continuously. On the other hand, we used platinum,

tungsten wire, graphite and glassy carbon electrodes as the cathode. In the case of employing the platinum and tungsten wires, Na and Na_2O was deposited on the electrode surface. Additionally, it was reported that the graphite forms the intermetallic compounds with alkali metals[19]. Therefore it is not appropriate to enrich the solute continuously using these electrodes and it was found that the best candidate for the cathode is the glassy carbon electrode. **Table 4-4** lists the results of the continuous electromigration in the NaCl-KCl system which contains CsCl, $SrCl_2$ and $BaCl_2$ (1mol%). This condition (Cs:Sr:Ba ≈ 1:1:1) means the first stage in applying the electromigration to the practical plant. Each bulk ratio of the melt bath after each electromigration was calculated from Eq. (4-6). The Sr/(Na+K) and Ba/(Na+K) ratios are about one order of magnitude larger than the bulk ratio and the Cs ratio is about two times larger than the bulk ratio during all experiments. This tendency is consistent with the result of the batch experiment as shown in Fig. 4-6. That is to say, it is possible to separate preferentially the enriched salt of multivalent ions, i.e., Sr^{2+} and Ba^{2+} from that of monovalent ion on the first stage. In addition, it is effective to recover the multivalent ions at the high current density continuously as mentioned above. On the other hand, **Table 4-5** shows the results after electromigration in the NaCl-KCl system which contains CsCl (1mol%), $SrCl_2$ and $BaCl_2$ (0.1mol%). This condition (Cs:Sr:Ba ≈ 1:0.1:0.1) means the second stage after removing the enriched Sr and Ba salts from the melt bath. It is possible to enrich Cs in this stage although the Cs/(Na+ K) ratio is not so high due to the small transported charge. Then, we attempted the electromigration at the condition of the high transported charge as shown in **Table 4-6**. Then the experimental results by using the different depth of the column are shown in **Tables 4-7** and **4-8**. These results as for Cs show that it is possible to take the more enriched Cs salt than that as shown in Table 4-5. Finally, the continuous countercurrent electromigration was successfully performed on the eleven time as tabulated in Table 4-8. The mass balance and the total recovery yield are also shown in **Table 4-9**. For the future, we should estimate the energy required for the continuous electromigration process by using cumulative results of these experiments as well as the data available for the fission yields at the equilibrium state.

Table 4-1 Main experimental conditions and the internal mobilities in the molten system (Na, K, Cs)Cl at 1023K.

(a) System of CsCl in the NaCl-KCl melt

Run No.	x_{Cs}	Q	i_d	Voltage	ε_{Cs}	κ	V_m	b_{Cs}	$b_{solvent}$
		(C)	(A/cm^2)	(V)		(Sm^{-1})	(10^{-6} m^3mol^{-1})	(10^{-8} $m^2V^{-1}s^{-1}$)	
a-1	0.011±0.003	2088	0.796	25～30	-0.003±0.009	245.4	43.18	10.95±0.03	11.12±0.03
a-2	0.013±0.005	6221	0.796	25～30	-0.014±0.006	245.0	43.22	10.82±0.03	10.98±0.02
a-3	0.013±0.005	7920	1.592	50～60	-0.020±0.007	245.0	43.22	10.76±0.02	10.98±0.02
a-4	0.019±0.008	9373	1.592	50～60	-0.029±0.005	243.5	43.34	10.63±0.01	10.98±0.02
a-5	0.040±0.002	4320	0.531	38～45	-0.010±0.008	239.1	43.71	10.73±0.03	10.94±0.03
a-6	0.099±0.001	5120	0.531	38～45	-0.005±0.003	225.9	44.91	10.47±0.06	10.84±0.07
a-7	0.137±0.007	4518	0.531	38～45	-0.002±0.005	218.6	45.62	10.32±0.03	10.52±0.04
a-8	0.157±0.002	6523	0.708	50～60	-0.002±0.003	214.9	46.00	10.23±0.08	10.34±0.06
a-9	0.574±0.018	5040	0.708	50～60	0.068±0.009	160.4	54.29	9.29±0.04	8.67±0.02
a-10	0.607±0.011	4320	0.531	38～45	0.066±0.006	157.7	54.99	9.22±0.06	8.63±0.04
a-11	0.674±0.011	6000	0.603	40～50	0.053±0.008	153.5	56.24	9.10±0.07	8.63±0.06
a-12	0.703±0.018	4500	0.531	38～45	0.062±0.003	151.3	57.01	9.10±0.02	8.55±0.01
a-13	0.713±0.015	5040	0.531	38～45	0.082±0.013	151.1	57.09	9.15±0.09	8.42±0.07
a-14	0.753±0.014	6300	0.603	40～50	0.084±0.011	149.2	57.81	9.12±0.08	8.37±0.06

The sign ± for x_{Cs}, ε and b indicates the errors due to the chemical analysis.

Table 4-2 Main experimental conditions and relative differences for Cs, Sr and Ba in internal mobilities at 1023K.

(b) System of CsCl, $SrCl_2$ and $BaCl_2$ in the NaCl-KCl melt in the condition of x_{Cs}=0.015 ±0.005, x_{Sr}=0.011±0.003 and x_{Ba}=0.014±0.004.

Run No.	Q (C)	i_d (A/cm^2)	Voltage (V)	ε_{Cs}	ε_{Sr}	ε_{Ba}
b-1	2520	0.796	25～30	-0.032±0.009	-0.378±0.010	-0.181±0.078
b-2	5040	0.796	25～30	-0.009±0.003	-0.197±0.040	-0.175±0.044
b-3	8100	1.194	40～60	-0.028±0.006	-0.334±0.064	-0.318±0.058

(c) System of CsCl, $SrCl_2$ and $BaCl_2$ in the NaCl-KCl melt in the condition of x_{Cs}=0.016 ±0.004, x_{Sr}=0.001±0.000 and x_{Ba}=0.001±0.000.

Run No.	Q (C)	i_d (A/cm^2)	Voltage (V)	ε_{Cs}	ε_{Sr}	ε_{Ba}
c-1	2160	0.796	25～30	-0.012±0.008	-0.267±0.025	-0.258±0.024
c-2	4323	0.796	25～30	-0.017±0.005	-0.361±0.021	-0.184±0.015
c-3	6515	1.194	40～60	-0.015±0.003	-0.349±0.020	-0.256±0.016
c-4	8525	1.194	40～60	-0.022±0.003	-0.576±0.038	-0.144±0.036

(d) System of CsCl, $SrCl_2$ and $BaCl_2$ in the NaCl-KCl melt.

Run No.	Q (C)	i_d (A/cm^2)	Voltage (V)	x_M	ε_M
d-1-Cs	4320	0.354	25～40	0.015±0.003	-0.0001±0.003
-Sr				0.014±0.002	-0.138±0.048
-Ba				0.007±0.003	-0.138±0.062
d-2-Cs	6528	0.531	35～50	0.015±0.005	-0.0004±0.004
-Sr				0.011±0.002	-0.132±0.094
-Ba				0.006±0.001	-0.073±0.090
d-3-Cs	8125	0.531	25～50	0.013±0.003	-0.0004±0.002

-Sr				0.001±0.000	-0.099±0.040
-Ba				0.002±0.000	-0.289±0.077
d-4-Cs	12660	0.531	25～50	0.014±0.002	-0.0008±0.000
-Sr				0.008±0.001	-0.417±0.028
-Ba				0.007±0.000	-0.346±0.021
d-5-Cs	4320	0.354	25～30	0.036±0.008	-0.002±0.003
-Sr				0.020±0.002	-0.140±0.039
-Ba				0.019±0.003	-0.097±0.036
d-6-Cs	4500	0.354	5～20	0.136±0.011	-0.008±0.003
-Sr				0.023±0.006	-0.118±0.046
-Ba				0.024±0.008	-0.125±0.084
d-7-Cs	3600	0.531	25～50	0.101±0.013	-0.005±0.004
-Sr				0.022±0.002	-0.135±0.095
-Ba				0.029±0.005	-0.149±0.092
d-8-Cs	5000	0.531	25～45	0.135±0.011	-0.006±0.002
-Sr				0.022±0.003	-0.230±0.043
-Ba				0.024±0.005	-0.274±0.067
d-9-Cs	5182	0.531	30～50	0.035±0.007	-0.006±0.003
-Sr				0.024±0.003	-0.227±0.038
-Ba				0.029±0.003	-0.171±0.041
d-10-Cs	8000	0.531	35～50	0.128±0.008	-0.004±0.005
-Sr				0.018±0.004	-0.108±0.059
-Ba				0.025±0.003	-0.106±0.060
d-11-Cs	4000	0.708	40～50	0.159±0.013	-0.003±0.003
-Sr				0.041±0.004	-0.178±0.046
-Ba				0.036±0.003	-0.198±0.078
d-12-Cs	10200	0.708	50～60	0.211±0.015	-0.006±0.002
-Sr				0.044±0.003	-0.097±0.043
-Ba				0.036±0.002	-0.126±0.057

Table 4-3 Relationship between the transported charge and the Cs/(Na+K) ratio for the salt stocked into the sub-units after electromigration

Run No.	Q (C)	i_d (A/cm^2)	Voltage (V)	Cs/(Na+K) ratio (%)	Recovered weight (mg)
1-1st	1087	<0.796	5～30	1.24±0.02	130
1-2nd	1937	<0.796	5～30	1.08±0.01	620
1-3rd	2057	<0.796	5～30	1.61±0.03	2612
Initial				0.90±0.01	
2-1st	2698	0.796	25～30	3.15±0.10	390
2-2nd	2027	0.796	25～30	2.53±0.06	116
2-3rd	2607	0.796	25～30	2.98±0.09	71
2-4th	3617	1.115	40～60	3.15±0.10	240
2-5th	2885	0.796	25～30	1.93±0.04	268
2-6th	1793	<0.796	5～30	1.39±0.02	102
Initial				1.01±0.01	
3-1st	2160	0.796	25～30	2.02±0.04	260
3-2nd	3504	1.194	40～60	3.13±0.10	214
3-3rd	2203	0.796	25～30	2.52±0.06	147
3-4th	2052	1.035	40～50	2.45±0.06	261
Initial				1.35±0.02	

Table 4-4 Main experimental conditions and the Sr, Ba, Cs/(Na+K) ratio for the salt stocked into the sub-units after electromigration.

Run No.	Q (C)	i_d (A/cm^2)	Voltage (V)	Sr ratio (%)	Ba ratio (%)	Cs ratio (%)	Weight (mg)
Initial				1.19±0.01	1.73±0.03	2.21±0.05	
4-1st	5004	1.592	50～60	13.72±1.88	13.07±1.71	3.30±0.11	88
bulk1				1.18±0.01	1.81±0.03	2.15±0.05	
4-2nd	1512	0.796	25～30	11.53±1.33	12.12±1.47	3.96±0.16	133
bulk2				1.09±0.01	1.77±0.03	2.05±0.04	
4-3rd	3246	0.796	25～30	10.96±1.20	13.68±1.87	2.27±0.05	114
bulk3				1.01±0.01	1.69±0.03	2.17±0.05	
4-4th	3096	0.955	40～50	10.49±1.10	11.50±1.32	3.08±0.09	156
bulk4				1.02±0.01	1.65±0.03	2.01±0.04	
4-5th	2520	0.955	40～50	7.42±0.55	10.77±1.16	2.90±0.08	240
bulk5				0.76±0.01	1.47±0.02	1.67±0.03	
4-6th	3060	0.955	35～50	6.86±0.47	7.28±0.53	3.11±0.10	198
Final				0.72±0.01	1.38±0.02	1.69±0.03	

Table 4-5 Main experimental conditions and the Sr, Ba, Cs/(Na+K) ratio for the salt stocked into the sub-units after electromigration.

Run No.	Q (C)	i_d (A/cm^2)	Voltage (V)	Sr ratio (%)	Ba ratio (%)	Cs ratio (%)	Weight (mg)
Initial				0.219±0.003	0.133±0.002	2.55±0.06	
5-1st	2160	0.796	25～30	0.668±0.009	0.368±0.005	3.57±0.13	85
bulk1				0.114±0.002	0.099±0.001	2.26±0.05	
5-2nd	3826	1.194	50～60	0.327±0.005	0.200±0.003	2.49±0.06	138
bulk2				0.187±0.003	0.143±0.002	2.58±0.07	
5-3rd	2772	0.796	25～30	0.249±0.003	0.196±0.003	2.64±0.07	231
bulk3				0.047±0.001	0.079±0.001	2.05±0.04	
5-4th	3456	0.955	40～50	0.296±0.004	0.245±0.003	2.76±0.08	245
bulk4				0.098±0.001	0.143±0.002	2.03±0.04	
5-5th	3744	0.796	25～30	0.304±0.004	0.262±0.004	2.70±0.07	196
bulk5				0.044±0.001	0.074±0.001	2.09±0.04	
5-6th	2880	0.955	40～50	0.076±0.001	0.172±0.002	2.52±0.06	251
Final				0.012±0.000	0.106±0.002	2.57±0.07	

Table 4-6 Main experimental conditions and the Sr, Ba, Cs/(Na+K) ratio for the salt stocked into the sub-units after electromigration.

Rùn No.	Q (C)	i_d (A/cm^2)	Voltage (V)	Sr ratio (%)	Ba ratio (%)	Cs ratio (%)	Weight (mg)
Initial				0.065±0.001	0.106±0.002	1.59±0.03	
6-1-1st	6080	0.796	15～20	0.301±0.004	0.211±0.003	2.69±0.07	177
6-1-2nd				0.186±0.003	0.151±0.002	2.14±0.05	176
bulk1				0.031±0.000	0.117±0.002	1.55±0.02	
6-2-1st	5872	0.557	20～60	0.126±0.002	0.135±0.002	2.46±0.06	202
6-2-2nd				0.064±0.001	0.129±0.002	2.44±0.06	193
bulk2				0.044±0.001	0.104±0.001	1.66±0.03	
6-3-1st	1008	<0.796	50～100	0.089±0.001	0.160±0.002	2.12±0.05	98
6-3-2nd				0.092±0.001	0.195±0.003	2.09±0.04	84
Final				0.057±0.001	0.135±0.002	1.66±0.03	

Table 4-7 Main experimental conditions and the Sr, Ba, Cs/(Na+K) ratio for the salt stocked into the sub-units after electromigration.

Run No.	Q (C)	i_d (A/cm^2)	Voltage (V)	Sr ratio (%)	Ba ratio (%)	Cs ratio (%)	Weight (mg)
Initial				0.471±0.007	0.249±0.004	1.99±0.04	
7-1-1st	8111	0.708	5～20	0.956±0.013	0.986±0.013	3.40±0.12	138
7-1-2nd				1.103±0.015	0.788±0.011	2.70±0.07	105
bulk1				0.629±0.009	0.327±0.005	2.07±0.04	
7-2-1st	5155	0.708	5～20	0.933±0.013	0.602±0.008	3.99±0.16	124
7-2-2nd				0.607±0.008	0.324±0.004	2.65±0.07	198
bulk2				0.208±0.003	0.164±0.002	1.86±0.03	
7-3-1st	6746	0.708	5～15	0.458±0.006	0.347±0.005	3.23±0.10	75
7-3-2nd				0.252±0.003	0.224±0.003	2.36±0.06	156
7-3-3rd				0.276±0.004	0.295±0.004	2.11±0.04	125
bulk3				0.085±0.001	0.053±0.001	1.70±0.03	
7-4-1st	5141	0.495	5～20	0.236±0.003	0.274±0.004	2.22±0.05	83
7-4-2nd				0.294±0.004	0.329±0.005	1.94±0.04	136
7-4-3rd				0.166±0.002	0.254±0.003	1.91±0.04	144
7-4-4th				0.097±0.001	0.205±0.003	1.70±0.03	254
bulk4				0.030±0.000	0.042±0.001	1.68±0.03	
7-5-1st	2916	0.425	5～20	0.088±0.001	0.182±0.003	2.12±0.05	112
7-5-2nd				0.057±0.001	0.175±0.002	2.06±0.04	137
Final				0.020±0.000	0.044±0.001	1.54±0.02	

Table 4-8 Main experimental conditions and the Sr, Ba, Cs/(Na+K) ratio for the salt stocked into the sub-units after electromigration.

Run No.	Q (C)	i_d (A/cm^2)	Voltage (V)	Sr ratio (%)	Ba ratio (%)	Cs ratio (%)	Weight (mg)
Initial				0.883±0.011	0.963±0.013	1.32±0.02	
8-1-1st	3434	0.495	5～20	10.27±0.14	7.197±0.100	3.23±0.04	105
8-1-2nd				9.476±0.132	6.036±0.084	3.49±0.05	100
8-1-3rd				5.847±0.082	3.822±0.054	2.89±0.04	153
8-1-4th				3.948±0.056	2.922±0.041	2.63±0.04	138
bulk1				1.075±0.016	0.990±0.014	1.38±0.03	
8-2-1st	5040	0.513	5～20	15.10±0.21	10.73±0.147	5.27±0.07	90
8-2-2nd				9.633±0.133	6.652±0.092	4.36±0.06	125
8-2-3rd				9.636±0.134	6.490±0.091	3.84±0.05	99
8-2-4th				6.757±0.095	4.262±0.060	3.50±0.05	168
8-2-5th				5.624±0.079	3.858±0.054	3.15±0.04	179
8-2-6th				5.800±0.082	3.905±0.055	3.66±0.05	86
bulk2				0.918±0.012	0.925±0.012	1.21±0.02	
8-3-1st	4680	0.531	5～20	11.99±0.17	8.805±0.122	3.81±0.05	117
8-3-2nd				10.33±0.14	7.889±0.110	4.11±0.06	95
8-3-3rd				9.544±0.134	5.614±0.079	4.12±0.06	117
8-3-4th				6.588±0.093	5.216±0.074	4.18±0.06	146
8-3-5th				6.966±0.098	5.480±0.077	4.18±0.06	122
bulk3				0.897±0.011	0.968±0.013	1.28±0.02	
8-4-1st	1500	0.354	5～15	7.565±0.106	6.473±0.091	4.53±0.06	96
8-4-2nd				4.263±0.060	4.631±0.065	3.84±0.05	85
8-4-3rd				4.081±0.058	4.449±0.063	3.69±0.05	82
8-4-4th				3.251±0.046	3.170±0.045	3.20±0.05	84
8-4-5th				3.205±0.045	3.041±0.043	3.44±0.05	137
bulk4				0.871±0.011	0.900±0.011	1.35±0.03	
8-5-1st	2880	0.495	5～20	11.88±0.17	10.47±0.145	4.53±0.06	80

8-5-2nd				9.280±0.129	8.405±0.117	4.27±0.06	74
8-5-3rd				7.599±0.106	6.615±0.093	4.12±0.06	146
8-5-4th				5.148±0.072	4.478±0.063	4.82±0.07	78
bulk5				0.838±0.010	0.936±0.012	1.34±0.03	
8-6-1st	3240	0.471	5～20	11.91±0.16	8.987±0.124	5.48±0.08	87
8-6-2nd				10.56±0.15	8.556±0.120	4.74±0.07	66
8-6-3rd				7.533±0.106	5.741±0.081	3.66±0.05	99
8-6-4th				7.098±0.100	5.313±0.075	3.51±0.05	77
8-6-5th				5.123±0.072	4.597±0.065	3.89±0.05	72
8-6-6th				4.411±0.062	3.749±0.053	4.49±0.06	70
bulk6				0.925±0.012	0.898±0.011	1.38±0.03	
8-7-1st	2700	0.602	5～25	12.41±0.17	8.635±0.119	3.30±0.05	42
8-7-2nd				7.909±0.111	5.915±0.083	3.29±0.05	33
8-7-3rd				5.742±0.081	4.591±0.065	3.03±0.04	64
8-7-4th				5.726±0.081	4.411±0.062	3.05±0.04	82
8-7-5th				4.625±0.065	4.250±0.060	2.70±0.04	53
bulk7				0.974±0.013	0.931±0.013	1.44±0.03	
8-8-1st	3060	0.354	5～20	11.69±0.16	9.540±0.133	3.60±0.05	43
8-8-2nd				13.75±0.19	10.93±0.152	4.69±0.07	46
8-8-3rd				9.214±0.129	7.847±0.110	3.02±0.04	41
8-8-4th				10.15±0.14	7.904±0.112	2.91±0.04	64
8-8-5th				10.24±0.15	9.090±0.128	3.23±0.05	40
8-8-6th				10.57±0.15	9.207±0.129	3.73±0.05	45
8-8-7th				10.27±0.15	8.400±0.119	3.18±0.04	63
bulk8				0.754±0.008	0.958±0.013	1.37±0.03	
8-9-1st	2880	0.354	5～20	11.10±0.15	9.757±0.135	4.88±0.07	39
8-9-2nd				8.617±0.119	5.734±0.080	5.30±0.07	38
8-9-3rd				5.997±0.084	5.657±0.079	3.63±0.05	85
8-9-4th				5.677±0.080	4.958±0.070	3.90±0.05	72
8-9-5th				6.513±0.092	5.572±0.078	4.38±0.06	64

bulk9				0.706±0.007	0.891±0.011	1.33±0.03	
8-10-1st	2160	0.283	5～15	9.519±0.133	8.870±0.124	3.30±0.05	58
8-10-2nd				8.859±0.124	7.211±0.101	3.52±0.05	65
8-10-3rd				5.411±0.076	5.996±0.084	3.83±0.05	72
8-10-4th				5.202±0.073	4.780±0.067	3.96±0.06	64
8-10-5th				4.764±0.067	3.413±0.048	3.72±0.05	82
8-10-6th				3.281±0.046	2.687±0.038	2.88±0.04	77
8-10-7th				5.530±0.078	5.320±0.075	4.25±0.06	55
bulk10				0.722±0.007	0.907±0.012	1.30±0.02	
8-11-1st	2160	0.283	5～15	9.743±0.137	8.931±0.125	4.18±0.06	65
8-11-2nd				6.693±0.094	5.947±0.083	4.02±0.06	72
8-11-3rd				4.324±0.061	4.117±0.058	3.66±0.05	78
8-11-4th				4.819±0.068	4.735±0.067	3.70±0.05	85
8-11-5th				4.210±0.059	4.413±0.062	3.51±0.05	52
Final				0.740±0.008	1.137±0.018	1.40±0.03	

Table 4-9 Mass balance and recovery yield for the electromigration

Run No.	Initial composition/g			Final composition/g			Sum of metal recovered/mg			Mass balance*	Recovery yield/%		
	Cs	Sr	Ba	Cs	Sr	Ba	Cs	Sr	Ba	(%)	Cs	Sr	Ba
	A	B	C	D	E	F	G	H	I				
4-1	18.04	6.33	14.54	17.56	6.31	15.24	2.90	12.07	11.50	101	0.32	1.84	1.47
4-2	17.56	6.31	15.24	16.70	5.79	14.89	5.27	15.34	16.12	96			
4-3	16.70	5.79	14.89	17.73	5.38	14.19	2.58	12.50	15.60	100			
4-4	17.73	5.38	14.19	16.40	5.44	13.82	4.80	16.37	17.94	96			
4-5	16.40	5.44	13.82	13.60	4.06	12.34	6.95	17.80	25.86	84			
4-6	13.60	4.06	12.34	13.72	3.82	11.56	6.16	13.58	14.42	97			
5-1	20.90	1.16	1.10	18.46	0.60	0.82	3.04	0.57	0.31	86	0.30	0.36	0.49
5-2	18.46	0.60	0.82	21.14	0.99	1.18	3.43	0.45	0.28	117			
5-3	21.14	0.99	1.18	16.76	0.25	0.66	6.10	0.58	0.45	76			
5-4	16.76	0.25	0.66	16.58	0.52	1.18	6.75	0.73	0.60	104			
5-5	16.58	0.52	1.18	17.03	0.23	0.61	5.29	0.60	0.51	98			
5-6	17.03	0.23	0.61	21.07	0.06	0.88	6.32	0.19	0.43	123			
6-1	12.91	0.34	0.88	12.59	0.17	0.97	8.53	0.86	0.64	97	0.29	0.51	0.31
6-2	12.59	0.17	0.97	13.50	0.23	0.86	9.69	0.37	0.52	106			
6-3	12.50	0.23	0.86	13.48	0.30	1.12	3.84	0.17	0.32	102			

7-1	16.24	2.49	2.06	16.91	3.34	2.71	7.52	2.48	2.19	110	0.51	0.38	0.64
7-2	16.91	3.34	2.71	15.12	1.10	1.36	10.20	2.36	1.40	77			
7-3	15.12	1.10	1.36	13.86	0.45	0.44	8.75	1.08	0.98	84			
7-4	13.86	0.45	0.44	13.69	0.16	0.35	11.55	1.08	1.56	96			
7-5	13.69	0.16	0.35	12.51	0.11	0.36	5.20	0.18	0.44	91			
8-1	10.69	4.70	8.03	11.19	5.73	8.26	14.93	34.65	23.47	108	3.52	10.32	7.50
8-2	11.19	5.73	8.26	9.79	4.88	7.71	28.66	61.57	41.82	89			
8-3	9.79	4.88	7.71	10.37	4.77	8.07	24.38	53.12	38.66	104			
8-4	10.37	4.77	8.07	10.94	4.63	7.50	18.04	21.36	20.63	100			
8-5	10.94	4.63	7.50	10.86	4.45	7.80	16.57	31.48	27.74	101			
8-6	10.86	4.45	7.80	11.19	4.92	7.48	20.15	37.03	29.18	102			
8-7	11.19	4.92	7.48	11.68	5.18	7.76	8.34	18.64	14.39	105			
8-8	11.68	5.18	7.76	11.10	4.00	7.99	11.78	36.95	30.48	94			
8-9	11.10	4.00	7.99	10.78	3.75	7.43	12.61	20.96	17.93	95			
8-10	10.78	3.75	7.43	10.53	3.83	7.56	17.10	27.98	25.00	100			
8-11	10.53	3.83	7.56	11.35	3.93	9.50	13.44	20.81	19.62	113			

*calculated from (D+E+F+G+H+I)/(A+B)×100

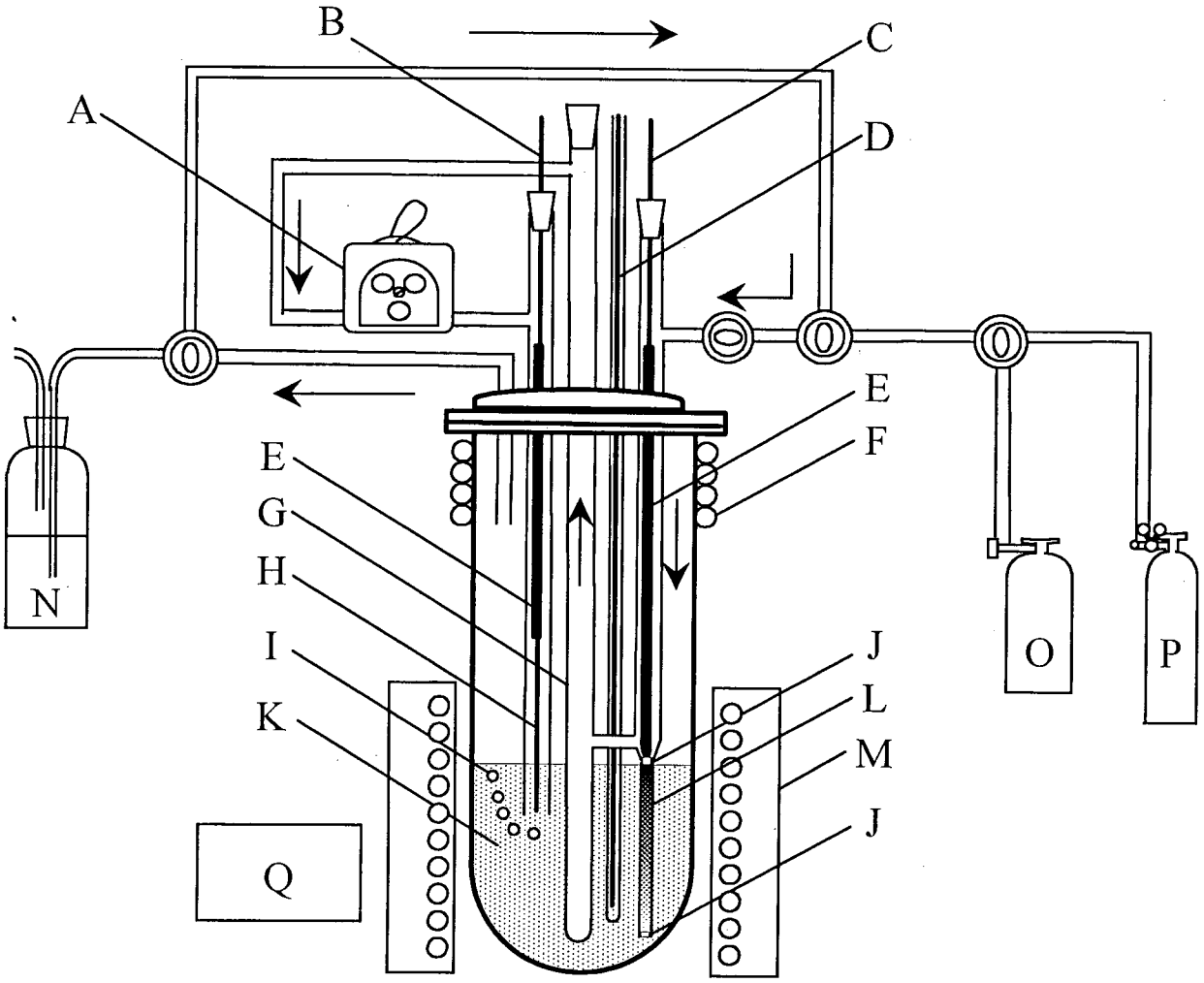

Fig. 4-1 The schematic diagram for continuously countercurrent electromigration
A: Roller pump (flow speed; 22.3ml/min), B: Tungsten wire (lead to graphite), C: Tungsten wire(lead to graphite; anode), D: Thermocouple, E: Graphite, F: Cooling water, G: Sub-unit, H: Glassy carbon electrode (cathode), I: Cl_2 gas, J: Quartz wool, K: Molten salt (NaCl-KCl system), L: Electromigration tube, M: Electric furnace, N: Gas trap, O: Cl_2 gas, P: Ar gas, Q: Thermoregulator

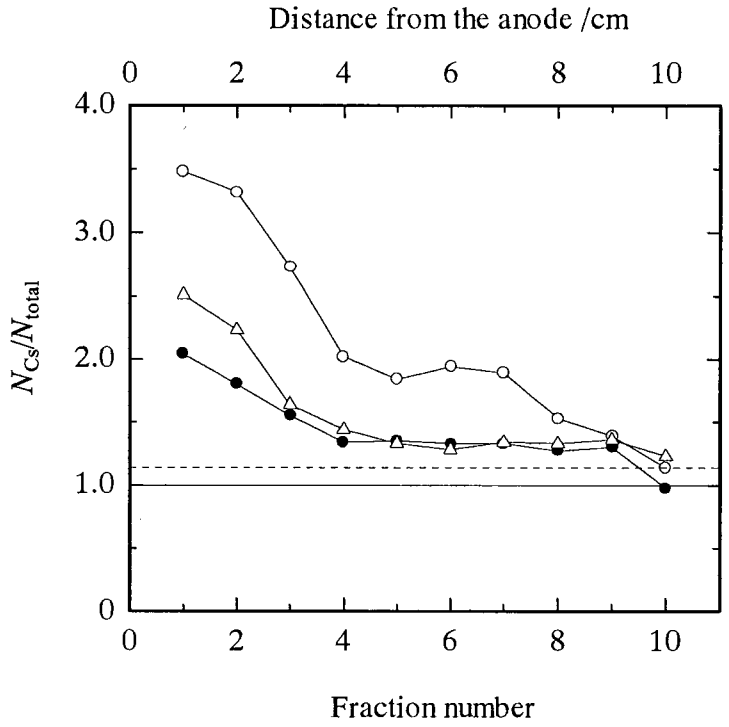

Fig. 4-2 One of the Cs concentration profile in the migration tubes containing CsCl in the NaCl-KCl system at 1023K,

—●—: N_{Cs}/N_{total} on Run a-2, —△—: N_{Cs}/N_{total} on Run a-3,

—○—: N_{Cs}/N_{total} on Run a-4

Initial composition; ———: x_{Cs}=0.010±0.003 on Run a-4, - - - : x_{Cs}=0.011±0.004 on Run a-2 and a-3

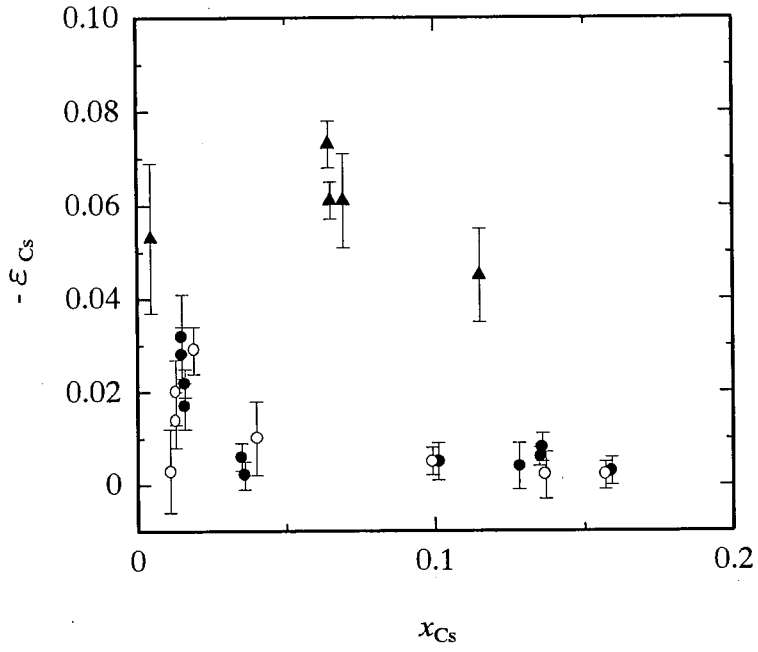

Fig. 4-3 Relationship between the relative differences of the mobilities and mole fraction as for Cs, ○: In the system of CsCl in the NaCl-KCl melt, ●: In the system of CsCl, $SrCl_2$ and $BaCl_2$ in the NaCl-KCl melt, ▲: In the system of CsCl, $SrCl_2$ and $GdCl_3$ in the LiCl-KCl eutectic melt[12]

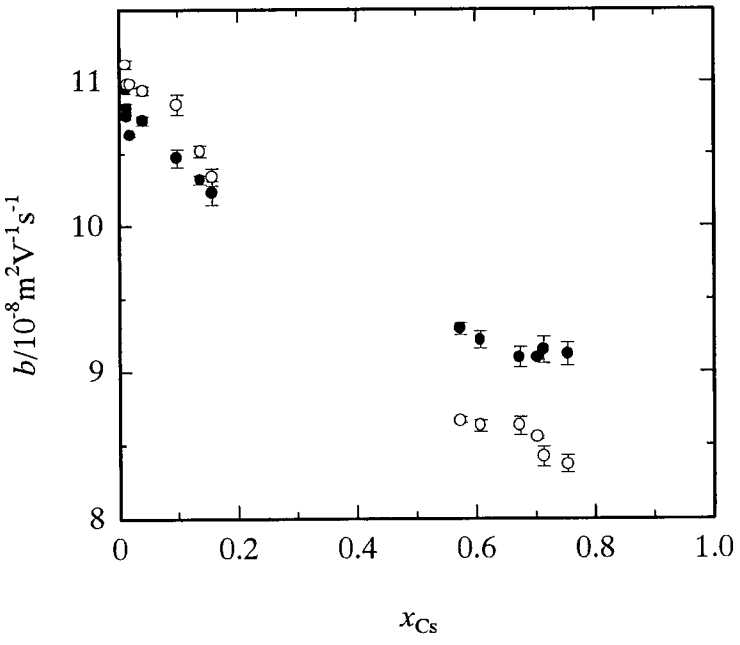

Fig. 4-4 Isotherms of the internal cation mobilities in the quasi-binary system (Cs, Na-K)Cl at 1023K, ●:b_{Cs}, ○:$b_{solvent}$

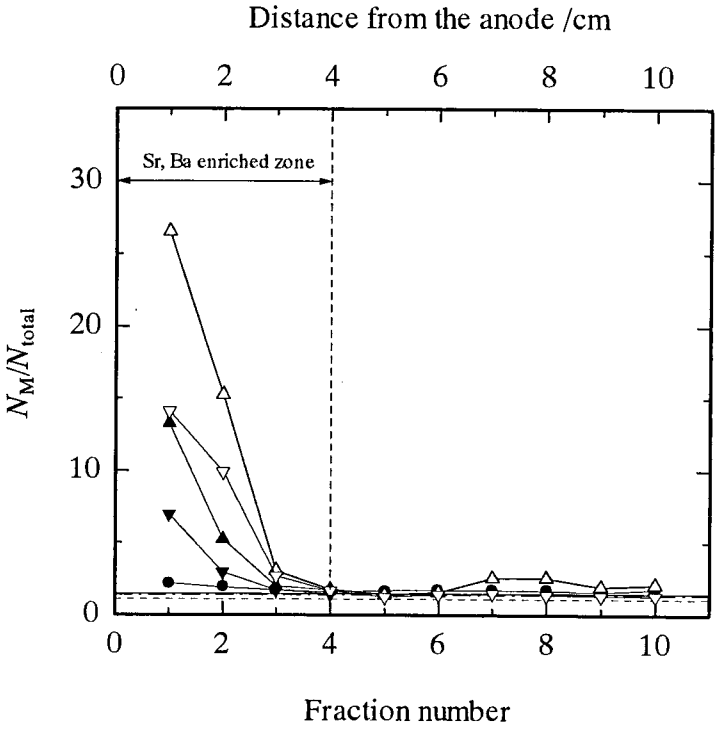

Fig. 4-5 One of the concentration profile in the migration tubes containing CsCl, $SrCl_2$ and $BaCl_2$ in the NaCl-KCl system at 1023K, Molar ratio in each fraction, N_M/N_{total};
—●—: N_{Cs}/N_{total} on Run b-1, —▲—: N_{Sr}/N_{total} on Run b-1,
—△—: N_{Sr}/N_{total} on Run b-2, —▼—: N_{Ba}/N_{total} on Run b-1,
—▽—: N_{Ba}/N_{total} on Run b-2,
Initial composition; ———: x_{Cs}=0.015±0.005, - - - : x_{Sr}=0.014±0.004,
— - —: x_{Ba}=0.014±0.004.

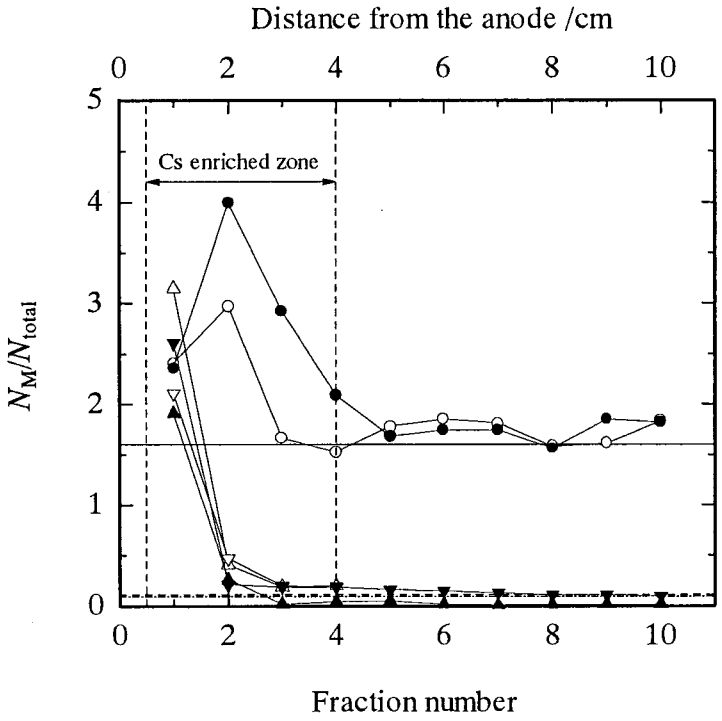

Fig. 4-6 One of the concentration profile in the migration tubes containing CsCl, $SrCl_2$ and $BaCl_2$ in the NaCl-KCl system at 1023K,

—●—: N_{Cs}/N_{total} on Run c-4, —○—: N_{Cs}/N_{total} on Run c-3,

—▲—: N_{Sr}/N_{total} on Run c-4, —△—: N_{Sr}/N_{total} on Run c-3,

—▼—: N_{Ba}/N_{total} on Run c-4, —▽—: N_{Ba}/N_{total} on Run c-3,

Initial composition; ———: x_{Cs}=0.016±0.004, - - - : x_{Sr}=0.001±0.000,

— - —: x_{Ba}=0.001±0.000

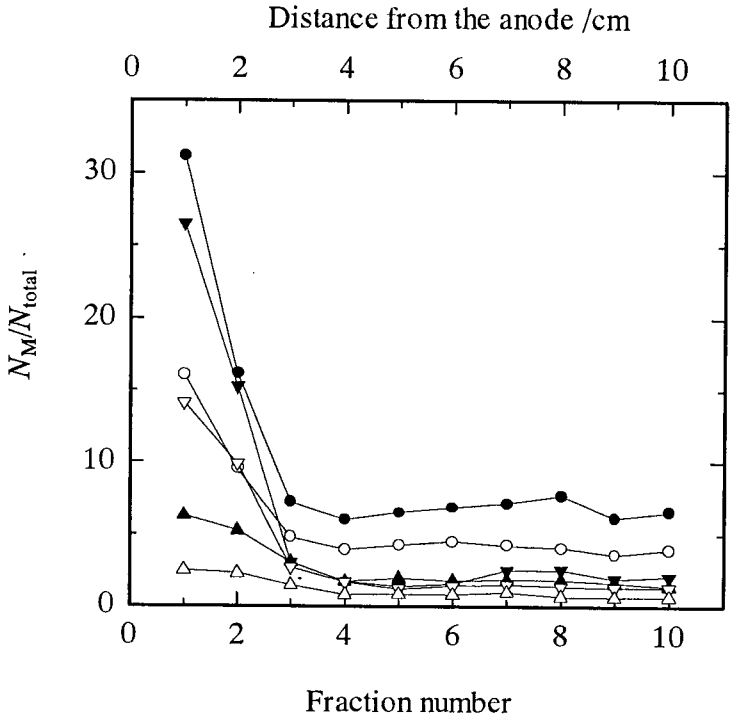

Fig. 4-7 One of the concentration profile in the migration tubes containing CsCl, $SrCl_2$ and $BaCl_2$ in the NaCl-KCl system at 1023K as for the difference of the current density, —▲—: N_{Sr}/N_{total} on Run d-5(i_d=0.354A/cm^2), —△—: N_{Ba}/N_{total} on Run d-5, —●—: N_{Sr}/N_{total} on Run d-11(i_d=0.708A/cm^2), —○—: N_{Ba}/N_{total} on Run d-11, —▼—: N_{Sr}/N_{total} on Run b-2(i_d=0.796A/cm^2), —▽—: N_{Ba}/N_{total} on Run b-2

§ Ⅳ-iv References

(1) A. Shimizu and Y. Fujii-e, *Prog. Nucl. Energy*, **29**, (Suppl.) 25 (1995).

(2) R. Takagi, H. Matsuura, Y. Fujii-e, R. Fujita and M. Kawashima, *Prog. Nucl. Energy*, **29**, (Suppl.) 471 (1995).

(3) A. Klemm, *Naturwissenshaften*, **32**, 59 (1944).

(4) A. Klemm and H. Hintenberger, P. Hoernes, *Z. Naturforsch.*, **2a**, 245 (1947).

(5) T. Haibara, O. Odawara, I. Okada, M. Nomura and M. Okamoto, *J. Electrochem. Soc.*, **136**, 1059 (1989).

(6) I. Okada and A. Lunden, *Z. Naturforsch.*, **38a**, 97 (1983).

(7) M. Iwasaki and R. Takagi, *J. Nucl. Sci. Technol.*, **31**, 751 (1994).

(8) H. Matsuura, I. Okada, R. Takagi and Y. Iwadate, Y, *Z. Naturforsch.*, **53a**, 45 (1998).

(9) H. Matsuura and I. Okada, *Denki Kagaku*, **61**, 732 (1993).

(10) H. Horinouchi and I. Okada, *J. Electroanal. Chem.*, **396**, 547 (1995).

(11) H. Matsuura, R. Takagi, M. Zablocka-Maricka, L. Rycerz and W. Szczepaniak, *J. Nucl. Sci. Technol.*, **33**, 895 (1996).

(12) H. Matsuura, R. Takagi, I. Okada and R. Fujita, *J. Nucl. Sci. Technol.*, **35**, 304 (1997).

(13) A. Lunden and I. Okada, *Z. Naturforsch.*, **41a**, 1034 (1986).

(14) A. Endoh and I. Okada, *Z. Naturforsch.*, **43a**, 638 (1988).

(15) A. Klemm, *Z. Naturforsch.*, **1**, 252 (1946).

(16) V. Ljubimov, A. Lunden, *Z. Naturforsch.*, **21a**, 1592 (1966).

(17) M. Matsumiya, H. Matsuura, R. Takagi and Y. Okamoto, to be submitted.

(18) J. Habasaki, C.-C. Yang and I. Okada, *Z. Naturforsch.*, **42a**, 695 (1987).

(19) J. F. Salzano and S. Aronson, *J. Chem. Phys.*, **42**, 1323 (1965).

Chapter V

Electrochemical Behavior of Cs^{+}, Eu^{2+}, Sr^{2+} and Ba^{2+}

Chapter V Electrochemical Behavior of Cs^+, Eu^{2+}, Sr^{2+} and Ba^{2+}

§ V-i Background

The Integral Fast Reactor (IFR) concept proposed by Argonne National Laboratory contains a sophisticated idea of pyrochemical treatment in a nuclear fuel cycle[1]. In the IFR concept, after removal of the fuel materials, the salt bath containing fission products will be occluded into the zeolites and stocked as the deposits. However, from a standpoint of the harmonization of nuclear systems with global environment, we should make an effort to separate the fission products each other for incineration or utilization of medical tracers, precious materials and so on.

It is difficult to recover some fission products like Cs^+ Eu^{2+}, Sr^{2+} and Ba^{2+} from salt phase because of their more negative reduction potentials[2] than the solvent components. Since it is found that liquid Cd metal forms stable alloy with Pu, if we can find adequate liquid metal which forms stable alloy with Eu and Sr making less interaction with the solvent, it will enable us to recover these at more positive potentials without interference by the solvent. Although Eu^{2+} and Sr^{2+} are also negative elements, we successfully recovered Eu^{2+} and Sr^{2+}[3]. In the case of using the chloride bath, Cs element may be recovered by forming the stable alloy like Cd-Pu alloy[4],[5], because it is possible to shift the deposition potential to more positive side by decreasing the activity of the deposited metal[3], which is understood by the Nernst-Equation

$$E = E^0 + \frac{RT}{nF} \ln \frac{a_{M^{n+}}}{a_M} \qquad (5\text{-}1)$$

where E is the apparent standard potential, E^0 the equilibrium potential of alloy formation, R the gas constant, T a temperature, n the charge transfer number, F the Faraday constant, $a_{M^{n+}}$ the activity of M^{n+} in the melt and a_M the activity of the deposited metal. However, it is known that Cs metal is not easy to make an alloy the other element from the Hume-Rothery rule and the phase diagrams. Then it is also known that Cs^+ has more positive decomposition potential[2] in the fluoride bath. Therefore we selected the FLINAK system (LiF:46.5mol%, NaF:11.5mol%, KF:42.0mol%, m.p.727K) as the solvent due to the low boiling point (b.p.951.4K) of Cs metal. Additionally, in the SCNES (Self-Consistent Nuclear Energy System) concept[6],

we must separate in particular ^{135}Cs and ^{93}Zr with significant yields from the recycle fuels in reprocessing, because these elements decrease breeding ratio due to large neutron adsorption cross sections. Then recovery of Zr and the electrochemical behavior of Zr^{3+} in fluoride bath were revealed in the previous works[7]-[11]. Furthermore, it was reported that the internal mobilities were measured in the molten LiCl-CsCl mixture[12]-[14], where Cs was enriched at the anode at $x_{Cs}<0.2$, where x is mole fraction of Cs. Then, we have proposed to apply the electromigration method to enrich and the electrowinnig, because the electromigration method has an advantage for the pyrochemical treatment due to its simple construction for being able to use the same container with the conductive melt bath. However, in these reports, electrochemical behavior of Cs^+/Cs and recovery of Cs after the enrichment by the electromigration method was not revealed. Therefore we have carried out the present experiments for the following purposes;

(a) Scientific aspects; electrochemical behavior of Cs^+/Cs on a solid graphite electrode in the FLINAK system at 773K.

(b) Technological aspects; possibility of recovery of Cs on three kinds of liquid metallic cathodes in the FLINAK system at 773K.

For this purpose, the electrochemical behavior of Cs^+ was analyzed on a solid graphite electrode by the cyclic voltammetry (CV) and the chronopotentiometry (CP) and we employed Pb, Sn and Zn as liquid metallic cathodes. Additionally, the following analyses were carried out, according to the CV in order to determine the charge transfer number and the diffusion coefficient, which will be compared each other. Moreover, in this work, the possibility of recovery of Eu, Sr and Ba was examined by liquid metallic cathodes. For this purpose, we selected Al, Bi, Cd, Pb, Sn, and Zn as liquid metallic cathode.

(1) Semi-integration electroanalysis of E-i curves was used to determine the charge transfer number and the diffusion coefficient precisely on the basis of Oldham's method[15]-[18].

(2) Semi-differential electroanalysis was also carried out on the basis of Goto's method[19]-[21].

§ V - ii Experimental

§ V - ii - i Melt preparation

(a) Preparation for Cs based on the fluoride bath

Fluoride reagents used as a solvent were LiF (Wako Chem. Ind. Ltd.:>98.0%), NaF (Wako Chem. Ind. Ltd.:>99.0%) and KF (Kanto Chem. Ind. Ltd.:>98.0%), and chloride reagent used as a solute is CsCl (Wako Chem. Ind. Ltd.:>99.0%). The KF was also introduced in a graphite crucible and kept at about 673K under vacuum for about 24h because it is hygroscopic. The finely crushed fluorides were mixed in the desired portion (LiF:46.5mol%, NaF:11.5mol%, KF:42.0mol%; FLINAK, m.p.727K) and were introduced in a graphite crucible. The mixture was kept at 973K under vacuum for about 7h and melted above 1173K. The solute CsCl was introduced in a quartz cell and kept at about 673K under vacuum for about 24h. Metal reagents used as liquid electrodes were Pb (Wako Chem. Ind. Ltd.:>99.9%), Sn (Wako Chem. Ind. Ltd.:>99.9%) and Zn (Kanto Chem. Co.:>99.9%).

(b) Preparation for Eu, Sr and Ba based on the chloride bath

Chloride reagents used were NaCl (Wako Chem. Ind. Ltd.:>99.5%), KCl (Kanto Chem. Ind. Ltd.:>99.5%) and $EuCl_2$ which was delivered in sealed glass ampoules (APL Engineered materials, Inc.:99.99%), $SrCl_2$ (Wako Chem. Ind. Ltd.:>99.5%), $BaCl_2$ (Wako Chem. Ind. Ltd.:>99.5%). The finely crushed chlorides were mixed in the following compositions (NaCl-50mol%;KCl-50mol%) and were introduced in a quartz cell. The mixture was dehydrated by heating under vacuum at 973K for about 7h and then melted at 1073K. The solute ($EuCl_2$, $SrCl_2$ and $BaCl_2$) was also introduced in the quartz cell and dehydrated by heating under vacuum at about 673K for about 24h because they are hygroscopic. Metal reagents used as liquid electrodes were Al (Wako Chem. Ind. Ltd.:>99.9%), Bi (Nilaco Co.:>99.999%), Cd (Wako Chem. Ind. Ltd.:>99.9%), Pb (Wako Chem. Ind. Ltd.:>99.9%), Sn (Wako Chem. Ind. Ltd.:>99.9%) and Zn (Kanto Chem. Co.: >99.9%).

§ V - ii - ii **Electrode and electrical devices**

(a) Electrochemical apparatus for Cs based on the fluoride bath

Preliminary, we found that there is no anodic peak and only a small cathodic peak on the voltammogram of Cs, when we used a solid tungsten electrode surface of which is downward. Since deposited Cs is liquid, it cannot retain at the electrode. Therefore, we devised a solid graphite electrode surface of which is upward as shown in **Fig. 5-1**. This solid graphite electrode was used to investigate the electrochemical behavior of Cs^+ in the molten FLINAK system. This solid electrode was constituted as follows. The BN rod (15mm ϕ, Denki-Kagaku Co.) and a graphite rod (D in Fig. 5-1, 10mm ϕ, Tokai Carbon:>99.9%) with a screw thread are tightened up each other in order to connect between the BN rod and the graphite. The large graphite (D) and the small graphite (C; 3mm ϕ, Tokai Carbon:>99.9%) with a screw thread are tightened up each other in order to connect them also. The small graphite has a hole (1mm ϕ) and was connect a tungsten to a lead wire (A) with ceramic binder. Additionally, the small graphite and the tungsten wire are covered with BN coating by using BN spray (Denki-Kagaku Co.) to prevent detection of the reaction between the tungsten wire and the melt bath. We devised a liquid metallic electrode in order to examine the possibility of recovery of Cs and the furnace-cell assembly used in this electrolytic experiments is shown in **Fig. 5-2a**. In the FLINAK melts the quasi-reference electrode (Q.R.E) was a Pt wire (1.5mm ϕ, Nilaco Co.:>99.98%) as also used by other authers[22)-(24)]. In our experiments Pt Q.R.E showed stable potentials. Pt does not make an alloy with Cs and the alkali metals. The electrode was rinsed in a 1N HCl solution and degreased with acetone before experiments. Prior to electrochemical experiments, pre-electrolysis was carried out with a tungsten cathode (1mm ϕ, Nilaco Co.:>99.5%) with a -10mA/mm^2 cathodic current density were made at 773K in order to eliminate metallic impurities and oxides. The pre-electrolysis was quitted before the deposition of the Cs and we identified no significant metallic impurities by CV before experiments. A graphite crucible (MS-G, Tokai Carbon:>99.9%) was used as a counter electrode. A tungsten lead wire was connected to this crucible with ceramic binder. Three kinds of liquid electrodes (Pb:m.p.600.5K, Sn:m.p.504.97K, Zn:m.p.692.6K) were used as a

working electrode. These liquid electrodes were constituted as follows. A small amount of Pb which was weighed by about 3g was introduced in the BN rod (E; 6.5mm inside diameter, 50mm length). A hole (L) with 6mm diameter locates about 2.5cm upper from the bottom of the BN rod. This BN rod was connected to a Mullite tube (D; $3Al_2O_3 \cdot 2SiO_2$) with ceramic binder, *i.e.*, the part immersed into the melt bath is only BN rod. The tungsten wire was almost covered by the BN coating and only the bottom edge of tungsten wire was immersed into this liquid Pb to prevent detection of the reaction between the tungsten wire and the melt bath. This liquid electrode was kept over the melt during pre-electrolysis. After the pre-electrolysis, this liquid electrode was immersed into the melt bath. The anodic and cathodic behaviors for Cs^+ in the FLINAK melt system containing CsCl (1mol%) were analyzed by the CV and CP at 773K. Voltammetry was carried out by a potentio/galvanostat (Type2001, Toho Tech.), a function-generator (Type2230, Toho Tech.) and X-Y and Y-T recorder (Type3036). In order to measure the transported charge on galvanostatic condition precisely we used the Desital Coulometer (HIOKI 3187, AC/DC Power HITESTER). After experiments for three kinds of electrodes were sliced to more than 10-layers. The sliced samples were dissolved into 1N HNO_3 in order to determine Cs concentration by adsorption spectrometry (Hitachi Corp. Z-6100) and alkali elements (Li, Na, K) concentrations by ICP Atomic Emission (Seiko Denshi Kogyo, SPS-1500-VR).

(b) Electrochemical apparatus for Eu, Sr and Ba based on the chloride bath

The furnace-cell assembly used in this electrolytic experiments is shown in **Fig. 5-2b**. Pt quasi-reference electrode (Q.R.E; 1.5mmϕ, Nilaco Co.:>99.98%) was used. Pt wire does not make an alloy with Eu, Sr and the alkali metals. It exhibits a high degree of electrochemical stability and its practical oxidation potential was close to the value at which chlorine gas was evolved. The electrode was rinsed in a 1N HCl solution and degreased with acetone before experiments. Before electrochemical experiments, pre-electrolysis was carried out with an iron rod cathode (3mmϕ,Nilaco Co.:>99.5%). Pre-electrolysis with a -10mA/cm^2 cathodic current were made at

1073K in order to eliminate metallic impurities and oxides. The pre-electrolysis was quitted before the deposition of the bath. A graphite crucible (MS-G, Tokai Carbon:>99.9%) was used as a counter electrode. A tungsten lead wire was connected to this crucible with ceramic binder. Five kinds of liquid electrodes (Al:m.p.933.4K, Bi:m.p.544.3K, Cd:m.p.593.9K, Pb:m.p.600.5K, Sn:m.p.504.97K and Zn:m.p.692.6K) were used as a working electrode. Al was used just for recovery of Sr, and other four were used for recovery of both Eu and Sr. These electrodes' area was calculated to be about 0.371cm^2 from cross section. This liquid electrode was constituted as follows. A small amount of Pb which was weighed by about 5g was introduced in the quartz tube (7.5mm inside diameter). A hole with 6mm diameter locates about 2.5cm upper from the bottom of the quartz tube. The tungsten wire was almost covered by the quartz tube (2.5mm inside diameter) and only the bottom edge of tungsten wire was immersed into this liquid Pb covered by the quartz tube to prevent detection of the reaction between the tungsten wire and the melt bath. This liquid electrode was kept over the melt during pre-electrolysis. After the pre-electrolysis, this liquid electrode was immersed into the bath. The anodic and cathodic behavior for Eu in the NaCl-KCl melt containing $EuCl_2$ (1mol%) and for Sr in the KCl melt containing $SrCl_2$ (1mol%) were analyzed by the CV and CP at 1073K. Voltammetry was carried out by a potentio/galvanostat (Type2001, Toho Tech.), a function-generator (Type2230, Toho Tech.) and X-Y and Y-T recorder (Type3036). After experiments for five kinds of electrodes were sliced to 6-layers samples. The samples in series of Bi, Pb, Sn and Zn electrode were dissolved into 5N HNO_3 and the samples of Al electrode ware dissolved into 1N HCl in order to determine their concentrations by ICP Atomic Emission (Seiko Denshi Kogyo, SPS-1500-VR).

§ V - iii Results and Discussion

§ V - iii - i Electrochemical behavior of Cs^+ in molten FLINAK system

The cyclic voltammetry and chronopotentiometry of Cs^+ were made on a solid graphite electrode and a liquid Pb electrode in order to obtain charge transfer numbers, kinetic parameters and diffusion coefficients by two kinds of conventional, semi-integral, semi-differential methods. The derived properties are compared with each other as follows.

(a) *Two kinds of conventional electroanalysis of a series of cathodic and anodic voltammograms with various sweep rates*

Typical cyclic voltammograms with various sweep rates for Cs^+ on the solid graphite electrode and on the liquid Pb electrode are shown in **Figs. 5-3a** and **5-3b**, respectively. Two peaks around -1.3V and -0.5V in Fig. 5-3a are not assigned so far. Typical values of anodic and cathodic peak potential (E_p) and half-peak potential ($E_{p/2}$) vs. Pt quasi-reference electrode in the FLINAK system at 773K obtained from the linear sweep voltammetry on the solid graphite electrode at various sweep rates were shown in **Tables 5-1a** and **5-1b**, respectively. In the case where the product, i.e., caesium metal, is hardly soluble, the following equation (5-2a) is preferred for calculating the charge transfer number involved in the electrode reaction[25]-[28]. Therefore the cathodic average charge transfer number (n=0.27) and the anodic average charge transfer number (n=0.32) are calculated from the following equation (5-2a) for a reversible electrochemical reaction. These charge transfer numbers are far from n=1. We conjectured that the electrochemical behavior of Cs^+ is not completely reversible system from the result mentioned above, because the anodic peak potential is slightly shifted to the positive side as increasing the sweep rate and ohmic drop is large as shown in Fig. 5-3a. Therefore we applied to the following equation (5-2b) for an irreversible electrochemical reaction. The cathodic average kinetic parameter ($\alpha n_a = 0.65$, where α is a transfer coefficient) and the anodic average kinetic parameter ($\alpha n_a = 0.86$) calculated from the following equation (5-2b) are also listed in Tables 5-1a and 5-1b, respectively. Compared with each result, we found that it is more reasonable for our conditions applying to an irreversible system than a reversible system. Therefore we

can deduce that the electrochemical behavior of Cs^+ is an irreversible system. Moreover, in the case of the liquid Pb electrode, we calculated the charge transfer number at 5mV/s in Fig. 5-3b by applying to the following equation (5-2c)[29]-[31] because the product can diffuse into the liquid Pb electrode. The calculated charge transfer number is n=0.80.

$$\Delta E_p^{rev} = \left|E_p - E_{p/2}\right| = \frac{0.774RT}{nF} = \frac{0.0516}{n} \quad \text{(Reversible for insoluble)} \qquad (5\text{-}2a)$$

$$\Delta E_p^{ir} = \left|E_p - E_{p/2}\right| = \frac{1.857RT}{\alpha n_a F} = \frac{0.1237}{\alpha n_a} \quad \text{(Irreversible)} \qquad (5\text{-}2b)$$

$$\Delta E_p^{rev} = \left|E_p - E_{p/2}\right| = \frac{2.2RT}{nF} = \frac{0.1465}{n} \quad \text{(Reversible for soluble)} \qquad (5\text{-}2c)$$

In addition, by adopting the Heyrovsky-Ilkovic equation[32],[33] to the cathodic peak as a reversible electrochemical reaction, we evaluated the charge transfer number.

$$E = E_{1/2} + \frac{RT}{nF}\ln\frac{i_p - i}{i} \qquad (5\text{-}3)$$

where E is the apparent standard potential, $E_{1/2}$ the half-wave potential, i_p the peak current and i the current. Then the equation applies to the range (0.4~0.9)i_p for the solid graphite electrode and to the range (0.5~0.9)i_p for the liquid Pb electrode. According to the above relation , the plot of E vs. $\ln\{(i_p - i)/i\}$ gives a straight line having slope of RT/nF. Typical examples for the solid graphite electrode and the liquid Pb electrode are shown in **Figs. 5-4a** and **5-4b**, respectively. We estimated that the charge transfer number for the solid graphite electrode is n=0.99 and for the liquid Pb electrode is n=0.73 from Figs. 5-4a and 5-4b. Then we determined the diffusion coefficient by the following relations[28],[34]. In the case of the solid graphite electrode, the following equation (5-4a) is preferred for calculating the diffusion coefficient because the product is hardly soluble. Then in the case of the liquid Pb electrode, the following equation (5-4b) is preferred for calculating the diffusion coefficient because the product can diffuse into the liquid Pb electrode.

$$i_p = 0.6105 \times 10^{-3} \frac{(nF)^{\frac{3}{2}} A D^{\frac{1}{2}} C^* \nu^{\frac{1}{2}}}{(RT)^{\frac{1}{2}}} \quad \text{(for insoluble)} \qquad (5\text{-}4a)$$

$$i_p = 0.4463 \times 10^{-3} \frac{(nF)^{\frac{3}{2}} A D^{\frac{1}{2}} C^* \nu^{\frac{1}{2}}}{(RT)^{\frac{1}{2}}} \quad \text{(for soluble)} \qquad (5\text{-}4b)$$

where i_p is the peak current, A a surface area of the working electrode, D the diffusion coefficient, C^* a bulk concentration and ν the sweep rate. The obtained values for the solid graphite electrode and for the liquid Pb electrode are listed in **Tables 5-2a** and **5-2b**, respectively. The conventional electroanalysis could not be adopted for peak width between the reduction peak and the oxidation peak, because there is no anodic peak corresponding to the reduction peak as shown in Fig. 5-3b. Therefore we determined the charge transfer number and the diffusion coefficient by applying semi-integral and semi-differential electroanalyses. We plotted the variations of the peak currents *vs.* the square root of the sweep rates from 0.005 to 1.0V/s in **Fig. 5-5**. The peak currents were found to be almost proportional to the square root of the sweep rates. Therefore, it is concluded that the main reaction is controlled by diffusion. Then it is also concluded the diffusion controlled as shown in **Fig. 5-6** because the current function $i_p / \nu^{1/2}$ remains virtually constant with increasing sweep rates.

(b) *Semi-integral and Semi-differential electroanalyses of the cathodic voltammograms*

As above mentioned about the conventional electroanalysis, the electrochemical behavior of Cs^+ is not completely reversible system. Therefore we calculated the charge transfer numbers and the kinetic parameters by applying to both a reversible and an irreversible systems. In the case of applying to a reversible system, a typical semi-integral curve (**Fig. 5-7**) obtained from a linear sweep voltammetric experiment with ν=0.5V/s (Fig. 5-3b, run6) yields a semi-integral limiting current density, $m^* = 0.015A \cdot s^{1/2}$ for the liquid Pb electrode. The occurrence of a plateau in the region of cathodic potentials proves that the rate of transfer is limited by diffusion; the plateau height is given by the following equation [15)-(18)]

$$m^* = nFAC\sqrt{D} \tag{5-5}$$

With the charger transfer number, this equation enables us to calculate the diffusion coefficient of Cs^+ in this melt. Calculated diffusion coefficients for the solid graphite electrode and for the liquid Pb electrode are listed in Tables 5-2a and 5-2b, respectively. In addition, by adopting the following equations to the cathodic peak as an electrochemically reversible (5-6a) and irreversible (5-6b) systems, we evaluated the charge transfer number and the standard rate constant, k^0.

$$E = E_{1/2} + \frac{RT}{nF}\ln\frac{m^* - m(t)}{m^*} \quad \text{(Reversible)} \tag{5-6a}$$

$$E = E^0 + \frac{RT}{\alpha n_a F}\ln\frac{k^0}{D^{1/2}} + \frac{RT}{\alpha n_a F}\ln\frac{m^* - m(t)}{i(t)} \quad \text{(Irreversible)} \tag{5-6b}$$

where E is the apparent standard potential, E^0 the equilibrium potential of Cs^+/Cs, m^* a semi-integral limiting value and m a semi-integral value calculated from current as a function of time t. This reversible equation (5-6a) is also regarded as the Heyrovsky-Ilkovic equation described equivalently above. According to the above relation for a reversible system, the plot of E vs. $\ln\{(m^* - m)/m^*\}$ gives a straight line with the slope of RT/nF. Typical example is shown in **Fig. 5-8** for the liquid Pb electrode with 0.5V/s. The calculated charge transfer number from the slope is listed in Table 5-2b. The kinetic parameter calculated from the equation (5-6b) for an irreversible system is also listed in Table 5-2b.

In semi-differential electroanalysis which provides clearer peak than the conventional cyclic voltammogram, the charge transfer number, the kinetic parameter and the diffusion coefficient can be obtained from the following equations (5-7a)-(5-7d) [19)-(21)].

$$W_p = \frac{3.53RT}{nF} = \frac{0.235}{n} \quad \text{(Reversible)} \tag{5-7a}$$

$$W_p = \frac{2.94RT}{\alpha n_a F} = \frac{0.196}{\alpha n_a} \quad \text{(Irreversible)} \tag{5-7b}$$

$$e_p = -\frac{n^2F^2A\nu C^*\sqrt{D}}{4RT} \quad \text{(Reversible)} \tag{5-7c}$$

$$e_p = -\frac{\alpha n_a^2F^2A\nu C^*\sqrt{D}}{3.367RT} \quad \text{(Irreversible)} \tag{5-7d}$$

where W_p is the peak width and e_p is the peak height. A typical semi-differential curve obtained from semi-integral curve (Fig. 5-7) is shown in **Fig. 5-9**. The observed peak width W_p=0.225V gives the charge transfer number n=1.04 in the case of a reversible system for the liquid Pb electrode. The kinetic parameters and the diffusion coefficients calculated from equations (5-7c)-(5-7d) for the solid graphite electrode and for the liquid Pb electrode are listed in Tables 5-2a and 5-2b, respectively.

(c) *General features and characterization of the chrnopotentiometric electroanalysis*

All these features for Cs^+ on the solid graphite electrode and on the liquid Pb electrode can also be depicted on the chronopotentiogram of **Figs. 5-10a** and **5-10b**, respectively. A series of chronopotentiograms on two kinds of electrodes for various current densities has also been examined.

Using the relations

$$E = E_{\tau/4} + \frac{RT}{nF}\ln\frac{\tau^{1/2} - t^{1/2}}{t^{1/2}} \quad \text{(Reversible)} \tag{5-8a}$$

$$E = E^0 + \frac{RT}{\alpha n_aF}\ln\frac{2k^0}{(\pi D)^{1/2}} + \frac{RT}{\alpha n_aF}\ln(\tau^{1/2} - t^{1/2}) \quad \text{(Irreversible)} \tag{5-8b}$$

where $E_{\tau/4}$ is quarter-wave potential and τ is a transition time, in the case of a reversible system, the charge transfer number was calculated from the slope of the E vs. $\ln\left\{(\tau/t)^{1/2} - 1\right\}$ plots. This method yields n=1.00 for the solid graphite electrode and n=1.17 for the liquid Pb electrode as shown in **Fig. 5-11** in the case of the solid graphite electrode. These values are reasonably similar to those determined by cyclic voltammograms as shown in Tables 5-2a and 5-2b. The kinetic parameters for the solid graphite electrode and for the liquid Pb electrode calculated from the equations (5-8a)-(5-8b) for an irreversible system are also listed in Tables 5-2a and 5-2b, respectively.

The diffusion coefficients for Cs^+ in this melt calculated from the following Sand's law[35],[36] are summarized in Tables 5-2a and 5-2b. This equation (5-9) can be applied to both a reversible and an irreversible systems.

$$\frac{i\tau^{1/2}}{C^*} = \frac{nFD^{1/2}\pi^{1/2}}{2} \tag{5-9}$$

The charge transfer numbers and the diffusion coefficients are also good agreement with the values determined from the various electroanalyses. Chronopotentiometric determinations showed that the Sand product was constant, *i.e.*, the square root of the transition time was found to be almost proportional to the reverse of the current density as shown in **Fig. 5-12**. Therefore, it is concluded that the main reaction is controlled by diffusion.

(d) *Electrochemical behavior of Cs^+ in molten FLINAK system*

We identified the decomposition potential of the bath before this electrochemical measurement and the cathodic limiting process in this melt is Cs metal deposition. In the case of the reversal sweep before -2.0V, there is no anodic peak around -1.2V. Therefore the cathodic peak around -2.0V for the solid graphite electrode corresponds to the reduction of Cs^+ as shown in Fig. 5-3a. The anodic peak around -1.2V corresponds to the oxidation of Cs was also observed. From the above mentioned for the various electroanalyses, we determined the charge transfer number and the kinetic parameter. We evaluated the electrochemical behavior of Cs by using the reversibility parameter (Λ) defined in general as follows.

$$\Lambda = \frac{k^0}{\sqrt{D_O^{1-\alpha} D_R^{\alpha} \left(\frac{nF}{RT}\right) \nu}} \tag{5-10a}$$

$$\Lambda > 15 \text{ reversible}, \quad \Lambda < 10^{-2(1+\alpha)} \text{ irreversible} \tag{5-10b}$$

We applied to the following assumption $D_O=D_R=D$, $\alpha=0.5$ and substituted the values calculated from the various electroanalyses to the above equation. Additionally, the standard rate constants calculated from the various electroanalyses which is listed in Table 5-2a are applied to the Matsuda and Ayabe criterion[37] for an irreversible system

as follows, which in our conditions yields

$$k^0 \leq 1.3 \times 10^{-6} \quad \text{(Irreversible)} \qquad (5\text{-}11)$$

The average standard rate constant obtained from the various electroanalyses falls in with the conditions above. Thus, the reaction of Cs^+/Cs can be qualified as an irreversible system. Therefore it is concluded that the behavior of Cs^+ is an electrochemically irreversible reactions (5-12).

In the molten FLINAK system on the solid graphite electrode at 773K

$$\begin{array}{ll} \text{Reduction} & Cs^+ + e^- \rightarrow Cs \\ \text{Oxidation} & Cs \rightarrow Cs^+ + e^- \end{array} \quad \text{(Irreversible)} \qquad (5\text{-}12)$$

In the case of the liquid Pb electrode, we identified the each reduction reaction for the each cathodic peak in Fig. 5-3b by referring to available decomposition potentials[2]. The first cathodic peak around -0.5V at 0.5V/s was observed and it was somewhat irreversible, since the peak positions depend on the sweep rates. The cathodic limit which is the third cathodic peak around -1.7V corresponds to the deposition of solvent, i.e., the reduction of K^+ ions. The second cathodic peak around -1.0V can be attributed to the reduction of Cs^+ because the deposition potential of Cs^+ is more negative than that of K^+. If Cs and Pb can make Cs-Pb alloy, it is possible to shift the decomposition potential of Cs^+ to more positive side by decreasing the activity of the deposition metal from the Nernst equation though there is no data for the phase diagram of Pb-Cs. The standard rate constants (Table 5-2b) calculated from the various electroanalyses are applied to the above Matsuda and Ayabe criterion[37] for an irreversible system as follows, which in our conditions yields

$$k^0 \leq 3.5 \times 10^{-6} \quad \text{(Irreversible)} \qquad (5\text{-}13)$$

Therefore it is concluded that the cathodic behavior of Cs^+ is an electrochemically irreversible reaction in the molten FLINAK system on the liquid Pb electrode at 773K

$$\text{Reduction} \quad Cs^+ + e^- \rightarrow Cs \quad \text{(Irreversible)} \qquad (5\text{-}14)$$

The diffusion coefficients of Cs^+ show good agreement with the values determined by the various electroanalyses. Although the self-diffusion coefficient and the diffusion coefficient are different from the definition, we compared with those values for reference. The diffusion coefficient of Cs^+ from experimental result is less than the

self-diffusion coefficient in the molten CsCl (1.4×10^{-5}; ^{134}Cs)[38]. It is known that Cs element has only one oxidation state, Cs^+. There is no disproportionation reaction in this melt. The electrochemical reaction of Cs^+ is more positive than the decomposition potential of the bath. However, we cannot recover Cs by using the solid electrode because the following reaction (5-15) take place in this melt due to the almost same reduction potential, which is calculated from the decomposition potentials[2], for Cs^+ and K^+.

$$K^+ + Cs \rightarrow K + Cs^+ \qquad (5\text{-}15)$$

Therefore we examined the possibility of the recovery of Cs on liquid metallic cathodes on Chapter VI.

§ V-iii-ii Electrochemical behavior of Eu^{2+} and Sr^{2+} in molten chloride system

The cyclic voltammogram and chronopotentiogram of Eu^{2+} and Sr^{2+} were made on liquid metallic cathode in order to obtain the kinetic parameters and diffusion coefficients by conventional, semi-integral and semi-differential methods. The derived properties are compared with each other as follows.

(a) Conventional electroanalysis of a series of voltammograms

Typical cyclic voltammograms for Eu^{2+} and Sr^{2+} on liquid Bi, Sn and Zn cathodes are shown in **Figs. 5-13a** and **5-13b**, respectively. In **Figs. 5-14a** and **5-14b**, typical cyclic voltammograms with various sweep rates are shown for the reduction of Eu^{2+} and Sr^{2+} on the liquid Pb cathode, respectively. There was found no prepeak and postpeak at the reduction part of Figs. 5-14a and 5-14b. On our recognition that there is negligible adsorption effect, we applied the following relation to the reduction reaction. Using the following relation[39] for conventional electroanalysis of the voltammograms,

$$\ln i_p = \frac{\alpha n_a F}{RT}(E_p - E_{1/2}) + \ln(0.227 \times 10^{-3} \times n_a FAC^* k^0) \qquad (5\text{-}16)$$

where i_p is the peak current, E_p is the peak potential, $E_{1/2}$ is the half wave potential, α is a transfer coefficient, k^0 is the standard rate constant, F is the Faraday constant, A is a surface area of the working electrode, C^* is a bulk concentration, R is a gas constant and T is an absolute temperature. According to this equation (5-16), αn_a is calculated

from the slope of the plot of $\ln i_p$ on $E_p - E_{1/2}$. In addition, we determined the diffusion coefficient by the following relation[39].

$$i_p = 0.4958 \times 10^{-3} n_a FAC^* D^{1/2} v^{1/2} \left(\frac{\alpha n_a F}{RT} \right)^{1/2} \quad (5\text{-}17)$$

where D is a diffusion coefficient and v is a sweep rate. The resultant value is tabulated in **Tables 5-3a** and **5-3b**. The conventional electroanalysis could not be adopted for peak width between the reduction peak and the oxidation peak, because there is no anodic peak corresponding to the reduction peak as shown in Figs. 5-14a and 5-14b. Therefore, we determined the kinetic parameters by applying semi-integral and the semi-differential electroanalyses. Since only one cathodic peak is observed, we assumed the number of electron transferred $n_a = 2$ hereafter. We plotted the variations of the peak currents *vs.* the square root of the sweep rates from 0.005 to 0.5V/s in **Fig. 5-15**. The peak currents were found to be almost proportional to the square root of the sweep rates. Therefore, it is concluded that the overall reaction is controlled by diffusion.

(b) Semi-integral and semi-differential electroanalyses of the cathodic voltammograms

A typical semi-integral curve (**Fig. 5-16**) obtained from a linear sweep voltammetric experiment with $v = 0.1\mathrm{V/s}$ (Fig. 5-14a, run 4) yields a semi-integral limiting current density, $m^* = 0.188\mathrm{A \cdot s^{1/2}}$ in case of Eu. The occurrence of a plateau in the region of cathodic potentials proves that the rate of transfer is limited by diffusion; the plateau height is given by the equation (5-5). Assuming that the number of electron transferred is 2, this equation enables us to calculate the diffusion coefficient of Eu^{2+} and Sr^{2+} in this melt. Calculated diffusion coefficients are listed in Tables 5-3a and 5-3b. In addition, by adopting the equation (5-6b) to the alloy formation peak as irreversible system, we evaluated the kinetic parameters. According to the above relation, the plot of E vs. $\ln\{(m^* - m(t)/i(t))\}$ gives a straight line having slope of $RT/\alpha n_a F$. Typical example is shown in **Fig. 5-17** with 0.1V/s. The αn_a and k^0 are listed in Tables 5-3a and 5-3b.

In semi-differential electroanalysis which provides clearer peak than the conventional voltammogram, both kinetic parameter and diffusion coefficient can be obtained from equation (5-7b) for peak width, W_p and equation (5-7d) for peak height, e_p. A typical semi-differential curve obtained from semi-integral curve (Fig. 5-16) is shown in **Fig. 5-18**. The observed peak width $W_p = 0.33V$ gives kinetic parameter $\alpha n_a = 0.824$ for Eu, and $W_p = 0.30V$ gives $\alpha n_a = 0.906$ for Sr. The diffusion coefficients obtained by the equation (5-7d) are given in Tables 5-3a and 5-3b.

(c) General features and characterization of the chronopotentiometric electroanalysis

All these features for Eu and Sr can also be depicted on the chronopotentiogram of **Figs. 5-19a** and **5-19b**, respectively. A series of chronopotentiograms at liquid Pb electrode for various current densities have also been examined. Using the equation (5-8b), the value of αn_a was calculated from the slope of the E *vs.* $\ln(\tau^{1/2} - t^{1/2})$ plots as shown in **Fig. 5-20** as for Eu^{2+}. This method yields $\alpha n_a = 0.804$ for Eu and $\alpha n_a = 1.124$ for Sr, which are reasonably similar to those determined from voltammogram as shown in Tables 5-3a and 5-3b. The diffusion coefficients of Eu^{2+} and Sr^{2+} in this melt calculated from Sand's law and the standard rate constant which is the one of kinetic parameter, extrapolated to $\ln(\tau^{1/2} - t^{1/2}) = 0$, are summarized in Tables 5-3a and 5-3b. The kinetic parameters and the diffusion coefficients are also good agreement with the values determined from the various electroanalyses. The diffusion coefficient of Sr^{2+} is also in reasonable agreement with the value of $1.46 \pm 0.18 \times 10^{-5}\ cm^2/s$ reported by A. V. Volkovich[40].

As the diffusion coefficient of Eu^{2+} obtained from experimental results is larger than that of Sr^{2+}, Eu^{2+} ion is more mobile than Sr^{2+}. Thus, the complexes made of Eu^{2+} may be less stable than that of Sr^{2+}. The transfer coefficient of Eu^{2+} is smaller than that of Sr^{2+}, which means that the activation energy of alloy formation for Eu^{2+} is smaller than that for Sr^{2+}, if transfer coefficient is regarded as symmetry factor equivalently[41]. Therefore, the high rate for alloy formation of Eu^{2+} ion may be attributed to the less stable complexes of Eu^{2+} ion.

Chronopotentiometric determinations showed that the Sand product was constant, i.e., the square root of the transition time was found to be almost proportional to the reverse of the current density in **Fig. 5-21**. Therefore, it is concluded that the overall reaction is controlled by diffusion.

(d) Cathodic behavior of Eu^{2+} in molten NaCl-KCl system

It was reported on the behavior of Eu^{3+}/Eu^{2+} in an eutectic mixture of NaCl-CsCl, as well as, in an equimolar mixture of NaCl-KCl on the solid electrode (vitreous carbon)[42),(43)]: The electromotive forces (emfs) were measured on liquid Pb cathode in the range of 809-973K during 0.42-3.42mol% of Eu concentration in the eutectic mixture of NaCl-CsCl. It was also reported that thermodynamic data of intermetallic compounds $EuBi_2$, $EuSn_3$, $EuPb_3$ with saturated liquid metal solutions were obtained by emf measurements[44]. However, in these reports, electrode behavior of Eu^{2+}/Eu on liquid metallic cathode was not electrochemically revealed.

In the case of liquid Bi, Sn and Zn electrodes, there was found no alloy formation peak at the reduction part as shown in Fig. 5-13a. The peak around -1.0V for liquid Bi electrode corresponds to the reduction of Bi^{3+}, which brought by the anodic dissolution. However, in the case of a liquid Pb electrode, we observed two cathodic peaks, as shown in Fig. 5-14a. The first cathodic peak around -2.3V at 0.1V/s was observed and it was somewhat irreversible, since peak positions depend on sweep rates. The cathodic limit which is the second cathodic peak around -3.0V corresponds to the deposition of solvent, i.e., the reduction of Na^+ ion. According to the report about the reduction of Eu on liquid Pb cathode, the deposition of Eu is in more positive side by 0.68V than the deposition of sodium[42]. Therefore, the second peak (Fig. 5-14a) at -2.32V (-3.0+0.68=-2.32) can be attributed to the reduction of Eu^{2+} by the following reaction.

$$Eu^{2+} + 2e^- + 3Pb \rightarrow EuPb_3 \qquad (5\text{-}18)$$

The Nernst equation for the above reaction (5-18) gives

$$E_{Eu^{2+}/Eu} = E^0_{Eu(Pb)} + \frac{RT}{2F} \ln \frac{a_{Eu^{2+}}}{a_{Eu(Pb)}} \qquad (5\text{-}19)$$

where $E_{Eu^{2+}/Eu}$ is the apparent standard potential of Eu, $E^0_{Eu(Pb)}$ is the equilibrium potential of Eu-Pb alloy, $a_{Eu^{2+}}$ is the activity of Eu in the melt, $a_{Eu(Pb)}$ is the activity of Eu-Pb alloy (from the deposition potential of Eu[5]). It is possible to shift $E_{Eu^{2+}/Eu}$ to more positive side by decreasing the activity of the deposition metal from equation (5-19).

It is known of two kinds of the oxidation state which is Eu^{3+} and Eu^{2+} for Eu metal. Eu^{3+} is not significantly included in this melt, because no Eu^{3+}/Eu^{2+} coupled peak exist in Fig. 5-14a. Moreover, the fact that Eu^{2+} is thermodynamically more stable than Eu^{3+} [42], so that no disproportionation reaction which is described as follows occurs in this melt at 1073K.

$$3Eu^{2+} \longrightarrow 2Eu^{3+} + Eu \qquad (5\text{-}20)$$

Chronopotentiogram of $EuCl_2$-NaCl-KCl shows that the peak around -0.65V corresponds to the deposition of Pb and the peak around -2.0V corresponds to the alloy formation of Eu by using the liquid metallic cathode and followed by the deposition of solvent Na around -2.6V in Fig. 5-19a.

The standard rate constants (k^0) determined from various electroanalyses show good agreement with the values obtained from linear sweep voltammetry with semi-integral electroanalysis. This value falls in with the Matsuda and Ayabe criterion[37], for a quasi-reversible system,

$$2.0\times10^{-5}\left(n_a\nu\right)^{1/2} \le k^0 \le 0.3\left(n_a\nu\right)^{1/2} \text{(Quasi-reversible)} \qquad (5\text{-}21)$$

which in our condition yields

$$8.9\times10^{-6} \le k^0 \le 0.1 \text{(Quasi-reversible)} \qquad (5\text{-}22)$$

Thus, the alloy formation reaction of Eu-Pb can be qualified as a quasi-reversible system at 1073K.

(e) Cathodic behavior of Sr^{2+} in molten NaCl-KCl and KCl system

In the case of liquid Bi, Sn and Zn electrodes, there was found no alloy formation peak at the reduction part as shown in Fig. 5-13b. The peak around +0.5V for liquid Sn electrode corresponds to the reduction of Sn^{2+} is brought by the anodic dissolution.

On the other hand, in the case of a liquid Pb electrode, we observed two cathodic peaks, as shown in Fig. 5-14b. The first cathodic peak around -1.8V with 0.1V/s was observed and it was also shifted depending on sweep rates, which means irreversible which is similar to Eu. The cathodic limit which is the second cathodic peak around -3.0V in Fig. 5-14b corresponds to the deposition of solvent, i.e., the reduction of K^+ ions. We should take the alloy composition of $SrPb_3$ which is stable at $x_{Pb} > 0.9$ on Pb-Sr phase diagram[45] into consideration and in view of the result obtained from Fig. 5-14b, it can be concluded that the first cathodic peak corresponds to the following reaction

$$Sr^{2+} + 2e^- + 3Pb \rightarrow SrPb_3 \qquad (5\text{-}23)$$

The Nernst equation for the reaction (5-23) also gives

$$E_{Sr^{2+}/Sr} = E^0_{Sr(Pb)} + \frac{RT}{2F}\ln\frac{a_{Sr^{2+}}}{a_{Sr(Pb)}} \qquad (5\text{-}24)$$

In the case of Sr, therefore, from the equation (5-24), it is possible to recover this element as well as Eu if it is possible to decrease the activity of the deposition metal by making an alloy formation between Sr and the liquid Pb electrode.

It is known that Sr metal has only one oxidation state, Sr^{2+}. There is no disproportionation reaction in this melt. We carried out the similar experiment to that in NaCl-KCl at 1073K. There is no Sr^{2+}/Sr(Pb) peak in the result of this experiment, because the Na deposited predominantly before the reduction of Sr. However, Fig. 5-19b for the $SrCl_2$-KCl system, it shows that the peak around -2.2V corresponds to the alloy formation of Sr by using the liquid Pb cathode and followed by the deposition of solvent KCl. The standard rate constants determined from various electroanalyses give good agreement each other as shown in Table 5-3b. This value falls in with the Matsuda and Ayabe criterion (5-22) and the alloy formation reaction of Sr-Pb can be qualified as a quasi-reversible system at 1073K.

§ V - iii - iii Electrochemical behavior of Ba^{2+} in molten chloride system

(a) Electrochemical behavior of Ba^{2+} using the liquid Pb cathode

Typical cyclic voltammograms for Ba^{2+} and no Ba^{2+} on liquid Pb electrode in the NaCl-KCl equimolar mixture are shown in **Figs. 5-22a** and **5-22b**, respectively. There are three cathodic peaks as shown in Fig. 5-22a. The peak 1 around 0V corresponds to the reduction of Pb^{2+}/Pb brought about by the anodic dissolution as shown in Fig. 5-22b on run 4. Additionally, it is conjectured that the cathodic peak 2 in Fig.5-22a indicates the alloy formation reation between Ba and Pb by comparison with Fig. 5-22b, since this figure shows no peak except for reduction of Pb^{2+}/Pb. In the case of carrying out the anodic dissolution of the liquid Pb electrode, there was the Ba-Pb alloy formation peak for the voltammogram shown in Fig. 5-22a. For the obtained cyclic voltammogram, the peak current is almost proportional to the square root of the sweep rate, as shown in **Fig. 5-23**. Therefore, this result allows us to conclude that the overall reaction is controlled by diffusion. It is speculated that the deposition mechanism of Ba as for Ba-Pb alloy formation might be different from that of Eu^{2+} and Sr^{2+}. Therefore, this result enables us to conclude that the deposition mechanism between Ba and Pb is associated with the alloy formation between them. According to the Ba-Pb phase diagram[46] in this condition at 1000K, this alloy formation reaction is considered to be $Ba^{2+} + 2e^- + Pb \rightarrow BaPb$. We determined the kinetic parameters and the diffusion coefficient for Ba^{2+} on the liquid Pb electrode by the electroanalysis of cyclic voltammogram with conventional, semi-integral and semi-differential methods. For conventional electroanalysis of the cyclic voltamogram, the kinetic parameters calculated from Eq. (5-16) is listed in **Table 5-3c**. The diffusion coefficient calculated from Eq. (5-17) is also shown in Table 5-3c. In this relation, we assumed the number of electron transferred is 2. In addition, in order to determine these parameters, we

applied the obtained voltammogram to semi-integral and semi-differential methods. A typical semi-integral curve obtained from the voltammogram was shown in **Fig. 5-24**. For the semi-integral electroanalysis, the estimated semi-integral limiting current density is $m^* = 0.815A \cdot s^{1/2}$ as shown in Fig. 5-24. Assuming the number of electron transferred is also 2, the diffusion coefficient calculated from Eq. (5-5) is shown in Table 5-3c with reported diffusion coefficient of Ba^{2+}, which is consistent with our results. According to the Eq. (5-6b), the typical example is shown in **Fig. 5-25** and the calculated kinetic parameters are also tabulated in Table 5-3c. In the semi-differential analysis which provides clearer peak than the conventional cyclic voltammogram, as shown in **Fig. 5-26**. In this work, the observed peak width W_p=0.548V gives the kinetic parameter $\alpha n_a = 0.84$. The diffusion coefficient obtained by the equation (5-7d) is given in Table 5-3c. Using the value of kinetic parameter, we estimated the reversibility of the Ba-Pb alloy formation reaction. According to Matsuda and Ayabe criterion, in our case,

$$8.6 \times 10^{-6} \le k^0 \le 7.0 \times 10^{-2} \text{ (Quasi-reversible)} \qquad (5\text{-}25)$$

Therefore, the alloy formation reaction is supposed to be the quasi-reversible reaction. A typical chronopotentiogram for Ba on the liquid Pb cathode is depicted in **Fig. 5-27**. It is difficult to electroanalyze for obtained chronopotentiograms and to estimate the kinetic parameters and the diffusion coefficient.

(b) Electrochemical behavior of Ba^{2+} using the liquid Sn cathode

Typical cyclic voltammograms for $BaCl_2$ and no Ba^{2+} in the NaCl-KCl system on liquid Sn electrode are shown in **Figs. 5-28a** and **5-28b**, respectively. There are several cathodic peaks in Fig. 5-28a. The peak 1 around 0~0.5V as shown in Figs. 5-28a and 5-28b corresponds to the reduction of Sn^{2+} as well as Pb^{2+}. In this condition at

1000K from the Ba-Sn phase diagram[47]-[50], we could not confirm what alloy was made between them because the phase diagram are not well defined at this temperature. However compared with Figs. 5-28a and 5-28b, it is conjectured that the decomposition mechanism of Ba^{2+} is related to the Ba-Sn alloy formation reaction. Additionally, the each plateau in a chronopotentiogram corresponds to a peak in the voltammogram as shown in **Fig. 5-29**.

On the other hand, there are no alloy formation peaks in the typical cyclic voltammograms and chronopotentiograms used liquid metallic cathodes (Al, Bi, Cd and Zn) as the working electrode.

Table 5-1a Typical values of cathodic peak potential (E_p^c) and half-peak potential ($E_{p/2}^c$) *vs.* Pt quasi-reference electrode for the Cs^+/Cs reduction in the FLINAK system at 773K obtained from linear sweep voltammetry on the solid graphite electrode at various potential sweep rates (ν)

ν (V/s)	E_p^c (V)	$E_{p/2}^c$ (V)	ΔE_p^c (V)	n	αn_a
1.0	-1.99	-1.78	0.21	0.25	0.59
0.5	-1.99	-1.78	0.21	0.25	0.59
0.3	-1.98	-1.79	0.19	0.27	0.65
0.2	-1.98	-1.80	0.18	0.29	0.69
0.1	-1.99	-1.80	0.19	0.27	0.65
0.05	-1.97	-1.80	0.17	0.30	0.73
0.03	-1.98	-1.76	0.22	0.24	0.56
0.01	-1.99	-1.81	0.18	0.29	0.69
0.005	-1.98	-1.81	0.17	0.30	0.73

Table 5-1b Typical values of anodic peak potential (E_p^a) and half-peak potential ($E_{p/2}^a$) *vs.* Pt quasi-reference electrode for the Cs/Cs^+ reduction in the FLINAK system at 773K obtained from linear sweep voltammetry on the solid graphite electrode at various potential sweep rates (ν)

ν (V/s)	E_p^a (V)	$E_{p/2}^a$ (V)	ΔE_p^a (V)	n	αn_a
1.0	-1.10	-1.28	0.18	0.29	0.69
0.5	-1.13	-1.31	0.18	0.29	0.69
0.3	-1.14	-1.33	0.19	0.27	0.65
0.2	-1.16	-1.31	0.15	0.35	0.83
0.1	-1.16	-1.31	0.15	0.35	0.83
0.05	-1.20	-1.35	0.15	0.35	0.83
0.03	-1.22	-1.35	0.13	0.40	0.95
0.01	-1.25	-1.36	0.11	0.47	1.13
0.005	-1.25	-1.36	0.11	0.47	1.13

Table 5-2a Charge transfer number, diffusion coefficient and kinetic parameter for Cs^+ in the FLINAK system on the solid graphite electrode at 773K from the various electroanalyses

n	$D \times 10^6$ (cm^2/s)	Method
0.99	1.1	CV(conventional from Eqs. (5-3), (5-4a))
-----	1.7	CV(semi-integral)
1.00	1.9	CP
αn_a	$k^0 \times 10^6$ (cm/s)	Method
0.65	------	CV(conventional from Eq. (5-2b))
0.83	1.1	CV(semi-integral)
0.86	1.0	CP

Table 5-2b Charge transfer number, diffusion coefficient and kinetic parameter for Cs^+ in the FLINAK system on the liquid Pb electrode at 773K from the various electroanalyses

n	$D \times 10^6$ (cm^2/s)	Method
0.73	1.6	CV(conventional from Eqs. (5-2c), (5-4b))
0.94	1.0	CV(semi-integral)
1.04	0.8	CV(semi-differential)
1.17	1.8	CP
αn_a	$k^0 \times 10^6$ (cm/s)	Method
0.73	------	CV(conventional from Eq. (5-2b))
0.81	1.2	CV(semi-integral)
0.87	------	CV(semi-differential)
1.00	2.1	CP

Table 5-3a Charge transfer number, diffusion coefficient and kinetic parameter for Eu^{2+} in the NaCl-KCl equimolar mixture on the liquid Pb electrode at 1073K from the various electroanalyses

αn_a *	$k^0 \times 10^4$ (cm/s)**	$D \times 10^5$ (cm^2/s)*	Method
0.66±0.06	3.3±0.8	6.5±0.5	CV(conventional)
0.84±0.05	4.6±0.5	8.5±0.5	CV(semi-integral)
0.82±0.04	----------	6.9±0.2	CV(semi-differential)
0.80±0.08	5.6±0.7	5.8±0.7	CP

* The errors of αn_a and D are due to potential and current in CV and CP.

** The error of k^0 is due to the least square method.

Table 5-3b Charge transfer number, diffusion coefficient and kinetic parameter for Sr^{2+} in the KCl system on the liquid Pb electrode at 1073K from the various electroanalyses

αn_a	$k^0 \times 10^4$ (cm/s)	$D \times 10^5$ (cm^2/s)	Method
0.90±0.05	3.8±0.6	1.3±0.3	CV(conventional)
0.88±0.06	2.2±0.5	1.7±0.2	CV(semi-integral)
0.91±0.05	----------	1.6±0.2	CV(semi-differential)
1.12±0.07	1.3±0.8	1.9±0.7	CP
		1.46±0.18	CP[40]

Table 5-3c Kinetic parameters and diffusion coefficient for Ba^{2+} in the NaCl-KCl system on the liquid Pb electrode at 1000K from the various electroanalyses

αn_a	$k^0 \times 10^4$ (cm/s)	$D \times 10^5$ (cm^2/s)	Method
0.86±0.04	----------	1.3±0.2	CV(conventional)
0.92±0.03	1.7±0.5	1.1±0.3	CV(semi-integral)
0.84±0.04	----------	1.2±0.3	CV(semi-differential)
0.87±0.06	2.2±0.4	1.0±0.2	CP
		1.08±0.16	CP[40]

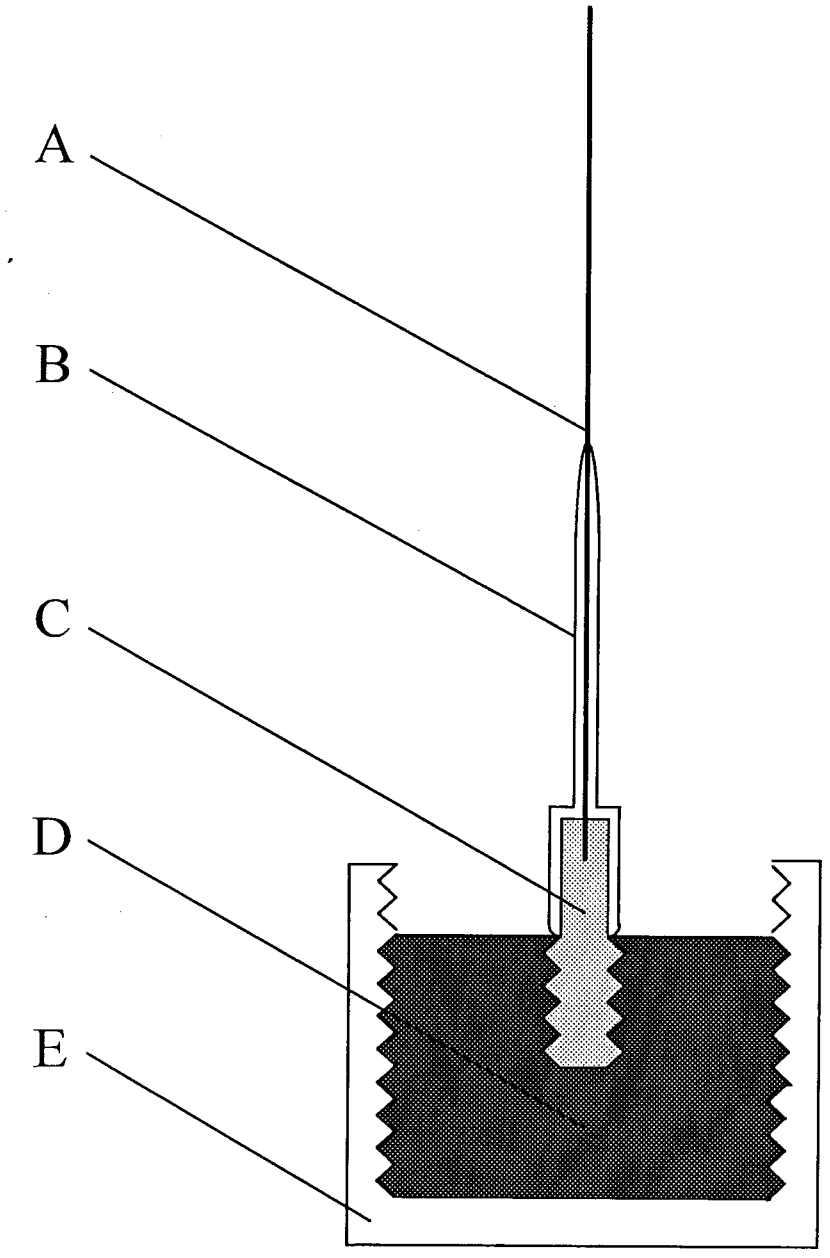

Fig. 5-1 The solid graphite electrode used in electrochemical measurement for Cs
A:Tungsten wire (lead to small graphite), B:BN coating, C:Small graphite
D:Large graphite (working electrode), E:BN rod

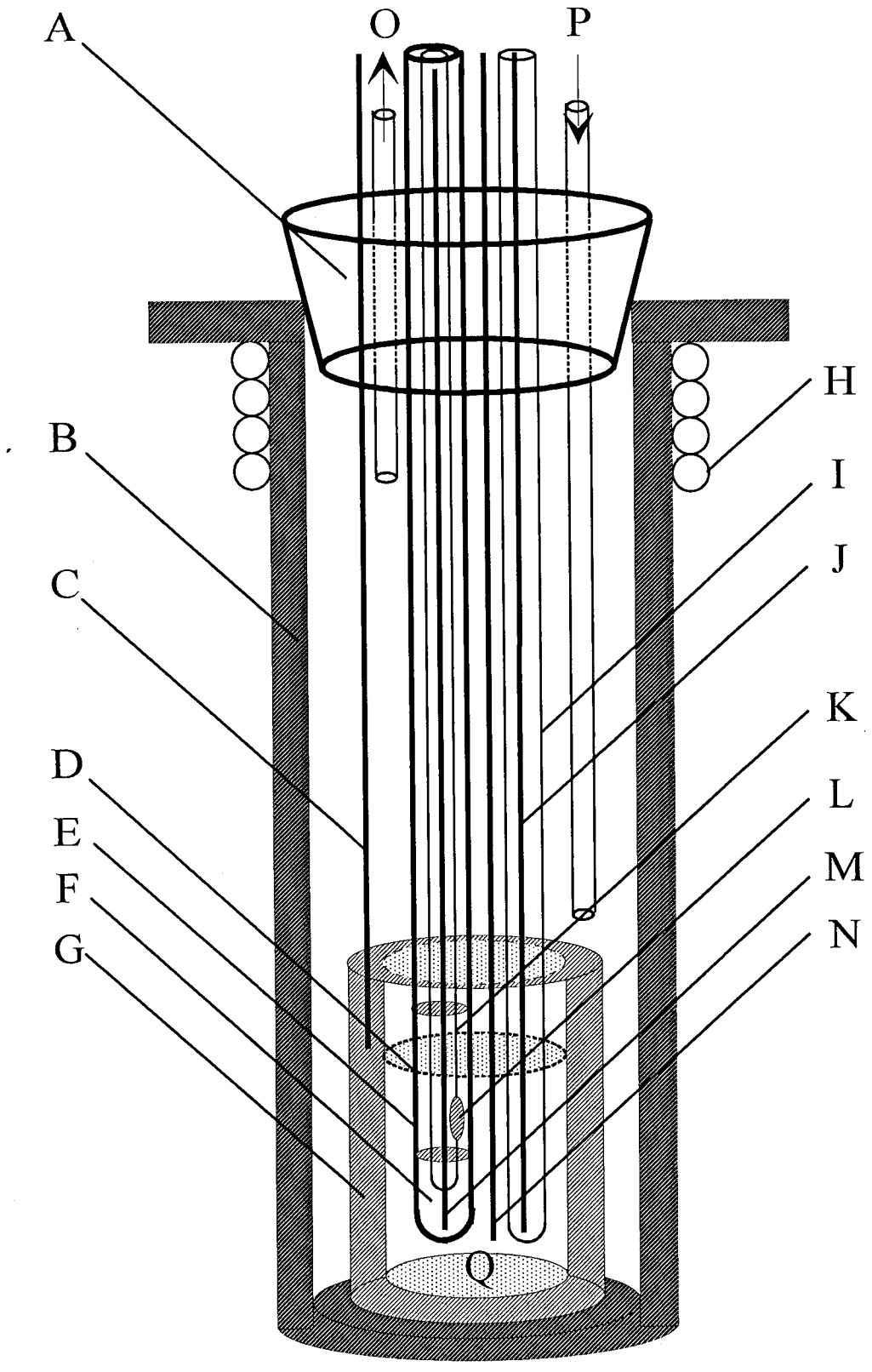

Fig. 5-2a The furnace cell assembly used in electrolytic experiments
A: Silicon stopper, B: Stainless steel cell, C: Tungsten wire (lead to crucible), D: Mullite tube, E: BN rod (covering liquid electrode), F: Liquid metallic electrode (Pb, Sn, Zn), G: Graphite crucible (counter electrode), H: Cooling water, I: Alumina tube (covering thermocouple), J: Thermocouple, K: BN rod (covering tungsten wire), L: 6mm ϕ hole, M: Tungsten wire (lead to liquid metal), N: Pt wire (quasi-reference electrode), O: Ar gas outlet, P: Ar gas inlet, Q: Molten salt (FLINAK system)

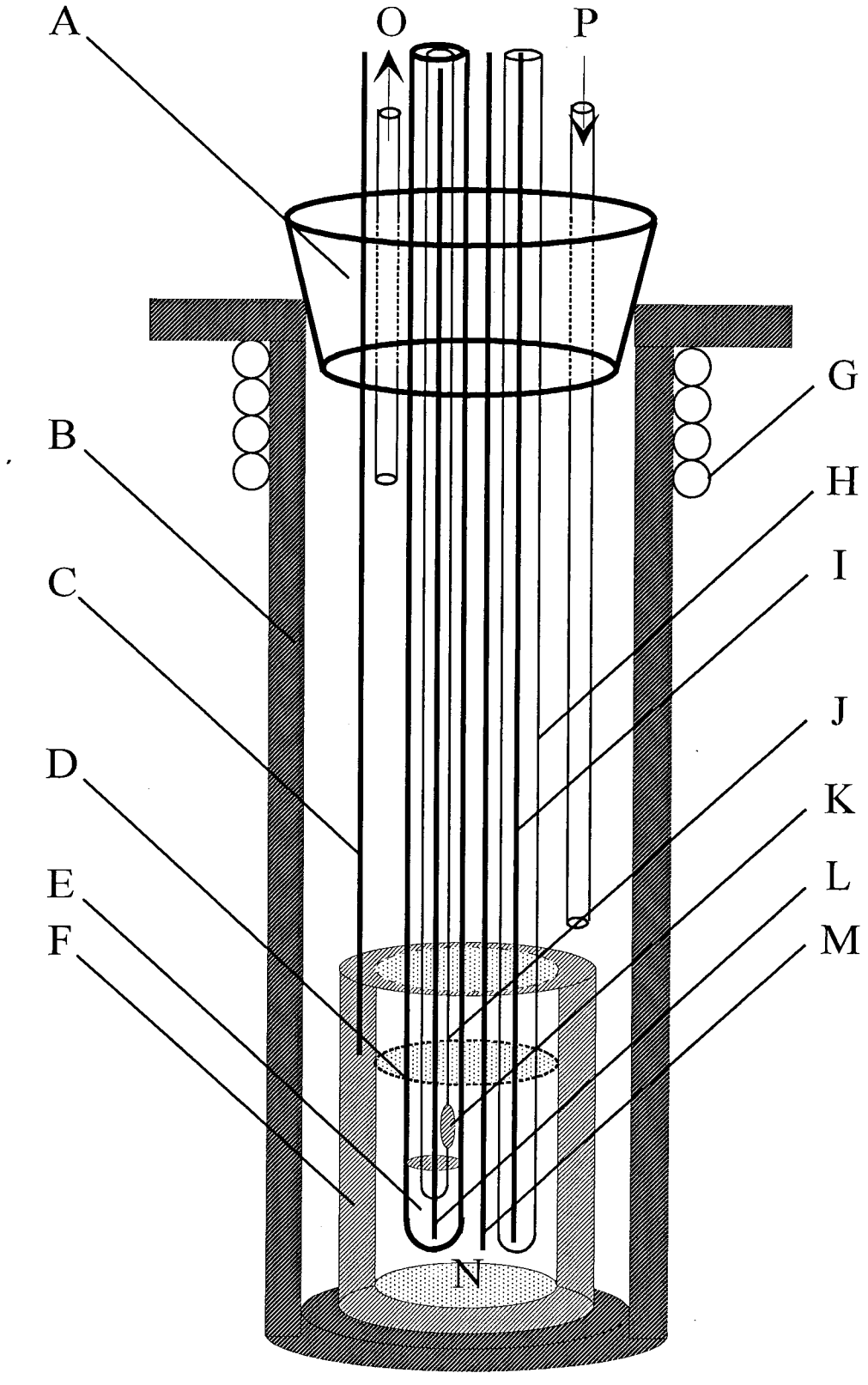

Fig. 5-2b The furnace cell assembly used in electrolytic experiments
A: Silicon stopper, B: Stainless steel cell, C: Tungsten wire (lead to crucible), D: Quartz tube (covering the liquid electrode), E: Liquid metallic working electrode (Al, Bi, Cd, Pb, Sn and Zn), F: Graphite crucible (counter electrode), G: Cooling water, I: Thermocouple, J: Quartz tube (covering tungsten wire), K: 6mmϕ hole, L: Tungsten wire (lead to liquid metal), M: Pt wire (quasi-reference electrode), N: Molten salt (NaCl-KCl equimolar mixture), O: Ar gas outlet, P: Ar gas inlet

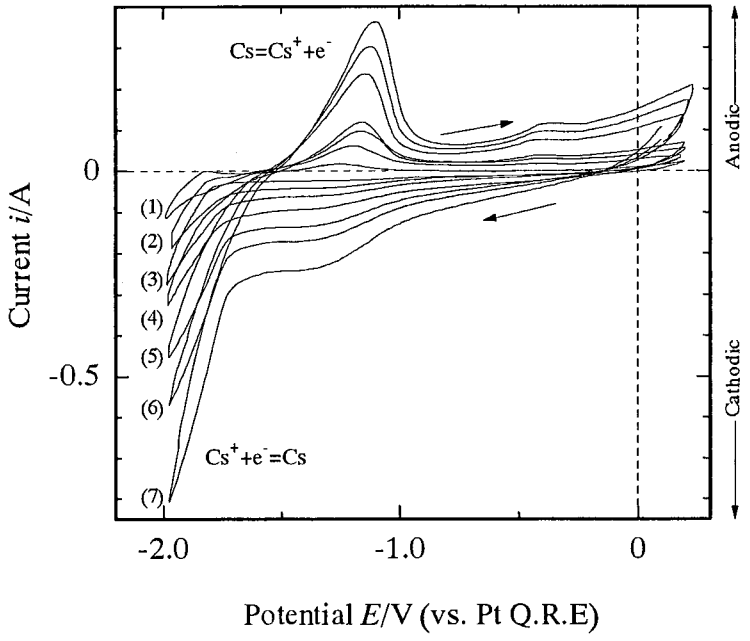

Fig. 5-3a Cyclic voltammogram for CsCl on the solid graphite electrode in the FLINAK system at 773K, sweep rate: (1) 0.005V/s (2) 0.01V/s (3) 0.05V/s (4) 0.1V/s (5) 0.3V/s (6) 0.5V/s (7) 1.0V/s.

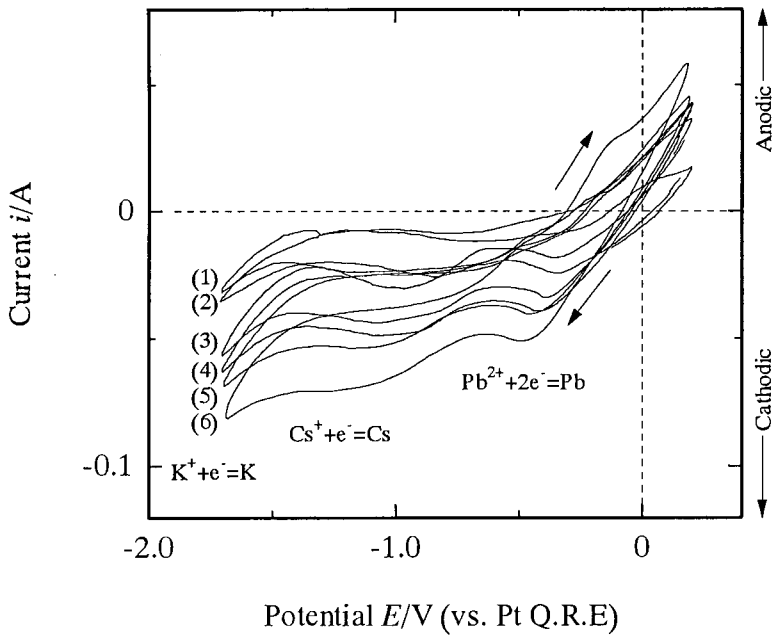

Fig. 5-3b Cyclic voltammogram for CsCl on the liquid Pb electrode in the FLINAK system at 773K, sweep rate: (1) 0.005V/s (2) 0.01V/s (3) 0.05V/s (4) 0.1V/s (5) 0.3V/s (6) 0.5V/s.

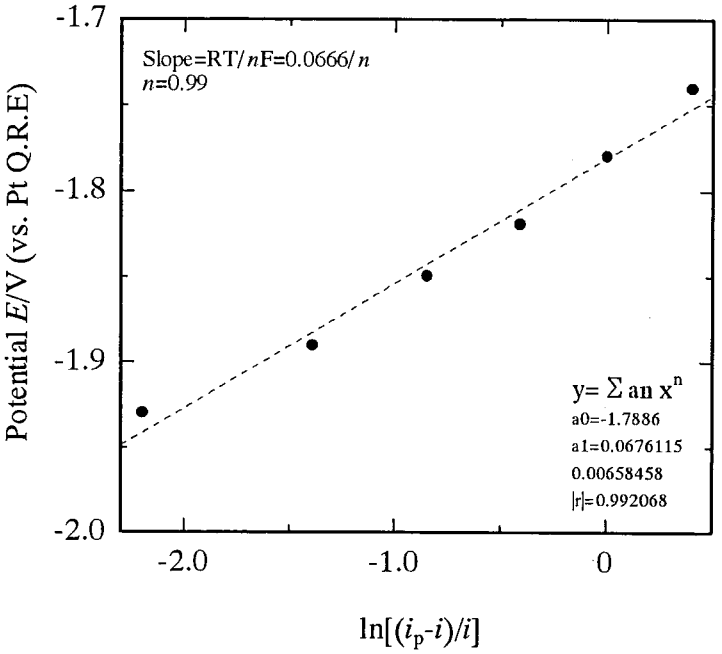

Fig. 5-4a Plots of E *vs.* $\ln\left\{\left(i_p - i\right)/i\right\}$ in the range (0.4-0.9)i_p for the reduction of Cs^+/Cs in the FLINAK system on the solid graphite electrode at 773K.

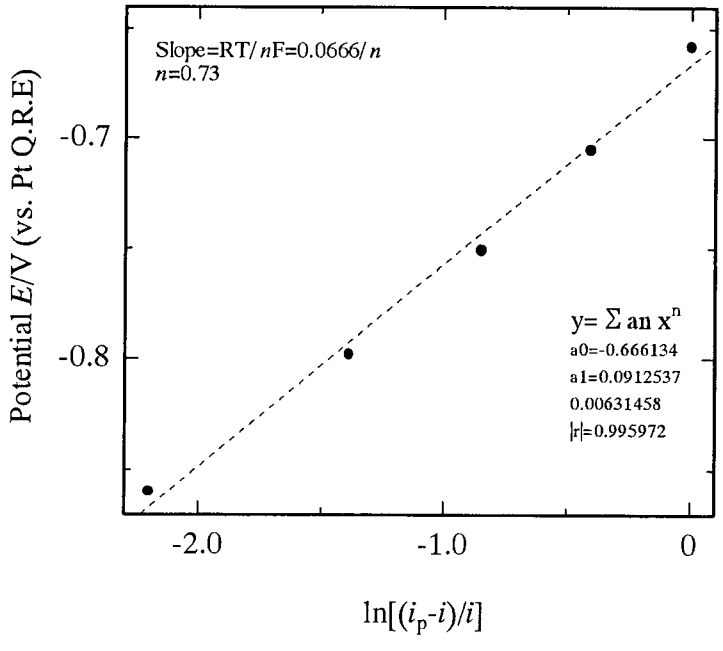

Fig. 5-4b Plots of E *vs.* $\ln\left\{\left(i_p - i\right)/i\right\}$ in the range (0.5-0.9)i_p for the reduction of Cs^+/Cs in the FLINAK system on the liquid Pb electrode at 773K.

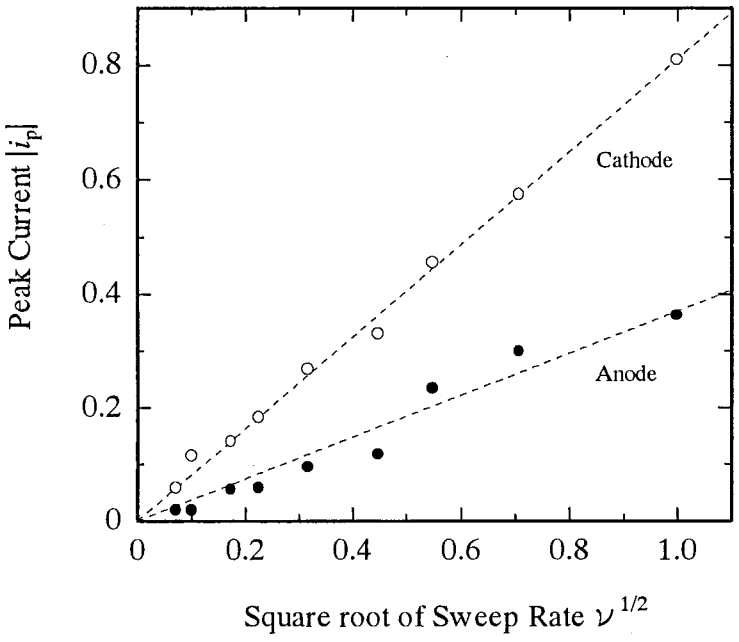

Fig. 5-5 Relationship between the square root of sweep rate and the peak current on the solid graphite electrode.

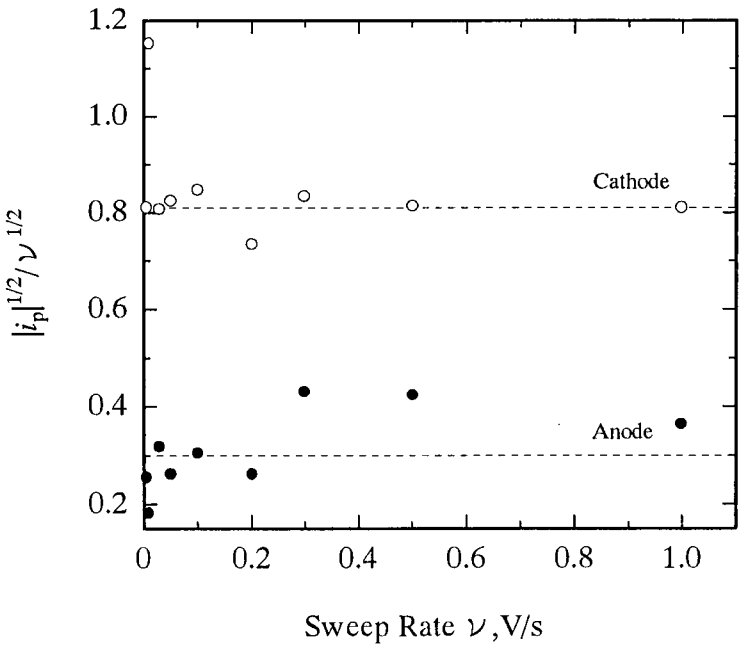

Fig. 5-6 Plots of $|i_p|/\nu^{1/2}$ vs. ν for the oxidation and reduction of CsCl in the FLINAK system on the solid graphite electrode.

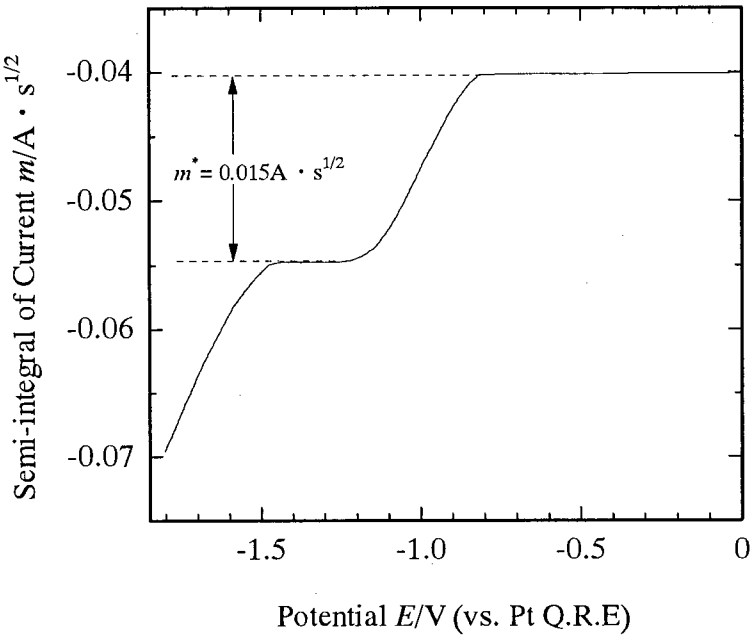

Fig. 5-7 Semi-integral of the curve plotted for CsCl in the FLINAK system on the liquid Pb electrode at 773K, sweep rate: 0.5V/s.

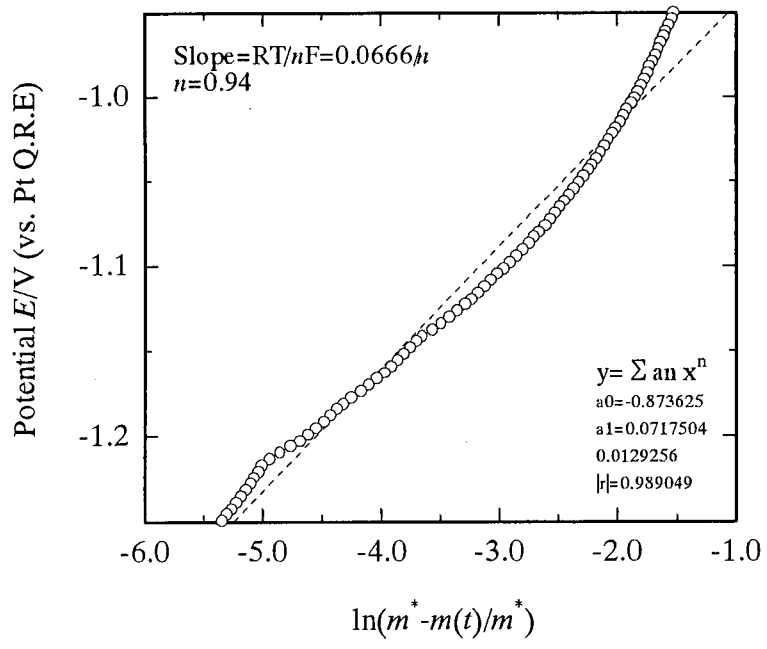

Fig. 5-8 Logarithmic analysis of semi-integral of the curve plotted for CsCl in the FLINAK system on the liquid Pb electrode at 773K, sweep rate: 0.5V/s.

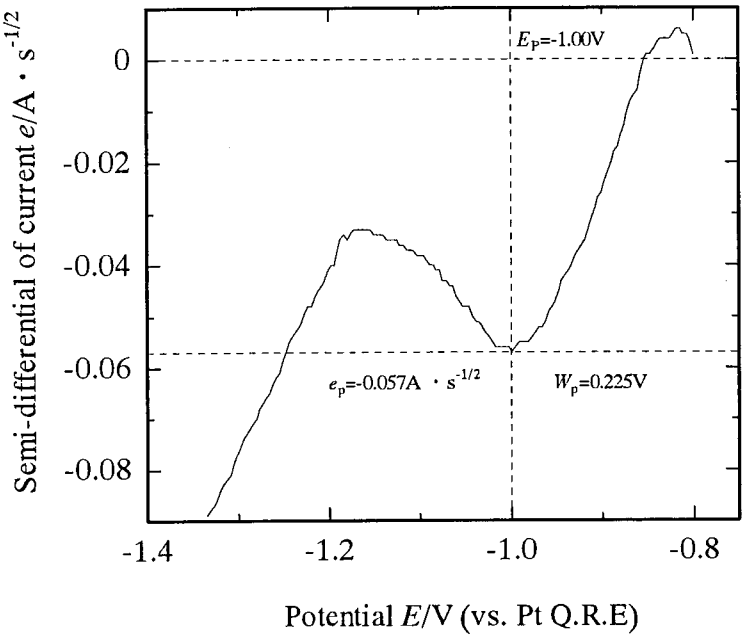

Fig. 5-9 Semi-differential of a voltammogram plotted at 0.5V/s for CsCl in the FLINAK system on the liquid Pb electrode at 773K.

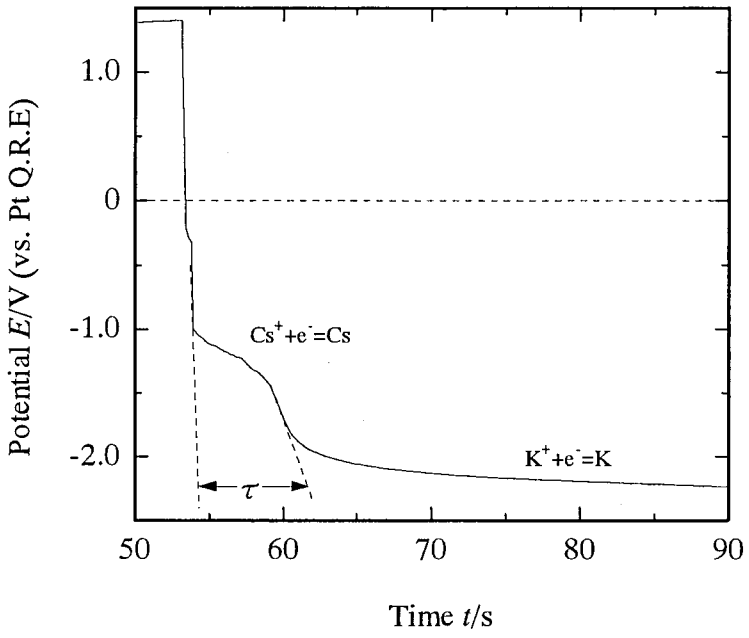

Fig. 5-10a Chronopotentiogram for CsCl on the solid graphite electrode in the FLINAK system at 773K, cathodic current density: -0.032A/cm^2.

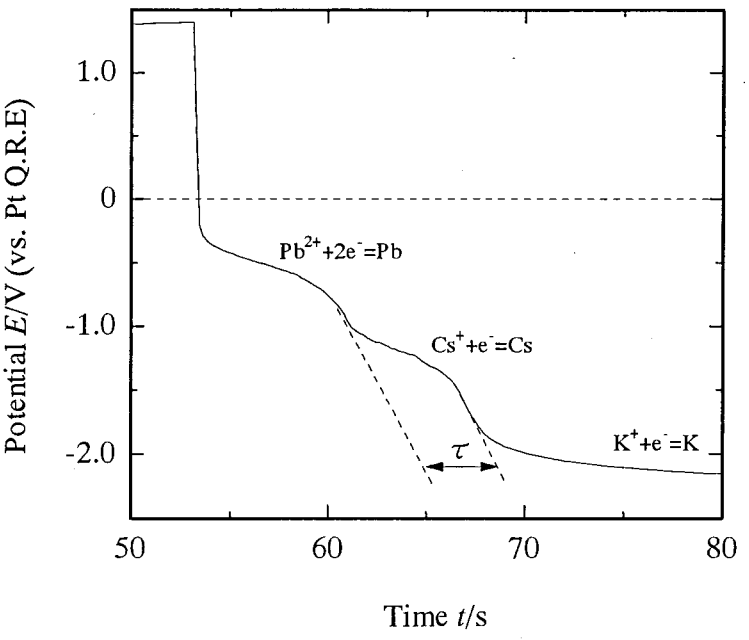

Fig. 5-10b Chronopotentiogram for CsCl on the liquid Pb electrode in the FLINAK system at 773K, cathodic current density: -0.089A/cm^2.

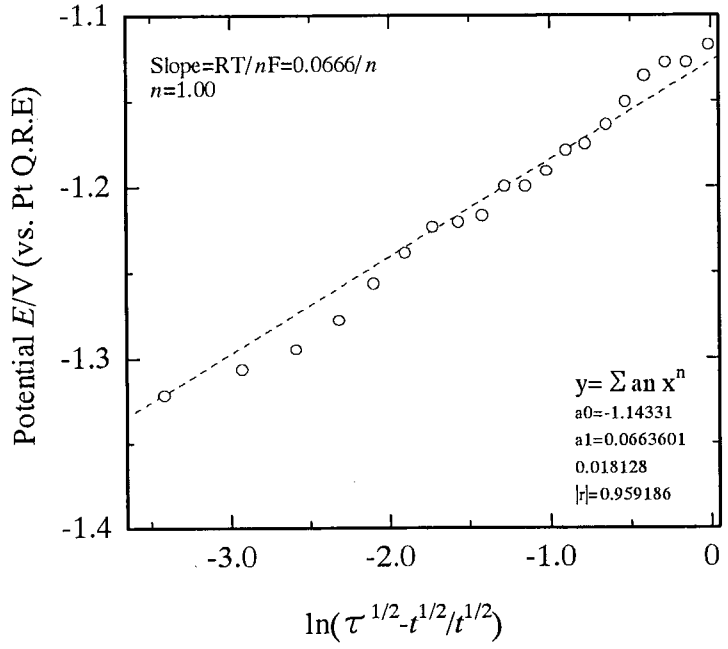

Fig. 5-11 Logarithmic analysis of chronopotentiogram for CsCl in the FLINAK system on the solid graphite electrode at 773K.

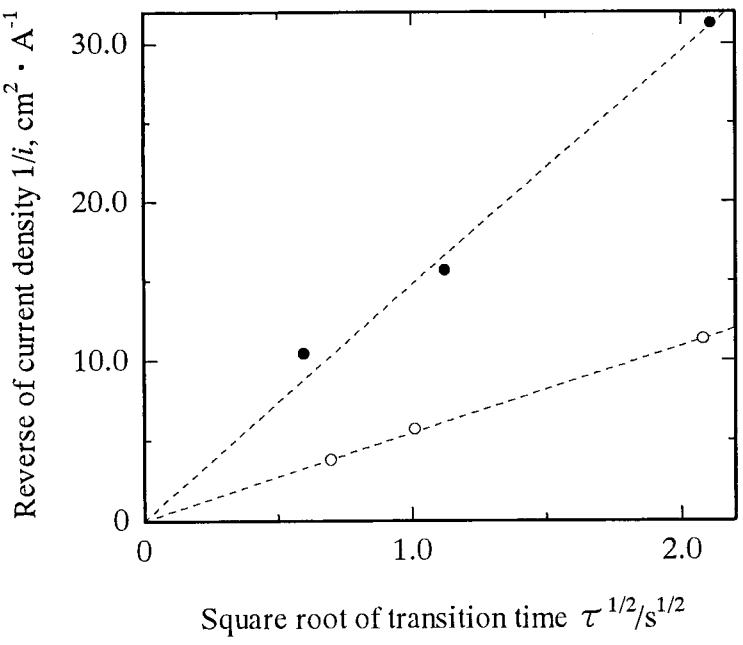

Fig. 5-12 Relationship between the reverse of electric current density and the square root of transition time in chronopotentiometric measurement, ●: solid graphite electrode, ○: liquid Pb electrode.

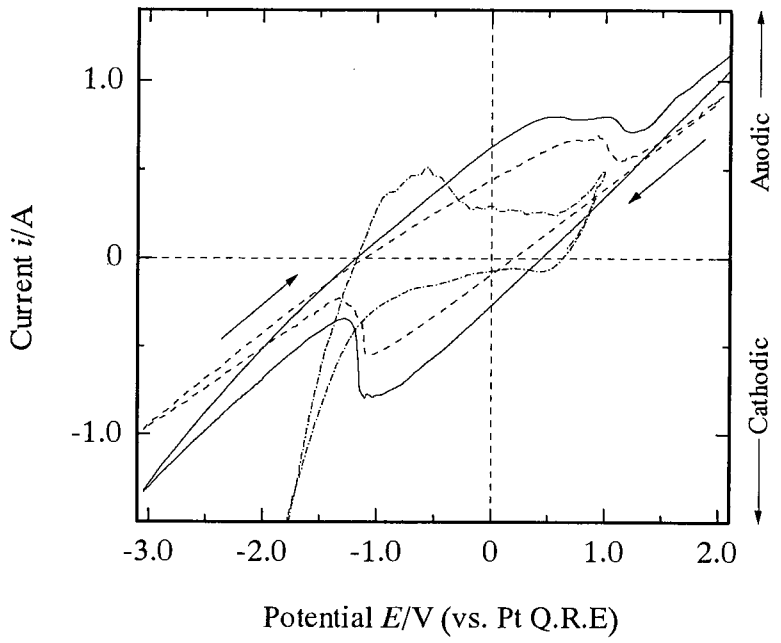

Fig. 5-13a Cyclic voltammogram for $EuCl_2$ on various liquid electrode in the NaCl-KCl equimolar mixture at 1073K, sweep rate: 0.1V/s, ———: Bi cathode, - - - -: Sn cathode, — - —: Zn cathode.

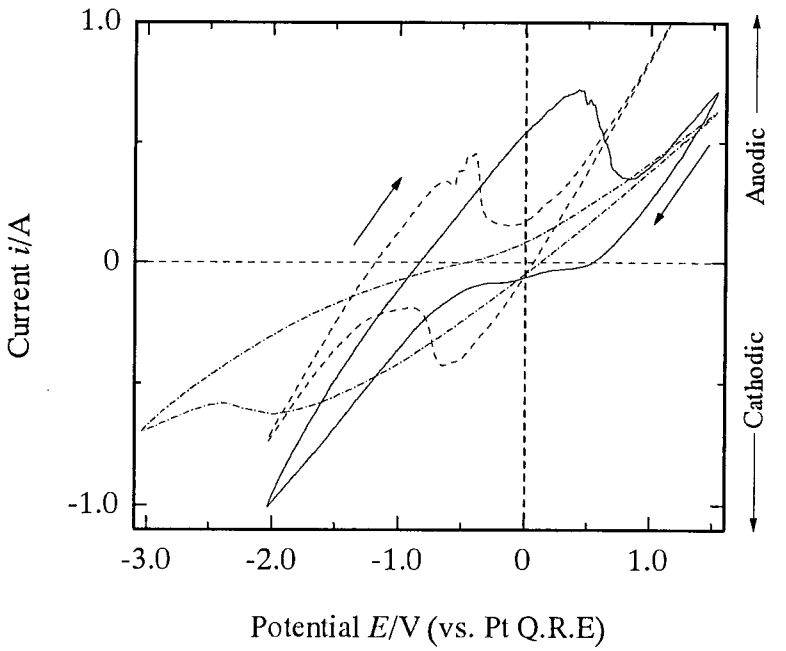

Fig. 5-13b Cyclic voltammogram for $SrCl_2$ on various liquid electrode in the NaCl-KCl equimolar mixture at 1073K, sweep rate: 0.1V/s, ———: Bi cathode, - - - -: Sn cathode, — - —: Zn cathode.

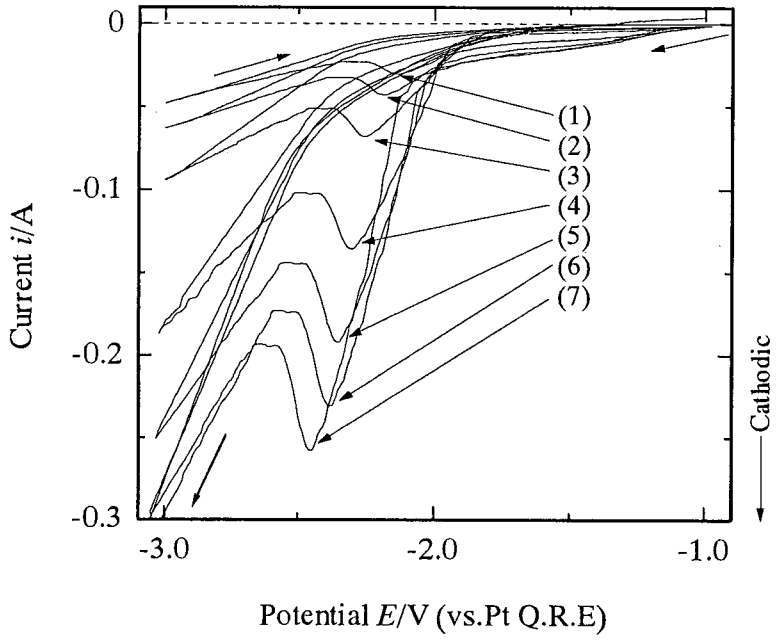

Fig. 5-14a Cyclic voltammogram for $EuCl_2$ on liquid Pb electrode in the NaCl-KCl equimolar mixture at 1073K, sweep rate: (1) 0.005V/s (2) 0.01V/s (3) 0.05V/s (4) 0.1V/s (5) 0.2V/s (6) 0.3V/s (7) 0.5V/s.

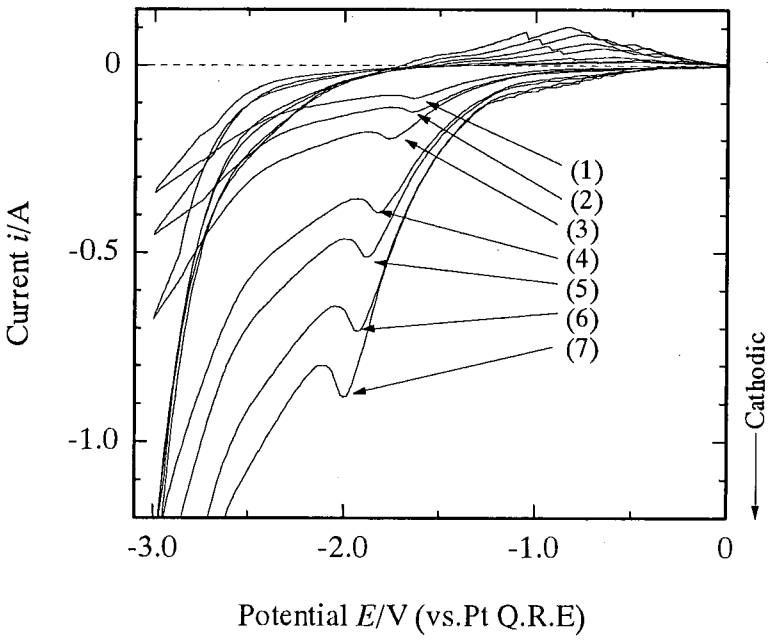

Fig. 5-14b Cyclic voltammogram for $SrCl_2$ on liquid Pb electrode in the KCl system at 1073K, sweep rate: (1) 0.005V/s (2) 0.01V/s (3) 0.05V/s (4) 0.1V/s (5) 0.2V/s (6) 0.3V/s (7) 0.5V/s.

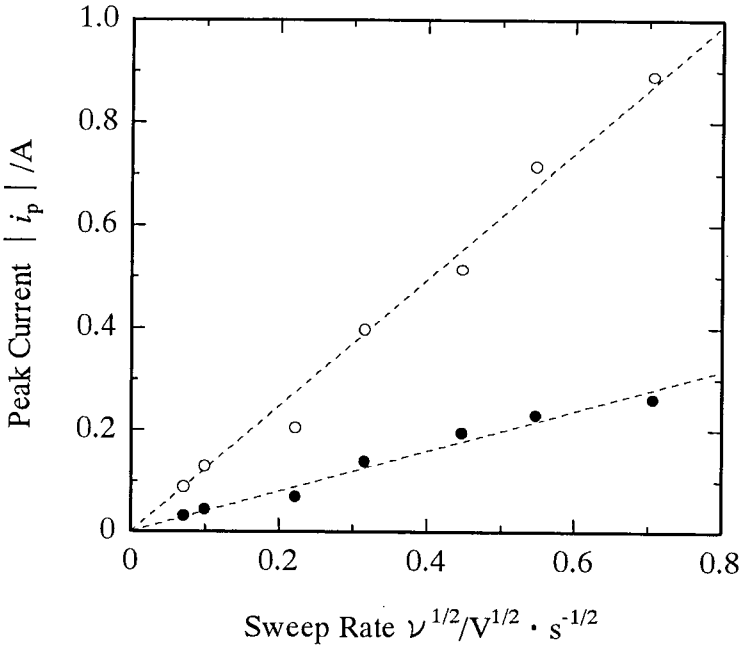

Fig. 5-15 Relationship between the square root of sweep rates and peak currents on the liquid Pb cathode at 1073K, ●: $EuCl_2$ in the NaCl-KCl system, ○: $SrCl_2$ in the KCl system.

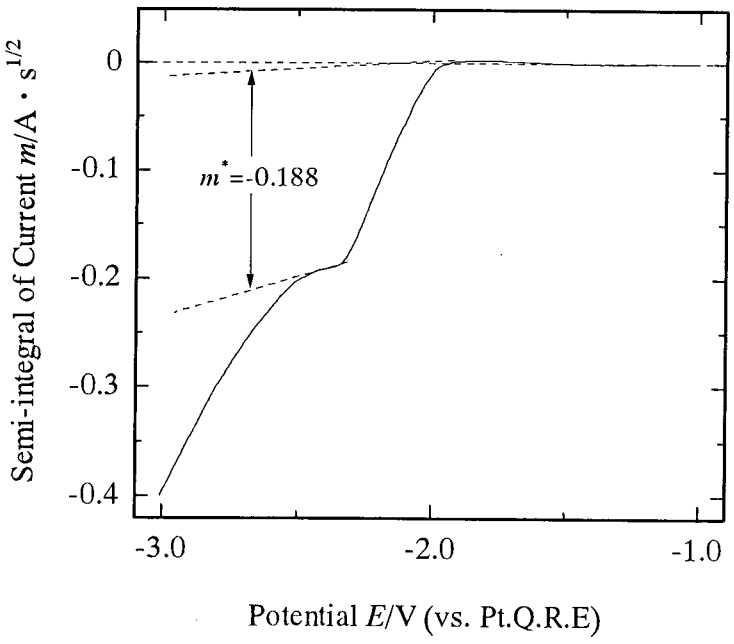

Fig. 5-16 Semi-integral of the curve plotted for $EuCl_2$ on the liquid Pb electrode in the NaCl-KCl equimolar mixture at 1073K, sweep rate: 0.1V/s

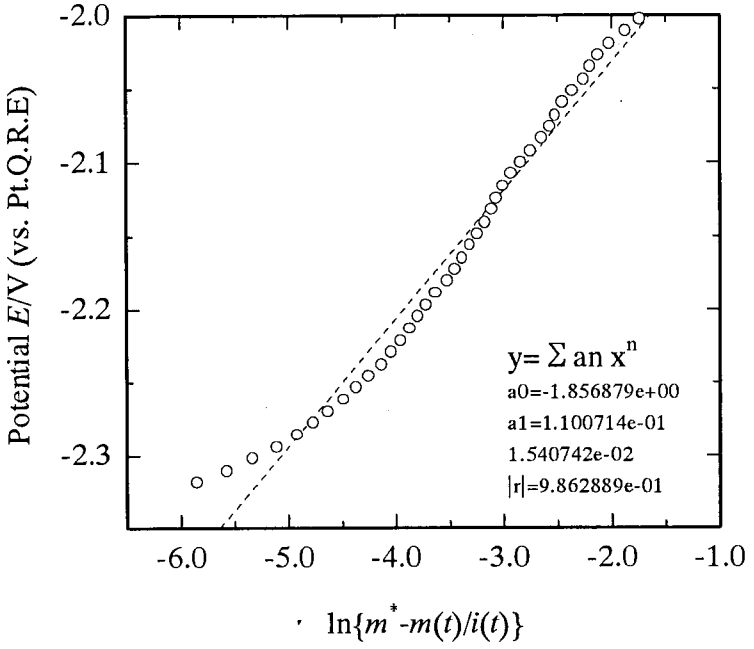

Fig. 5-17 Logarithmic analysis of semi-integral of the curve plotted for $EuCl_2$ on the liquid Pb electrode in the NaCl-KCl equimolar mixture at 1073K

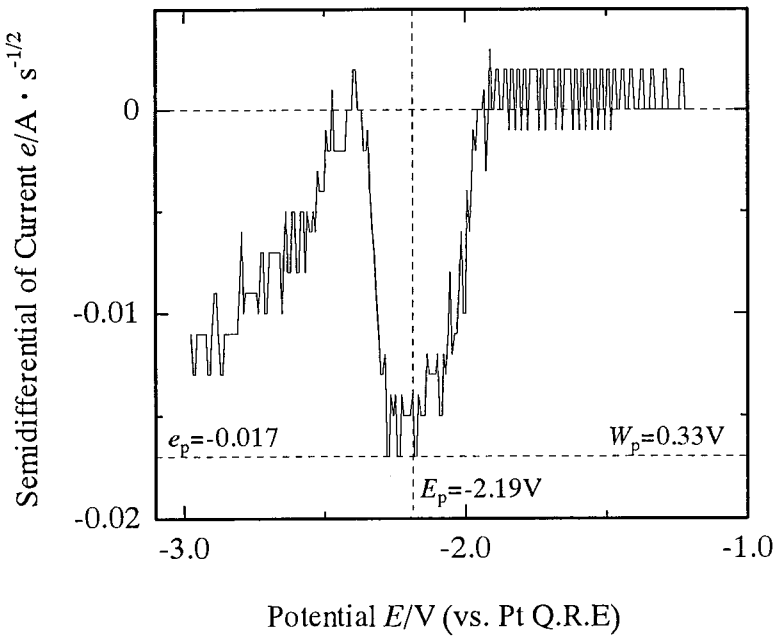

Fig. 5-18 Semi-differential of the curve plotted for $EuCl_2$ on the liquid Pb electrode in the NaCl-KCl equimolar mixture at 1073K

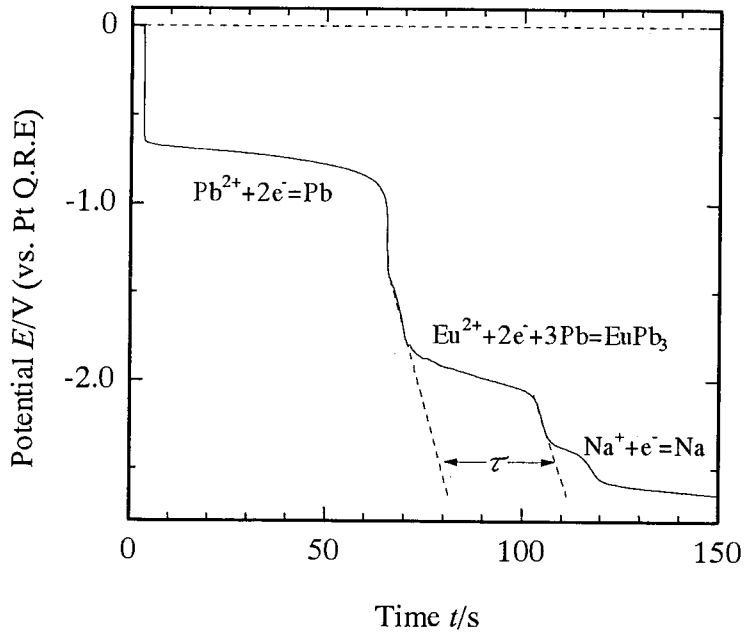

Fig. 5-19a Chronopotentiogram for $EuCl_2$ on the liquid Pb cathode in the NaCl-KCl equimolar mixture at 1073K

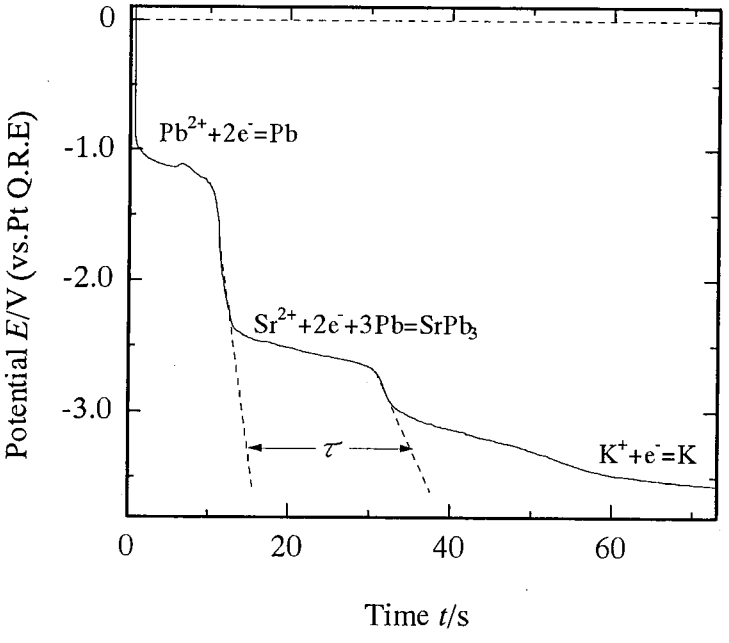

Fig. 5-19b Chronopotentiogram for $SrCl_2$ on the liquid Pb cathode in the KCl system at 1073K.

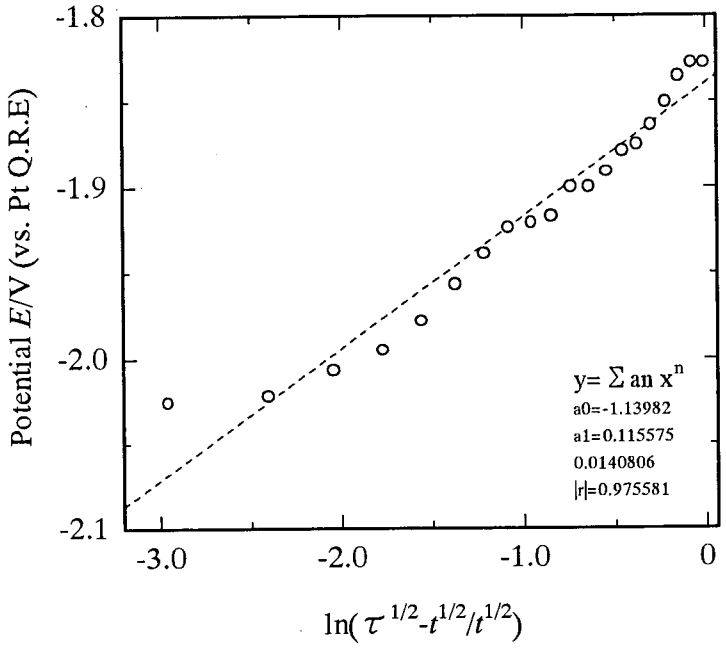

Fig. 5-20 Logarithmic analysis of chronopotentiogram for $EuCl_2$ on the liquid Pb cathode in the NaCl-KCl equimolar mixture at 1073K.

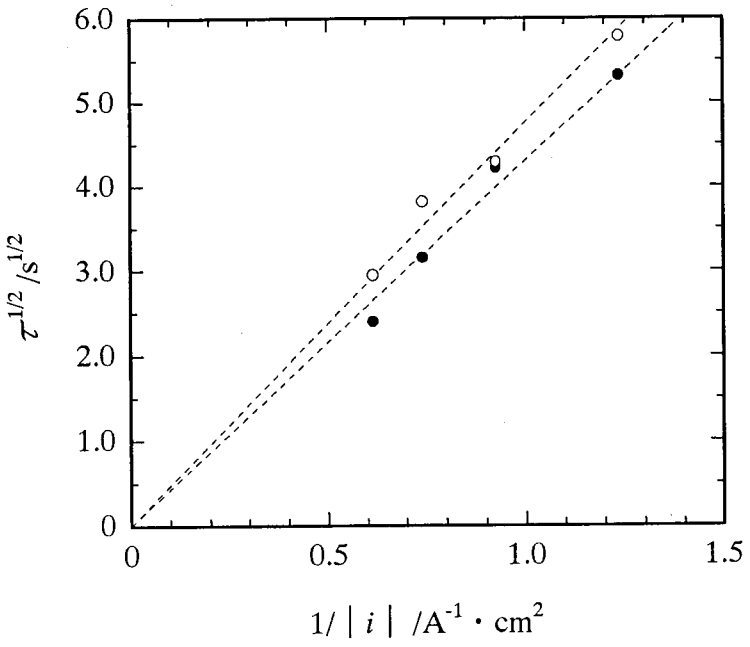

Fig. 5-21 Relationship between the reverse of electric current density and the square root of transition time in chronopotentiometric measurement, ●: $EuCl_2$ in the NaCl-KCl system, ○: $SrCl_2$ in the KCl system.

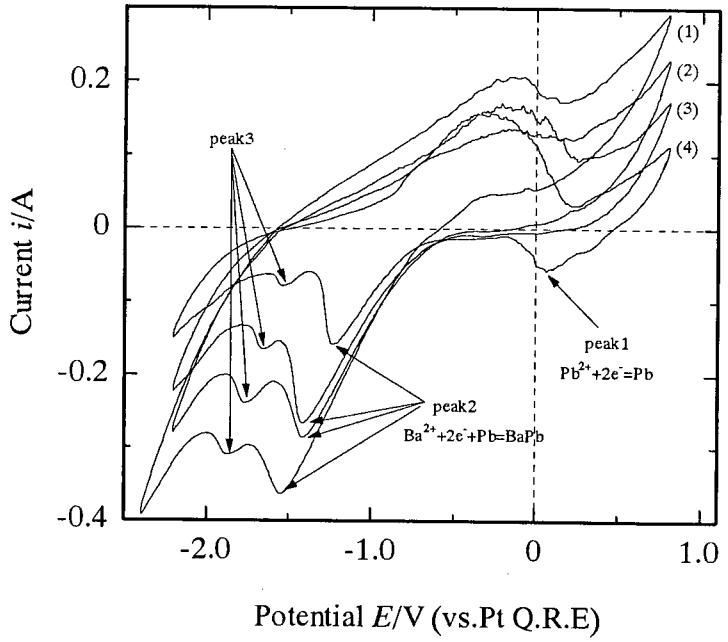

Fig. 5-22a Cyclic voltammogram for $BaCl_2$ on liquid Pb cathode in the NaCl-KCl equimolar mixture at 1000K, sweep rate: (1) 0.2V/s (2) 0.1V/s (3) 0.05V/s (4) 0.01V/s.

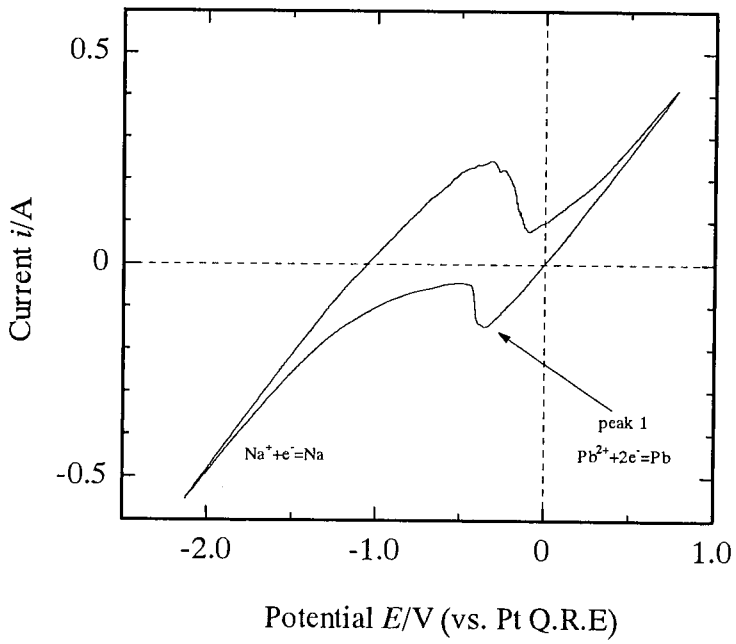

Fig. 5-22b Cyclic voltammogram for NaCl-KCl on liquid Pb cathode at 1000K, sweep rate: 0.1V/s.

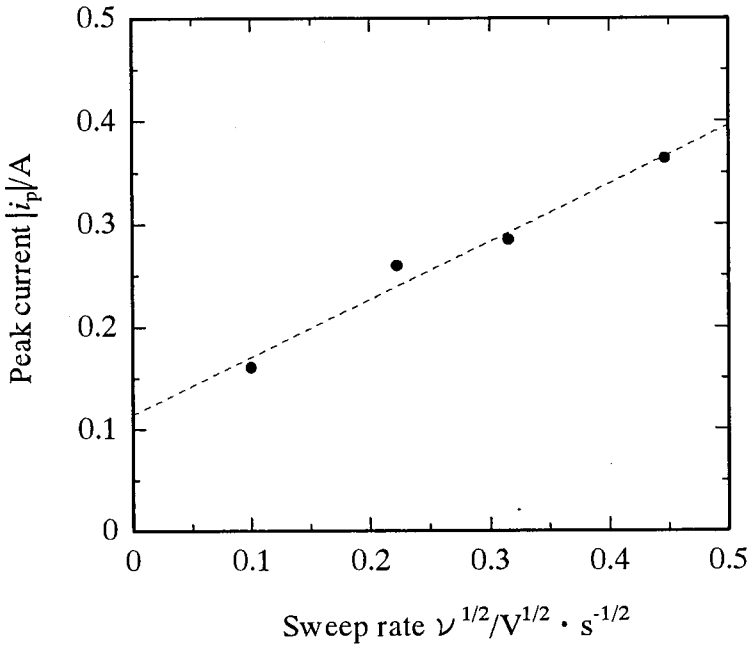

Fig. 5-23 Relationship between the square root of sweep rates and peak currents on the liquid Pb cathode at 1000K.

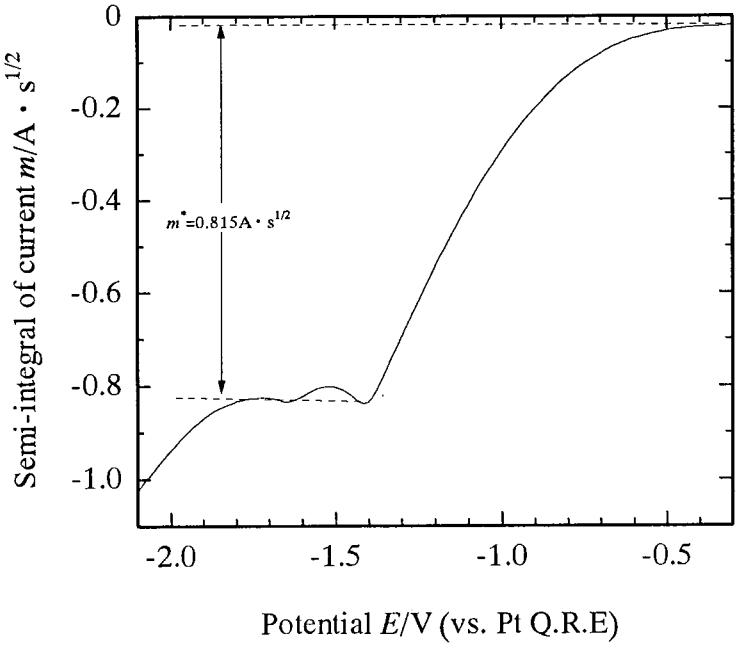

Fig. 5-24 Semi-integral of the curve plotted for $BaCl_2$ on the liquid Pb electrode in the NaCl-KCl equimolar mixture at 1000K, sweep rate: 0.1V/s.

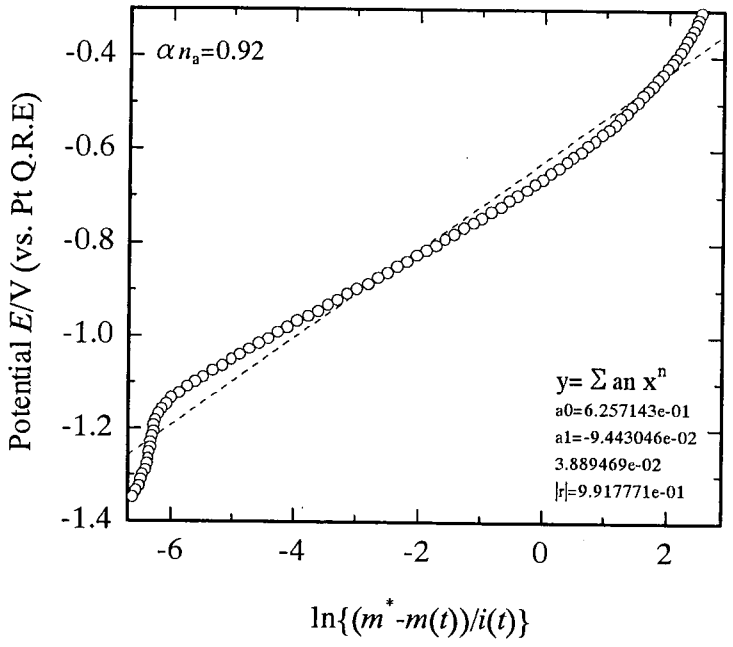

Fig. 5-25 Logarithmic analysis of semi-integral of the curve plotted for $BaCl_2$ on liquid Pb cathode in the NaCl-KCl equimolar mixture at 1000K.

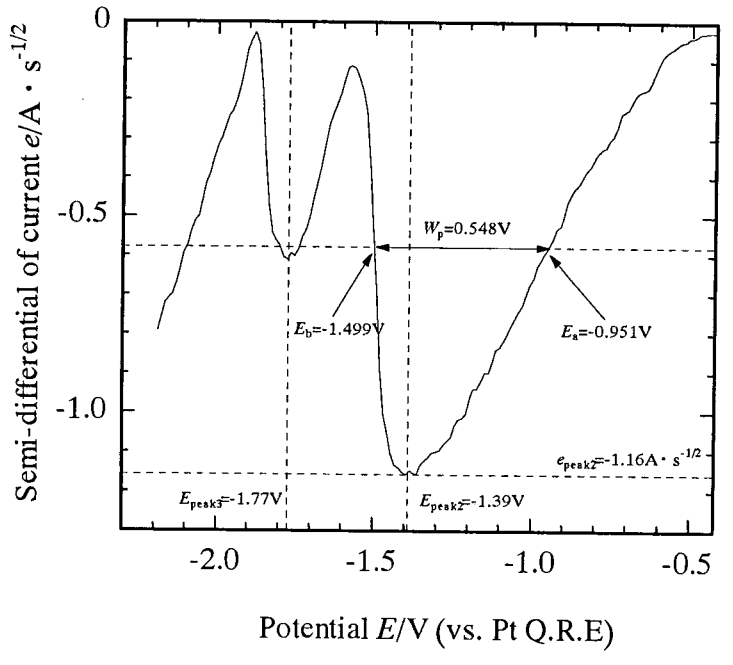

Fig. 5-26 Semi-differential of the curve plotted for $BaCl_2$ on the liquid Pb electrode in the NaCl-KCl equimolar mixture at 1000K, sweep rate: 0.1V/s.

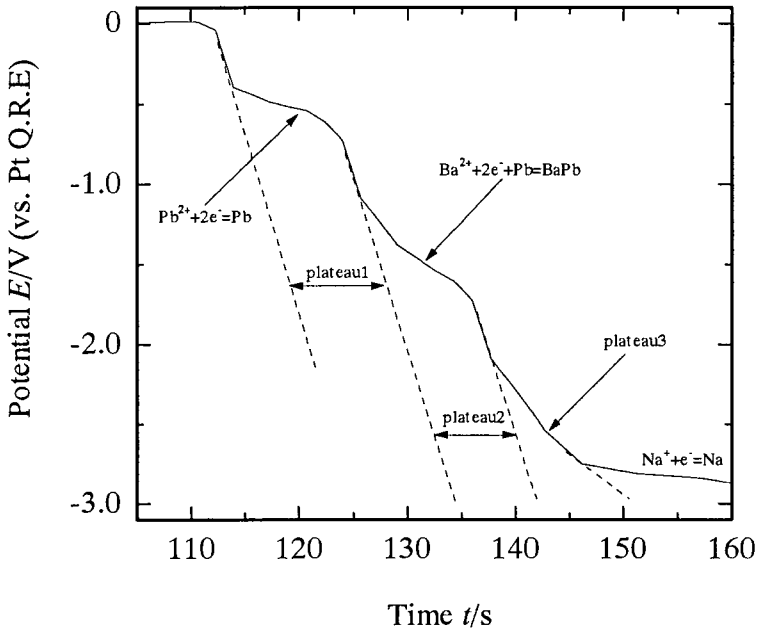

Fig. 5-27 Chronopotentiogram for $BaCl_2$ on the liquid Pb cathode in the NaCl-KCl equimolar mixture at 1000K.

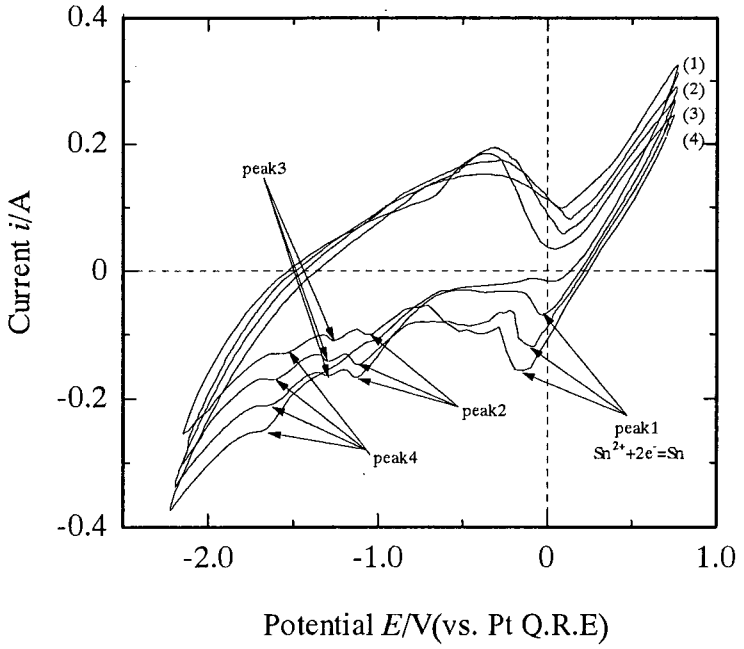

Fig. 5-28a Cyclic voltammogram for $BaCl_2$ on liquid Sn cathode in the NaCl-KCl equimolar mixture at 1000K, sweep rate: (1) 0.4V/s (2) 0.2V/s (3) 0.1V/s (4) 0.05V/s

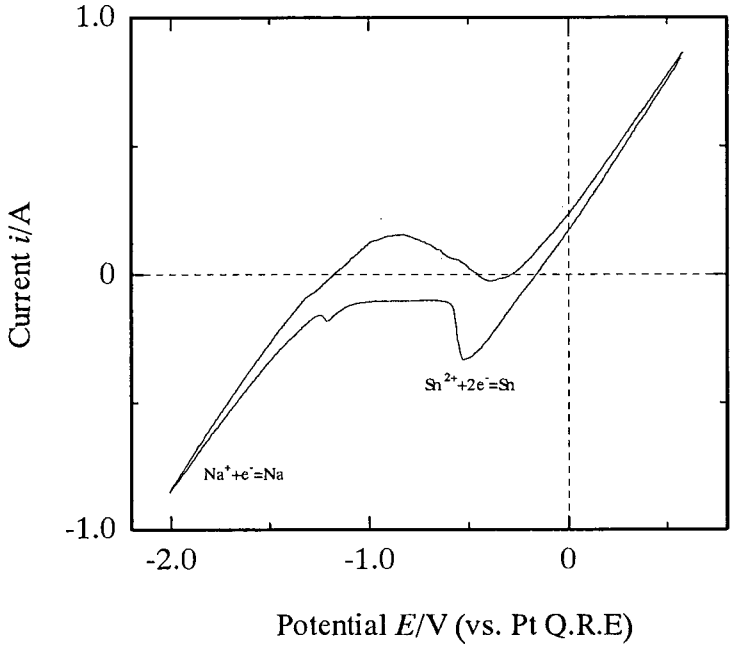

Fig. 5-28b Cyclic voltammogram for NaCl-KCl on liquid Sn cathode at 1000K, sweep rate: 0.1V/s

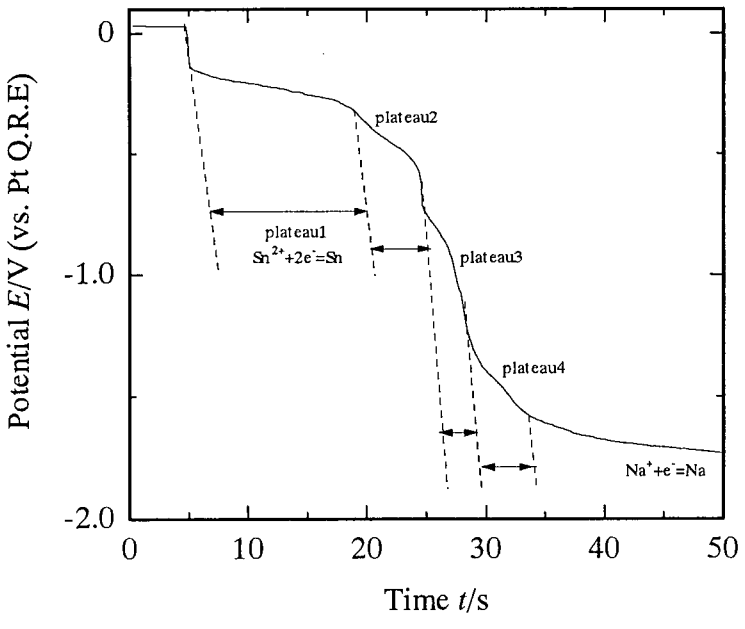

Fig. 5-29 Chronopotentiogram for $BaCl_2$ on the liquid Sn cathode in the NaCl-KCl equimolar mixture at 1000K.

§ V-iv References

(1) Y. I. Chang, L. C. Walters, J. E. Battles, D. R. Pedersen, D. C. Wade, D and M. J. Lineberry, *ANL-IFR-125*, (1990).

(2) W. J. Hamer, M. S. Malmberg and B. Rubin, *J. Elecrochem. Soc.*, **112**, 750 (1965).

(3) M. Matsumiya, R. Takagi and R. Fujita, *J. Nucl. Sci. Technol.*, **34**, 310 (1997).

(4) J. L. Willit, W. E. Miller and J. E. Battes, *J. Nucl. Mater.*, **195**, 229 (1992).

(5) K. M. Goff and A. Schneider, *Nucl.Technol.*, **102**, 331 (1993).

(6) A. Shimazu and Y. Fujii-e, *Prog. Nucl. Energy*, **29**, 25 (1995).

(7) L. P. Polyakova and P. T. Stangrit, *Electochim. Acta*, **27**, 1641 (1982).

(8) G. L. Kiporos and S. N. Flengas, *J. Electrochem. Soc.*, **132**, 1087 (1985).

(9) M. Yamane and R. Takagi, *Denki Kagaku*, **60**, 900 (1992).

(10) D. L. Manning and G. Mamantov, *J. Electroanal. Chem.*, **6**, 328 (1963).

(11) G. W. Mellors and S. Senderoff, *J. Electrochem. Soc.*, **113**, 60 (1966).

(12) H. Horinouchi and I. Okada, *J. Electroanal. Chem.*, **396**, 547 (1995).

(13) I. Okada, S. Okazaki, H. Horinouchi and Y. Miyamoto, *Mat. Sci. Forum*, **73-75**, 175 (1991).

(14) H. Matsuura, R. Takagi and R. Fujita, *J. Nucl. Sci. Technol.*, **34**, 304 (1997).

(15) K. B. Oldham, *J. Electroanal. Chem.*, **26**, 331 (1970).

(16) M. Grenness and K. B. Oldham, *Anal. Chem.*, **44**, 1121 (1972).

(17) M. Goto and K. B. Oldham, *Anal. Chem.*, **45**, 2043 (1973).

(18) K. B. Oldham, *Anal. Chem.*, **44**, 196 (1972).

(19) P. Dalrymple-Alford, M. Goto, K. B. Oldham, *J. Electroanal. Chem.*, **85**, 1 (1977).

(20) M. Goto and D. Ishii, *J. Electroanal. Chem.*, **61**, 361 (1975).

(21) K. B. Oldham, *J. Electroanal. Chem.*, **121**, 341 (1981).

(22) D. Elwell and G. M. Rao, *Electrochim. Acta*, **27**, 673 (1982).

(23) J. De Lepinay, S. Bouteillon, D. Renaud and M. J. Barbier, *J. appl. Electrochem.*, **17**, 294 (1987).

(24) T. Yoko and A. Hellawell, *J. Electrochem. Soc.*, **131**, 2590 (1984).

(25) T. Berzins and P. Delahay, *J. Am. Chem. Soc.*, **75**, 555 (1953).

(26) N. M. Nicholson, *J. Am. Chem. Soc.*, **79**, 7 (1957).

(27) T. Shimada, M. Iizuka and Y. Ito, Y, *Denki Kagaku*, **60**, 200 (1992).

(28) S. Hikino, Xie. Gang, K. Ema, K and Y. Ito, *J. Electrochem. Soc.*, **139**, 1820 (1992).

(29) R. S. Nicholson and I. Shain, *Anal. Chem.*, **36**, 706 (1964).

(30) Z. Galus, "*Fundamentals of Electrochemical Analysis*", Ellis Horwood, Chichester (1976).

(31) A. J. Bard and L. R. Faulkner, Editors, "*Electrochemical Methods, Fundamentals and Applications*", 219, John Wiley and Sons, New York (1980).

(32) G. Mamantov, D. L. Manning and M. Dale, *J. Electroanal. Chem.*, **9**, 253 (1965).

(33) C. A. C. Sequeira, *J. Electrochem. Soc.*, **9**, 140 (1993).

(34) A. J. Bard and L. R. Faulkner, Editors, "*Electrochemical Methods, Fundamentals and Applications*", 288, John Wiley and Sons, New York (1980).

(35) A. J. Bard and L. R. Faulkner, Editors, "*Electrochemical Methods, Fundamentals and Applications*", 253, John Wiley and Sons, New York (1980).

(36) P. Delahay, "*New Instrumenttal Methods in Electrochemistry*", 117, Interscience Publishers, Inc., New York (1954).

(37) H. Matsuda and Y. Ayabe, *Z. Electrochem.*, **59**, 494 (1955).

(38) J.O'M. Bockris, G. W. Hooper, *Disc. Faraday Soc.*, **32**, 218 (1961).

(39) R. S. Nicholson and I. Shain, *Anal. Chem.*, **36**, 706 (1964).

(40) A. V. Volkovich, *Rasplavy*, **2**, 43 (1993), [in Russian].

(41) A. R. Despic, *Electrochim. Acta*, **21**, 63 (1976).

(42) B. D. Vasin, A. V. Vasil'ev, V. A. Ivanov and S. P. Raspopin, *Melts*, **3** , 244 (1989).

(43) M. V. Smirnov, "*Electrode Potentials in Molten Chlorides*", Nauka, Moscow (1973), [in Russian].

(44) V. I. Kober, V. A. Dubinin, V. I. Kochkin and S. P. Raspopin, *Fiz. Khim.*, **9**, 2124 (1985).

(45) E. Piwowarsky, *Z. Metallkunde*, **14**, 300 (1922).

(46) T. B. Massalski, "*Binary Alloy Phase Diagrams Vol. 1*", Am. Soc. Metals, (1986).

(47) K. W. Ray and R. G. Thompson, *Metals Alloys*, **1**, 314 (1930).

(48) W. Rieger and E. Parthe, *Acta Crystallogy*, **22**, 919 (1967).

(49) W. Dorrsheild, A. Widera and A. Schafer, *Z. Nuturforsch.*, **B32**, 1097 (1977).

(50) G. Bruzzone, E. Franceschi and F. Merlo, *J. Less-Common Met.*, **60**, 59 (1978).

Chapter VI

Recovery System of Electrochemically Negative Elements

Chapter VI Recovery System of Electrochemically Negative Elements

§ VI- i Background

The Self-Consistent Nuclear Energy System (SCNES)[1] requires zero release of radioactive materials out of the fuel cycle[2]. In this system we need to recover fuel elements and fission products separately. For SCNES, we have proposed one of the revised ideas of the Integral Fast Reactor (IFR) concept[3]-[5]. The IFR concept proposed by Argonne National Laboratory contains a sophisticated idea of pyrochemical treatment in a nuclear fuel cycle[3]. In the IFR concept, after removal of the fuel materials, the salt bath containing fission products will be occluded into the zeolites and stocked as the deposits. However, from a standpoint of the harmonization of nuclear systems with global environment, we should make an effort to separate the fission products each other for incineration or utilization of medical tracers, precious materials and so on. As one of the most feasible candidates for the SCNES is a metallic fuel fast breeder reactor, we have adopted pyrochemical treatment of metallic fuel as a chemical separation process. After the electrorefining and drawdown process, all alkali halides, alkaline-earth halides and some amounts of rare earth halides from fission products still remain in the salt bath. Thus it is difficult to recover some fission products like alkali and alkaline-earth elements from the salt phase, because of their more negative reduction potentials[6] than those of the solvent components. Although Eu^{2+}, Sr^{2+}, Ba^{2+} and Cs^{+} are also negative elements, we successfully recovered Eu^{2+}, Sr^{2+}[7] and Ba^{2+}[8] in the different liquid metallic cathodes in the chloride bath and Cs^{+}[9] in the liquid Pb cathode in the fluoride bath in the previous works. Because it is possible to shift the deposition potential to more positive side by decreasing the activity of the deposited metal, which is interpreted from the Nernst-Equation

$$E = E^0 + \frac{RT}{nF} \ln \frac{a_{M^{n+}}}{a_M} \tag{6-1}$$

where E is the apparent standard potential, E^0 the equilibrium potential of alloy formation, R the gas constant, T an absolute temperature, n the charge transfer number, F the Faraday constant, $a_{M^{n+}}$ the activity of M^{n+} in the melt and a_M the activity of the deposited metal. The distribution behavior of U, Np, rare-earth elements and alkaline-

earth metals in the LiCl-KCl/Cd and LiCl-KCl/Bi systems was reported[10]. The distribution behaviors of the lanthanide and the actinide elements between the molten fluoride salts and the liquid bismuth were also reported[11,12]. However, in these reports, the possibility of recovery of the electrochemically negative elements in the other liquid metallic cathodes in the fluoride bath was not revealed. We therefore carried out the present experiment which is investigation for the selective recovery of Cs, Sr and Ba in three kinds of liquid metallic cathodes in the FLINAK system and in six kinds of liquid metallic cathodes in the chloride system from the technological aspects. Additionally, a pyrometallurgical partitioning process is being developed for recovering transuranic elements from high-level waste[13,14]. However, the recovery system for the elements which has in particular electrochemically negative potential than the solvent components was not developed. Therefore we have suggested the original recovery process in the pyrochemical reprocessing on the basis of the experimental results for the continuous countercurrent electromigration[15] and the electrowinning methods using electrochemical technique in this thesis.

§ VI- ii Experimental

§ VI- ii - i Melt preparation for electrowinning method

(a) Sample preparation for electrolysis in fluoride bath

Fluoride reagents used as a solvent were LiF (Wako Chem. Ind. Ltd.:>98.0%), NaF (Wako Chem. Ind. Ltd.:>99.0%) and KF (Kanto Chem. Ind. Ltd.:>98.0%), and chloride reagents used as a solute were CsCl, $SrCl_2$ and $BaCl_2$. The KF was introduced in a graphite crucible and kept at about 673K under vacuum for about 24h because it is hygroscopic. The finely crushed fluorides were mixed in the desired portion (LiF:46.5mol%, NaF:11.5mol%, KF:42.0mol%; FLINAK, m.p.727K) and were introduced in a graphite crucible. The mixture was kept at 973K under vacuum for about 7h and melted above 1173K. The treatment as for the solute is the same way as the electromigration method. Metal reagents used as liquid electrodes were Pb (Wako Chem. Ind. Ltd.:>99.9%), Sn (Wako Chem. Ind. Ltd.:>99.9%) and Zn (Kanto Chem. Co.:>99.9%).

(b) Sample preparation for electrolysis in chloride bath

Chloride reagents used were NaCl (Wako Chem. Ind. Ltd.:>99.5%), KCl (Kanto Chem. Ind. Ltd.:>99.5%) and $EuCl_2$ which was delivered in sealed glass ampoules (APL Engineered materials, Inc.:99.99%), $SrCl_2$ (Wako Chem. Ind. Ltd.:>99.5%), $BaCl_2$ (Wako Chem. Ind. Ltd.:>99.5%). The finely crushed chlorides were mixed in the following compositions (NaCl-50mol%;KCl-50mol%) and were introduced in a quartz cell. The mixture was dehydrated by heating under vacuum at 973K for about 7h and then melted at 1073K. The solute ($EuCl_2$, $SrCl_2$ and $BaCl_2$) was also introduced in the quartz cell and dehydrated by heating under vacuum at about 673K for about 24h because they are hygroscopic. Metal reagents used as liquid electrodes were Al (Wako Chem. Ind. Ltd.:>99.9%), Bi (Nilaco Co.:>99.999%), Cd (Wako Chem. Ind. Ltd.:>99.9%), Pb (Wako Chem. Ind. Ltd.:>99.9%), Sn (Wako Chem. Ind. Ltd.:>99.9%) and Zn (Kanto Chem. Co.: >99.9%).

§ VI- ii - ii Elctrowinning method

The electrowinning cell is shown in **Fig. 6-1**, which is similar one of the previous work[9]. The quasi-reference electrode (Q.R.E) was a platinum wire (1.5mmϕ, Nilaco Co.:>99.98%) as also used by other authors[16]-[18]. In our experiments Pt Q.R.E showed the stable potentials. The electrode was rinsed in a 1N HCl solution and degreased with acetone before experiments. Prior to electrochemical experiments, pre-electrolysis was carried out with a tungsten wire (1mmϕ, Nilaco Co.:>99.5%) in order to ,eliminate metallic impurities and oxides. A graphite crucible (MS-G, Tokai Carbon:>99.9%) was used as a counter electrode. A tungsten lead wire was connected to this crucible with ceramic binder. Three kinds of liquid electrodes (Pb, Sn and Zn) and six kinds of liquid electrodes (Al, Bi, Cd, Pb, Sn and Zn) were used as a working electrode in fluoride and chloride baths, respectively. These liquid electrodes were constituted as follows. A small amount of Pb which was weighed by about 3g was introduced in the BN rod (F; 6.5mm inside diameter, 50mm length) for fluorides and quartz cell for chlorides. Two holes (N) in each side with 6mm diameter locates about 2.5cm upper from the bottom of the BN rod and quartz cell. This BN rod was connected to a Mullite tube (D; $3Al_2O_3 \cdot 2SiO_2$) with ceramic binder, *i.e.*, the part immersed into the fluoride bath is only BN rod. The tungsten wire was almost covered by the BN coating and only the bottom edge of tungsten wire was immersed into this liquid Pb to prevent detection of the reaction between the tungsten wire and the melt bath. This liquid electrode was kept over the melt during pre-electrolysis. After the pre-electrolysis, this liquid electrode was immersed into the melt bath. In order to measure the transported charge on the electrolytic conditions precisely, the Desital Coulometer was used in this experiment. The electrowinning was performed under Ar bubbling because the convection effect can be useful to recover Cs by Ar bubbling. The three kinds of electrodes which have different electrode areas and the amounts of Pb were used in the FLINAK which contains CsCl as the solute. These electrodes were sliced to more than 10-layers and dissolved into acid solutions in order to determine Cs concentration by adsorption and other elements by ICP Atomic Emission Spectrometry.

§ VI-iii Results and Discussion

§ VI-iii-i Selectivity of Eu and Sr in the liquid metallic cathodes in molten chlorides

The liquid electrodes in which Eu^{2+} and Sr^{2+} are deposited around -3V under galvanostatic conditions are rapidly quenched. In order to reveal the presence of alloy formation, the contents of metals in the liquid electrodes were measured by ICP-emission analysis. The distribution of the solute absorbed in the liquid metal along the depth of the electrode was analyzed. **Figs. 6-2** and **6-3** indicate the molar ratio of Eu and Sr/Na+K or K at various depths, respectively. The vertical dotted line expresses the boundary between the electrode surface and the salt. The horizontal dotted line expresses the initial ratio of the bath. As shown in Figs. 6-2 and 6-3, in the case of both Eu and Sr, liquid Bi, Sn and Zn cathodes, as the depth increases, the ratio of recovered Eu and Sr decrease or remain constant. The contents of recovered Eu and Sr in liquid Bi, Sn and Zn cathodes are as small as <0.1ppm. Therefore we found it difficult to recover Eu and Sr on these cathodes. On the other hand, in the case of liquid Pb cathode, the significant contents of Eu and Sr were observed and the ratio of recovered Eu and Sr drastically increases from the initial ratio as the depth of electrode increases. Therefore we found it obvious that recovered Eu and Sr are concentrated in this cathode and these elements are selectively recovered in liquid cathode. In the case of Al cathode, we recovered Sr and the ratio of recovered Sr in the KCl melt drastically increases from the initial ratio as the depth increases. We found that recovered Sr is concentrated in the bulk of this cathode and we can selectively recover the contents of Sr by using liquid Al cathode. The ratio of recovered Sr in the NaCl-KCl melt is less than the initial ratio due to the large amount of deposited Na and K. Therefore, in the NaCl-KCl melt, the contents of recovered Sr is concentrated as well as Na and K.

§ VI-iii-ii Selectivity of Ba in the liquid metallic cathodes in molten chlorides

The distribution of Ba absorbed in the liquid metal along the depth of the electrode was analyzed in order to estimate the ratio of Ba to (Na+K). The molar ratio of Ba/(Na+K) at each depth is shown in **Fig. 6-4**. The ordinate and abscissa indicate the

ratios of molar quantity of Ba in the electrode to that of (Na+K) in the electrode and the number of sliced layer from the surface to the bulk, respectively. The vertical and horizontal dotted lines indicate the boundary between electrode surface and the salt, and the initial ratio of the melt bath, respectively. We can compare the selectivity for each liquid cathodes because the molar quantities of the deposited bulk constituents were no obvious difference for each liquid cathode.

In the case of the using liquid Al and Bi, the ratio of recovered Ba decreases as the depth increases and we found it facilitate not to recover Ba on these cathodes effectively. Although the phase diagram of Al-Ba[19] shows Al_4Ba compound would be formed at 1000K, Ba did not actually deposit on the Al cathode, it might be speculated that Gibbs formation energy of Al_4Ba is not so negative than the salt bath. As for Bi, phase diagram of Ba-Bi[20] was not well defined at 1000K.

For the liquid Cd, Pb, Sn and Zn cathodes, the ratio of recovered Ba to (Na+K) was higher than the initial ratio. Especially, in the case of the liquid Pb and Sn cathodes, the ratio of recovered Ba to (Na+K) drastically increases and the selectivity is about one order of magnitude larger than the initial ratio. Then the contents of recovered Ba almost remain constant as the depth increases. In addition we found that recovered Ba is concentrated in these cathodes and we can selectively recover the contents of Ba. In this condition at 1000K, we could not confirm what alloy was made since Ba-Sn[21-24] ,Ba-Pb[25] and Ba-Zn[26] phase diagrams are not well defined at this temperature. There is no information as to the constitution of Ba-Cd alloys. However, it is speculated that in the case of these cathodes, Ba forms the stable alloys with each cathode and possibly shifts the decomposition potential to more positive side by decreasing the activity of the deposited metal.

The order of the selectivity is estimated with respect to Eu^{2+}, Sr^{2+} and Ba^{2+} as follows.

Pb>1>Bi>Sn>Zn (for Eu^{2+})

Pb>1>Al≈Sn>Bi>Zn (for Sr^{2+} in the NaCl-KCl system)

Pb>Al>1 (for Sr^{2+} in the KCl system)

Sn>Pb>Zn>Cd>1>Al>Bi (for Ba^{2+})

where unity means original ratio before electrolysis. These results allow us to conclude that the use of the liquid Sn cathode is considered to be more hopeful for the separation of Ba^{2+} from Eu^{2+} and Sr^{2+}, and it is effective to recover Ba^{2+} selectively using liquid Sn cathode before electrowinning Eu^{2+} and Sr^{2+} on the liquid Pb cathode.

The partial molar excess thermodynamic characteristics and the activity coefficients of Ba metals in each liquid metal estimated from the thermodynamic characteristics are shown in **Tables 6-1** and **6-2**, respectively[27]-[30]. These calculations are assumed to be independent of the concentration of each constituent in the liquid metal phase. The partial molar excess Gibbs energy and the activity coefficient correspond to the miscibility of Ba in each liquid metal. The order of the thermodynamic characteristics and the activity coefficients for each cathode is shown as follows.

$$Sn<Pb<Bi\approx Zn<Cd<Al$$

This order means that Ba is most stable in Sn and the more unstable in each cathode as increasing the activity coefficients. This tendency excepted for Bi is consistent with the order of the selectivity in our results. Additionally, it was also described that there is the significant deviation for Ba-Bi system in this reference[27], and therefore this order of Bi may be inconsistent with our results. It is reported that the separation factor of Ba in the LiCl-KCl/Pb system is larger than that of Ba in the LiCl-KCl/Cd system[11]. This tendency is also consistent with our results. However, it is also reported that the distribution coefficient of Ba as a function of distribution coefficient of Li for the LiCl-KCl/Cd system is larger than that of Ba for the LiCl-KCl/Bi system[10], *i.e.*, the selectivity of Ba in LiCl-KCl/Cd system is smaller than that of Ba in LiCl-KCl/Bi system and this tendency is inconsistent with our results. This is due to the smaller activity coefficient[31],[32] of Li in Bi than that of Li in Cd, that is to say, Li is more stable in Bi than that of Li in Cd to divalent elements. However, it is difficult to discuss the activity coefficient of Na in each cathode in our results.

In the previous work[9], we tried to recover Cs^+ in the NaCl-KCl equimolar mixture and KCl system by adding the 10mol% NaF or KF in order to shift the decomposition potential of Cs^+ to more positive side. However, we could not recover Cs^+ on the

liquid Pb cathode, because Cs^+ might have more negative decomposition potential[6] even in the chloride bath. The results indicate that the use of the liquid Pb cathode is suitable to separate Eu^{2+}, Sr^{2+} and Ba^{2+} from Cs^+ in the chloride bath. It is reported that the separation factor of Cs in the LiCl-KCl/Pb system is very small[11] and this result is also consistent with our results.

§ VI-iii-iii Selectivity of Cs in the in the liquid metallic cathodes in molten chlorides and fluorides

Preliminary, we tried to recover Cs in the chloride bath (NaCl-KCl equimolar mixture and KCl system) by adding the 10mol% NaF or KF in order to shift the decomposition potential of Cs to more positive side. However, we failed to recover Cs on the liquid Pb cathode, because Cs^+ might have more negative decomposition potential even in the chloride bath. Therefore we selected the FLINAK system as the solvent in this work.

The liquid electrodes in which Cs^+ is deposited under galvanostatic conditions (-0.1A, 400C) are rapidly quenched. In order to investigate the selectivity, the contents of Cs in the liquid electrodes were measured by absorption spectrometry and the contents of alkali elements (Li, Na, K) were measured by ICP-emission analysis. The distribution of Cs absorbed in the liquid metal along the depth of the electrode was analyzed. The molar ratio of Cs/(Li+Na+K) at various depths is shown in **Fig. 6-5**. The vertical dotted line expresses the boundary between electrode surface and the salt. The horizontal dotted line expresses the initial ratio of the melt bath. As shown in Fig. 6-5, in the case of using liquid Sn cathode, the ratio of recovered Cs does not drastically increase and almost remain constant as the depth increases. In the case of using liquid Zn cathode, the ratio of recovered Cs decreases as the depth increases and the selectivity is less than the initial ratio. Therefore, we found that we can not recover Cs on these cathodes effectively. However in the case of using liquid Pb cathode, the ratio of recovered Cs drastically increases from the initial ratio as the depth increases and the selectivity is about ten times more than the initial ratio. Therefore we found that recovered Cs is concentrated in this cathode and we can selectively recover the contents

of Cs. However, in the case of using liquid Pb cathode, the current efficiency is less than that of liquid Zn cathode. Because Pb element is not strong affinity between Pb and K compared with affinity between Zn and K, i.e., there is only a few contents of K in the bulk of liquid Pb cathode and the loss is due to the reduction reaction of K^+ on the surface of liquid Pb cathode.

(a) System of CsCl on the liquid Pb cathode in the FLINAK melts

The analyzed distribution of Cs and solvent components absorbed in the liquid metal along the depth of the electrode is shown in **Fig. 6-6**. The selectivity of each element is defined as follows[9]:

$$\frac{C_{M(N)}}{C_{total}} = \frac{C_{M(N)}}{C_{Li} + C_{Na} + C_K} \times 100(\%) \qquad (6\text{-}2)$$

where $C_{M(N)}$ is the mole concentration of each element (M=Li, Na ,K, Cs, Sr and Ba) in the liquid metallic cathodes (N=Pb, Sn and Zn) and C_{total} is the total mole concentration of the solvent components in the liquid metallic cathodes. The ordinate and abscissa indicate the selectivities for Cs and solvent components which is defined in the same way in the previous paper[9], and the depth from the electrode surface to the bulk, respectively. The selectivity for Cs is about one order of magnitude larger than the initial ratio as shown in Fig. 6-6, while the selectivity for each solvent components in the liquid Pb cathode remains almost the initial ratio or lower. This result, of course, is consistent with the previous work[9] and we can recover Cs in the liquid Pb cathode preferentially. Although there is no information as to the constitution of Cs-Pb alloys, it is speculated that it is possible to shift the decomposition potential of Cs^+ to more positive side by decreasing the activity of the deposition metal, if Cs forms the stable alloys with Pb cathode. Additionally, it is conjectured that the another factor in order to recover Cs preferentially in this experiment is effective for the fluoride bath, i.e., the decomposition potential of Cs^+ in the fluoride bath is more positive side than that of Cs^+ in the chloride bath because we failed to recover Cs^+ in the chloride bath in the previous work[9]. **Table 6-3** shows a series of experimental results together with the main conditions. The current efficiency is not so high for all experiments. This might

possibly be ascribed to the oxide ion in the fluoride bath, since it is reported that the decomposition potential is shifted more negative side by the oxide ion which is containing in the fluoride bath[33].

(b) System of CsCl, $SrCl_2$ and $BaCl_2$ in the FLINAK melts

In the previous work, it is possible to recover Cs[9] in the liquid Pb cathode in the FLINAK system and Sr[7] in the liquid Pb cathode in the chloride bath. On the other hand, it is possible to recover Ba[8] effectively in the liquid Sn cathode in the chloride bath. In the present study, we attempt to recover Cs, Sr and Ba in the galvanostatic condition (-0.1A, 400C) in the FLINAK system. The analyzed distribution of Cs, Sr and Ba absorbed in the liquid Pb metal along the depth of the electrode is shown in **Fig. 6-7**. In this case, the selectivity for Cs is about one order of magnitude larger than the initial ratio and that for Sr and Ba is about two times larger than the initial ratio, i.e., we can selectively recover Cs, Sr and Ba in the liquid Pb cathode in the FLINAK system. It was reported that Pb cathode is suitable to separate alkaline earth elements from the salt[13,14] and this tendency is consistent with our results. Then the contents of recovered Cs, Sr and Ba almost remain constant as the depth increases. The experimental result as for the liquid Sn cathode is also shown in **Fig. 6-8**. In this case, the selectivity for Ba is drastically increasing and we can selectively recover Ba on the liquid Sn cathode in this system. This tendency for Sn-Ba in the FLINAK system is similar to that for Sn-Ba in the chloride bath. It is speculated that this result means that Ba is most stable in Sn because the activity coefficients[28,29], which is corresponding to the miscibility of Ba in the liquid Sn cathode, decreases. On the other hand, we failed to recover these elements selectively in the liquid Zn cathode as shown in **Fig. 6-9**. This tendency is consistent with the previous results for Cs and Sr in the chloride bath. As for Ba, it is speculated that the activity coefficient of Ba-Zn[30] is larger than that of Ba-Sn system and the decomposition potential of Ba might be shifted to more negative side in the fluoride bath. **Table 6-4** shows a series of the experimental results. In this condition, it is difficult to discuss what alloy was made since there is no information as for the constitution of Cs-Pb, Cs-Sn and Cs-Zn alloys.

The recovery yield for the each electrowinning in the FLINAK system is also shown in **Table 6-5**.

§ VI-iii-iv One of the recovery system in the pyrochemical reprocessing using electrochemical technique

In this thesis we have suggested one of the recovery system in the pyrochemical reprocessing using electrochemical technique as shown in **Fig. 6-10**. This system is appropriate for the condition after removing the fuel elements and electrochemically positive elements by electrolysis. The flow sheet of salt wastes treatment is on the basis of the previous and present experimental results. There are two types of recovery methods, which are the continuous countercurrent electromigration[15] and the electrowinning methods[7]-[9]. At first, on the condition which is containing CsCl, $SrCl_2$ and $BaCl_2$ (1mol%) in the NaCl-KCl system, it is possible to enrich the multivalent ions and separate them from the monovalent ions by the continuous countercurrent electromigration. Additionally, on the condition which is containing CsCl (1mol%), $SrCl_2$ and $BaCl_2$ (0.1mol%) in the NaCl-KCl system, it is possible to significantly enrich the Cs ion in the low concentration of Cs. After that, on the next electrowinning process, it is desirable to use the enriched salt because the decomposition potential is more positive than before electromigration. Then the previous results[7],[8] allow us to conclude that the use of the liquid Sn cathode is considered to be more hopeful for the separation of Ba^{2+} from Eu^{2+}, Sr^{2+} and Cs^{+} in the chloride bath, and it is effective to recover Ba^{2+} selectively using liquid Sn cathode before electrowinning Eu^{2+}, Sr^{2+} and Cs^{+} in the liquid Pb cathode. Ba is preferentially removed into the liquid Sn phase and is separated from Sr^{2+} and Cs^{+} by the difference of the selectivity, which means the separation of the stable isotope from the long-lived radioactive wastes. Additionally, it is reported that the alkaline-earth and rare earth metals were recovered into Pb cathode[13,14] and that is similar to our proposing process. Then it is possible to re-use the chloride bath after removing the multivalent ions. On the other hand, as for the recovery of Cs, the previous results[8] indicate that the use of the liquid Pb cathode is suitable to separate Eu^{2+}, Sr^{2+} and Ba^{2+} from Cs^{+} in the chloride bath. However, this

result also means that it is difficult to recover Cs in the chloride bath and we proposed the enriched Cs chlorides can be converted into Cs fluorides because it is not so difficult to convert alkali chlorides to alkali fluorides thermodynamically. Moreover, it was demonstrated that it was possible to recover Cs in the liquid Pb cathode selectively in the fluoride bath in the present work. Then it is reported that Cs was recovered in the liquid Pb cathode at high cesium concentration in the molten chloride bath[13] although the separation factor is not so high. It might be possible to recover Cs in the chloride bath without converting the Cs chlorides into the Cs fluorides if the Cs concentration is high. Furthermore, if it is demonstrated that the enrichment of Cs in the fluoride bath by the electomigration method is much better than that in the chloride bath, the recovery process based on the fluoride bath will be developed in the future.

Table 6-1 The partial molar excess thermodynamic characteristics of Ba in liquid metals in reference[27]-[30]

System	$-\Delta H_M^*$ (kJ/mol)	$-\Delta S_M^*$ (J/mol K)	$-\Delta G_M^*$ at 1000K
Ba-Al	79.7	26.0	53.7
Ba-Bi	122.9	8.3	114.6
Ba-Cd	164.2	73.9	90.3
Ba-Pb	189.6	20.8	168.8
Ba-Sn	209.3	20.8	188.5
Ba-Sn[28],[29]	174.4	5.0	169.4
Ba-Zn[30]	186.6	79.4	107.2

Table 6-2 The activity coefficients of Ba in liquid metals estimated from the thermodynamic characteristics in reference[27]-[30]

System	$\log\gamma = a + b/T$		γ at 1000K
	a	$-b$	
Ba-Al	1.36	4164	1.6×10^{-3}
Ba-Bi	0.43	6420	1.0×10^{-6}
Ba-Cd	3.86	8578	1.9×10^{-5}
Ba-Pb	1.09	9905	1.5×10^{-9}
Ba-Sn	1.09	10934	1.5×10^{-10}
Ba-Sn[28],[29]	0.26	9111	1.4×10^{-9}
Ba-Zn[30]	4.15	9750	2.5×10^{-6}

Table 6-3 Selectivity and weights of Cs recovered at cathodes in the FLINAK system

Run No.	Condition of electrodeposition			Selectivity	Initial		Final		Weight of Cs	Mass balance	Current
	Potential	Coulomb	Current	(%)	Ratio	Cs metal	Ratio	Cs metal	at cathode	(B+C)/A×100	efficiency
	(V vs. Pt Q.R.E)		(mA)		(%)	A(g)	(%)	B(g)	C(g)	(%)	(%)
A-1	------	400	-100	12.5±0.8	1.00	4.42	-------	-------	0.376±0.003	-----	61
A-2	-1.8	1000	<-30	15.8±1.9	1.38	5.89	1.17	4.98	0.645±0.008	96	45
A-3	-1.8	2000	<-30	8.2±0.5	1.96	8.42	1.17	4.98	0.697±0.014	68	37
A-4	-1.8	3000	<-50	11.4±1.6	4.07	17.86	2.49	10.75	1.603±0.025	69	64

------ Not recorded

Table 6-4 Selectivity and weights of each metal recovered at cathodes in the FLINAK system under the galvanostatic condition.

RunNo.	Liquid	Condition of electrodeposition			Selectivity			Weight of Cs recovered			Current
	metal	Potential	Coulomb	Current	(%)			at cathode(mg)			efficiency
		(V vs. Pt Q.R.E)		(mA)	Cs	Sr	Ba	Cs	Sr	Ba	(%)
B-1	Pb	------	400	-100	7.44±0.64	2.29±0.05	2.13±0.05	265±4	60.0±0.8	95.3±1.2	71
B-2	Sn	------	400	-100	1.44±0.23	0.47±0.02	4.78±0.25	31.0±0.4	8.7±0.1	106±1	48
B-3	Zn	------	400	-100	0.90±0.08	1.22±0.12	1.59±0.21	18.5±0.3	16.0±0.2	29.2±0.4	37

Table 6-5 Recovery yield for the electrowinning in the FLINAK system

RunNo.	Recovery yield/%			Liquid metal
	Cs	Sr	Ba	
A-1	8.52	-----	-----	Pb
A-2	14.61	-----	-----	Pb
A-3	15.79	-----	-----	Pb
A-4	36.31	-----	-----	Pb
B-1	6.00	2.06	2.09	Pb
B-2	0.70	0.30	2.32	Sn
B-3	0.42	0.55	0.64	Zn

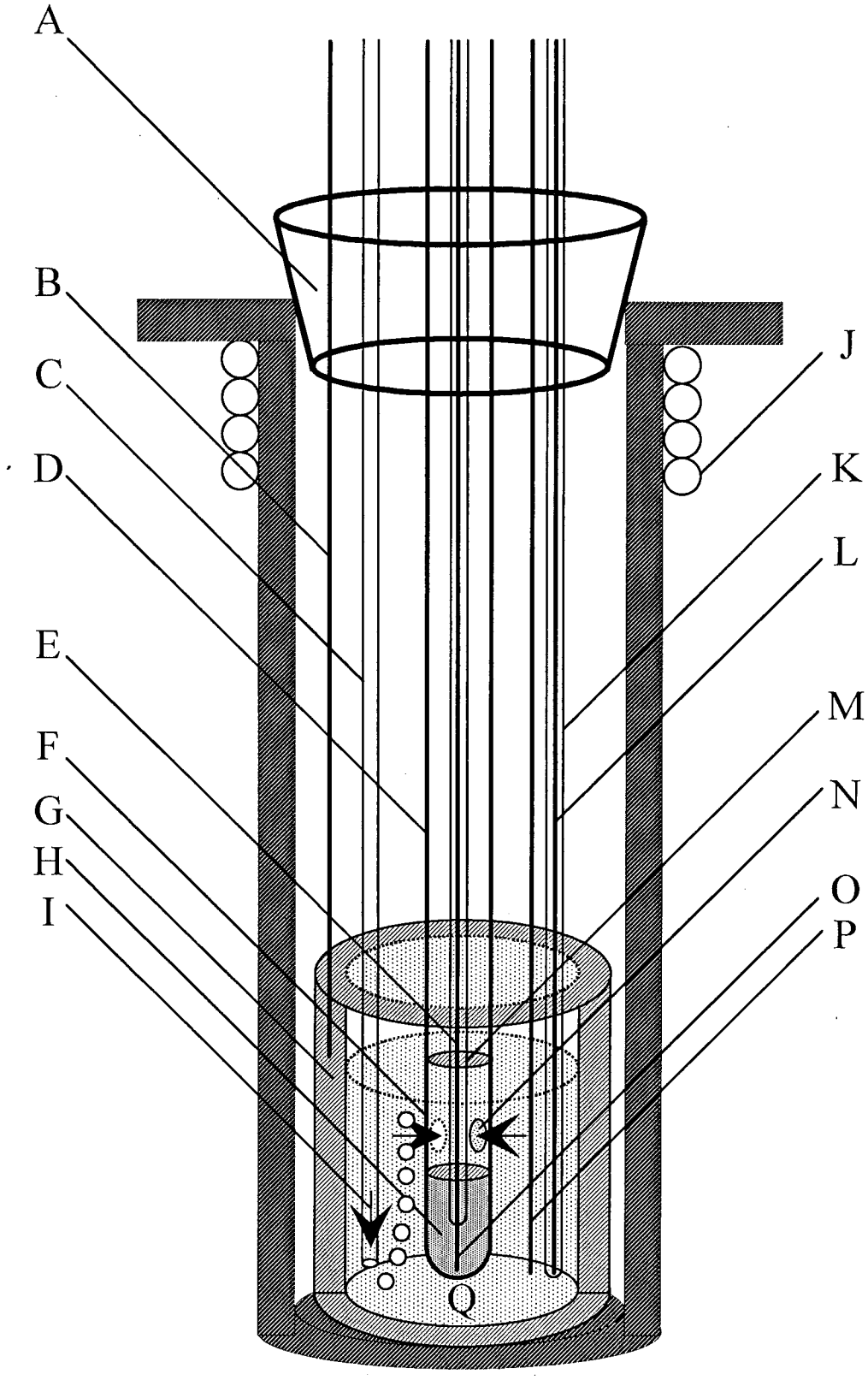

Fig. 6-1 The furnace-cell assembly used in electrowinning experiments
A: Silicon stopper, B: Tungsten wire (lead to crucible) , C: Alumina tube, D: Mullite tube, E: Tungsten wire, F: BN rod (covering liquid electrode), G: Graphite crucible (counter electrode), H: Liquid metallic electrode (Pb, Sn, Zn), I: Ar gas, J: Cooling water, K: Alumina tube (covering thermocouple), L: Thermocouple, M: BN coating (covering tungsten wire), N: 6mm ϕ hole, O: Tungsten wire (lead to liquid metal), P: Pt wire (quasi-reference electrode), Q: Molten salt (FLINAK system)

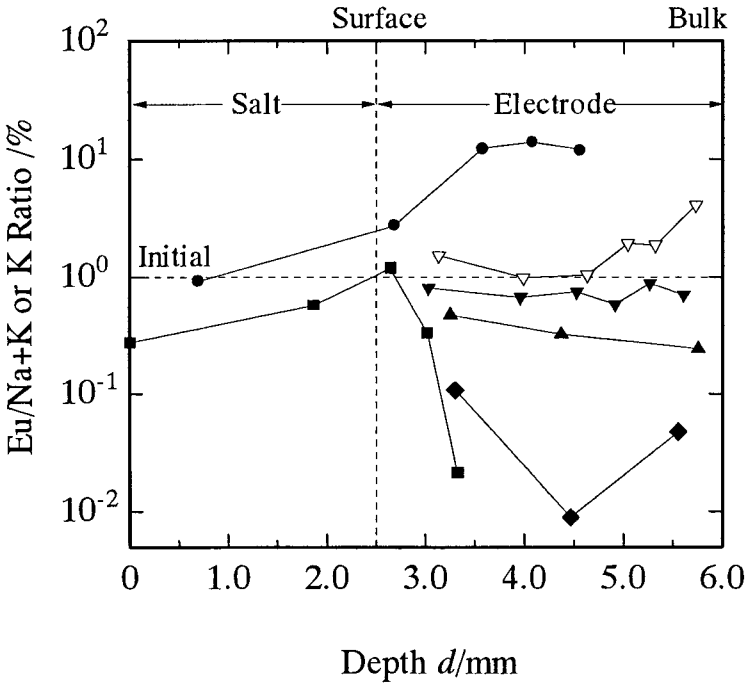

Fig. 6-2 Relationship between the depth and the Eu/(Na+K) ratio for $EuCl_2$ on various liquid electrode in the NaCl-KCl equimolar mixture at 1073K

—●—: Pb cathode, —▲—: Sn cathode, —■—: Bi cathode,

—◆—: Zn cathode, —▼—: Al cathode, —▽—: Al cathode (KCl system)

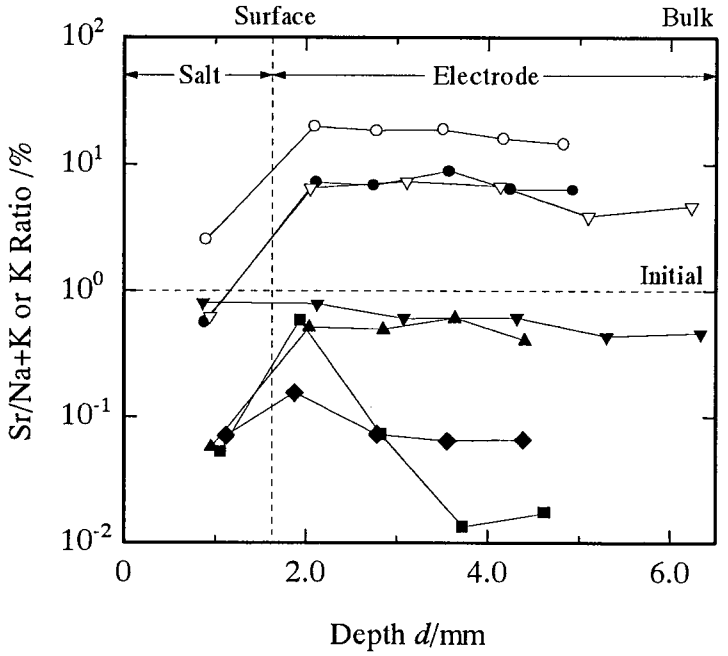

Fig. 6-3 Relationship between the depth and the Sr/(Na+K) or Sr/K ratio for $SrCl_2$ on various liquid electrode in the NaCl-KCl equimolar mixture or KCl system at 1073K

—●—: Pb cathode, —▲—: Sn cathode, —■—: Bi cathode,

—▼—: Al cathode, —◆—: Zn cathode,

—▽—: Al cathode (KCl system), —○—: Pb cathode (KCl system)

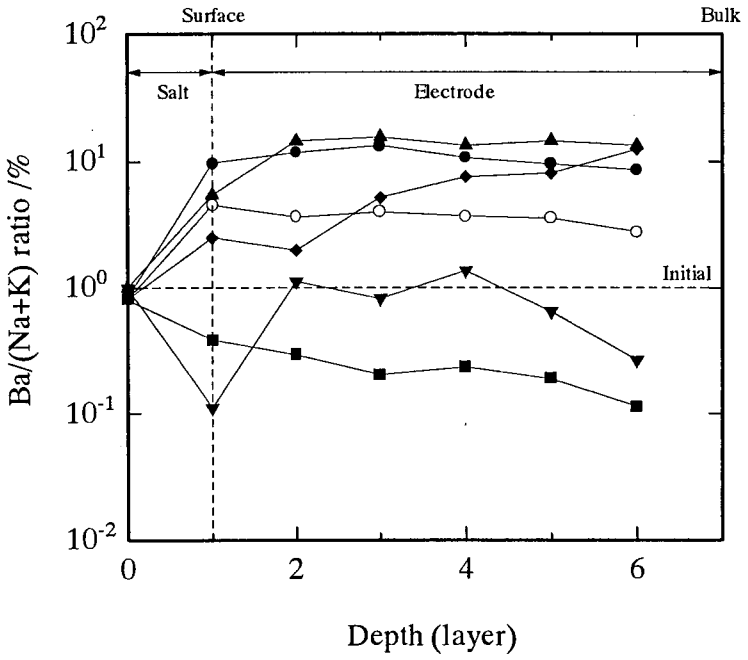

Fig. 6-4 Relationship between the depth and the Ba/(Na+K) ratio for $BaCl_2$ on various liquid electrode in the NaCl-KCl equimolar mixture at 1000K

—●—: Pb cathode, —▲—: Sn cathode, —■—: Bi cathode,

—▼—: Al cathode, —◆—: Zn cathode, —○—: Cd cathode

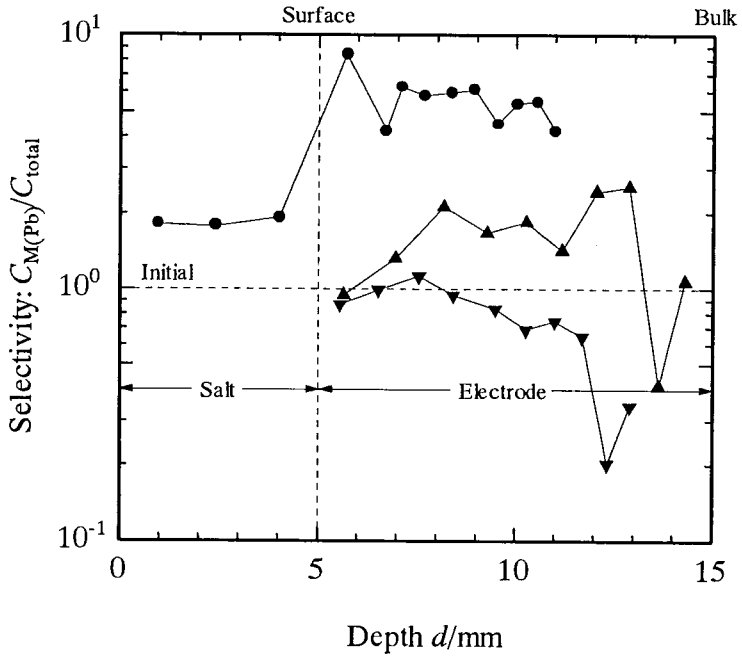

Fig. 6-5 Relationship between the depth and the Cs/(Li+Na+K) ratio for CsCl on various liquid electrode in the FLINAK system at 773K

—●—: Pb cathode, —▲—: Sn cathode, —▼—: Zn cathode

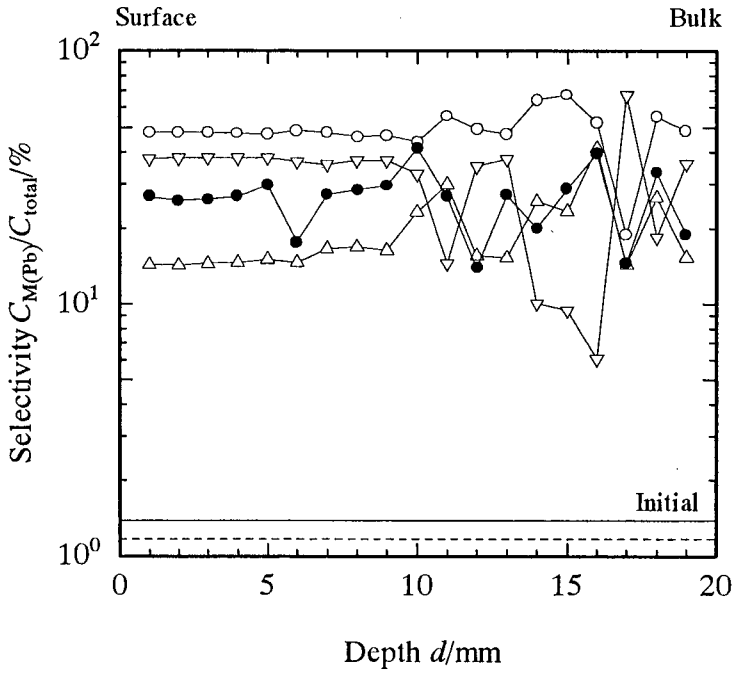

Fig. 6-6 Relationship between the depth and the selectivity for Cs and solvent components on the liquid Pb cathode in the FLINAK system at 873K, Total transported charge is 1000C under potentiostatic condition,

—●—: $C_{Cs(Pb)}/C_{total}$, —○—: $C_{K(Pb)}/C_{total}$, —△—: $C_{Na(Pb)}/C_{total}$, —▽—: $C_{Li(Pb)}/C_{total}$,

————: Initial ratio=1.38, - - - : Final ratio=1.17

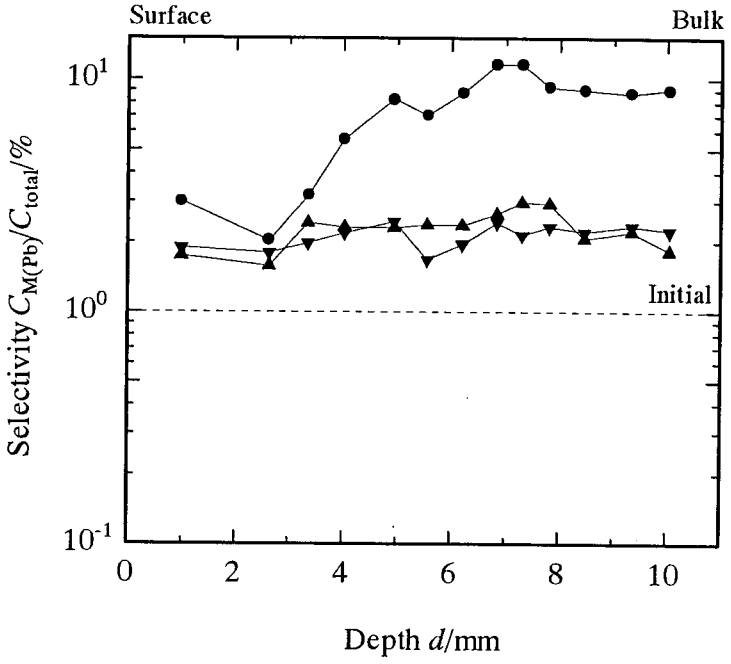

Fig. 6-7 Relationship between the depth and the selectivity for Cs, Sr and Ba on the liquid Pb cathode in the FLINAK system at 873K,

—●—: $C_{Cs(Pb)}/C_{total}$, —▲—: $C_{Sr(Pb)}/C_{total}$, —▼—: $C_{Ba(Pb)}/C_{total}$

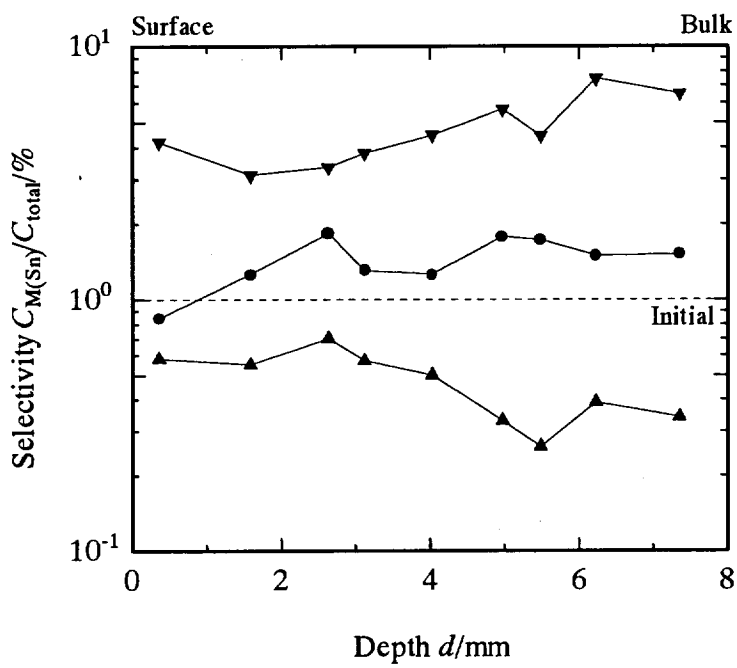

Fig. 6-8 Relationship between the depth and the selectivity for Cs, Sr and Ba on the liquid Sn cathode in the FLINAK system at 873K,

—●—: $C_{Cs(Sn)}/C_{total}$, —▲—: $C_{Sr(Sn)}/C_{total}$, —▼—: $C_{Ba(Sn)}/C_{total}$

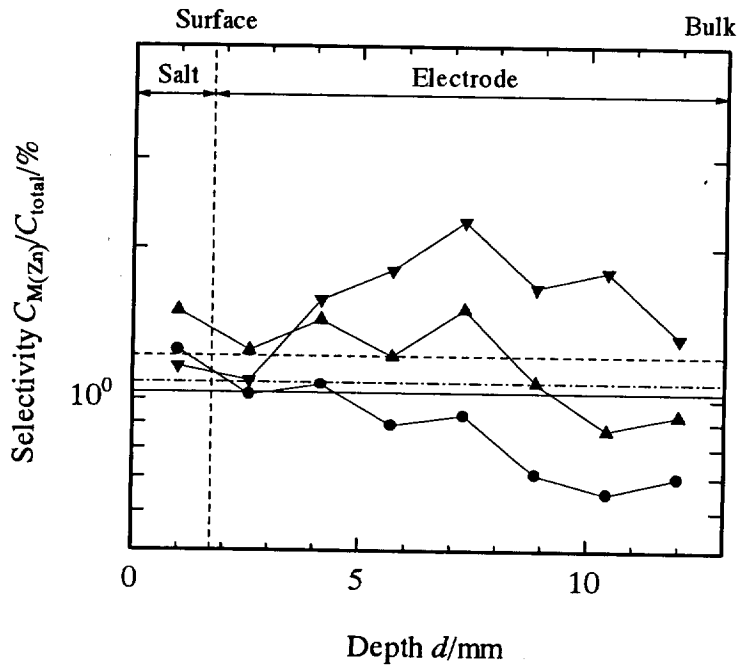

Fig. 6-9 Relationship between the depth and the selectivity for Cs, Sr and Ba on the liquid Zn cathode in the FLINAK system at 873K,

—●—: $C_{Cs(Zn)}/C_{total}$, —▲—: $C_{Sr(Zn)}/C_{total}$, —▼—: $C_{Ba(Zn)}/C_{total}$,

Initial composition; ———: x_{Cs}=0.010±0.004, - - - : x_{Sr}=0.012±0.002,

— - —: x_{Ba}=0.011±0.003

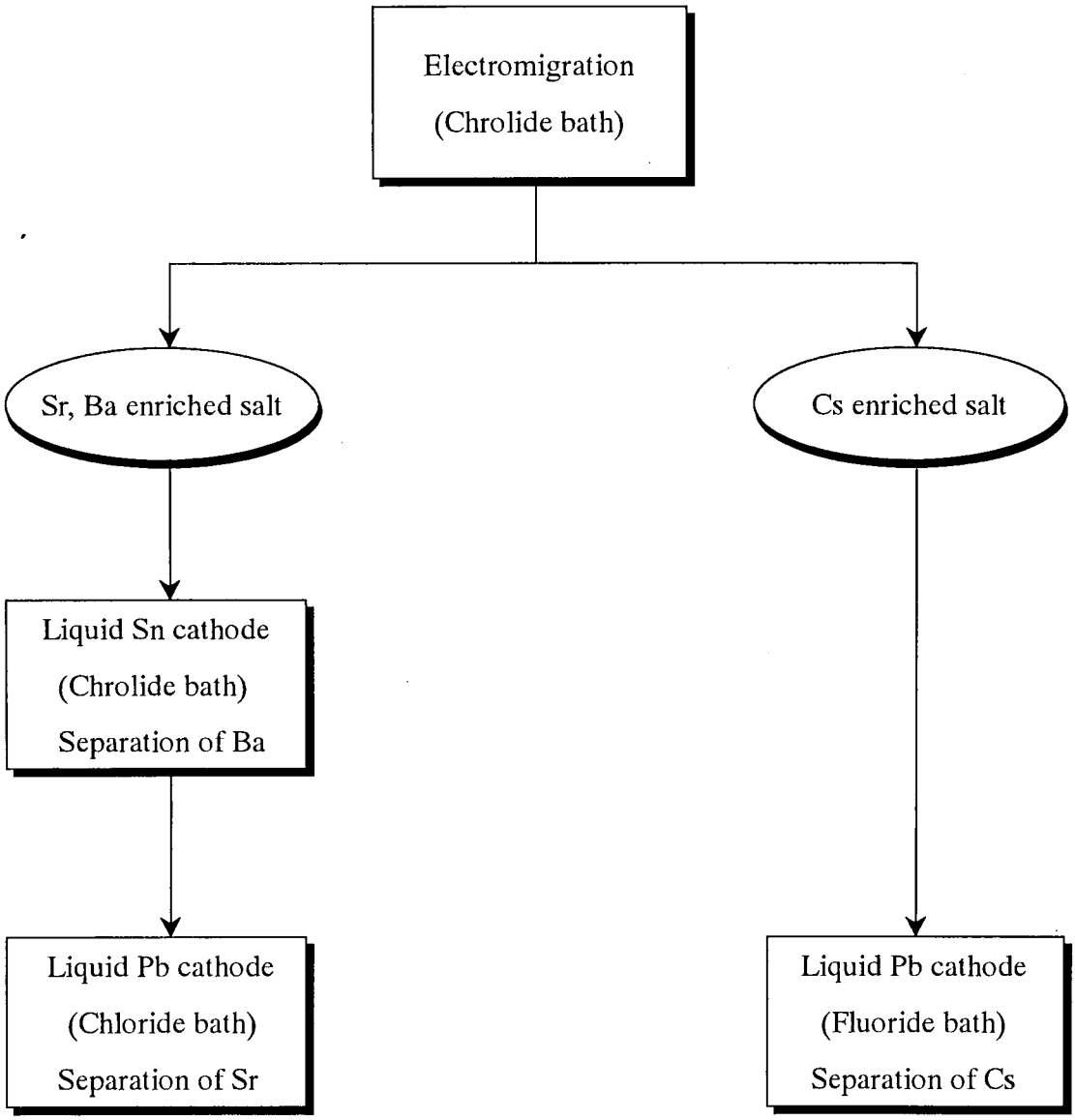

Fig. 6-10 The schematic diagram for one of the recovery system in the pyrochemical reprocessing process

§ VI-iv References

(1) A. Shimizu and Y. Fujii-e, *Prog. Nucl. Energy*, **29**, (Suppl.) 25 (1995).

(2) R. Takagi, H. Matsuura, Y. Fujii-e, R. Fujita and M. Kawashima, *Prog. Nucl. Energy*, **29**, (Suppl.) 471 (1995).

(3) Y. I. Chang, L. C. Walters, J. E. Battles, D. R. Pedersen, D. C. Wade and M. J. Lineberry, *ANL-IFR-125*, (1990)

(4) Y. I. Chang et al., *ANL-IFR-149*, (1991).

(5) Y. I. Chang et al., *ANL-IFR-246*, (1994).

(6) W. J. Hamer, M. S. Malmberg and B. Rubin, *J. Elecrochem. Soc.*, **112**, 750 (1965).

(7) M. Matsumiya, R. Takagi and R. Fujita, *J. Nucl. Sci. Technol.*, **34**, 310 (1997).

(8) M. Matsumiya, M. Takano, R. Takagi and R. Fujita, *J. Nucl. Sci. Technol.*, **35**, 836 (1998).

(9) M. Matsumiya, R. Takagi and R. Fujita, *J. Nucl. Sci. Technol.*, **35**, 137 (1998).

(10) M. Kurata, Y. Sakamura, T. Hijikata and K. Kinoshita, *J. Nucl. Mater.*, **227**, 110 (1995).

(11) M. L. Ferris, C. J. Maulen, J. J. Lawrance, J. F. Smith and D. E. Nogueira, *J. inorg. nucl. Chem.*, **32**, 2019 (1970).

(12) M. L. Ferris, C. J. Mailen and J. F. Smith, *J. inorg. nucl. Chem.*, **33**, 1325 (1971).

(13) Y. Sakamura, T. Inoue, T. Shimizu and K. Kobayashi, "*Development of pyrometallurgical partitioning technology for TRU in high level radioactive wastes vitrification process for salt waste*", Proc. GLOBAL'97, Vol. 2, 1222 (1997).

(14) K. Kinoshita, T. Inoue, P. S. Fusselman, L. D. Grimmett, J. J. Roy, L. R. Gay, L. C. Krueger, R. C. Nabelek and S. T. Storvick, *J. Nucl. Sci. Technol.*, **36**, 189 (1999).

(15) M. Matsumiya, H. Matsuura, R. Takagi and R. Fujita, *J. Alloys Comp.*, to be submitted.

(16) D. Elwell and G. M. Rao, *Electrochim. Acta*, **27**, 673 (1982).

(17) J. De Lepinay, S. Bouteillon, D. Renaud and M. J. Barbier, *J. Appl. Electrochem.*, **17**, 294 (1987).

(18) T. Yoko and A. Hellawell, *J. Electrochem. Soc.*, **131**, 2590 (1984).

(19) I. Motosada, *Nippon Kinzoku Gakkaishi*, **17**, 632 (1953).

(20) G. Grube and A. Dietrich, *Z. Electrochem.*, **44**, 755, (1938).

(21) K. W. Ray and R. G. Thompson, *Metals and alloys*, **1**, 314 (1930).

(22) W. Rieger and E. Parthe, *Acta Crystallogy*, **22**, 919 (1967).

(23) W. Dorrsheild, A. Widera and A. Schafer, *Z. Nuturforsch.*, **B32**, 1097 (1977).

(24) G. Bruzzone, E. Franceschi and F. Merlo, *J. Less-Common Met*, **60**, 59 (1978).

(25) T. B. Massalski, *"Binary alloy phase diagrams vol.1"*, American Society for Metals (1986).

(26) I. I. Kornilov, *Tsvet. Metally*, **10**, 73 (1935) [in Russian].

(27) V. A. Lebedev, *Melts*, **7**, 285 (1994).

(28) R. C. King, O. J. Kleppa, *Acta Metallurgica*, **12**, 87 (1964).

(29) A. Sh. Avaliani, O. O. Tvaradze, A. G. Morachevskii and L. N. Shulaya, *Zh. Prikl. Khim.*, **57**, 438 (1984) [in Russian].

(30) V. I. Zhuravlev, V. A. Lebedev, I. F. Nichkov and A. V. Volkovich, *Izv. Akad. Nauk SSSR, Met.*, **5**, 62 (1980) [in Russian].

(31) A. I. Demidov and A. G. Morachevskii, *Elektrokhimiya*, **9**, 1393 (1973).

(32) G. Langen, G. Schwitzgebel and H. Ruppertsberg, *Z. Metallk.*, **74**, 425 (1983).

(33) P. L. Polyakova, A. Z. Kononova, G. V. Kremenetsky and G. E. Polyakov, *Refractory Metals in Molten Salts*, 259 (1998).

Chapter VII

Conclusion

ChapterⅦ Conclusion

In the present work, in order to use the salt bath repeatedly, we have applied two methods, which are continuous countercurrent electromigration and electrowinning methods, to the practical plant for nuclear waste treatment system. For this purpose, the electromigration and molecular dynamics (MD) simulation for alkali chloride ternary system (Na, K, Cs)Cl have been performed at first, because it is necessary for us to interpret the cation mobilities of alkali chlorides from the scientific aspects. For molten (Na, K, Cs)Cl system, the relative differences in the internal cation mobilities at 1023K are investigated by the Klemm method and the electric conductivity by a direct current method as there will not exist a conductivity in this ternary system. From these data and the molar volumes which are evaluated from those of the pure salts on the assumption of additivity, the internal mobilities of the each cation, i.e., b_{Na}, b_K and b_{Cs} have been calculated. This result allows us to conclude that the internal mobilities of each cation becomes $b_{Cs}<b_{Na}<b_K$ at $x_{Cs}=0.1$, $b_{Na}<b_{Cs}<b_K$ at $x_{Cs}=0.14$ and $b_{Na}<b_K<b_{Cs}$ at $x_{Cs}>0.6$. In addition, MD simulation has been performed on molten (Na, K, Cs)Cl of the various compositions at 1023K. The employed pair potential parameters are based on the Tosi-Fumi ones. Then, the self-exchange velocities (SEV's) of Na^+, K^+ and Cs^+ with reference to Cl^- have been calculated. The sequence of the internal mobilities of these cations is well reproduced by the corresponding SEV's. Moreover, the transport numbers are calculated by the original equations. The result is also well reproduced by the corresponding internal mobilities.

Then, we have carried out a series of experiments of continuous countercurrent electromigration using the NaCl-KCl system from the technological aspects. We have measured the relative differences in internal mobilities for each experiment with respect to that of the solvent salt, where the mobilities of Na and K are regarded as practically equal. As long as the concentration of CsCl is low, Cs was concentrated in the CsCl-NaCl-KCl system. Since the multivalent cations ,i.e., Sr and Ba were enriched better than the monovalent cation, Cs, we can propose the electromigration method for separation of multivalent materials and monovalent materials. Furthermore, we

designed a new countercurrent electromigration system which is arranged to take out concentrated solute in the column from the melt, and it is necessary to introduce the Cl_2 gas into the cell before electromigration in order to prevent the corrosion caused by Na deposited. Consequently, it was demonstrated that the electromigration method was applicable to the salt bath cleaning process.

On the other hand, for the recovery by the electrodeposition of electrochemically negative elements using the liquid metallic cathodes, we have investigated the electrochemical behavior for Cs^+, Eu^{2+}, Sr^{2+} and Ba^{2+} in molten chloride and fluoride baths. In order to investigate the electrochemical behavior of Cs^+ in the molten FLINAK system and the recovery of Cs, the solid graphite electrode and the three kinds of the liquid metallic cathodes were examined. Then we determined that the total reaction of Cs^+ is expressed by the following irreversible reactions on the solid graphite electrode.

$$Cs^+ + e^- \rightarrow Cs$$
$$Cs \rightarrow Cs^+ + e^-$$

The charge transfer numbers and the diffusion coefficients show good agreement with the values determined by the various electroanalyses. The contents of Cs in the bulk of each liquid metallic cathode are confirmed by adsorption spectrometry. Furthermore, we found that Cs is concentrated in the liquid Pb cathode and we can selectively recover Cs on using the liquid Pb cathode in the FLINAK system.

In order to show electrolytic recovery of Eu^{2+},Sr^{2+} and Ba^{2+} the reduction reaction of these elements in the molten NaCl-KCl or KCl system into five or six kinds of liquid cathodes (Al, Bi, Cd, Pb, Sn and Zn) were examined. Then we investigated the reduction reaction for these elements on using these liquid metallic cathodes. As a result, we speculated that their alloy formation reactions are expressed by the following quasi-reversible reactions on liquid Pb electrodes.

$$Eu^{2+} + 2e^- + 3Pb \rightarrow EuPb_3$$
$$Sr^{2+} + 2e^- + 3Pb \rightarrow SrPb_3$$

$$Ba^{2+} + 2e^{-} + Pb \rightarrow BaPb$$

It was also clarified that we can recover Eu, Sr and Ba because it is possible to shift the deposition potential to more positive side by decreasing the activity of the deposited metal. The standard rate constants and the diffusion coefficients show good agreement with the values determined by the various electroanalyses. The existence of these elements in the bulk of each liquid Pb electrode is confirmed by ICP-emission analysis. Furthermore, we found it obvious that recovered these elements are concentrated in the liquid Pb cathode and we can selectively recover these elements on liquid Pb cathode or Sr^{2+} in the KCl melt on liquid Al and Pb cathodes. Moreover, we found that recovered Ba^{2+} is drastically concentrated in the liquid Pb and Sn cathodes, and we can selectively recover Ba^{2+} on liquid Pb and Sn cathodes. Furthermore, we found that it is effective to recover Ba^{2+} selectively using liquid Sn cathode before electrowinning Eu^{2+} and Sr^{2+} on the liquid Pb cathode, and we can separate Eu^{2+}, Sr^{2+} and Ba^{2+} from Cs^{+} by using liquid Pb cathode in the chloride bath.

Furthermore, we have investigated the possibility of recovery of Cs, Sr and Ba in the different liquid metallic cathodes in the FLINAK system. We found that the recovered Cs, Sr and Ba were concentrated in the liquid Pb cathode and selectively recovered Ba was concentrated in the liquid Sn cathode in this system. Therefore these results allow us to conclude that it is effective to recover Ba selectively using liquid Sn cathode before electrowinning Sr in the liquid Pb cathode in the chloride bath and to recover Cs selectively using liquid Pb cathode in the fluoride bath after electromigration. Finally we have proposed one of the recovery system in the pyrochemical reprocessing using electrochemical technique in this thesis.

List of Publications

1. M. Matsumiya, R. Takagi and R. Fujita, "Recovery of Eu^{2+} and Sr^{2+} Using Liquid Metallic Cathodes in Molten NaCl-KCl and KCl system", *J. Nucl. Sci. Technol.*, **34**, 310 (1997).

2. M. Matsumiya, R. Takagi and R. Fujita, "Recovery of Caesium Using Liquid Metallic Cathodes in Molten Fluoride system", *J. Nucl. Sci. Technol.*, **35**, 137 (1998).

3. M. Matsumiya, M. Takano, R. Takagi and R. Fujita, "Recovery of Ba^{2+} Using Liquid Metallic Cathodes in Molten Chlorides", *J. Nucl. Sci. Technol.*, **35**, 836 (1998).

4. R. Ohashi, M. Matsumiya, H. Matsuura and R. Takagi, "Internal Cation Mobilities in the Molten Binary System $NdCl_3$-KCl", *Electrochemistry*, **67**, 550 (1999).

5. M. Matsumiya and R. Takagi, "Internal Cation Mobilities in the Ternary Molten System (Na, K, Cs)Cl", *Proceedings of J. Electrochem. Soc.*, in press.

6. M. Matsumiya, M. Takano, R. Takagi and R. Fujita, "Electrochemical Behavior of Ba^{2+} Using Liquid Metal Cathodes in Molten Chlorides", *Z. Naturforsch.*, **54a**, 739 (1999).

7. M. Matsumiya, H. Matsuura, R. Takagi and R. Fujita, "Continuous Recovery of Concentrated Solute from the Melt by Countercurrent Electromigration", *J. Alloys Comp.*, to be submitted.

8. M. Matsumiya, H. Matsuura, R. Takagi and R. Fujita, "Recovery System of Electrochemically Negative Elements of Cs^{+}, Sr^{2+} and Ba^{2+} in Molten Chloride and Fluoride System", *J. Alloys Comp.*, to be submitted.

9. M. Matsumiya, H. Matsuura, R. Takagi and Yoshihiro Okamoto, "Internal Cation Mobilities in the Ternary Molten System (Na, K, Cs)Cl", *J. Electrochem. Soc.*, in preparation.

List of Presentations

1. Masahiko Matsumiya, Ryuzo Takagi and Reiko Fujita, "Recovery of Eu^{2+} and Sr^{2+} on Using Liquid Metallic Cathodes", Proc. of the 28th Symposium on Molten Salt Chemistry, Kofu, p259, Nov. 1st, (1996) [in Japanese].

2. Masatoshi Takano, Masahiko Matsumiya, Ryuzo Takagi and Reiko Fujita, "Recovery of Ba^{2+} from Molten Salt Chloride on Liquid Metallic Cathodes", Proc. of the 29th Symposium on Molten Salt Chemistry, Fukuoka, p47, Oct. 31th, (1997) [in Japanese].

3. Haruaki Matsuura, Masahiko Matsumiya, Ryuzo Takagi and Reiko Fujita, "Equipment to take out Continuously Concentrated Solute from the Melt by Countercurrent Electromigration", Proc. of the 29th Symposium on Molten Salt Chemistry, Fukuoka, p49, Oct. 31th, (1997) [in Japanese].

4. Masahiko Matsumiya, Ryuzo Takagi and Reiko Fujita, "Study of Electrochemical Behavior for Cs in Molten Fluoride Bath", Proc. of the 29th Symposium on Molten Salt Chemistry, Fukuoka, p51, Oct. 31th, (1997) [in Japanese].

5. Haruaki Matsuura, Masahiko Matsumiya, Ryuzo Takagi and Reiko Fujita, "Equipment to take out Continuously Concentrated Solute from the Melt by Countercurrent Electromigration", Proc. of 1998 Annual Meeting of the Atomic Energy Society of Japan, Osaka, p661, March 28th, (1998) [in Japanese].

6. Masahiko Matsumiya, Ryuzo Takagi and Reiko Fujita, "Selective Recovery of Cs, Sr and Ba Using Liquid Metallic Cathodes in Molten Fluoride System", Proc. of 1998 Fall Meeting of the Atomic Energy Society of Japan, Fukui, p810, Sep. 30th, (1998) [in Japanese].

7. Haruaki Matsuura, Masahiko Matsumiya, Ryuzo Takagi and Reiko Fujita, "Equipment to take out Continuously Concentrated Solute from the Melt by Countercurrent Electromigration (2)", Proc. of 1998 Fall Meeting of the Atomic Energy Society of Japan, Fukui, p811, Sep. 30th, (1998) [in Japanese].

8. Masahiko Matsumiya, Haruaki Matsuura, Ryuzo Takagi and Reiko Fujita, "Investigation for the Separation-Recovery System of the Fission Products in the Pyrochemical Reprocessing of the Spent Metallic Fuels", Proc. of the 30th Symposium on Molten Salt Chemistry, Osaka, p37, Nov. 13th, (1998) [in Japanese].

9. Ryo Ohashi, Masahiko Matsumiiya, Haruaki Matsuura and Ryuzo Takagi, "Internal Cation Mobilities in the Molten Binary System $NdCl_3$-KCl", Proc. of the 30th Symposium on Molten Salt Chemistry, Osaka, p81, Nov. 13th, (1998) [in Japanese].

10. Masahiko Matsumiya and Ryuzo Takagi, "Internal Cation Mobilities in the Ternary Molten System (Na, K, Cs)Cl", Proc. of the 30th International Symposium on Electrochemistry, Hawaii, Abstract No. 2286, Oct. 20th, (1999).

11. Masahiko Matsumiya, Mitsuo Akabori, Fumiaki Kobayashi and Toru Ogawa, "Spectrophotometric Study for Disproportionation Reaction of Nd^{2+}/Nd^{3+} in Molten LiCl-KCl Eutectic", Proc. of 31th Symposium on Molten Salt Chemistry, Sendai, p5, Nov. 11th, (1999) [in Japanese].

Acknowledgements

The work presented in this thesis has been performed mainly at Research Laboratory for Nuclear Reactors, Tokyo Institute of Technology and the work, in particular, MD simulation described in Chapter III performed at Japan Atomic Energy Research Institute. I am deeply indebted to Professor R. Takagi and Professor H. Tomiyasu for his continuing guidance and valuable discussion during the present work. However, suddenly Professor Takagi passed away in being regrettable. Professor Tomiyasu succeeded to Professor Takagi.

I am also especially indebted to Dr. H. Matsuura, Research Laboratory for Nuclear Reactors, Tokyo Institute of Technology, for kind and helpful assistance in organization of the experiment and for many valuable discussions and to Dr. R. Fujita, Nuclear Engineering Laboratory, Toshiba Corporation, for many valuable discussions for the electrochemical measurements mentioned in Chapter V.

I am grateful to Dr. T. Ogawa and Dr. Y. Okamoto for their useful suggestions and encouragement during the last one-year study at JAERI.

Lastly, I would like to express my gratitude to Dr. Pao-Hwa Chou, Mr. M. Takano, Mr. R. Ohashi and all of the colleagues of Professor Takagi's and Professor Tomiyasu's laboratory.